ASTROBIOLOGY AT THE INTERFACE: INTERACTIONS BETWEEN BIOSPHERES, GEOSPHERES, HYDROSPHERES AND ATMOSPHERES UNDER PLANETARY CONDITIONS

EDITED BY: Tetyana Milojevic, Adrienne Kish and Akihiko Yamagishi
PUBLISHED IN: Frontiers in Microbiology

frontiers Research Topics

frontiers

ISSN 1664-8714
ISBN 978-2-88966-618-8
DOI 10.3389/978-2-88966-618-8

About Frontiers

Frontiers is more than just an open-access publisher of scholarly articles: it is a pioneering approach to the world of academia, radically improving the way scholarly research is managed. The grand vision of Frontiers is a world where all people have an equal opportunity to seek, share and generate knowledge. Frontiers provides immediate and permanent online open access to all its publications, but this alone is not enough to realize our grand goals.

Frontiers Journal Series

The Frontiers Journal Series is a multi-tier and interdisciplinary set of open-access, online journals, promising a paradigm shift from the current review, selection and dissemination processes in academic publishing. All Frontiers journals are driven by researchers for researchers; therefore, they constitute a service to the scholarly community. At the same time, the Frontiers Journal Series operates on a revolutionary invention, the tiered publishing system, initially addressing specific communities of scholars, and gradually climbing up to broader public understanding, thus serving the interests of the lay society, too.

Dedication to Quality

Each Frontiers article is a landmark of the highest quality, thanks to genuinely collaborative interactions between authors and review editors, who include some of the world's best academicians. Research must be certified by peers before entering a stream of knowledge that may eventually reach the public - and shape society; therefore, Frontiers only applies the most rigorous and unbiased reviews.
Frontiers revolutionizes research publishing by freely delivering the most outstanding research, evaluated with no bias from both the academic and social point of view. By applying the most advanced information technologies, Frontiers is catapulting scholarly publishing into a new generation.

What are Frontiers Research Topics?

Frontiers Research Topics are very popular trademarks of the Frontiers Journals Series: they are collections of at least ten articles, all centered on a particular subject. With their unique mix of varied contributions from Original Research to Review Articles, Frontiers Research Topics unify the most influential researchers, the latest key findings and historical advances in a hot research area! Find out more on how to host your own Frontiers Research Topic or contribute to one as an author by contacting the Frontiers Editorial Office: frontiersin.org/about/contact

ASTROBIOLOGY AT THE INTERFACE: INTERACTIONS BETWEEN BIOSPHERES, GEOSPHERES, HYDROSPHERES AND ATMOSPHERES UNDER PLANETARY CONDITIONS

Topic Editors:
Tetyana Milojevic, University of Vienna, Austria
Adrienne Kish, Muséum National d'Histoire Naturelle, France
Akihiko Yamagishi, Tokyo University of Pharmacy and Life Sciences, Japan

The Topic Editors would like to acknowledge Dr. Yuko Kawaguchi for her contribution in designing and organizing this editorial project.

Citation: Milojevic, T., Kish, A., Yamagishi, A., eds. (2021). Astrobiology At The Interface: Interactions Between Biospheres, Geospheres, Hydrospheres And Atmospheres Under Planetary Conditions. Lausanne: Frontiers Media SA.
doi: 10.3389/978-2-88966-618-8

Table of Contents

frontiers in Microbiology

EDITORIAL
published: 12 February 2021
doi: 10.3389/fmicb.2021.629961

Editorial: Astrobiology at the Interface: Interactions Between Biospheres, Geospheres, Hydrospheres and Atmospheres Under Planetary Conditions

Tetyana Milojevic[1]*, *Adrienne Kish*[2] and *Akihiko Yamagishi*[3]

[1] Space Biochemistry Group, Department of Biophysical Chemistry, University of Vienna, Vienna, Austria, [2] Muséum National d'Histoire Naturelle, Paris, France, [3] Department of Applied Life Sciences, School of Life Sciences, Tokyo University of Pharmacy and Life Sciences, Hachioji, Japan

Keywords: astrobiology, outer space, extremophiles, ISS, Universe, Mars, space simulating facilities, biosignatures

Editorial on the Research Topic

Astrobiology at the Interface: Interactions Between Biospheres, Geospheres, Hydrospheres and Atmospheres Under Planetary Conditions

OPEN ACCESS

Edited by:
André Antunes, Macau University of Science and Technology, China

Reviewed by:
Michael Macey, The Open University, United Kingdom

***Correspondence:**
Tetyana Milojevic
tetyana.milojevic@univie.ac.at

Specialty section:
This article was submitted to Extreme Microbiology, a section of the journal Frontiers in Microbiology

Received: *16 November 2020*
Accepted: *26 January 2021*
Published: *12 February 2021*

Citation:
Milojevic T, Kish A and Yamagishi A (2021) Editorial: Astrobiology at the Interface: Interactions Between Biospheres, Geospheres, Hydrospheres and Atmospheres Under Planetary Conditions. Front. Microbiol. 12:629961. doi: 10.3389/fmicb.2021.629961

Astrobiology is a young, rapidly developing branch of science that seeks to address the question of whether life exists, or has existed, elsewhere in the Universe. It is by nature an interdisciplinary field that explores the origins of life, the conditions and processes that support or challenge life, the influence of different environmental conditions on the preservation and detection of biosignatures of past and present life, and the spread of life across the Universe.

As highly interdisciplinary field, astrobiology requires an integrative approach to link the efforts of microbiologists exploring the origins, evolution, and limits of life to the work of geologists exploring both planetary conditions (past and present) and preservation of biosignatures in the geological record. In the search for potential life on other planetary bodies, efforts are being made to combine exoplanet discovery, the study of asteroids and comets, ground-based analyses of recovered meteorites, microbial space exposure experiments with analog planetary-scale biosignature detection. Being a few steps in front of retrieving and returning the first samples from the surface of Mars, we have already gained extensive knowledge from the field, laboratory, and space exposure experiments (McKay and Stoker, 1989; Grotzinger and Milliken, 2012; Westall et al., 2015; Hays et al., 2017). This should enable a comprehensive characterization of the first Mars returned samples in terms of potential exobiology.

Outer space, along with ground-based simulating facilities, provides a research tool for studying life in the Universe. Multiple microbial exposure experiments have been successfully performed on board and outside of the International Space Station under the environmental conditions of low Earth orbit (Cockell et al., 2011; Nicholson et al., 2012; Vaishampayan et al., 2012; Kawaguchi et al., 2020; Ott et al., 2020) or mimicking planetary constraints (galactic cosmic and solar UV radiation, temperature fluctuations, microgravity, freezing, desiccation, and extreme vacuum) (Nicholson et al., 2012; Billi et al., 2019; de Vera et al., 2019; Panitz et al., 2019). Exposure experiments at ground-based simulating facilities have enabled the investigation of the effects of space-related parameters on microbial survival and adaptation capacities (Mastroleo et al., 2013; Ott et al., 2019a,b; Beblo-Vranesevic et al., 2020).

Revealing unknown boundaries for prokaryotic life under multiple extremes is a prerequisite to understanding the extent of biology on Earth, and to discover its possible wider presence in the Universe. Understanding freezing tolerance and survival limits of thermophiles in permanently cold habitats is important for studies of microbial transfer through space and between celestial bodies. The peculiar presence of thermophiles in permanently cold marine and terrestrial habitats, including Arctic marine sediments (Hubert et al., 2009; Hanson et al., 2019), cold seawaters (Mora et al., 2014; Wirth, 2017), Antarctic accretion ice (Bulat et al., 2004; Lavire et al., 2006), permafrost (Gilichinsky et al., 2007; Demidov and Gilichinsky, 2009), and laboratory investigations of thermophiles under low temperatures (Marchant et al., 2008; Milojevic et al., 2020) has been known for many years. However, our understanding of the molecular and physiological mechanisms of thermophilic adaptation to low temperatures is still poor.

The papers in this Research Topic cover a range of microbiological and biochemical research in extreme environments, from cold marine sediments with permanent low temperatures to hot springs in Yellowstone National Park, and to drilling samples from millions-year-old oceanic crust with deep fractured rock ecosystems. These papers provide a snapshot of current research activities in the field of astrobiology that have evolved at the boundaries of biosphere, geosphere, hydrosphere and atmosphere. In this research collection we present one review and 8 original research papers exploring the interactions between the biological, geological, hydrological, and atmospheric elements in the Universe. These works seek to address the impact of planetary conditions on the evolution of microorganisms, molecular mechanisms driving the limits of life under different physiochemical regimes, and traces of life that can be detected in the physiochemical conditions of Earth and beyond.

Several papers in this collection are addressing the survival limits of extremophiles exposed to harsh space-related parameters and drastic planetary constraints. Mosca et al. studied the desert cyanobacterium *Chroococcidiopsis* exposed to a Mars-like UV flux and long-termed desiccation. Their study reshaped the boundaries of *Chroococcidiopsis* desiccation and UV tolerance and revealed several molecular determinants of DNA damage and repair response of *Chroococcidiopsis*.

A review by Milojevic and Weckwerth presents further detailed analysis of molecular mechanisms behind microbial survival and adaptation to an outer space environment. This review is focused on molecular strategies revealed with the help of the global and integrative –omics approaches of systems biology that have been recently used to study microorganisms exposed to real and simulated space conditions. Popall et al. investigated the influence of UV-C radiation on cultures dominated by the cyanobacterium *Geitlerinema* sp., which was obtained from a laboratory-maintained stromatolite originating from a Precambrian analog lagoonal system Lagoa Vermelha, Brazil. The *Geitlerinema* sp. was able to withstand long-term exposure to UV-C radiation, building and maintaining filamentous mats after harmful irradiation.

The other papers in this Research Topic issue illustrate co-evolution of biosphere, geosphere, and hydrosphere, and consider biosignatures of life formed at their interfaces. Boyer et al. analyzed the influence of redox geochemistry on lipid composition of microbial communities inhabiting hot springs in Yellowstone National Park. This study proposed chemical signatures in lipid biomarkers that could potentially represent a fingerprint of the geochemical paleoredox conditions on microorganisms inhabiting these paleoenvironments. Sueoka et al. investigated a basaltic rock core sample of 104-million-year-old oceanic crust and proposed that deep saponite-bearing fractures could harbor extant life and/or host the remnants of bygone life on Mars. Hamilton-Brehm et al. described a novel anaerobic and thermophilic bacterium *Thermoanaerosceptrum fracticalcis* isolated from deep fractured rock ecosystems of the US Great Basin and provided insights into metabolic strategies of the deep subsurface biosphere. Glamoclija et al. studied subsurface microbial ecology of hypersaline playa Lake Lucero at the White Sands National Monument in New Mexico and proposed this region as a terrestrial analog for future astrobiological explorations. The limits of microbial life in saline and cold environments with potential implications for habitability of Martian cryobrines were a focus of investigations by Waajen et al. Their laboratory investigations showed that salt concentration, anion parameters and the water activity are crucial factors in the survival of the cryo- and halotolerant bacterial strain *Planococcus halocryophilus* in concentrated brines. Thus, anion brine composition, the salt concentration and water activity were proposed as a set of environmental parameters to be considered when investigating potential habitability of Martian cryobrines. Microbial life under extremely low temperatures was also investigated by Cramm et al., who studied the influence of freezing temperatures on the survival of thermophilic endospore-forming bacteria. Their laboratory study showed that thermospores remain viable after freezing at temperatures as low as −80°C, making them suitable for microbial viability investigations in Martian surface soil with temperature fluctuations between 20 and −76°C.

In summary, this Research Topic includes both novel research strategies and methodologies that should yield promising results in the future, expanding our current view of life-search across the Universe.

AUTHOR CONTRIBUTIONS

The authors are co-editors which organized this Research Topic, substantially, directly, and intellectually contributed to the work on this Research Topic and the manuscript, and approved it for publication. All authors contributed to the article and approved the submitted version.

ACKNOWLEDGMENTS

We warmly thank all contributing authors for submission of their papers to the Research Topic. The authors gratefully acknowledge the reviewers for their time spent on the manuscripts and valuable suggestions.

REFERENCES

Beblo-Vranesevic, K., Bohmeier, M., Schleumer, S., Rabbow, E., Perras, A. K., Moissl-Eichinger, C., et al. (2020). Impact of simulated martian conditions on (facultatively) anaerobic bacterial strains from different Mars analogue sites. *Curr. Issues Mol. Biol.* 38, 103–122. doi: 10.21775/cimb.038.103

Billi, D., Staibano, C., Verseux, C., Fagliarone, C., Mosca, C., Baqu,é, M., et al. (2019). Dried biofilms of desert strains of chroococcidiopsis survived prolonged exposure to space and Mars-like conditions in low Earth orbit. *Astrobiology* 19, 1008–1017. doi: 10.1089/ast.2018.1900

Bulat, S. A., Alekhina, I. A., Blot, M., Petit, J. R., Angelis, M., Waggenbach, D., et al. (2004). DNA signature of thermophilic bacteria from the aged accretion ice of Lake Vostok, Antarctica: implications for searching for life in extreme icy environments. *Int. J. Astrobiol.* 3, 1–12. doi: 10.1017/S1473550404001879

Cockell, C. S., Rettberg, P., Rabbow, E., and Olsson-Francis, K. (2011). Exposure of phototrophs to 548 days in low Earth orbit: microbial selection pressures in outer space and on early earth. *ISME J.* 5, 1671–1682. doi: 10.1038/ismej.2011.46

de Vera, J.-P. P., Alawi, M., Backhaus, T., Baqu,é, M., Billi, D., Böttger, U., et al. (2019). Limits of life and the habitability of Mars: the ESA space experiment BIOMEX on the ISS. *Astrobiology* 19, 145–157. doi: 10.1089/ast.2018.1897

Demidov, N. E., and Gilichinsky, D. A. (2009). "Terrestrial permafrost models and analogues of martian habitats and inhabitants," in *Permafrost Soils*, ed R. Margesin (Berlin: Springer), 334.

Gilichinsky, D. A., Wilson, G. S., Friedmann, E. I., McKay, C. P., Sletten, R. S., Rivkina, E. M., et al. (2007). Microbial populations in Antarctic permafrost: biodiversity, state, age, and implication for astrobiology. *Astrobiology* 7, 275–311. doi: 10.1089/ast.2006.0012

Grotzinger, J. P., and Milliken, R. E. (2012). "The sedimentary rock record of Mars: Distribution, origins, and global stratigraphy," in *Sedimentary Geology of Mars, SEPM*, eds J. P. Grotzinger and R. E. Milliken (Tulsa, OK: Society for Sedimentary Geology).

Hanson, C. A., Müller, A. L., Loy, A., Dona, C., Appel, R., Jørgensen, B. B., et al. (2019). Historical factors associated with past environments influence the biogeography of thermophilic endospores in Arctic marine sediments. *Front. Microbiol.* 10:245. doi: 10.3389/fmicb.2019.00245

Hays, L. E., Graham, H. V., Des Marais, D. J., Hausrathm, E. M., Horgan, B., McCollom, T. M., et al. (2017). Biosignature preservation and detection in mars analog environments. *Astrobiology* 4, 363–400. doi: 10.1089/ast.2016.1627

Hubert, C., Loy, A., Nickel, M., Arnosti, C., Baranyi, C., Brüchert, V., et al. (2009). A constant flux of diverse thermophilic bacteria into the cold Arctic seabed. *Science* 325, 1541–1544. doi: 10.1126/science.1174012

Kawaguchi, Y., Shibuya, M., Kinoshita, I., Yatabe, J., Narumi, I., Shibata, H., et al. (2020). DNA damage and survival time course of deinococcal cell pellets during 3 years of exposure to outer space. *Front. Microbiol.* 11:2050. doi: 10.3389/fmicb.2020.02050

Lavire, C., Normand, P., Alekhina, I., Bulat, S., Prieur, D., Birrien, J. L., et al. (2006). Presence of Hydrogenophilus thermoluteolus DNA in accretion ice in the subglacial Lake Vostok, Antarctica, assessed using rrs, cbb and hox. *Environ. Microbiol.* 8, 2106–2114. doi: 10.1111/j.1462-2920.2006.01087.x

Marchant, R., Franzetti, A., Pavlostathis, S. G., Tas, D. O., Erdbrugger, I., Unyayar, A., et al. (2008). Thermophilic bacteria in cool temperate soils: are they metabolically active or continually added by global atmospheric transport? *Appl. Microbiol. Biotechnol.* 78, 841–852. doi: 10.1007/s00253-008-1372-y

Mastroleo, F., Van Houdt, R., Atkinson, S., Mergeay, M., Hendrickx, L., Wattiez, R., et al. (2013). Modelled microgravity cultivation modulates N-acylhomoserine lactone production in *Rhodospirillum rubrum* S1H independently of cell density. *Microbiology* 159, 2456–2466. doi: 10.1099/mic.0.066415-0

McKay, C. P., and Stoker, C. R. (1989). The early environment and its evolution on Mars: implication for life. *Rev. Geephys.* 2, 189–214.

Milojevic, T., Zebec, Z., and Schimak, M. P. (2020). Cultivation with powdered meteorite (NWA 1172) as the substrate enhances low-temperature preservation of the extreme thermoacidophile *Metallosphaera sedula*. *Front. Astron. Space Sci.* 7:37. doi: 10.3389/fspas.2020.00037

Mora, M., Bellack, A., Ugele, M., Hopf, M., and Wirth, R. (2014). The temperature gradient forming device: an accessory unit for normal light microscopes to study the biology of hyperthermophilic microorganisms. *Appl. Environ. Microbiol.* 80, 4764–4770. doi: 10.1128/AEM.00984-14

Nicholson, W. L., Moeller, R., PROTECT Team and Horneck, G. (2012). Transcriptomic responses of germinating Bacillus subtilis spores exposed to 1.5 years of space and simulated martian conditions on the EXPOSE-E experiment PROTECT. *Astrobiology* 12, 469–486. doi: 10.1089/ast.2011.0748

Ott, E., Fuchs, F., Moeller, R., Hemmersbach, R., Kawaguchi, Y., Yamagishi, A., et al. (2019a). Molecular response of *Deinococcus radiodurans* to simulated microgravity explored by proteometabolomic approach. *Sci. Rep.* 9:18462. doi: 10.1038/s41598-019-54742-6

Ott, E., Kawaguchi, Y., Kölbl, D., Rabbow, E., Rettberg, P., Mora, M., et al. (2020). Molecular repertoire of *Deinococcus radiodurans* after 1 year of exposure outside the International Space Station within the Tanpopo mission. *Microbiome* 8:150. doi: 10.1186/s40168-020-00927-5

Ott, E., Kawaguchi, Y., Özgen, N., Yamagishi, A., Rabbow, E., Rettberg, P., et al. (2019b). Proteomic and metabolomic profiling of *Deinococcus radiodurans* recovering after exposure to simulated low earth orbit vacuum conditions. *Front. Microbiol.* 10:909. doi: 10.3389/fmicb.2019.00909

Panitz, C., Frösler, J., Wingender, J., Flemming, H. C., and Rettberg, P. (2019). Tolerances of *Deinococcus geothermalis* biofilms and planktonic cells exposed to space and simulated Martian conditions in low Earth orbit for almost two years. *Astrobiology* 19, 979–994. doi: 10.1089/ast.2018.1913

Vaishampayan, P. A., Rabbow, E., Horneck, G., and Venkateswaran, K. J. (2012). Survival of *Bacillus pumilus* spores for a prolonged period of time in real space conditions. *Astrobiology* 12, 487–497. doi: 10.1089/ast.2011.0738

Westall, F., Foucher, F., Bost, N., Bertrand, M., Loizeau, D., Vago, J. L., et al. (2015). Biosignatures on Mars: what, where, and how? Implications for the search for Martian life. *Astrobiology* 11, 998–1029. doi: 10.1089/ast.2015.1374

Wirth, R. (2017). Colonization of black smokers by hyperthermophilic microorganisms. *Trends Microbiol.* 2, 92–99. doi: 10.1016/j.tim.2016.11.002

Conflict of Interest: The authors declare that the research was conducted in the absence of any commercial or financial relationships that could be construed as a potential conflict of interest.

frontiers in Microbiology

ORIGINAL RESEARCH
published: 03 May 2019
doi: 10.3389/fmicb.2019.00945

Freezing Tolerance of Thermophilic Bacterial Endospores in Marine Sediments

*Margaret A. Cramm[1], Anirban Chakraborty[1], Carmen Li[1], S. Emil Ruff[2†], Bo Barker Jørgensen[3] and Casey R. J. Hubert[1]**

[1] Geomicrobiology Group, Department of Biological Sciences, University of Calgary, Calgary, AB, Canada, [2] Energy Bioengineering Group, Department of Geoscience, University of Calgary, Calgary, AB, Canada, [3] Center for Geomicrobiology, Department of Bioscience, Aarhus University, Aarhus, Denmark

OPEN ACCESS

Edited by:
Adrienne Kish, Muséum National d'Histoire Naturelle, France

Reviewed by:
Michael Pester, German Collection of Microorganisms and Cell Cultures GmbH (DSMZ), Germany
Siavash Atashgahi, Radboud University Nijmegen, Netherlands

***Correspondence:**
Casey R. J. Hubert
chubert@ucalgary.ca

†Present address:
S. Emil Ruff, Ecosystems Center/Josephine Bay Paul Center, Marine Biological Laboratory, Woods Hole, MA, United States

Specialty section:
This article was submitted to Extreme Microbiology, a section of the journal Frontiers in Microbiology

Received: *27 January 2019*
Accepted: *15 April 2019*
Published: *03 May 2019*

Citation:
Cramm MA, Chakraborty A, Li C, Ruff SE, Jørgensen BB and Hubert CRJ (2019) Freezing Tolerance of Thermophilic Bacterial Endospores in Marine Sediments. Front. Microbiol. 10:945. doi: 10.3389/fmicb.2019.00945

Dormant endospores of anaerobic, thermophilic bacteria found in cold marine sediments offer a useful model for studying microbial biogeography, dispersal, and survival. The dormant endospore phenotype confers resistance to unfavorable environmental conditions, allowing dispersal to be isolated and studied independently of other factors such as environmental selection. To study the resilience of thermospores to conditions relevant for survival in extreme cold conditions, their viability following different freezing treatments was tested. Marine sediment was frozen at either −80°C or −20°C for 10 days prior to pasteurization and incubation at +50°C for 21 days to assess thermospore viability. Sulfate reduction commenced at +50°C following both freezing pretreatments indicating persistence of thermophilic endospores of sulfate-reducing bacteria. The onset of sulfate reduction at +50°C was delayed in −80°C pretreated microcosms, which exhibited more variability between triplicates, compared to −20°C pretreated microcosms and parallel controls that were not frozen in advance. Microbial communities were evaluated by 16S rRNA gene amplicon sequencing, revealing an increase in the relative sequence abundance of thermophilic endospore-forming *Firmicutes* in all microcosms. Different freezing pretreatments (−80°C and −20°C) did not appreciably influence the shift in overall bacterial community composition that occurred during the +50°C incubations. Communities that had been frozen prior to +50°C incubation showed an increase in the relative sequence abundance of operational taxonomic units (OTUs) affiliated with the class *Bacilli*, relative to unfrozen controls. These results show that freezing impacts but does not obliterate thermospore populations and their ability to germinate and grow under appropriate conditions. Indeed the majority of the thermospore OTUs detected in this study (21 of 22) could be observed following one or both freezing treatments. These results are important for assessing thermospore viability in frozen samples and following cold exposure such as the very low temperatures that would be encountered during panspermia.

Keywords: thermophiles, endospores, microbial ecology, extremophiles, microbial dispersal, panspermia, frozen environments, spores

INTRODUCTION

Thermophilic endospore-forming bacteria (thermospores) have been discovered in cold marine sediments through conducting high-temperature (50°C) incubation experiments (Hubert et al., 2009; de Rezende et al., 2013; Müller et al., 2014; Volpi et al., 2017; Bell et al., 2018; Chakraborty et al., 2018; Hanson et al., 2019). These misplaced thermophiles are members of the dormant microbial seed bank and are conspicuously alien to these cold environments where they cannot grow and divide. By existing in a dormant state at temperatures below their growth and activity range they can be passively dispersed through hostile environments without suffering adverse effects. Because thermospores must originate in warm environments, their presence in cold sediments imply mechanisms of passive dispersal distribute thermospores making them unique models for studying microbial biogeography. Petroleum reservoirs and oceanic spreading centers associated with geofluid flow have been proposed as warm source environments for thermospores found in cold marine sediment (Hubert et al., 2009; Chakraborty et al., 2018).

The rate at which thermospores are dispersed is considerable. Hubert et al. (2009) found that thermospores are supplied to Arctic marine sediment at a rate of 10^8 m^{-2} y^{-1}. Many studies have observed intriguingly high numbers of thermospores in cold or mild environments (Bartholomew and Paik, 1966; Fields and Chen Lee, 1974; Marchant et al., 2002, 2008; Rahman et al., 2004; de Rezende et al., 2013; Volpi et al., 2017; Bell et al., 2018). These apparently paradoxical observations, and the fact that warm environments hospitable to thermospore germination and growth are limited, point to thermospores being well adapted for dispersal and survival (Zeigler, 2014).

Understanding the survival limits of thermospores is important if they are to be used as model organisms for studying survival in frozen ecosystems, passive dispersal on Earth, or between Earth and other planets in the context of panspermia – the theory that life is dispersed throughout the universe by vectors, including but not limited to comets, meteors, or spacecraft. While the heat tolerance of endospores is well known (Nicholson et al., 2000; Setlow, 2006; O'Sullivan et al., 2015), fewer studies have investigated the ability of endospores to withstand low temperatures including freezing conditions (Fairhead et al., 1994). Whereas sporulation at warmer temperatures results in more heat-resistant endospores (Melly et al., 2002; O'Sullivan et al., 2015), it is unclear whether endospores of thermophiles are able to survive very low sub-zero temperatures. Although thermophilic endospores are unlikely to ever encounter extreme temperatures such as −80°C on Earth, the low temperature tolerance of thermospores is interesting for several reasons. Due to their dormancy and resistance to radiation, temperature, and pressure extremes, endospore-forming bacteria have been used to study interstellar transport of microbial life by meteors or other ancient dispersal vectors (Fajardo-Cavazos et al., 2007; Nicholson, 2009).

Endospores have been shown to survive stresses associated with the three main stages of lithopanspermia, (i.e., panspermia where a rock, such as a meteorite, is the life-carrying vector). The stages are ejection from the donor planet, travel through space, and capture by the recipient planet. *Bacillus subtilis* endospores were shown to remain viable (40–100%) following simulations of the velocity, acceleration, and jerk forces encountered during impact-ejection from Mars (Mastrapa et al., 2001). Endospores of both mesophilic *B. subtilis* and thermophilic *Thermoanaerobacter siderophilus* survived entry through the Earth's atmosphere on artificial meteorites (Fajardo-Cavazos et al., 2005; Slobodkin et al., 2015), and *B. subtilis* endospores survived the extremely high deceleration of impact onto Earth coming out of orbit (Barney et al., 2016). Horneck et al. (2008) showed that *Bacillus* endospores survive temperatures and pressures experienced by Martian meteorites found on earth as well as the stresses experienced by a trip from Earth to Mars (Horneck et al., 2012).

Surviving the stresses of ejection from a donor planet and capture by a recipient planet is not enough; panspermia also demands that endospores survive the harsh conditions of space over timescales allowing for the transit between the donor planet and a recipient planet. Irradiation is likely the harshest biocidal factor spores engaged in panspermia experience (Nicholson et al., 2005; Horneck et al., 2012) and while endospores are more resistant to UV radiation than their vegetative counterparts (Nicholson et al., 2000; Riesenman and Nicholson, 2000; Setlow, 2001, 2006), they are quickly inactivated by direct exposure to UV (Schuerger et al., 2003; Horneck et al., 2012; Panitz et al., 2015; Khodadad et al., 2017). Yet several studies showed that with minor shelter from UV endospores maintain viability (Horneck et al., 2012; Moeller et al., 2012; Vaishampayan et al., 2012) and, under protection from UV, tolerance of other stresses of the space environment, such as extremely low temperatures, may determine endospore survival. Interstellar particle temperature is ten degrees Kelvin (i.e., −263°C). While mesophilic *B. subtilis* and *B. pumilus* endospores have been used to study viability at low temperature, in vacuum pressures, and in the intense UV environment of space (Weber and Greenberg, 1985; Horneck, 1993; Nicholson et al., 2000; Horneck et al., 2012; Vaishampayan et al., 2012; Panitz et al., 2015; Khodadad et al., 2017), less is known about the survival of thermophiles.

Based on thermal inactivation kinetics, Nicholson (2003) suggested that thermophilic endospores are more likely than their mesophilic relatives to survive dormancy on panspermia-relevant timescales. Thermospores have only recently been studied with regards to the maintenance of viability during exposure to the conditions encountered during panspermia (Slobodkin et al., 2015). We therefore investigated whether thermospores survive exposure to different freezing temperatures. For this investigation we used marine sediment from an Arctic fjord of Svalbard known to contain high concentrations of thermospores (Hubert et al., 2009). We tested the hypothesis that thermospores remain viable after freezing at temperatures as low as −80°C, and that different temperature pretreatments furthermore select for a greater diversity of germinating endospores during subsequent incubation at high temperature permissive to thermophile germination and growth.

MATERIALS AND METHODS

Freezing Pretreatment

Marine surface sediment from Smeerenburgfjorden, Svalbard, (79°42.82′ N 11°05.19′ E), previously determined to harbor thermophilic endospore-forming sulfate-reducing bacteria (Hubert et al., 2009), was used in this study. The year-round *in situ* temperature in this sediment is close to 0°C. Sediment was sampled in the summer of 2007 and stored in anoxic plastic bags at +4°C until it was used for these experiments. Wet sediment (15 g) was added to 120 mL serum bottles that were stoppered and flushed with N_2/CO_2 (90:10%) gas to ensure anoxic conditions. Anoxic bottles containing only sediment were frozen at either −20°C or −80°C for 10 days. The minimum temperature a cell is exposed to and the rate at which it freezes have been shown to be the factors causing the most injury to a frozen cell (Mazur and Schmidt, 1968). Both factors are accounted for in these 10-day freezing pretreatments. A parallel set of microcosms remained in a +4°C cold room during the pretreatment period and served as unfrozen positive controls.

High-Temperature Incubation

After the freezing pretreatments, 30 mL of artificial seawater medium (Isaksen et al., 1994) amended with sulfate (20 mM), ethanol (1 mM), and six organic acids, i.e., formate, lactate, acetate, succinate, propionate, and butyrate (each to a final concentration of 1 mM), was added to each of the microcosm bottles using a syringe flushed with N_2/CO_2 gas. All microcosms were again flushed with N_2/CO_2 gas and then pasteurized at +80°C for 1 h. Immediately following pasteurization, microcosms were incubated at +50°C for 21 days to promote germination and growth of thermophilic endospore-forming bacteria.

Triplicate microcosms were prepared for each of the experimental conditions. Triplicates were subsampled immediately before and after pasteurization and then daily for the first 7 days at +50°C, and then at 10, 14, and 21 days of incubation. Subsampled aliquots were centrifuged at 14,800 rpm for 5 min to separate supernatant and pellet fractions, that were both stored at −20°C until further analysis.

Sulfate and Organic Acid Measurement

Sulfate and organic acid concentrations were measured in supernatant subsamples at various time points during the incubation to monitor activity of thermophilic populations in the microcosms. Sulfate concentrations were determined in a Dionex ICS-5000 reagent-free ion chromatography system (Thermo Scientific) equipped with an anion-exchange column (Dionex IonPac AS22; 4 × 250 mm; Thermo Scientific), and EGC-500 K_2CO_3 eluent generator cartridge and a conductivity detector. The mobile phase consisted of 4.5 mM K_2CO_3 and 1.4 mM $KHCO_3$ and was passed through the column at a constant flow rate of 1.3 mL min^{-1} while maintaining column temperature of 30°C. The sulfate detection limit was 100 μM. Organic acid concentrations were measured in an UltiMate 3000 RSLC ultra-high performance liquid chromatography system (Thermo Scientific) with a 5 mM H_2SO_4 mobile phase at a flow rate of 0.6 mL min^{-1} and a temperature of 60°C using an Aminex HPX-87H column (5 μm, 7.8 × 300 mm, Bio Rad). The organic acid detection limit was 2.5 μM.

DNA Extraction and 16S rRNA Gene Amplicon Sequencing

DNA was extracted from the subsample pellets (0.3 g) using the DNeasy PowerSoil Kit (Qiagen) (formerly the PowerSoil DNA Isolation Kit, MoBio) as per the manufacturer's protocol with the addition of a 70°C incubation for 10 min prior to bead beating as per the manufacturer's troubleshooting guide. DNA was extracted directly from the sediment following pretreatment at −80°C or −20°C, and from the +4°C unfrozen control (i.e., prior to pasteurization), from slurry subsamples before the +50°C incubation (i.e., immediately after pasteurization) and again after 7 days of incubation at +50°C. Assessing the community composition after 7 days is consistent with observations that this is a sufficient time frame for uncovering thermospore richness in heated sediment incubations (Chakraborty et al., 2018; Hanson et al., 2019). Procedural blank DNA extractions, i.e., without any subsample added, were performed in parallel with each batch of DNA extractions. Subsequent PCR stages were performed on these blank DNA extractions to confirm the absence of contaminating DNA sequences due to the DNA extraction process.

A 427 bp fragment of the V3–V4 hypervariable region of the 16S rRNA gene was amplified using the primer pair S-D-Bact-0341-a-S-17 and S-D-Bact-0785-a-A21 (Klindworth et al., 2013). To minimize PCR bias, triplicate 25 μl PCR reactions were performed using 2 × KAPA HiFi Hot Start Ready Mix (KAPA Biosystems), a final concentration of 0.1 mM of each primer, 4–10 ng template DNA, and sterile nuclease-free water and then pooled. Touchdown PCR conditions were as follows: an initial denaturation at 95°C for 5 min, then 10 touchdown cycles of denaturation at 95°C for 30 s, a decreasing annealing temperature at 60°C to 51°C for 45 s, and extension at 72°C for 1 min. The touchdown sequence started 60°C, rather than 65°C as would be done in a classical PCR touchdown protocol, to minimize preferential amplification of high G+C sequences. After the 10 touchdown cycles, 20 additional cycles with denaturation at 95°C for 30 s, annealing at 55°C, and extension at 72°C for 1 min were performed, for a total of 30 cycles, prior to a final extension at 72°C for 5 min. Amplified 16S rRNA gene fragments 427 bp in length were prepared for sequencing as per Dong et al. (2017) and sequenced on a MiSeq Benchtop DNA sequencer (Illumina) resulting in an average library size of 44,937 reads after quality filtering. DNA extraction negatives were performed using only the buffer solutions provided for the DNA extraction protocol. PCR of the DNA extraction negatives following the same PCR conditions outlined above confirmed the absence of

contamination introduced during the extraction process and these samples were not sequenced.

Community Analysis

Community analysis was performed using the MetaAmp pipeline (Dong et al., 2017). Sequencing reads were clustered into operational taxonomic units (OTUs) using a 97% sequence identity threshold. Representative sequences for each OTU were chosen based on the UPARSE-OTU algorithm and were used for assigning taxonomy using the SILVA (version 132) database (Pruesse et al., 2012). Paired-end merging options for the MetaAmp program were 100 bp for the minimum length of overlap, and 8 as the maximum number of mismatches in the overlap region. Quality filtering allowed a maximum of 1 mismatch per primer sequence, and the maximum number of expected errors was 1. The length of the amplicon was trimmed to 350 bp. Amplicon sequences can be found in the NCBI Sequence Read Archive under accession PRJNA496528.

Operational taxonomic unit tables generated by MetaAmp (version 2.0) were used to calculate Bray–Curtis dissimilarity matrices in the R software environment (R Core Team, 2013) using a community analysis workflow based on the 'vegan' version 2.5–3 (Oksanen et al., 2016) and 'cluster' version 2.0.6 (Maechler et al., 2018) packages and custom R scripts (Ruff et al., 2019). The Bray–Curtis algorithm was chosen because it considers OTU presence/absence as well as OTU abundance, giving relatively more weight to OTUs with higher relative sequence abundance. This is especially important when a few populations dominate the communities, as is the case in thermospore enrichment experiments (Müller et al., 2014; Chakraborty et al., 2018). Microbial community similarity was visualized using non-metric multidimensional scaling (NMDS) based on dissimilarity matrices. The significance of the variance within the NMDS ordinated groups was tested using Analysis of Similarity (ANOSIM).

High-temperature (+50°C) germination experiments were required to detect viable thermospore OTUs in this study. OTUs were identified as thermospores and considered for further analyses based on the following criteria: OTUs had to be present in at least one post-incubation (day 7) sample in greater than 0.5% relative sequence abundance. Furthermore, the percent relative abundance of these OTUs had to increase by at least a factor of 10 relative to the corresponding pre-incubation library (i.e., after freezing and pasteurization, but before +50°C incubation). These criteria limited analysis only to OTUs that showed substantial increases in relative abundance. The significance of OTU relative sequence abundance between two subsampling intervals was confirmed using the STAMP application (Parks et al., 2014) using a two-sided Fisher's Exact test, which is preferred for its accuracy with small counts (Parks and Beiko, 2010), and the Bonferroni multiple test correction to prevent false positives, resulting in a p-value of <0.001.

Phylogenetic analysis of OTUs was performed using the ARB software environment (Ludwig et al., 2004). Sequences included in the annotated phylogenetic tree are those of the closest cultured relatives as well as representatives of the closest uncultured relatives, in addition to the thermospore OTU sequences. Thermospore OTU representative sequences generated from MetaAmp, as well as their closest relatives (determined by BLASTn searching; Johnson et al., 2008) were aligned using the SINA aligner (Pruesse et al., 2012) and imported into the ARB-SILVA SSU Ref NR 99 132 database (Quast et al., 2013). A phylogenetic tree was calculated in ARB (Ludwig et al., 2004) using the maximum likelihood (phyML) algorithm using near-full-length (>1,300 bp) 16S rRNA reference sequences of 243 bacteria, calculated based on 1,072 alignment positions using a positional variability filter. Only conserved regions with a calculated site mutation rate of less than 8.3% were considered. The topology of the tree was validated with bootstrap support (100 re-samplings). Sequences of the thermospore OTUs and their closest relatives were added to the phylogenetic tree using the ARB Parsimony function and applying the positional variability filters for bacteria along 337 alignment positions respectively. Phylogenetic trees were visualized using iTOL version 4.2.3 (Letunic and Bork, 2006).

RESULTS

Sulfate Reduction and the Production and Consumption of Organic Acids in +50°C Incubations

Patterns of net sulfate consumption in each microcosm incubated at +50°C differed depending on the freezing pretreatment. During 21 days at +50°C, the sulfate concentrations in −20°C pretreated microcosms and the +4°C unfrozen controls were similar, showing a drop in all triplicates between 3 and 6 days (**Figures 1A,B**). Sulfate reduction in −80°C pretreated microcosms was not observed during the first 6 days of incubation at +50°C (**Figure 1C**), with sulfate eventually dropping to concentrations similar to those observed in the other microcosms in two out of three replicates. In all cases where a decrease in sulfate concentration was observed, it was 7–9 mM lower than in the medium-only controls (**Figures 1A–C**), in agreement with the expected amount of sulfate reduction (8.75 mM) that corresponds to all organic acids being oxidized to CO_2.

Triplicate +4°C unfrozen controls (**Figures 1D,G,J**) showed very similar changes in organic acid concentrations during the +50°C incubation. Formate and lactate were rapidly consumed, reaching 0 mM within 1.5 days at +50°C; it cannot be concluded with certainty whether or not this was coupled to sulfate reduction as has been observed in the early hours in similar experiments with different marine sediment (de Rezende et al., 2013, 2017). The concomitant increase in acetate during this period could be due to incomplete oxidation of lactate coupled to sulfate reduction, or acetogenesis from formate. Stoichiometric conversion of succinate to propionate was observed between day 1 and day 3 in unfrozen controls, followed by complete consumption of propionate as well as butyrate by 4–6 days. Both propionate and butyrate consumption occurred concomitantly with decreases in sulfate concentration. Acetate concentration

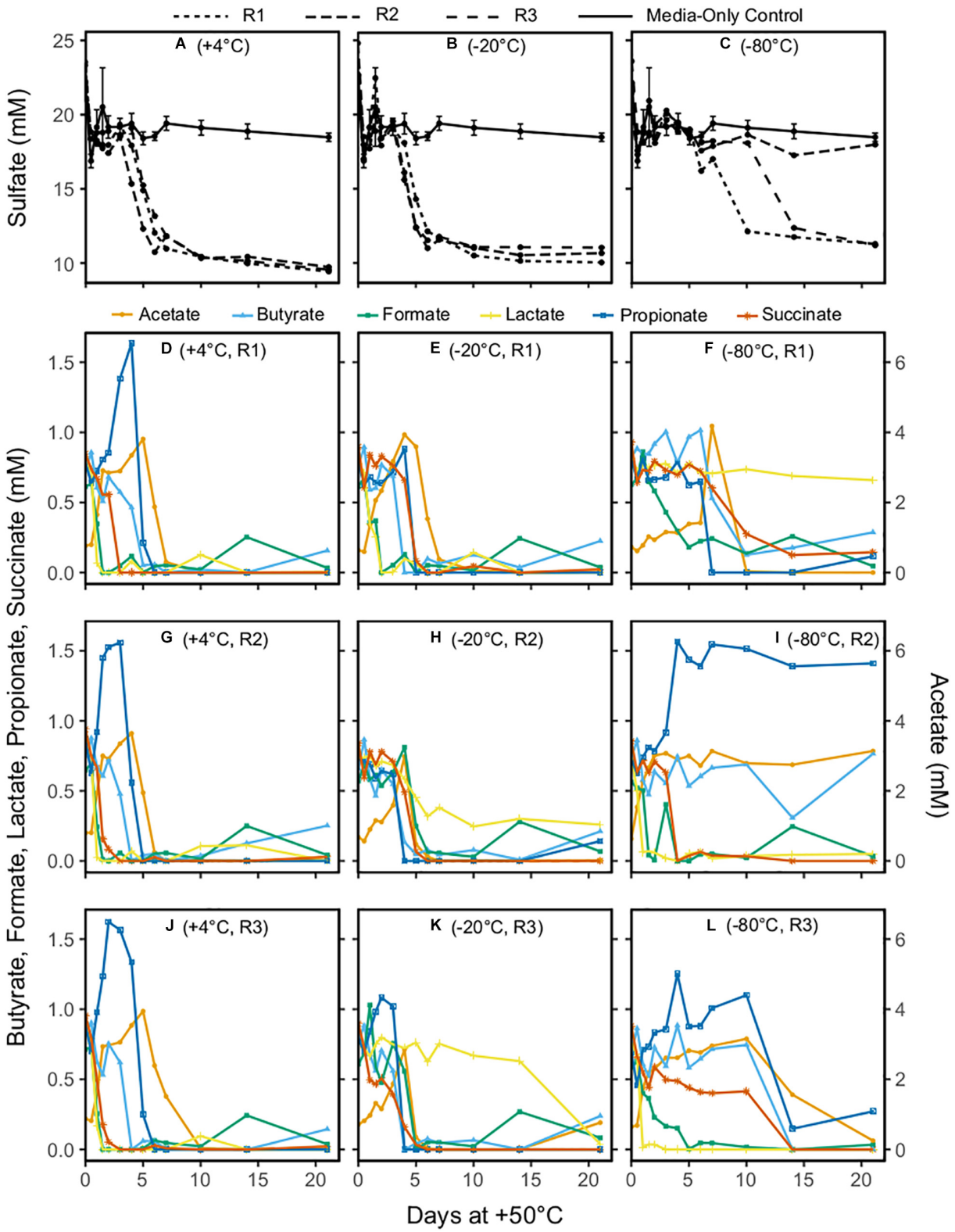

FIGURE 1 | Concentrations of sulfate **(A–C)** and the organic acids acetate, butyrate, formate, lactate, propionate, and succinate **(D–L)** in sediment microcosms incubated at +50°C for 21 days. Acetate is shown on the secondary *y*-axis owing to its higher concentrations. Replicates are identified as R1, R2, and R3. In panels **(A–C)**, line types denote the medium-only control (mean of triplicates) and the individual replicates for the –20 and –80°C pretreatments and the unfrozen control. In panels **(D–L)**, symbol shapes and colors indicate the six different organic acids measured.

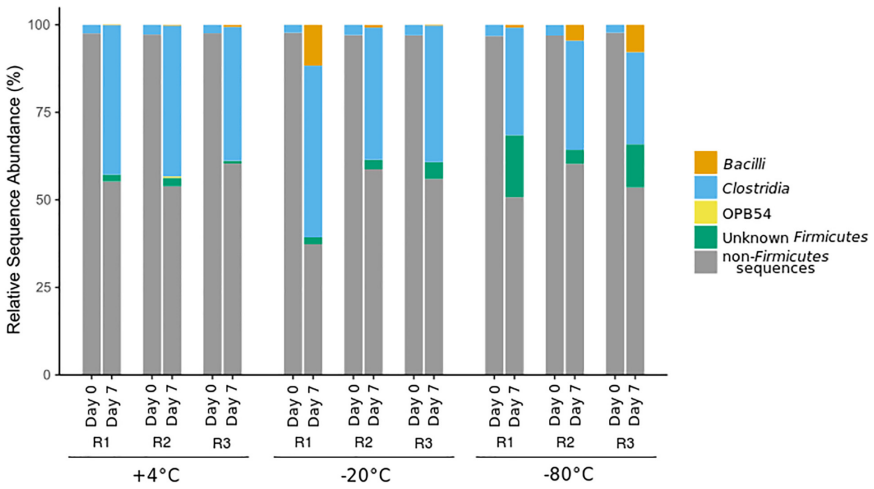

FIGURE 2 | Class-level community structure within the phylum *Firmicutes* based on 16S rRNA gene amplicon sequencing before (day 0) and after (day 7) incubation at +50°C. Sequences affiliated with other phyla (not *Firmicutes*) are represented in gray. Replicates are identified as R1, R2, and R3.

increased by up to fourfold during the first 6 days of incubation, and then decreased to 0 mM between 6 and 10 days.

Organic acid profiles for the −20°C pretreatment showed more variability (**Figures 1E,H,K**) than the +4°C unfrozen controls. One replicate was similar to +4°C unfrozen control microcosms (**Figure 1E**) with the exception of succinate conversion to propionate (this feature was apparently less pronounced from all −20°C pretreated microcosms). The other two replicates had similar patterns to each other, with formate and lactate consumption delayed (observed after 3 days) relative to +4°C unfrozen controls. Organic acid profiles for −80°C pretreated microcosms showed the most variability between triplicates (**Figures 1F,I,L**), though a rapid change in organic acid concentration at +50°C was detected in some instances. Formate was consumed rapidly in one replicate (**Figure 1I**) and slowly in the other two (**Figures 1F,L**), whereas lactate was consumed rapidly in two replicates (**Figures 1I,L**) and was not removed at all in one replicate (**Figure 1F**). A threefold to fourfold increase in acetate during the first few days of incubation was observed in all three −80°C pretreated replicates. Patterns of subsequent acetate consumption in the −80°C pretreated microcosms differed from the −20°C pretreated microcosms and +4°C unfrozen controls, with either rapid, slow or no depletion (**Figures 1F,I,L**, respectively). In general, in all replicates following the −80°C pretreatment, changes in organic acid concentration could be observed at times when sulfate concentration was unchanging, suggesting that thermophilic sulfate reducers as well as non-sulfate-reducing thermophiles survived the freezing pretreatment and became active during +50°C incubations.

Microbial Community Structure and Phylogeny of Thermospore OTUs

An increase in the relative sequence abundance of *Firmicutes*, the phylum containing all known endospore-forming bacteria, was observed after all +50°C incubations, regardless of freezing pretreatment. *Clostridia*, the class containing all known sulfate-reducing thermospores, showed the largest increase in relative sequence abundance after +50°C incubation in all microcosms (**Figure 2**). Increases in the relative sequence abundance of the class *Bacilli,* and of *Firmicutes* that were unclassified at the class level, varied between replicates (R1, R2, and R3), and were most pronounced in microcosms that experienced a freezing pretreatment. *Bacilli* were 8−12% of the sequence reads in −20°C and −80°C pretreated microcosms, and <1% in +4°C pretreated unfrozen controls. In two out of three of the −80°C pretreated microcosms, the relative sequence abundance of *Firmicutes* of unknown class was >10%, whereas this category was <5% of the sequence reads in the −20°C pretreatment group, and <3% in the +4°C pretreated controls.

Alpha and beta diversity of the bacterial communities were calculated at the OTU level (clustered at 97% sequence identity) and are shown in **Table 1** and **Figure 3**, respectively. Alpha diversity based on richness (OTU count and Chao1 Index), and evenness (Inverse Simpson Index), decreased after +50°C incubation without any notable differences in these indices between freezing pretreatments (**Table 1**). NMDS illustrates that the beta diversity in microcosms is significantly more variable after 7 days of incubation at +50°C compared to before the +50°C incubation (**Figure 3**). ANOSIM comparing the similarity between the three pretreatment groups after 7 days of incubation shows that variation in beta diversity between the groups is significant ($p < 0.011$) although the effect is relatively small (R statistic is 0.4239).

Twenty-two thermospore OTUs were identified from 16S rRNA gene libraries of +50°C incubations with different pretreatments. Between 8 and 16 thermospore OTUs were identified in each of the microcosms, and on average between 10 and 13 thermospore OTUs were identified within each pretreatment group (**Table 2**). Numbers of thermospores were not significantly different following different pretreatments based

TABLE 1 | Alpha diversity indices.

		Alpha Diversity Index					
		Inverse Simpson		Richness		Chao1	
Pretreatment	Days of incubation	Average	SD	Average	SD	Average	SD
+4°C	0	49.2	2.7	861.4	20.4	551.8	30.9
	7	24.6	3.7	655.8	29.1	427.0	36.4
−20°C	0	43.1	7.7	821.0	33.6	519.1	14.7
	7	16.4	1.6	579.6	115.5	350.1	75.3
−80°C	0	43.1	4.1	820.3	58.7	530.0	47.2
	7	20.4	7.6	568.9	70.8	385.7	37.0

Values are based on the average of triplicates. Standard deviation (SD) is listed in the column to the right of the averages.

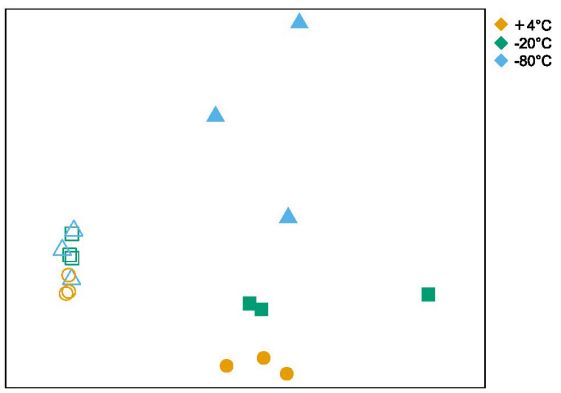

FIGURE 3 | Non-metric multidimensional scaling of bacterial community similarity based on 16S rRNA gene amplicon sequencing, for samples before and after incubation at +50°C that received +4°C, –20 or –80°C freezing pretreatments. Open symbols correspond to microbial communities after pretreatment but before +50°C incubation, and closed symbols correspond to communities after 7 days of incubation at +50°C. The stress is 0.076 after 20 iterations. ANOSIM comparing the communities belonging to different pretreatment groups (after-incubation) resulted in an R statistic of 0.42 and a *p*-value of 0.011 after 999 permutations.

on a Kruskal-Wallis test. These OTUs accounted for 36.1–61.1% of the sequence reads for each of the microcosms after 7 days, consistent with germination subsequent and growth at +50°C by thermophiles that survived the freezing pretreatments as endospores. Of the 22 thermospore OTUs, 18 were affiliated with the class *Clostridia,* three with the class *Bacilli,* and one could not be assigned at the Class level (**Table 3**). The majority of identified thermospores (19 of 22) belong to spore-forming orders of *Bacilliales* within the class *Bacilli* and to spore-forming orders of *Clostridiales* within the class *Clostridia* (**Table 3**). A comparison of the thermospore OTUs detected following the freezing pretreatments is shown in **Figure 4**, revealing that 12 of the 22 thermospore OTUs were found in at least one replicate of all the pretreatment temperatures. One thermospore OTU was identified only in the +4°C unfrozen control and not in any of the −20°C or −80°C pretreated microcosms. Interestingly, six thermospore OTUs were identified only in microcosms that had been frozen (−20°C or −80°C) prior to +50°C incubation, with two of these identified only in the −80°C pretreatment group.

Four of the 22 thermospore OTUs identified were affiliated with the genus *Desulfotomaculum*, a clade known to contain thermophilic sulfate-reducing endospore-formers. *Desulfotomaculum* thermospore OTUs were identified in all nine microcosms after 7 days of +50°C incubation. **Figure 5** shows that increased relative sequence abundance of *Desulfotomaculum* thermospores corresponds with decreases in sulfate concentration at +50°C. The sulfate concentration in two of the replicates that were pretreated at −80°C drops only minimally after 10 days at +50°C (**Figure 1C**) compared to the other microcosms; these replicate bottles (R2, R3) have much lower levels of *Desulfotomaculum* thermospores in the corresponding amplicon libraries (**Figure 5**). Specifically, Thermospore 2, most closely related to *Desulfotomaculum thermosapovorans*, is identified in all microcosms that experience a rapid drop in sulfate concentration before 10 days, but not in these two microcosms. This OTU had on average the highest relative sequence abundance in the other seven microcosms

TABLE 2 | Number of thermospore OTUs and total thermospore OTU relative sequence abundance detected after pretreatment at +4°C, −20°C, and −80°C and incubation for 7 days at +50°C.

	+4°C			−20°C			−80°C		
	R1	R2	R3	R1	R2	R3	R1	R2	R3
Number of thermospore OTUs	15	11	14	16	9	10	8	12	11
Total thermospore relative abundance (%)	42.6	43.0	37.4	61.1	39.4	42.4	47.4	36.1	44.2

Replicates are identified as R1, R2, and R3.

TABLE 3 | Individual thermospore OTU relative sequence abundance detected after pretreatment at +4°C, −20°C, and −80°C and incubation for 7 days at +50°C.

		Relative abundance of thermospore OTU (%)								
		+4°C			−20°C			−80°C		
Thermospore #	**Family**	**R1**	**R2**	**R3**	**R1**	**R2**	**R3**	**R1**	**R2**	**R3**
Order *Bacillales* of Class *Bacilli*										
6	*Bacillaceae*				11.0				3.6	
13	Unknown	0.1		0.5	0.6	0.7	0.2	0.6	0.8	4.5
17	*Bacillaceae*									3.2
Order *Clostridiales* of Class *Clostridia*										
2	*Peptococcaceae*	11.6	12.4	12.5	12.7	20.4	21.9	8.7		
3	*Clostridiaceae*	4.2	7.4	1.2	3.7	5.5	5.4	9.1	4.9	10.8
4	*Clostridiaceae*	4.0	3.6		13.3					0.5
5	*Clostridiales Incertae Sedis*	12.1	11.1	6.7	6.1		1.2			
7	Unknown	2.6	2.3	4.2	1.7					
8	*Peptococcaceae*	0.7			2.7				8.3	
10	Cluster XI	0.3	0.5	1.1	2.7	2.8	1.6	1.9	5.1	4.5
11	Unknown	1.5		0.6					2.2	5.2
14	*Peptococcaceae*	0.2		0.4	0.5	1.5			0.3	
15	*Clostridiaceae*	0.2	0.6	0.3	0.1	0.8	0.5	0.6	0.3	0.5
16	*Clostridiaceae*						2.5			
18	*Defluviitaleaceae*	1.2	0.4	0.7	1.2	1.9	0.9	1.1	1.3	1.4
19	*Clostridiaceae*	1.9	2.2	4.9	0.2	3.1	3.4		0.5	1.3
20	*Peptostreptococcaceae*								4.7	
21	*Clostridiaceae*	0.1	0.5	0.7	1.2					0.1
22	*Clostridiaceae*			3.0						
Unknown Order of Class *Clostridia*										
9	Unknown				1.5			7.7		
12	Unknown	2.0	2.2	0.8	1.9				4.0	
Order Unknown of Class Unknown of Phylum *Firmicutes*										
1	Unknown					2.7	4.8	17.7		12.2

Taxonomy of the thermospore OTUs are assigned at the family level. OTUs with bootstrap values <80% at the class, order, or family level are labeled as Unknown. Replicates are identified as R1, R2, and R3.

(14%) pointing to this organism as being a key driver of sulfate reduction in these experiments (**Table 2**).

The thermospores identified in this study are closely related to cultured bacteria and environmental sequences from similar biogeographical studies (i.e., sediment heating experiments) as well as from warm environments inhabited by thermophiles. Of the 22 thermospores identified here, 16 are closely related to thermospores that have previously been detected in sediment heating experiments (**Figure 6**). Only four (thermospore OTUs 5, 7, 16, and 22) of the 22 OTUs were not identified in any of the −80°C pretreated microcosms, supporting the notion that many thermospores can be enriched from sediments frozen at temperatures as low as −80°C, potentially enabling biogeography studies using samples preserved in this way. Out of the 22 thermospores identified in this study, 16 were not identified in other thermospore studies using sediment from the same site (Hubert et al., 2009, 2010).

DISCUSSION

Previous studies have shown that thermospores from cold marine sediments germinate upon incubation at high temperature (Hubert et al., 2009, 2010; de Rezende et al., 2013; Müller et al., 2014; Volpi et al., 2017; Bell et al., 2018; Chakraborty et al., 2018; Hanson et al., 2019). In this study, as in previous studies, sulfate consumption at +50°C after pasteurization corresponded with an increase in the relative sequence abundance of putative sulfate-reducing bacteria. This is consistent with the survival, germination and growth of thermophilic *Desulfotomaculum* endospores. Sulfate reduction and organic acid consumption observed in the microcosms for both experimental pretreatments (−20°C, −80°C) and the +4°C unfrozen control point to thermophile activity at +50°C and the ability of different thermospores to remain viable after freezing at −20°C and −80°C. Nearly all of the thermospores identified in this study

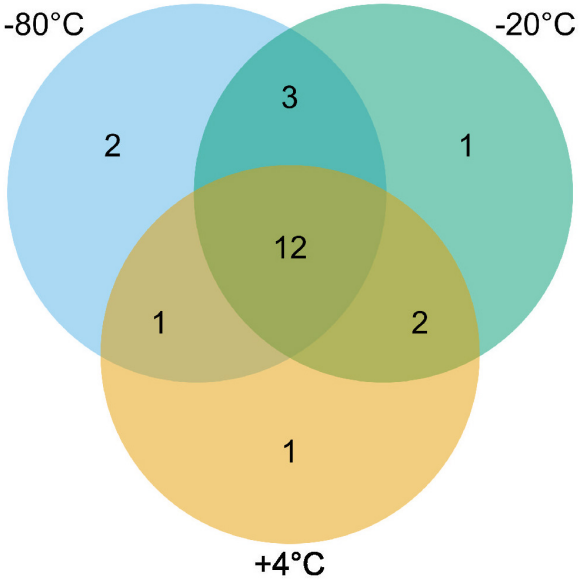

FIGURE 4 | Venn diagram showing the unique and shared thermospore OTUs detected after 7 days incubation at +50°C in microcosms in each pretreatment (–80°C, –20°C, and +4°C). In total, 22 thermospore OTUs were detected in this study, out of which 12 were detected in all experimental conditions.

(21 out of 22 OTUs) were detected following a 10-day freezing pretreatment, with the great majority (18 out of 22) observed to increase in relative abundance after being exposed to −80°C. This suggests that the viability of these thermospores is largely unaffected by freezing, and that the low temperature tolerance of thermospores extends to −80°C. These results are in alignment with previous reports suggesting no loss in endospore viability after −20°C storage (Freeman and Wilcox, 2003; Mah et al., 2009) and extend the lower temperature limit for maintaining viability to −80°C for many endospores of thermophilic bacteria. The discovery that many of the thermospores identified here, from different pretreatment groups, share phylogenetic similarity to thermospores that have been the focus of other thermospore germination studies, indicates that frozen storage of marine sediment should not preclude their use in studies of biogeography and dispersal that rely on sediment heating to germinate thermospores.

While bacterial activity was evident after freezing pretreatments (**Figure 1**), variability between triplicates was also common and may be driven by differences in the thermospore diversity and/or abundance of viable endospores within each individual microcosm bottle following different experimental pretreatments, or by purely stochastic effects. Differences in organic acid production and consumption were more pronounced within the −20°C and −80°C pretreatment microcosms, compared to the +4°C unfrozen controls, suggesting freezing and freezing temperature affect the number of viable thermospores. Non-uniform sulfate depletion among triplicates following the −80°C pretreatment, and the later onset of sulfate reduction in these incubations (compared to the −20°C and +4°C pretreatments) suggests that some sulfate reducers may be present in low abundance or have reduced viability following freezing at −80°C. For example, thermospore OTU 2 (related to *Desulfotomaculum thermosapovorans*) was consistently detected in microcosms pretreated at −20°C or +4°C prior to heating, but not in microcosms pretreated at −80°C, suggesting that fewer viable endospores were present after the −80°C exposure. On the other hand, other thermospores that were only detected after freezing, or only detected after −80°C freezing, albeit sporadically across triplicates

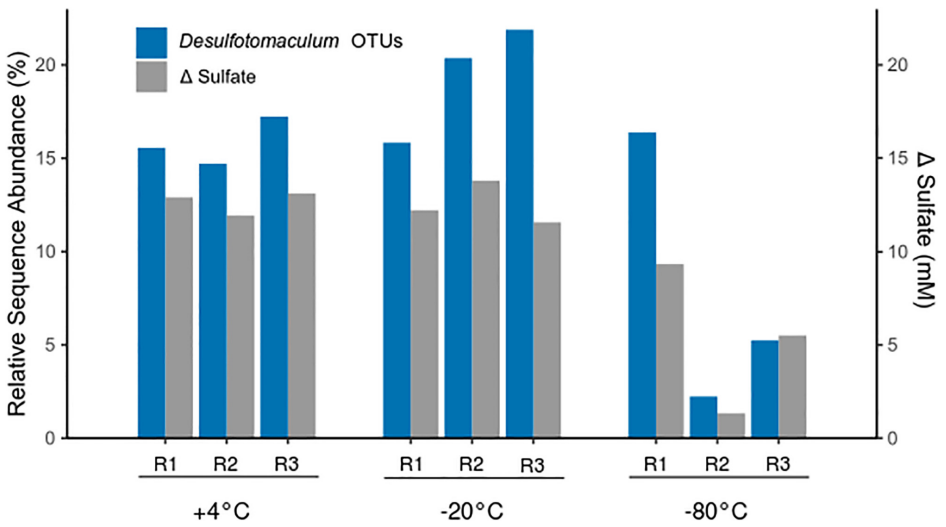

FIGURE 5 | Relative sequence abundance of thermospore OTUs within the genus *Desulfotomaculum* after 7 days of incubation at +50°C (left *Y*-axis), and the corresponding amount of sulfate consumed during the first 10 days of incubation (right *Y*-axis). Replicates are identified as R1, R2, and R3. The relative sequence abundance of *Desulfotomaculum* OTUs before high-temperature incubation (i.e., day 0) was on average <0.005% in all microcosms (not shown).

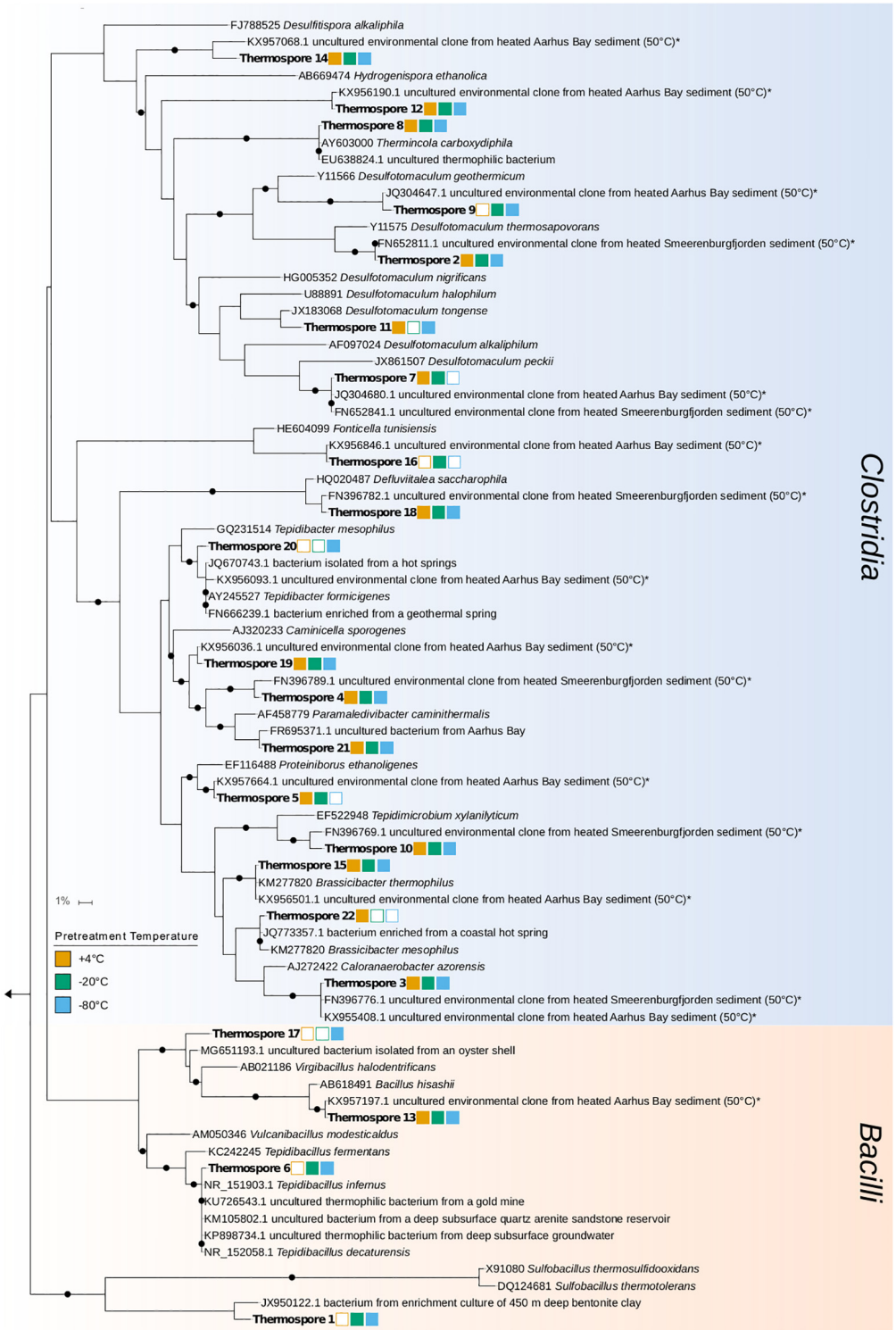

FIGURE 6 | Phylogenetic tree of annotated 16S rRNA gene sequences from 22 thermospore OTUs identified in this study (in bold) and their closest cultured and uncultured relatives (determined by BLASTn searching; Johnson et al., 2008). Percent identity for uncultured relatives is between 98 and 100%, and for cultured relatives is between 87 and 100%. Uncultured relatives identified in similar sediment heating experiments are indicated by an asterisk. Bootstrap values greater than 80% after 100 re-samplings are indicated by black circles at the nodes. Squares to the right of the thermospore OTUs indicate the pretreatments prior to the +50°C incubations in which that thermospore was identified (an empty square indicates that the OTU was not identified in any replicates in that pretreatment). The scale bar indicates 1% sequence divergence as inferred by PhyML.

(thermospore OTUs 1, 6, 9, 16, 17, and 20) may simply be robust freeze-tolerant endospores that are present *in situ* in low abundance.

This latter group of thermospores indicates that freezing pretreatment is able to reveal a different complement of thermospores from a given sediment sample and thereby uncover a greater diversity of these target organisms when multiple different pretreatments are employed before high-temperature enrichment. It is possible that some thermospores experience competitive exclusion when unfrozen sediment is incubated at +50°C (i.e., this study and previous studies), and that freezing pretreatment impairs other thermospores in the sediment sample (those less tolerant to freezing) allowing the otherwise-excluded thermospores to become enriched and therefore detectable in +50°C incubations following freezing. This ability to uncover a greater diversity of organisms engaged in potential long-distance and long-term passive dispersal is valuable for biogeography studies employing the thermospore study system. The results presented here also further confirm that samples can be frozen and still used in such investigations as was done by Chakraborty et al. (2018) in an investigation of thermospores in Gulf of Mexico sediments. Given the long-term survival potential of endospores, this feature is particularly useful in instances where study design depends on compilations of samples from various different archives to address specific biogeography questions (e.g., Müller et al., 2014).

The larger representation of *Bacilli* sequences in the microcosms that were frozen (−20°C and −80°C) before +50°C incubation have not been observed in previous studies of this sediment (Hubert et al., 2009, 2010). Presumably these *Bacilli* endospores are sufficiently abundant in the sediment and are thus present initially in all microcosms, but only become detectable in the +50°C-active thermospore community after freezing renders certain *Clostridia* non-viable or otherwise impairs their germination. This suggests that these *Bacilli* are better able to tolerate freezing compared to certain *Clostridia* thermospores (e.g., thermospore OTUs 5, 7, 12, and 21 were reproducibly detected only in the +4°C unfrozen control microcosms). Genes for the sporulation process are generally conserved among spore-forming *Firmicutes* (Galperin, 2013), yet there are differences between the complement of sporulation genes possessed by different endospore-formers that may explain differential freezing tolerance. Fairhead et al. (1994) observed that the absence of small acid-soluble proteins (SASPs) contributed to a decrease in endospore viability after freeze-drying suggesting that SASPs may play an important role in endospore tolerance to low temperature stress. SASPs bind to DNA within the spore core and are well known to offer protection against radiation and dry heat (Fairhead et al., 1993; Setlow, 2001, 2007; Paredes-Sabja et al., 2008). At the class level, *Bacilli* and *Clostridia* differ notably in their SASP complement; *Bacilli* generally contain between 11 and 22 different SASP genes, whereas *Clostridia* often contain only two (Galperin et al., 2012). Meaney et al. (2016) suggest that the protections conferred by different SASPs encoded by *Clostridium botulinum* are additive (i.e., in protecting DNA against chemical damage). It is possible that the greater number of SASP genes leads to increased tolerance to freezing in certain *Bacilli* and other thermospores, including those corresponding to thermospore OTUs that were detected in higher relative sequence abundance in microcosms that were frozen prior to +50°C incubation (**Table 3**). Further studies into the relationship between SASP genes and thermospore freezing tolerance may shed light on genomic determinants to freezing tolerance.

CONCLUSION

This is the first study exploring the freezing tolerance of bacterial endospore populations from the natural environment, and from geologic samples in particular. Furthermore, while some previous studies have explored the freezing tolerance of mesophilic endospores in pure culture (Weber and Greenberg, 1985; Fairhead et al., 1994; Jafari et al., 2016), this is the first study exploring the freezing tolerance of thermospores specifically, discovering a number of different bacteria that form spores that survive freezing conditions. Our results suggest that storage of thermospores at −20°C or −80°C does not preclude their use in biogeography investigations relying on high-temperature incubation experiments. Endospore freezing tolerance is relevant to their proposed usefulness as model organisms for studying microbial dispersal and broadens the scope of such investigations to consider capabilities of microorganisms for dispersal not only on Earth but between Earth and other planets in our solar system. For example, our results show that thermospores that survive dispersal from Earth to Mars should remain viable in soil on the surface of Mars, where the average temperature fluctuates between −10 and −76°C (Schofield et al., 1997; Horneck et al., 2012).

The lower temperature tolerance of thermophilic endospores for maintaining viability during dormancy, if one exists at all, remains unconstrained given that many thermospores were able to survive at −80°C. These may be good candidates for additional studies of tolerance to other extreme conditions. Thermospores presumably exhibit tolerances to radiation, extreme temperature, and pressure extremes similar to their mesophilic counterparts, and are projected to remain viable for much longer time scales (Nicholson, 2003). Thermospores may thus be uniquely prepared to withstand conditions required for panspermia and should be considered in studies exploring interplanetary dispersal.

AUTHOR CONTRIBUTIONS

BJ and CH planned and conducted the Arctic sampling expeditions. MC and CH designed the sediment freezing experiments with input from AC. MC conducted all experiments. MC and CL prepared the 16S rRNA gene amplicon libraries. MC performed the data analysis with support from SR and AC. MC and CH wrote the manuscript with input from AC, CL, SR, and BJ.

FUNDING

This research was supported by a Campus Alberta Innovates Program (CAIP) chair, research grants from the Canadian Marine Environmental Observation, Prediction and Response (MEOPAR) network, ArcticNet, Genome Canada, the Canada Foundation for Innovation (CFI-JELF, 33752), and the Max Planck Society. SR was supported by an AITF/Eyes High Postdoctoral Fellowship.

ACKNOWLEDGMENTS

We wish to thank Captain Stig Hennigsen, Carol Arnosti, Joanna Sawicka, Tom Gihring, Hans Røy, and the crew of the R/V *Farm* expeditions. We gratefully acknowledge the Alfred Wegener Institute for collaborative support and providing laboratory space at the Koldewey station in Ny Ålesund, Svalbard (RIS 3298; KOP 56). We also wish to thank Rhonda Clark for research support, and China Hanson for valuable scientific discussions.

REFERENCES

Barney, B. L., Pratt, S. N., and Austin, D. E. (2016). Survivability of bare, individual *Bacillus subtilis* spores to high-velocity surface impact: implications for microbial transfer through space. *Planet. Space Sci.* 125, 20–26. doi: 10.1016/j.pss.2016.02

Bartholomew, J. W., and Paik, G. (1966). Isolation and identification of obligate thermophilic sporeforming Bacilli from ocean basin cores. *J. Bacteriol.* 92, 635–638.

Bell, E., Blake, L. I., Sherry, A., Head, I. A., and Hubert, C. R. J. (2018). Distribution of thermophilic endospores in temperate estuary indicate that dispersal history structures sediment microbial communities. *Environ. Microbiol.* 20, 1134–1147. doi: 10.1111/1462-2920.14056

Chakraborty, A., Ellefson, E., Li, C., Gittens, D., Brooks, J. M., Bernard, B. B., et al. (2018). Thermophilic endospores associated with migrated thermogenic hydrocarbons in deep Gulf of Mexico marine sediments. *ISME J.* 12, 1895–1906. doi: 10.1038/s41396-018-0108-y

de Rezende, J. R., Hubert, C. R. J., Røy, H., Kjeldsen, K. U., and Jørgensen, B. B. (2017). Estimating the abundance of endospores of sulfate-reducing bacteria in environmental samples by inducing germination and exponential growth. *Geomicrobiol. J.* 34, 338–345. doi: 10.1080/01490451.2016.1190805

de Rezende, J. R., Kjeldsen, K. U., Hubert, C. R. J., Finster, K., Loy, A., and Jørgensen, B. B. (2013). Dispersal of thermophilic *Desulfotomaculum* endospores into Baltic Sea sediments over thousands of years. *ISME J.* 7, 72–84. doi: 10.1038/ismej.2012.83

Dong, X., Kleiner, M., Sharp, C. E., Thorson, E., Li, C., Liu, D., et al. (2017). Fast and simple analysis of MiSeq amplicon sequencing data with MetaAmp. *Front. Microbiol.* 8:1461. doi: 10.3389/fmicb.2017.01461

Fairhead, H., Setlow, B., and Setlow, P. (1993). Prevention of DNA damage in spores and in-vitro by small, acid-soluble proteins from *Bacillus* species. *J. Bacteriol.* 175, 1367–1374.

Fairhead, H., Setlow, B., Waites, W. M., and Setlow, P. (1994). Small, acid-soluble proteins bound to DNA protect *Bacillus subtilis* spores from being killed by freeze-drying. *Appl. Environ. Microbiol.* 60, 2647–2649.

Fajardo-Cavazos, P., Link, L., Melosh, H. J., and Nicholson, W. L. (2005). *Bacillus subtilis* spores on artificial meteorites survive hypervelocity atmospheric entry: implications for lithopanspermia. *Astrobiology* 5, 726–736. doi: 10.1089/ast.2005.5.726

Fajardo-Cavazos, P., Schuerger, A. C., and Nicholson, W. L. (2007). Testing interplanetary transfer of bacteria between Earth and Mars as a result of natural impact phenomena and human spaceflight activities. *Acta Astronaut.* 60, 534–540. doi: 10.1016/j.actaastro.2006.09.018

Fields, M. L., and Chen Lee, P. P. (1974). *Bacillus stearothermophilus* in soils of Iceland. *Appl. Microbiol.* 28, 638–640.

Freeman, J., and Wilcox, M. H. (2003). The effects of storage conditions on viability of *Clostridium difficile* vegetative cells and spores and toxin activity in human faeces. *J. Clin. Pathol.* 56, 126–128. doi: 10.1136/jcp.56.2.126

Galperin, M. (2013). Genome diversity of spore-forming *Firmicutes*. *Microbiol. Spectrum* 1:TBS-0015-2012. doi: 10.1128/microbiolspectrum.TBS-0015-2012

Galperin, M. Y., Mekhedov, S. L., Puigbo, P., Smirnov, S., Wolf, Y. I., and Rigden, D. J. (2012). Genomic determinants of sporulation in *Bacilli* and *Clostridia*: towards the minimal set of sporulation-specific genes. *Environ. Microbial.* 14, 2870–2890. doi: 10.1111/j.1462-2920.2012.02841.x

Hanson, C., Müller, A. L., Loy, A., Dona, C., Appel, R., Jørgensen, B. B., et al. (2019). Historical factors associated with past environments influence the biogeography of thermophilic endospores in arctic marine sediments. *Front. Microbiol.* 10:245. doi: 10.3389/fmicb.2019.00245

Horneck, G. (1993). Responses of *Bacillus subtilis* spores to space environment: results from experiments in space. *Orig. Life Evol. Biosph.* 23, 37–52. doi: 10.1007/BF01581989

Horneck, G., Moeller, R., Cadet, J., Douki, T., Mancinelli, R. L., Nicholson, W., et al. (2012). Resistance of bacterial endospores to outer space for planetary protection purposes – experiment PROTECT of the EXPOSE-E mission. *Astrobiology* 12, 445–456. doi: 10.1089/ast.2011.0737

Horneck, G., Stöffler, D., Ott, S., Hornemann, U., Cockell, C. S., Moeller, R., et al. (2008). Microbial rock inhabitants survive hypervelocity impacts on Mars-like host planets: first phase of lithopanspermia experimentally tested. *Astrobiology* 8, 17–44. doi: 10.1089/ast.2007.0134

Hubert, C., Arnosti, C., Brüchert, V., Loy, A., Vandieken, V., and Jørgensen, B. B. (2010). Thermophilic anaerobes in Arctic marine sediments induced to mineralize complex organic matter at high temperature. *Environ. Microbiol.* 12, 1089–1104. doi: 10.1111/j.1462-2920.2010.02161.x

Hubert, C., Loy, A., Nickel, M., Arnosti, C., Baranyi, C., Brüchert, V., et al. (2009). A constant flux of diverse thermophilic bacteria into the cold Arctic seabed. *Science* 325, 1541–1544. doi: 10.1126/science.1174012

Isaksen, M. F., Bak, F., and Jørgensen, B. B. (1994). Thermophilic sulfate-reducing bacteria in cold marine sediment. *FEMS Microbiol. Ecol.* 14, 1–8.

Jafari, M., Alebouyeh, M., Mortazavian, A. M., Hosseini, H., Ghanati, K., Amiri, Z., et al. (2016). Influence of heat shock temperatures and fast freezing on viability of probiotic sporeformers and the issue of spore plate count versus true numbers. *Nutr. Food Sci. Res.* 3, 35–42. doi: 10.18869/acadpub.nfsr.3.1.35

Johnson, M., Zaretskaya, I., Raytselis, Y., Merezhuk, Y., McGinnis, S., and Madden, T. L. (2008). NCBI BLAST: a better web interface. *Nucleic Acids Res.* 36, W5–W9. doi: 10.1093/nar/gkn201

Khodadad, C. L., Wong, G. M., James, L. M., Thakrar, P. J., Lane, M. A., Catechis, J. A., et al. (2017). Stratosphere conditions inactivate bacterial endospores from a mars spacecraft assembly facility. *Astrobiology* 17, 337–350. doi: 10.1089/ast.2016.1549

Klindworth, A., Pruesse, E., Schweer, T., Peplies, J., Quast, C., Horn, M., et al. (2013). Evaluation ofgeneral 16S ribosomal RNA gene PCR primers for classical and next-generation sequencing-based diversity studies. *Nucleic Acids Res.* 41:e1. doi: 10.1093/nar/gks808

Letunic, I., and Bork, P. (2006). Interactive Tree Of Life (iTOL): an online tool for phylogenetic tree display and annotation. *Bioinformatics* 23, 127–128. doi: 10.1093/bioinformatics/btl529

Ludwig, W., Strunk, O., Westram, R., Richter, L., Meier, H., Yadhukumar, et al. (2004). ARB: a software environment for sequence data. *Nucleic Acids Res.* 32, 1363–1371. doi: 10.1093/nar/gkh293

Maechler, M., Rousseeuw, P., Struyf, A., Hubert, M., and Hornik, K. (2018). *Cluster: Cluster Analysis Basics and Extensions. R Package Version 2.0.7-1.* .

Mah, J.-H., Kang, D.-H., and Tang, J. (2009). Comparison of viability and heat resistance of *Clostridium sporogenes* stored at different temperatures. *J. Food Sci.* 74, M23–M27. doi: 10.1111/j.1750-3841.2008.00984.x

Marchant, R., Banat, I. M., Rahman, T. J., and Berzano, M. (2002). The frequency and characteristics of highly thermophilic bacteria in cool soil environments. *Environ. Microbiol.* 4, 595–602. doi: 10.1046/j.1462-2920.2002.00344.x

Marchant, R., Franzetti, A., Pavlostathis, S. G., Tas, D. O., Erdbrûgger, I., Ûnyayar, A., et al. (2008). Thermophilic bacteria in cool temperate soils: are they metabolically active or continually added by global atmospheric

transport? *Appl. Microbiol. Biotechnol.* 78, 841–852. doi: 10.1007/s00253-008-1372-y

Mastrapa, R. M. E., Glanzberg, H., Head, J. N., Melosh, H. J., and Nicholson, W. L. (2001). Survival of bacteria exposed to extreme acceleration: implications for panspermia. *Earth Planet Sci. Lett.* 189, 1–8.

Mazur, P., and Schmidt, J. (1968). Interactions of cooling velocity, temperature, and warming velocity on the survival of frozen and thawed yeast. *Cryobiol* 5, 1–17. doi: 10.1016/S0011-2240(68)80138-5

Meaney, C. A., Cartman, S. T., McClure, P. J., and Minton, N. P. (2016). The role of small acid-soluble proteins (SASPs) in protection of spores of *Clostridium botulinum* against nitrous acid. *Int. J. Food Micrbiol.* 216, 25–30. doi: 10.1016/j.ijfoodmicro.2015.08.024

Melly, E., Genest, P. C., Gilmore, M. E., Little, S., Popham, D. L., Dirks, A., et al. (2002). Analysis of the properties of spores of *Bacillus subtilis* prepared at different temperatures. *J. Appl. Microbiol.* 92, 1105–1115. doi: 10.1046/j.1365-2672.2002.01644.x

Moeller, R., Reitz, G., Nicholson, W. L., the Protect Team, and Horneck, G. (2012). Mutagenesis in bacterial spores exposed to space and simulated martian conditions: data from the EXPOSE-E spaceflight experiment PROTECT. *Astrobiology* 12, 457–468. doi: 10.1089/ast.2011.0739

Müller, A. L., de Rezende, J. R., Hubert, C. R. J., Kjeldsen, K. U., Lagkouvardos, I., Berry, D., et al. (2014). Endospores of thermophilic bacteria as tracers of microbial dispersal by ocean currents. *ISME J.* 8, 1153–1165. doi: 10.1038/ismej.2013.225

Nicholson, W. L. (2003). Using thermal inactivation kinetics to calculate the probability of extreme spore longevity: implications for paleomicrobiology and lithopanspermia. *Orig. Life Evol. Biosph.* 33, 621–631. doi: 10.1023/A:1025789032195

Nicholson, W. L. (2009). Ancient micronauts: interplanetary transport of microbes by cosmic impacts. *Trends Microbiol.* 17, 243–250. doi: 10.1016/j.tim.2009.03.004

Nicholson, W. L., Munakata, N., Horneck, G., Melosh, H. J., and Setlow, P. (2000). Resistance of *Bacillus* endospores to extreme terrestrial and extraterrestrial environments. *Microbiol. Mol. Biol. Rev.* 64, 548–572. doi: 10.1128/MMBR.64.3.548-572.2000

Nicholson, W. L., Schuerger, A. C., and Setlow, P. (2005). The solar UV environment and bacterial spore UV resistance: considerations for earth-to-mars transport by natural processes and human spaceflight. *Mutat. Res.* 571, 249–264. doi: 10.1016/j.mrfmmm.2004.10.012

Oksanen, J., Blanchet, F., Kindt, R., Legendre, P., Minchin, P., O'Hara, R., et al. (2016). *Vegan: Community Ecology Package. R Package Version 2.3-4.*

O'Sullivan, L. A., Roussel, E. G., Weightman, A. J., Webster, G., Hubert, C. R., Bell, E., et al. (2015). Survival of *Desulfotomaculum* spores from estuarine sediments after serial autoclaving and high-temperature exposure. *ISME J.* 9, 922–933. doi: 10.1038/ismej.2014.190

Panitz, C., Horneck, G., Rabbow, E., Rettberg, P., Moeller, R., Cadet, J., et al. (2015). The SPORES experiment of the EXPOSE-R mission: *Bacillus subtilis* spores in artificial meteorites. *Int. J. Astrobiol.* 14, 105–114. doi: 10.1017/S1473550414000251

Paredes-Sabja, D., Raju, D., Torres, J. A., and Sarker, M. R. (2008). Role of small, acid-soluble spore proteins in the resistance of *Clostridium perfringens* spores to chemicals. *Int. J. Food Microbiol.* 122, 333–335. doi: 10.1016/j.ijfoodmicro.2007.12.006

Parks, D. H., and Beiko, R. G. (2010). Identifying biologically relevant difference between metagenomic communities. *Bioinformatics* 26, 715–721. doi: 10.1093/bioinformatics/btq041

Parks, D. H., Tyson, G. W., Hugenholtz, P., and Beiko, R. G. (2014). STAMP: statistical analysis of taxonomic and functional profiles. *Bioinformatics* 30, 3123–3124. doi: 10.1093/bioinformatics/btu494

Pruesse, E., Peplies, J., and Glöckner, F. O. (2012). SINA: Accurate high-throughput multiple sequence alignment of ribosomal RNA genes. *Bioinformatics* 28, 1823–1829. doi: 10.1093/bioinformatics

Quast, C., Pruesse, E., Yilmaz, P., Gerken, J., Schweer, T., Yarza, P., et al. (2013). The SILVA ribosomal RNA gene database project: improved data processing and web-based tools. *Nucleic Acids Res.* 41, 590–596. doi: 10.1093/nar/gks1219

R Core Team (2013). *R: A Language and Environment for Statistical Computing*. Vienna: R Foundation for Statistical Computing.

Rahman, T. J., Marchant, R., and Banat, I. M. (2004). Distribution and molecular investigation of highly thermophilic bacteria associated with cool soil environments. *Biochem. Soc. Trans.* 32, 209–213. doi: 10.1042/bst0320209

Riesenman, P. J., and Nicholson, W. L. (2000). Role of the spore coat layers in *Bacillus subtilis* spore resistance to hydrogen peroxide, artificial UV-C, UV-B, and solar UV radiation. *Appl. Environ. Microbiol.* 66, 620–626. doi: 10.1128/AEM.66.2.620-626.2000

Ruff, S. E., Felden, J., Gruber-Vodicka, H. R., Marcon, Y., Knittel, K., Ramette, A., et al. (2019). In situ development of a methanotrophic microbiome in deep-sea sediments. *ISME J.* 13, 197–213. doi: 10.1038/s41396-018-0263-1

Schofield, J. T., Barnes, J. R., Crisp, D., Haberle, R. M., Larsen, S., Magalhães, J. A., et al. (1997). The mars pathfinder atmospheric structure investigation/meteorology (ASI/MET) experiment. *Science* 278, 1752–1758. doi: 10.1126/science.278.5344.1752

Schuerger, A. C., Mancinelli, R. L., Kern, R. G., Rothschild, L. J., and McKay, C. P. (2003). Survival of endospores of *Bacillus subtilis* on spacecraft surfaces under simulated martian environments: implications for the forward contamination of Mars. *Icarus* 165, 253–276. doi: 10.1016/S0019-1035(03)00200-8

Setlow, P. (2001). Resistance of spores of *Bacillus* species to ultraviolent light. *Environ. Mol. Mutagen.* 38, 97–104. doi: 10.1002/em.1058

Setlow, P. (2006). Spores of *Bacillus subtilis*: their resistance to and killing by radiation, heat and chemicals. *J. Appl. Microbiol.* 101, 514–525. doi: 10.1111/j.1365-2672.2005.02736.x

Setlow, P. (2007). I will survive: DNA protection in bacterial spores. *Trends. Microbiol.* 15, 172–180. doi: 10.1016/j.tim.2007.02.004

Slobodkin, A., Gavriloc, S., Ionov, V., and Iliyin, V. (2015). Spore-forming thermophilic bacterium within artificial meteorite survives entry into the Earth's atmosphere on FOTON-M4 satellite landing module. *PLoS One* 10: e0132611.

Vaishampayan, P. A., Rabbow, E., Horneck, G., and Venkateswaran, J. J. (2012). Survival of *Bacillus pumilus* spores for a prolonged period of time in real space conditions. *Astrobiology* 12, 487–497. doi: 10.1089/ast.2011.0738

Volpi, M., Lomstein, B. A., Sichert, A., Røy, H., Jørgensen, B. B., and Kjeldsen, K. U. (2017). Identity, abundance, and reactivation kinetics of thermophilic fermentative endospores in cold marine sediment and seawater. *Front. Microbiol.* 8:131. doi: 10.3389/fmicb.2017.00131

Weber, P., and Greenberg, J. M. (1985). Can spores survive in interstellar space? *Nature* 316, 403–407. doi: 10.1038/316403a0

Zeigler, D. R. (2014). The Geobacillus paradox: why is a thermophilic bacterial genus so prevalent on a mesophilic planet? *Microbiology* 160, 1–11. doi: 10.1099/mic.0.071696-0

Conflict of Interest Statement: The authors declare that the research was conducted in the absence of any commercial or financial relationships that could be construed as a potential conflict of interest.

frontiers in Microbiology

ORIGINAL RESEARCH
published: 27 September 2019
doi: 10.3389/fmicb.2019.02224

Thermoanaerosceptrum fracticalcis gen. nov. sp. nov., a Novel Fumarate-Fermenting Microorganism From a Deep Fractured Carbonate Aquifer of the US Great Basin

Scott D. Hamilton-Brehm[1,2], Laura E. Stewart[3], Mavrik Zavarin[4], Matt Caldwell[5], Paul A. Lawson[5], Tullis C. Onstott[6], Joseph Grzymski[1], Iva Neveux[1], Barbara Sherwood Lollar[7], Charles E. Russell[8] and Duane P. Moser[1,8]**

[1] Division of Earth and Ecosystems Sciences, Desert Research Institute, Las Vegas, NV, United States, [2] Department of Microbiology, Southern Illinois University Carbondale, Carbondale, IL, United States, [3] Madison Area Technical College, Madison, WI, United States, [4] Lawrence Livermore National Laboratory, Livermore, CA, United States, [5] Department of Microbiology and Plant Biology, University of Oklahoma, Norman, OK, United States, [6] Department of Geosciences, Princeton University, Princeton, NJ, United States, [7] Department of Earth Sciences, University of Toronto, Toronto, ON, Canada, [8] Division of Hydrologic Sciences, Desert Research Institute, Las Vegas, NV, United States

OPEN ACCESS

Edited by:
Akihiko Yamagishi,
Tokyo University of Pharmacy and Life Sciences, Japan

Reviewed by:
Susan Childers,
Colby College, United States
Juliane Hopf,
University of Notre Dame, United States

***Correspondence:**
Scott D. Hamilton-Brehm
Scott.Hamilton-Brehm@siu.edu
Duane P. Moser
Duane.Moser@dri.edu

Specialty section:
This article was submitted to Microbiological Chemistry and Geomicrobiology, a section of the journal Frontiers in Microbiology

Received: 04 June 2019
Accepted: 11 September 2019
Published: 27 September 2019

Citation:
Hamilton-Brehm SD, Stewart LE, Zavarin M, Caldwell M, Lawson PA, Onstott TC, Grzymski J, Neveux I, Lollar BS, Russell CE and Moser DP (2019) Thermoanaerosceptrum fracticalcis gen. nov. sp. nov., a Novel Fumarate-Fermenting Microorganism From a Deep Fractured Carbonate Aquifer of the US Great Basin. Front. Microbiol. 10:2224. doi: 10.3389/fmicb.2019.02224

Deep fractured rock ecosystems across most of North America have not been studied extensively. However, the US Great Basin, in particular the Nevada National Security Site (NNSS, formerly the Nevada Test Site), has hosted a number of influential subsurface investigations over the years. This investigation focuses on resident microbiota recovered from a hydrogeologically confined aquifer in fractured Paleozoic carbonate rocks at 863 – 923 meters below land surface. Analysis of the microorganisms living in this oligotrophic environment provides a perspective into microbial metabolic strategies required to endure prolonged hydrogeological isolation deep underground. Here we present a microbiological and physicochemical characterization of a deep continental carbonate ecosystem and describe a bacterial genus isolated from the ecosystem. Strain DRI-13^T is a strictly anaerobic, moderately thermophilic, fumarate-respiring member of the phylum *Firmicutes*. This bacterium grows optimally at 55°C and pH 8.0, can tolerate a concentration of 100 mM NaCl, and appears to obligately metabolize fumarate to acetate and succinate. Culture-independent 16S rRNA gene sequencing indicates a global subsurface distribution, while the closest cultured relatives of DRI-13^T are *Pelotomaculum thermopropionicum* (90.0% similarity) and *Desulfotomaculum gibsoniae* (88.0% similarity). The predominant fatty acid profile is iso-$C_{15:0}$, $C_{15:0}$, $C_{16:0}$ and $C_{14:0}$. The percentage of the straight-chain fatty acid $C_{15:0}$ is a defining characteristic not present in the other closely related species. The genome is estimated to be 3,649,665 bp, composed of 87.3% coding regions with an overall average of 45.1% G + C content. Strain DRI-13^T represents a novel genus of subsurface bacterium isolated from a previously uncharacterized rock-hosted geothermal habitat.

The characterization of the bacterium combined with the sequenced genome provides insights into metabolism strategies of the deep subsurface biosphere. Based on our characterization analysis we propose the name *Thermoanaerosceptrum fracticalcis* (DRI-13^T = DSM 100382^T = ATCC TSD-12^T).

Keywords: 16S rRNA, subsurface, deep biosphere, *Firmicutes*, fractured carbonate, aquifer, borehole, Death Valley Regional Flow System

INTRODUCTION

Biomass in the continental crust may be greater than that on the surface of the Earth (Gold, 1992; Whitman et al., 1998; McMahon and Parnell, 2014; Magnabosco et al., 2018). The deep biosphere is an untapped reservoir of microbial biodiversity that may hold novel solutions to industrial, medical, and origin of life questions. While the concept of subsurface life was proposed in the 1920s (Bastin and Greer, 1930), research into deep terrestrial subsurface environments did not begin in earnest until the 1980s (Jorgensen, 2012). Exploration of subsurface microbial biogeochemical processes remain largely unmapped and uncharacterized, due partly to limited access to the terrestrial subsurface and the low biomass densities often found there. Primary sampling opportunities occur through caves, mines, springs, and boreholes. A high level of novel microbial diversity has been discovered in the subsurface through cultivation-independent sequencing of the 16S rRNA gene (Pedersen and Ekendahl, 1990; Kotelnikova and Pedersen, 1997; Takai et al., 2001; Chapelle et al., 2002; Moser et al., 2005; Lin et al., 2006; Osburn et al., 2014). However, only a modest fraction of known lineages are currently represented in culture collections (Daumas et al., 1988; Boone et al., 1995; Ravot et al., 1995; Nilsen et al., 1996; Puspita et al., 2012).

With some notable exceptions (Stevens and McKinley, 1995; Colwell et al., 1997; Fredrickson et al., 1997; Krumholz et al., 1997; Lehman et al., 2001; Osburn et al., 2014), the deep fractured rock ecosystems across most of North America have been relatively little studied for microbiology. However, the US Great Basin, in particular the Nevada National Security Site (NNSS, formerly the Nevada Test Site, Bowen et al., 2001), has hosted a number of influential subsurface investigations over the years (Amy et al., 1992; Haldeman and Amy, 1993; Haldeman et al., 1993; Kieft et al., 1997). Most of the NNSS lies entirely within a geologic extensional zone and is underlain by the "Death Valley Regional Flow System (DVRFS)." This expansive set of groundwater basins is dominated by fractured rock aquifers that comprises ∼100,000 km^2 of mountain ranges (up to 3,600 m above mean sea level) and valleys which can reach below sea level (e.g., Death Valley, at −86 m, the lowest point in North America) (D'Agnese et al., 1997; Belcher et al., 2002; Ye et al., 2008; Bushmann et al., 2010). Within this system groundwater flows long distances (i.e., Interbasin Flow), from high-elevation recharge zones in central Nevada to large-discharge springs in and near Death Valley, CA, United States (Winograd and Thordarson, 1975; Winograd and Pearson, 1976; Belcher et al., 2009). Direct access to the DVRFS is achievable through an ongoing Department of Energy (DOE) sponsored environmental management activity tasked with tracking groundwater contamination associated with underground nuclear testing at the NNSS, the Underground Test Area (UGTA) sub-project. The hundreds of monitoring boreholes/wells established and maintained by this program represent a unique regional-scale observatory for deep life study.

This study focuses on resident microbiota in fluids from 863–923 meters below land surface (mbls), accessed via a monitoring borehole, U-3cn#5 (Garber and Johnson, 1967; Bangerter and Giblin, 1998). Intercepting a hydrogeologically confined aquifer within the fractured Paleozoic carbonate rocks of a prominent regional feature termed the "Lower Carbonate Aquifer" (LCA), this well provides a portal into a pristine deep ecosystem that would otherwise be very difficult to access. Analysis of the microorganisms living in this restricted oligotrophic environment provides a perspective into microbial metabolic strategies required to endure prolonged hydrogeological isolation deep underground. The isolation of this unit is demonstrated by the very low radiocarbon content (4.65 pmc ^{14}C) and absence of contamination related to past nuclear testing in the overlying units. Here we present a microbiological and physicochemical characterization of one window into the NNSS portion of the DVRFS and describe the isolation of a representative bacterium from this ecosystem, DRI-13^T, a novel, moderately thermophilic, strict fumarate-respiring organism belonging to the phylum *Firmicutes* from the deep terrestrial biosphere, here designated *Thermoanaerosceptrum fracticalcis*.

MATERIALS AND METHODS

Field Site and Sample Collection

Well U-3cn#5 (Garber and Johnson, 1967; Bangerter and Giblin, 1998) is located in central Yucca Flat, Nevada, United States on the NNSS (latitude 37.06, longitude −116.02, surface elevation 1223 m). Yucca Flat is an arid, intermontane valley partially filled with tuffs and alluvium (260 – 290 m thickness), underlain by partially welded and zeolitized Tertiary-age ash-flow tuffs and bedded tuffs (∼536 m thickness). A highly fractured Paleozoic carbonate layer (colluvium transitioning to dolomite/dolomitic quartzite) of about 41 m thickness completes the sequence and is the source of groundwater for this study. The borehole was drilled in 1965 to a total depth of 923.5 mbls, 120 m southwest of surface ground zero and outside the collapse chimney of the Bilby underground nuclear test conducted in 1963 (249 kt, 63.7 m cavity radius) (Zavarin, 2014) (**Figures 1A,B**). The hole intersects the local groundwater table at 493.9 mbls and carbonate rocks at 863.2 mbls. Borehole gamma logs conducted within U-3cn#5 indicated the presence of elevated radionuclides within

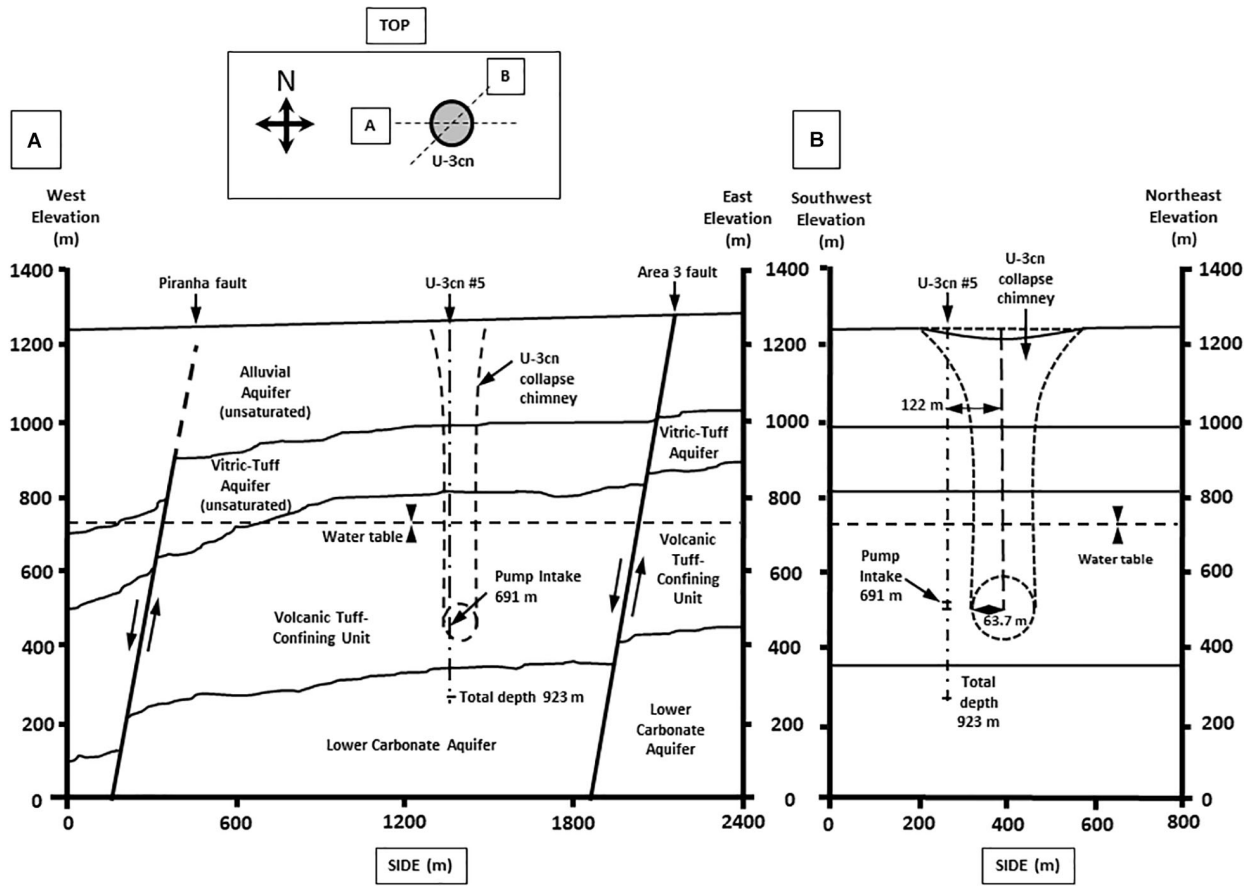

FIGURE 1 | Geological cross section of well U-3cn #5. Cross section from **(A)** West to East and **(B)** Southwest to Northeast. Cross sections show borehole U-3cn#5 pump position, Total depth (TD) at 923 m, and relative location below the water table. (Image modified from McCall, RL, Raytheon Services Nevada, 1994, DOE/NV/-500-UC-700) [DOE cleared].

the unsaturated zone tertiary volcanic rock. These radionuclides were thought to have been emplaced by prompt injection during the underground test. Radionuclides have not been detected in the water-saturated fractured carbonates intersected by U-3cn#5, indicating no impact by the nearby underground nuclear test (Thompson, 1999). This volcanic confining unit overlying the carbonate aquifer serves to hydrogeologically isolate a nearly anoxic, slightly geothermal (∼45°C) portion of the LCA. The well is continuously cased through the vadose zone and confining unit (stainless steel below the water table) and was recompleted in 1996/1997, when the permanent 50-horsepower tandem pump used for this study was installed at 691.3 mbls. During pumping, water is obtained from an isolated open hole segment (863.2–923.5 mbls) within the LCA below the casing terminus; most likely derived from distinct fractured zone in core logs at 863.5, 864.4, and 866.2 mbls or a highly fractured zone from 868.7 to 876.3 mbls (Bangerter and Giblin, 1998).

Prior to sampling, U-3cn#5 was pumped and sampled on a semi-regular basis since 1967 (Total of 3×10^6 m^3 of water), including March 29, 2011, the subject of this report. Water samples were obtained on the surface from an in-line sampling port affiliated with a hydrologic pump test (104.9 gpm) after removal of 440 m^3 of water over a period of days via an autoclaved gas-tight manifold. Water samples for microbial cultivation and dissolved gas sampling were transferred from flowing lines (LS-24 Nuprene Tubing, Masterflex) fitted with 24 Ga needles into sterile crimp-sealed, pre-evacuated, N_2 flushed, 120 mL serum bottles (gas samples fixed with 5 μL of saturated $HgCl_2$). Samples for aqueous chemistry were collected from the flowing sample lines and analyzed offsite. Samples for microbial community analysis were collected in two sterile 8 L polypropylene carboys and cells collected offsite on 0.2 μm filters (Sterivex, EMD Millipore, Bedford MA, 2 L per filter).

Physical and Geochemical Analysis

Field measurements of temperature, dissolved O_2 (dO_2), conductivity, and pH were made onsite with an MP20 Sonde fitted with a flow cell (Yellow Springs Instruments, Yellow Springs, OH). Most chemical analytes were obtained during routine analysis by the DOE Underground Test Area (UGTA) Program. Additional analyses were performed at the Desert Research Institute (DRI) Water Analysis Laboratory (Reno, NV, United States) or at Princeton University (Princeton, NJ,

United States). Nitrite, nitrate, and ammonia were analyzed at DRI using Alpkem RFA 300 and Technicon Automated Colorimetric Analyzers using EPA method SM 4500-NO_3 F and SM 4500-NH_4 F. Dionex Model ICS 2000 Ion Chromatograph was used for the measurement of Cl^-, Br^-, and SO_4^{2-}. A Brinkmann Metrohm Titrando automated titrator, capable of potentiometric titrations to fix inflection end points, was used in the determination of CO_3^{2-}, HCO_3^-, pH, EC, and F^-. An OI Analytical 1030W Carbon Analyzer was used for determination of dissolved organic carbon (DOC) and total organic carbon (TOC) in water samples. A Thermo Elemental SOLAAR M5 Atomic Absorption Spectrometer with air-acetylene flame and vapor generation capabilities was used for major cation and many metal analyses.

A subset of samples were analyzed in duplicate for anions (F^-, Cl^-, NO^{2-}, SO_4^{2-}, Br^-, NO_3^-, PO_4^{3-}) and for short chain fatty acids (acetate, lactate, formate, and propionate) at Princeton University using a Dionex IC25 ion chromatograph (Thermo Scientific, Waltham, MA, United States) coupled to an MSQ Plus™ ESI-quadrupole mass spectrometer (Thermo Scientific, Waltham, MA, United States) (Lau et al., 2014).

Total and Live/Dead cell counts were determined for groundwater samples using mfgr-provided reagents and protocols with a MicroPro Flow Cytometer (Benton Dickenson).

Environmental DNA and Clone Libraries

Planktonic microorganisms, concentrated by filtration, were extracted using the UltraClean™ Soil DNA Isolation kit (Mo Bio Laboratories Inc., Carlsbad, CA, United States), according to manufacturer's protocol amended with three freeze/thaw cycles (−80°C/65°C; 20 min each) at the beginning of DNA extraction procedure. Given the proximity of the site to prior nuclear testing, filters were screened for radioactivity by scintillation at the Harry Reid Center for Environmental Studies at the University of Nevada, Las Vegas as a precaution (all were below detection limits). The extracted DNA was used for PCR-amplified clone libraries, universal bacterial primers 27F-YM/1492R (AGAGTTTGATYMTGGCTCAG/TACCTTGTTACGACTT) and universal archaeal primers were used 21F/1492R (TTCCGGTTGATCCYGCCGGA/TACCTTGTTACGACTT) to generate near-full-length 16S rRNA gene amplicons (Lane, 1991). PCR was performed using LATaq (Clontech, Mountain View, CA, United States) and thermocycler settings of 95°C, 30 s; 53°C, 30 s; 72°C, 60 s; for 30 cycles. PCR amplicons were purified with an UltraClean GelSpin DNA Purification Kit (Mo Bio Laboratories Inc., Carlsbad, CA, United States), cloned (TOPO-TA, Invitrogen, Carlsbad, CA, United States) and contigs were completely sequenced for bacteria and partially sequenced for archaea by Functional BioSciences (Madison, WI, United States) using vector primers. Contigs were generated using Sequencher™ 4.9 (Gene Codes, Ann Arbor, MI, United States), aligned, matched with nearest neighbors and checked for chimeras using Silva (v1.2.11) (Glöckner et al., 2017) and MEGA 5.2 (Tamura et al., 2011).

Enrichment Cultivation and Isolation

Microbial cultivation enrichments were performed in 160 mL serum bottles with 25 mL of a custom artificial groundwater medium (AGM), composed of per liter 3.6 g 2-[4-(2-hydroxyethyl)piperazin-1-yl]ethanesulfonic acid (HEPES), 1.5 g Na_2SO_4, 0.174 g K_2PO_4, 0.138 g Resazurin, 0.4 g $MgCl_2$6 H_2O, 0.5 g KCl, 0.268 g NH_4Cl, 0.25 g $NaHCO_3$, 1 mL ATCC Minimal Vitamins (ATCC, Manassas, VA, United States), and 1 mL ATCC Minimal Minerals. AGM was prepared anaerobically using a modified Hungate technique with 600 mg/L $Na_2S \cdot 9H_20$ as a reducing agent (Miller and Wolin, 1974). The water sample was maintained at 4°C for 2 years prior to attempting enrichments. The primary enrichment consisted of 1 mL inoculum from the environmental sample, incubated in AGM amended with 0.1% (w/v) peptone (BD Bacto, Franklin Lakes, NJ, United States) at 45°C with a headspace of 100% N_2. Cell numbers were monitored using a Petroff-Hausser counter (Hausser Scientific Co., Horsham, PA, United States) and an Axioskop2 Plus microscope under phase contrast. Cells reached a density of 10^6 cells/mL after 1 month and were subsequently transferred three times prior to final isolation by low-intensity heat shock, serial dilution, and streak plating. Heat shocks were performed first on the environmental enrichment by rapidly raising the incubation temperature during logarithmic growth from 45°C to 60°C for 1 h and then rapidly cooling to 45°C. This was repeated for three transfers, the resulting cultures were then serial diluted to sub single cell concentrations. Finally, the putative isolate was streaked on anaerobic 1% w/v agar plates (AGM with agar added) amended with 10 mM fumarate/0.05% (w/v) yeast extract and one of the apparently identical colonies was selected as the type strain.

Cell Growth Assays

Growth experiments were conducted in 160-mL serum bottles, containing 25 mL volume of AGM and 10 mM fumarate with a headspace of 100% N_2. Cultivation experiments to define temperature optima were incubated at 37, 45, 50, 55, 60, and 65°C in the dark without shaking. Cultivation experiments to determine optimal pH utilized alternative buffers, replacing the HEPES buffer when not appropriate. A final concentration of 10 mM for each buffer was used to achieve the desired pH value. The buffers used were: 1,4-Piperazinediethanesulfonic acid (PIPES) for pH 6.5-7.5, HEPES for pH 8-8.5, and 3-([1,1-Dimethyl-2-hydroxyethyl]amino)-2-hydroxypropanesulfonic acid (AMPSO) for pH 9. All culturing optimization tests were completed in quadruplicate.

Substrate utilization was determined by transferring strain DRI-13^T three times at 55°C into AGM media containing 10 mM of the following defined substrates: glucose, formate, fumarate, lactate, acteate, pyruvate, methanol, propionate, ribose, xylose, oxaloacetate, succinate, tartarate, butyrate, malate, citrate, aspartate, methionine, valine, alanine/glycine, leucine/glycine, and glutamate/glycine. Undefined substrates were added to AGM media in concentrations of 0.1% wt/vol for casamino acids, peptone, and yeast extract. Gas phase substrates were added to the serum bottle headspace to a pressure of 30 psi for H_2/CO_2 (80:20) and CO (100). Electron acceptors 5 mM nitrite, 5 mM nitrate, 10 mM sulfate, 10 mM sulfite, 10 mM thiosulfate, and 0.01% wt/vol elemental sulfur were individually added to AGM medium with each defined and undefined substrate. Success was determined when cultures were successfully transferred three

times and reached cell densities of 10^8 cells/mL by microscopy observations using a Petroff-Hauser cell counting chamber.

Co-culture experiments of strain DRI-13^T with wild type *Methanothermobacter thermoautotrophicum* were conducted in AGM medium containing 10 mM fumarate or 30 psi H_2/CO_2 (80/20 headspace) at 55°C. Enumeration of both microorganism's growth was monitored by microscopy based on their distinct morphologies.

Fumarate depletion was monitored by high-performance liquid chromatography (HPLC). Supernatants were filtered and acidified with 200 mM sulfuric acid to a final concentration of 5 mM. A sample of 5 μL was injected into AcclaimTM OA 5 μm column (4 × 250 mm), (Thermo Scientific), housed in Agilent 1100 series HPLC system for each time point. Separation was achieved under an isocratic gradient at a temperature of 38°C and flow of 0.5 mL/min. The DAD detector was adjusted to a wavelength of 210 nm and full scale sensitivity. Retention times of obtained peaks were compared with known standards (Organic Acids Kit, Supelco Analytical) and the quantity calculated using linear standard curves. The results were assessed with Chromeleon 7 software.

16S rRNA Gene Sequence Analysis and Genomic DNA Extraction

Strain DRI-13^T isolate was identified by centrifuging 5 mL of planktonic cells during logarithmic growth at 10,000 × *g* for 15 min at 4°C. DNA was extracted from the resulting cell pellet using an UltraClean Microbial DNA Isolation Kit (Mo Bio, Carlsbad, CA, United States). Universal bacterial primers 27F/1492R (5′-AGAGTTTGATCMTGGCTCAG-3′/5′-ACCTTGTTACGACTT-3′) were used to PCR amplify the small subunit ribosomal RNA (SSU rRNA or 16S rRNA gene) (Weisburg et al., 1991). The PCR product was then sequenced by Functional Biosciences (Madison, WI, United States) to determine identification of the isolate. With other 16S rRNA gene sequences recovered from the National Center for Biotechnology Information (NCBI) website, the sequences were aligned and phylogenetic relationships determined by Silva (v1.2.11) (Glöckner et al., 2017) and MEGA 5.2 (Tamura et al., 2011). Taxonomic classification sequences were obtained from the "List of Prokaryotic names with Standing in nomenclature" (LPSN,[1]).

High-molecular weight DNA was extracted from DRI-13^T by cultivating the organism in five, 1-L batch cultures grown on 10 mM fumarate. Cells were harvested by centrifugation at 15,000 × *g* for 30 min, and DNA was precipitated and extracted by cetyltrimethyl ammonium bromide (CTAB) buffer/phenol/chloroform (Sambrook and Russell, 2001). DNA was RNase treated, quality-checked on 1% agarose gel and shipped to the DOE Joint Genome Institute (JGI) for draft sequencing using Illumina and PacBio sequencing technology (PacBio RS; Illumina HiSeq 2500). The sequences were assembled according to JGI protocols using Velvet, annotated using a suite of gene characterization tools, and made available as a part of the JGI-IMG data warehouse (Markowitz et al., 2014). The genome of DRI-13^T was released to the public as per JGI protocol and is available both through the DOE IMG platform and via NCBI (Accession# PRJNA234897). The full length 16S rRNA gene sequence was submitted to NCBI and assigned accession number KR014122.

[1]http://www.bacterio.net/index.html

Electron Microscopy and Sample Preparation

For SEM, the samples were moved to a 13 mm Swinney micofilter holder with 0.2 μm Millipore filters and dehydrated. Dehydration of the cells was done with 25% increases of ethanol for 15 min each step from 25 to 95%, then three washes of 100%. Once dehydrated, the filters were critical point dried with a Tousimis Samdri CPD (Tousimis, Rockville MD, United States), mounted on aluminum stubs and coated with approximately 25 nm layer of gold with a SPI sputter coater (SPI supplies, West Chester, PA, United States). Images were taken on a Zeiss 1450EP SEM at 10 kV.

Cells for transmission electron microscopy (TEM) and scanning electron microscopy (SEM) were aseptically removed from anaerobic serum bottles and immediately fixed with 2% v/v glutaraldehyde in 0.1 M sodium cacodylate buffer for 1 h at 4°C. Cells were pelleted by centrifugation (10,000 × *g* for 10 min) between all steps and then re-suspended each time. The sample was then rinsed with 0.1 M sodium cacodylate buffer for 10 min each for three times and re-suspended in 1% OsO_4 in 0.1 M sodium cacodylate buffer for an hour at 4°C, then rinsed in distilled water for 10 min twice. TEM dehydration of the cells was performed with 25% increases of ethanol for 15 min each step from 25 to 95%, then three washes of 100%. Samples were then infiltrated with Spurr's low viscosity resin (EMS, Hatfield, PA, United States), with increasing concentrations of 100% ethanol and resin. After three changes of 100% resin and 1 h between each change, the samples were then placed in a 70°C oven for polymerization for 12 h. The resin was cut into 50–70 nm thick sections on a MT-X ultramicrotome (RMC, Tuscon, AZ, United States) and images were obtained on a JEOL 1011 TEM (JEOL, United States, Peabody, MA, United States) operating at 80 kV and equipped with an AMT camera system.

Lipid Analysis

For analysis of cellular fatty acids, biomass was harvested from cells grown in fumarate-amended (10 mM) mineral media for 72 h at 55°C. Analysis was performed at the Center for Microbial Identification and Taxonomy (University of Oklahoma). Fatty acid methyl esters were extracted, separated, and analyzed using the Sherlock Microbial Identification System (MIDI) version 6.1 as described previously (Kampfer and Kroppenstedt, 1996; Sasser, 2001). Analysis was performed with an Agilent Technologies 6890N gas chromatograph equipped with a phenyl methyl silicone fused silica capillary column (HP-Ultra 2, 25 m × 0.2 mm × 0.33 μm film thickness) coupled with a flame ionization detector. Hydrogen was used as the carrier gas. The temperature program was preset at 170°C and increased at 5°C min^{-1} to a final temperature of 270°C. The identification and

relative abundance of each fatty acid was expressed in terms of the percentage of total fatty acids using the QTSA1 database.

RESULTS

Hydrogeological Setting

The physiological and geochemical characteristics of the water samples from the pump test of U-3cn#5 on March 29, 2011 are presented in **Table 1**. Borehole water was fresh (845 μS/cm or 540 ppm TDS) (Kang and Jackson, 2016), slightly alkaline (pH 7.7), and was 44.7°C, as recorded at the surface. The dissolved oxygen (DO) was measured at 0.19 mg/L (3.2% of saturation), with no detectable sulfide. Reduction/oxidation potential was not measured. Total inorganic carbon (TIC) was 50.3 mg C/L, which at this pH would have been mostly bicarbonate. Major ions were defined by sodium > calcium > sulfate > silica (53.5, 37.2, 36, and 35 mg/L, respectively), followed by lesser amounts of chloride, magnesium, and potassium. Total metals were dominated by iron (1.57 mg/L), followed by lesser amounts of strontium (248 μg/L), manganese (101 μg/L), zinc (10.9 μg/L), and molybdenum (4.8 μg/L). Inorganic nitrogen was dominated by ammonium and nitrate, which were detected at 0.05 mg/L and 0.26 mg/L; while nitrite was below the 0.01 mg/L detection limit. Phosphate was detectable at 0.033 mg/L. Total organic carbon (TOC) was present at 1.5 mg/L, a substantial proportion of which is represented by the short chain fatty acids formate, acetate, and lactate, measured at 0.65, 0.4, and 0.4 mg/L, respectively. Propionate and fumarate were below detection limits. Tritium, a marker for the impact of nuclear device testing, was <7 pCi/L. Stable isotope signatures of $d^{13}C$ for dissolved inorganic carbon (DIC) of −12.8‰, and $d\ ^{2}H$ of -108‰ were detected as well.

TABLE 1 | Physical and chemical characteristics of source water from borehole U-3cn#5.

Latitude	37.06	Mn (μg/L)	101
Longitude	−116.02	Mo (μg/L)	4.8
Depth of sample (m)	863–923	Zn (μg/L)	10.9
Total Depth of well (m)	924	Cu (μg/L)	<0.09
Sampling method	Pump	Cr (μg/L)	<0.18
Temperature (°C)	44.7	Ni (μg/L)	2.6
pH	7.69	U (μg/L)	0.83
Rock type	carbonate	Pb (μg/L)	0.072
DO (mg/L)	0.193	Sr (μg/L)	248
DO (%Sat.)	3.2	Cs (μg/L)	2.11
^{3}H (pCi/L)	<6.5	W (μg/L)	0.49
TOC (mg C/L)	1.5	Acetate (mg/L)	0.4
TIC (mg C/L)	50.3	Lactate (mg/L)	0.4
Live/Dead Cell counts	4245	Formate (mg/L)	0.65
Total cell counts	10887	Propionate (mg/L)	<0.01
Conductivity (μS/cm)	845	Fumarate (mg/L)	<0.01
Turbidity (NTU)	3.675	He (% vol/vol)	<0.01
SO_4^{2-} (mg/L)	36	H_2 (% vol/vol)	<0.01
NO_3^- (mg/L)	0.26	O_2 (% vol/vol)	17.1
NO_2^- (mg/L)	<0.14	N_2 (% vol/vol)	65.0
NH_4^+ (mg/L)	0.05	CO_2 (% vol/vol)	16.9
PO_4^{3-} (mg/L)	0.033	CH_4 (% vol/vol)	0.17
SiO_2 (mg/L)	35	C_2H_6 (% vol/vol)	<0.01
Cl (mg/L)	27.4	C_3H_8 (% vol/vol)	<0.01
Na (mg/L)	53.5	iso-C_4H_{10} (% vol/vol)	<0.002
K (mg/L)	8.5	n-C_4H_{10} (% vol/vol)	0.002
Ca (mg/L)	37.2	$d^{13}C$ CO_2 (in ‰ V-PDB)	−12.8
Mg (mg/L)	16.5	$d^{13}C$ Methane (in ‰ V-PDB)	b.d.
Br (mg/L)	0.09	$d\ ^{2}H$ (‰)	−108
Fe (mg/L)	1.57	^{14}C (pmc)	4.65

b.d., below detection limit of instrument.

Indigenous Microbial Communities

Cell enumeration indicated a total planktonic cell density in borehole water of 1.1×10^4 cells/mL. Of these, a substantial proportion (∼half, 4.2×10^3 cells/mL) were reported as viable based on the output of a flow cytometric Live/Dead assay. To gain a better understanding of microbial community structure in these samples, total DNA from 0.2 micron filters was amplified by PCR and used to construct bacterial and archaeal 16S rRNA gene libraries. A total of 84 complete (∼1400 bp) bacterial sequences were constructed and consolidated into 23 representative taxa that were submitted to NCBI (Accession #:MK682771-MK682793). A total of 35 partial (∼850 bp) archaeal sequences were consolidated into 3 representative taxa that were also submitted to NCBI (Accession #: MK675956-MK675958). Bacterial communities were dominated by Proteobacteria (81% - a mix of Alphaproteobacteria, Betaproteobacteria, Deltaproteobacteria, and Gammaproteobacteria), Acidobacteria (11%), and Firmicutes (8%) (**Supplementary Figure S1**). Among the archaea, clones were distributed between Euryarchaeota (71%) predominantly a species related to *Methanothermobacter thermautotrophicus* and *Methanococcus igneus*, and Crenarchaeota (29%) (**Supplementary Figure S2**). Close relatives of strain DRI-13^T were not detected in these libraries.

Isolate Properties and Identification

Strain DRI-13^T was purified from a 45°C anaerobic enrichment in a synthetic groundwater medium supplemented with 0.1% wt/vol peptone as the sole carbon and energy source. After 3 weeks of isolation techniques (see methods), the DRI-13^T colonies were 0.5 mm in diameter, circular (with entire margins), glossy, and convex. The resulting isolate was a Gram-stain-positive bacillus (∼2–6 μm long and ∼0.5 μm wide) which reached a density of $\sim 10^6$ cells/mL in culture. The strain was motile and was observed by phase contrast microscopy to form a central endospore. Phylogenetic analysis of the full-length 16S rRNA gene (GenBank accession no. KR014122) indicated that DRI-13^T possessed 90.0% similarity to *Pelotomaculum propionicicum* (Imachi et al., 2007) and *P. thermopropionicum* (Imachi et al., 2002) and 88.0% similarity to *Desulfotomaculum gibsoniae* (Kuever et al., 1999). The most closely related 16S rRNA gene sequences in available databases affiliated with as-yet uncultured bacteria discovered from subsurface environments in Denmark (99.0% similarity, AY538172.1), Australia (97.0% similarity, EU400652.1), and Japan (97.0%

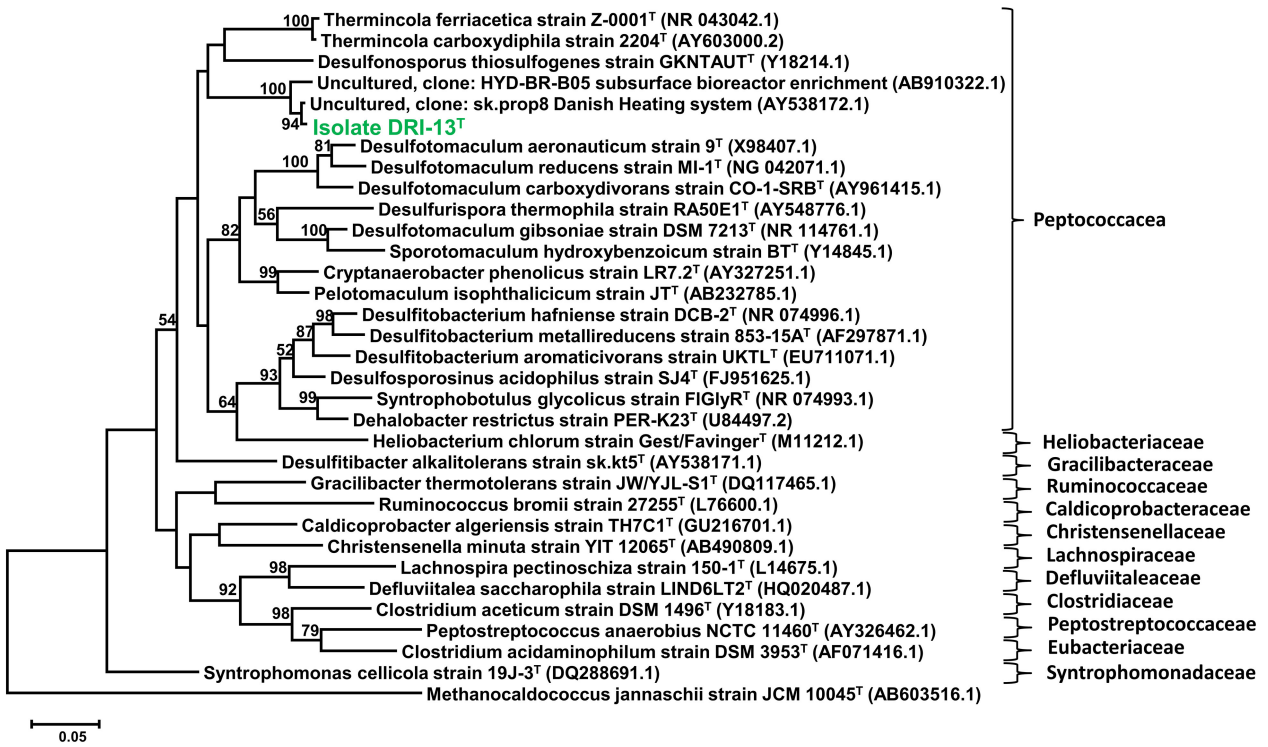

FIGURE 2 | Taxonomic placement of isolate DRI-13^T by full length 16S rRNA genes aligned by SILVA (v1.2.11), and maximum-likelihood method based on 1,000 permutations of all bacterial families with nomenclature standing within the class *Clostridiales*. The scale bar represents 5% identity dissimilarity between sequences.

similarity, AB910322.1). By comparing the 16S rRNA gene sequence to selected type strains representing all families under the order *Clostridiales*, it appears strain DRI-13^T is a previously undescribed genus within the family *Peptococcacea* (**Figure 2**).

Physiological Characterization of Strain DRI-13^T

Analysis by SEM of isolate DRI-13^T revealed a distinctive thin rod-shaped morphology characterized by an average length of 4–6 μm and 0.5 μm width (**Figure 3A**). TEM revealed a distinct inner and outer membrane with an electron-dense matrix and what appears to be a vacuole (**Figure 3B**).

Strain DRI-13^T is a fastidious obligate anaerobe. The isolate grew poorly with 0.1% wt/vol casamino acids, 10 mM glucose, 0.1% wt/vol peptone, or 0.1% wt/vol yeast extract when used as the sole carbon and energy source. No growth was observed when supplemented with H_2/CO_2 (80:20), CO, formate, lactate, acetate, pyruvate, CH_4, methanol, propionate, ribose, xylose, oxaloacetate, succinate, tartarate, butyrate, malate, citrate, aspartate, methionine, and valine. Stickland reactions of alanine/glycine, leucine/glycine, and glutamate/glycine also failed to support growth (Nisman, 1954). Likewise, accessory electron acceptors including nitrite, nitrate, sulfate, sulfite, thiosulfate, and elemental sulfur failed to stimulate growth. The only substrate tested that was successful in supporting growth was fumarate (**Table 2**).

Specific growth rates of DRI-13^T during anaerobic respiration on fumarate display a maximal specific growth rate of 0.4 h^{-1} under optimal conditions of temperature and pH (55°C and pH 8.0) (**Figures 4A,B**). Metabolic analysis of DRI-13^T shows growth vs. substrate utilization experiment (30 mM fumarate) performed over 70 h (**Figure 5**). This experiment revealed an initial lag phase of 15–20 h, after which cellular growth commenced along with consumption of fumarate, reaching the lower limit of detection at 65 h. Temporally corresponding to the depletion of fumarate was the coincident production of succinate and acetate, which reached maxima at about 50 h. These experiments revealed a conversion rate of one equivalent of fumarate to approximately 0.83 and 0.33 equivalents of succinate and acetate.

Lipid analysis indicates that the major fatty acids (>10%) present for strain DRI-13^T are the branched-chain fatty acid iso-$C_{15:0}$ (22.8%), straight-chain $C_{15:0}$ (15.0%), $C_{16:0}$ (12.0%), and $C_{14:0}$ (11.6%), as compared to phylogenetically related bacteria (**Table 3**).

Genome Sequencing and Analysis

High-quality genomic DNA was extracted from isolate DRI-13^T for genome sequencing by the DOE Joint Genome Institute

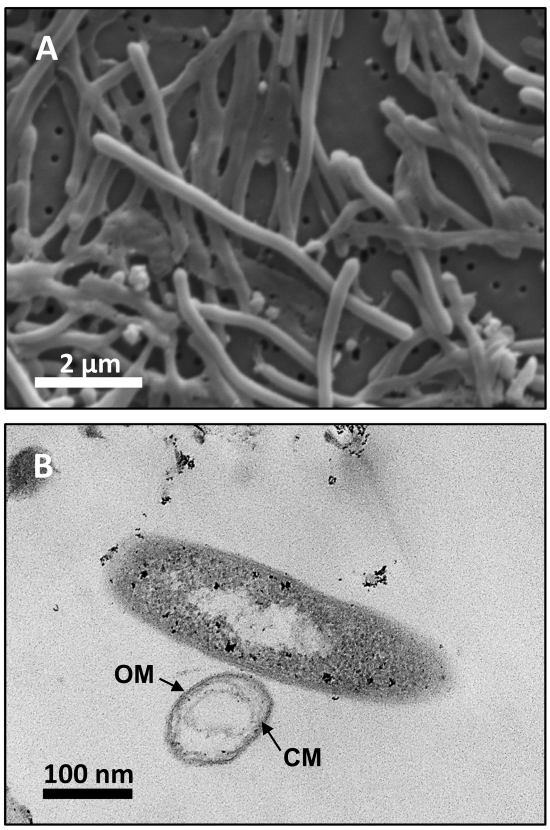

FIGURE 3 | Microscopy images of strain DRI-13^T: **(A)** scanning electron micrograph showing average 4–6 µm length morphology; **(B)** transmission electron micrograph showing outer membrane (OM) and cytoplasmic membrane (CM).

(JGI, JGI GOLD Gi0054453, NCBI Taxonomic ID 1449126, and Assembly #ASM74602v1). The completed draft genome of DRI-13^T is 3,649,665 bp, with an average G + C content of 45% and composed of 105 contigs (**Supplementary Table S1**). A total of 3,749 genes were identified, of which 3,671 (98%) are predicted to code for proteins (PCGs). Predicted function could be assigned to 2874 (77%) of the total number of PCGs, while 797 (21%) had no known functional prediction[2]. Genes were identified for assimilatory/dissimilatory sulfate and sulfite reduction, anaerobic fumarate respiration, tripartite ATP-independent secondary passive transport, endospore formation/germination, and flagella biosynthesis (**Supplementary Table S2**).

DISCUSSION

Within North America's Basin and Range (B&R) physiographic province lies the Great Basin (Grayson, 2011), a hydrogeologically defined, internally draining province that comprises portions of the US states of California, Oregon, Idaho, Arizona, and most of Nevada. Fault-controlled flow of deep groundwater within this tectonic extensional zone results in hydrographic basins and sub-basins (Winograd and Thordarson, 1975, Winograd et al., 2005), with the subject of this study, the Death Valley Regional Flow System (DVRFS), being the largest. Borehole U-3cn#5 (**Figure 1**) intercepts a hydrologically confined lobe of the DVRFS's and represents a novel window for deep biosphere study of the Basin and Range and extensional zones in general.

The fracture carbonate-hosted aquifer from which DRI-13^T was isolated possesses chemistries (e.g., circumneutral pH, relatively high sulfate, low TOC) and overall microbial community structure typical of subsurface fractured carbonate aquifers studied elsewhere (**Table 1**) (Hohnstock-Ashe et al., 2001; Farnleitner et al., 2005; Gihring et al., 2006; Pfiffner et al., 2006; Park et al., 2009). Nutrients, fixed organic carbon, and energy resources are all relatively limited in this environment. As with other fractured carbonate aquifers, it is unclear how microbial populations are sustained, especially with regard to carbon sources (Hohnstock-Ashe et al., 2001). In U-3cn#5, rRNA gene libraries reveal a microbial community composed of predicted thermophilic anaerobes from the domain Bacteria and Archaea (**Supplementary Figures S1**, **S2**). The geothermal/carbonate-controlled nature of this subsurface environment makes it a distinct environment compared to surrounding monitoring wells, which are emplaced in shallower lower temperature systems and other rock types (e.g., volcanics and alluvium), with one exception: borehole BLM-1. Located approximately 75 km South of U-3cn#5 in the discharge zone of the DVRFS, this latter well intersects anoxic geothermal waters (57°C) of the regional fractured carbonate aquifer. In spite of this distance, these two wells share similar bacterial and archaeal profiles, including the presence of important marker subsurface bacteria such as "*Candidatus* Desulforudis audaxviator," *Desulfotomaculum putei*, and the archaeon *Methanothermobacter thermautotrophicus* (Chivian et al., 2008; Thomas et al., 2013; Sackett, 2018).

Enrichment cultivations from U-3cn#5 water samples in a strictly anaerobic minimal salts medium amended with peptone produced a slowly growing thermophilic bacillus after ∼1 month at 50°C. Sugar and short chain carbohydrate substrates did not promote growth (**Table 2**). While not directly detected in the subsurface environment of U-3cn#5, the citric acid cycle intermediate fumarate was the only substrate that enabled routine culturing of the microorganism. Isolation techniques yielded a pure culture which was given the strain name, DRI-13^T. Analysis of the 1463 nucleotide 16S rRNA gene sequence revealed that DRI-13^T affiliates at the species level with uncultured clones from other geothermally influenced subsurface locations including Japan, Australia (unpublished), and Denmark (AB910322.1, EU400652.1, AY538172.1) (Kjeldsen et al., 2007; Baito et al., 2015). Within the family *Peptococcaceae*, DRI-13^T is most closely related (∼90.0% similarity to the 16S rRNA gene) to three type strains *Pelotomaculum propionicicum*, *P. thermopropionicum*, and *P. isophthalicicum*. This establishes DRI-13^T as a novel genus using the parameters defined by Yarza et al. (2014) (**Figure 2**). Of these phylogenetic relatives, only *P. thermopropionicum* share thermophilic characteristics and utilization of fumarate

[2]https://img.jgi.doe.gov

TABLE 2 | Carbon and electron utilization of DRI-13^T and closest relatives.

Characteristic	DRI-13^T	*Pelotomaculum propionicicum* DSM 15578[1]	*Pelotomaculum thermopropionicum* DSM 13744[2]
Isolation source and depth	Nevada well U-3cn#5 at 0.7 km	Anaerobic sludge blanket reactor	Anaerobic sludge blanket reactor
Morphology	Rod	Rod	Rod
Cell size (μm)	0.5 × 6.0	1.0 × 3.0	0.7 × 2.0
Motility	Yes	No	No
Spore former	Yes	Yes	Yes
Spore location	Central	Central	Central
Optimal Temperature for growth (°C)	55	37	55
Temperature range (°C)	35–65	25–45	45–65
Optimal pH for growth (range)	8.0 (7.0–8.5)	7.0 (6.5–7.4)	7.0 (6.5–8.0)
NaCl limit of growth (mM)	100	85	68
Genome Sequenced	Yes	No	Yes
Doubling time (hours)	2.5	120	14.5
Utilization of electron/carbon donors			
H_2/CO_2	–	–	–
CO	–	ND	ND
Formate	–	–	–
Lactate	–	–	+*
Acetate	–	–	–
Pyruvate	–	–	+
Methane	–	ND	ND
Methanol	–	–	–
Propionate	–	+	+*
Ribose	–	–	–
Glucose	(+)	–	–
Xylose	–	–	–
Casamino acids	(+)	–	–
Peptone	(+)	–	+
Yeast Extract	(+)	–	+
Fumarate	+	–	–
Oxaloacetate	–	ND	ND
Succinate	–	–	–
Tartarate	–	ND	ND
Butyrate	–	–	–
Malate	–	–	–
Citrate	–	ND	ND
Aspartate	–	–	ND
Methionine	–	ND	ND
Alanine + glycine	–	–	ND
Leucine + glycine	–	–	ND
Glutamate + glycine	–	–	ND
Valine	–	ND	ND
Utilization of electron acceptors			
Fumarate	+	–	+
Nitrite	–	ND	ND
Nitrate	–	–	–
Sulfate	–	–	–
Thiosulfate	–	–	–
Sulfite	–	–	–
Inorganic Sulfur	–	–	–

*ND, not determined. (), limited growth observed over 2–3 weeks. *, only in co-culture with Methanothermobacter themautotrophicus strain DH^T. –, no observed growth; +, growth was observed. [1]Imachi et al. (2007). [2]Imachi et al. (2002).*

(**Table 2**). Unlike DRI-13^T, *P. thermopropionicum* can utilize a wider range of substrates and is described under certain conditions to support a syntrophic interaction with the methanogen *Methanothermobacter thermoautotrophicus*. The most abundant archaeon in our U-3cn#5 rRNA gene libraries was *M. thermoautotrophicus* (71% of reads). *P. propionicicum* and *P. isophthalicicum* have been reported to have syntrophic interactions with other methanogens as well, though no interactions were established between DRI-13^T and an isolated wild type *M. thermoautotrophicum* from the borehole. Growth combinations only resulted in DRI-13^T becoming the majority within the culture bottle and causing no change in growth performance with or without *M. thermoautotrophicum* (not shown).

Examination of DRI-13^T by SEM indicates a bacillus-type morphology, averaging 6 μm in length and 0.5 μm width (**Figure 3A**). TEM reveals features of the outer membrane and cytoplasmic membrane, including what appears to be a vacuole (**Figure 3B**), though it is possible that the space within the cell may be an artifact from TEM preparation. If real, the presence of a vacuole may explain an apparent buoyant property of DRI-13^T cells requiring centrifugation times greater than 30 min at or above 15,000 × *g*, which is typical for very small cells or for cells with natural buoyancy. Lab-standard cells from the phylum *Firmicutes*, such as *Desulfotomaculum putei*, can be pelleted with less rigorous effort similar to *E. coli*. While not a feature noted in other subsurface microorganisms, it is conceivable that innate buoyancy control could be advantageous to fracture-dwelling subsurface microorganisms during planktonic growth.

Measureable DRI-13^T growth was observed to occur between 37°C (minimum) and 65°C (maximum). While the environmental temperature of U-3cn#5 was recorded at 44.7°C, the optimal temperature for DRI-13^T is 55°C (**Figure 4A**). Although not determined, the *in situ* temperature from the interval where DRI-13^T was obtained was likely higher than that recorded at the wellhead due to the long distance pumped water was lifted through presumably cooler conditions in the aquifer above the confining layer and ∼500 m of vadose zone. As might be expected for an organism adapted to strongly

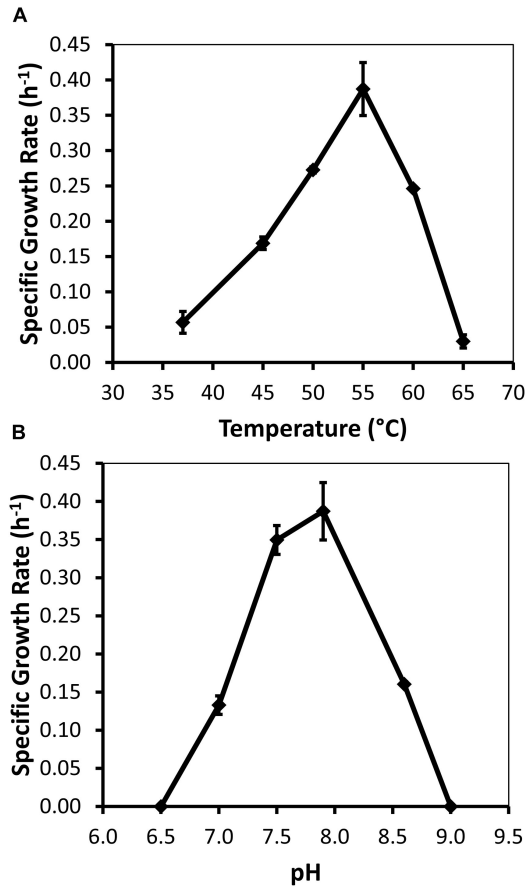

FIGURE 4 | Growth characteristics of strain DRI-13^T for: **(A)** optimal temperature of 55°C; and **(B)** optimal pH of 8. Data points averaged from quadruplicate cultures using a standardized medium of salts with 10 mM fumarate.

buffered carbonate aquifers, the pH tolerance of DRI-13^T is narrow, with observable growth occurring only between 7.0 and 8.5, and optimal growth at pH 8.0 (**Figure 4B**). As compared to close relatives, the optimal temperature is similar to *P. thermopropionicum* and *P. propionicicum* (55°C and 37°C). The growth rate of DRI-13^T appears to be substantially faster, doubling every 2.5 h, as opposed to 14.5 and 120 h for *P. propionicicum* and *P. thermopropionicum,* respectively (Imachi et al., 2002, 2007). This faster growth rate possibly reflects the independent lifestyle of DRI-13^T as opposed to the syntrophic associations of the others. In addition, cells cultured beyond stationary phase (approximately 48 h) exhibit endospore formation, as observed by microscopy and the presence of endospore related genes (**Supplementary Table S2**). While no discernable cellular movement was consistently observed, DRI-13^T genome appears to have flagella related genes as well (**Supplementary Table S2**).

Lipid analysis indicates that the major fatty acids (>10%) for strain DRI-13^T are the branched-chain fatty acid iso-$C_{15:0}$ (22.8%) along with the straight-chain $C_{15:0}$ (15.0%), $C_{16:0}$ (12.0%) and $C_{14:0}$ (11.6%). The higher proportion of the branched-chain iso-$C_{15:0}$ in strain DRI-13^T is also characteristic of its nearest neighbor, *P. thermopropionicum* strain SI^T in which iso-$C_{15:0}$ represents the majority of all fatty acids at 76.4% (Imachi et al., 2002), and in *P. terephthalicicum* strain JT^T (28.7%) (Qiu et al., 2006), *Cryptanaerobacter phenolicus* strain LR7.2^T (Juteau et al., 2005), and *Desulfotomaculum gibsoniae* Groll^T (Kuever et al., 1999) (**Table 3**). While the overall fatty acid methyl ester (FAME) profile for strain DRI-13^T clearly differentiates it from its nearest phylogenetic neighbors, the significant percentage of the straight-chain fatty acid $C_{15:0}$ is a defining characteristic, as it is not present in other closely related species, with the exception of *C. phenolicus* strain LR7.2^T, in which it is only a minor component (Juteau et al., 2005). Interestingly, C15 lipids were not detected in any of 44 fracture and mine water samples from a comprehensive survey of environmental lipids in the ultradeep mines of South Africa (Pfiffner et al., 2006). Another defining characteristic is the detection of $C_{16:1\omega\ 7c}/C_{16:\ 1\omega\ 6c}$ (5.8%), which is not present in other phylogenetic neighbors such as *C. phenolicus* strain LR7.2^T (Juteau et al., 2005), and *D. gibsoniae* strain Groll^T (Kuever et al., 1999). $C_{16:1\omega\ 7c}$ was detected in the South African study, but statistically corresponded with mine service water samples rather than pristine fracture water.

Fumarate catabolism was typical as described previously in other Firmicutes (Dorn et al., 1978; Imachi et al., 2002). High-pressure liquid chromatography (HPLC) detected the removal of fumarate and the concomitant production of succinate and acetate. This supports the idea that fumarate is both being metabolized and used as an electron acceptor in anaerobic respiration (**Figure 5**). No other observable products such as oxalate, tartrate, lactate, malate, citrate, or propionate were observed by HPLC. Headspace pressure in culture bottles remained stable (∼1 bar) with no obvious over-pressurization. The source of fumarate in the subsurface is unclear. Gelling agents associated with drilling can be a source of fumarate (Borchardt, 1989). However, in this case residue from the drilling of U-3cn#5 may be unlikely given the borehole age (1965) and its flushing with multiple millions of liters of water pumped over the years. Samples of 1 g fractured carbonate from U-3cn#5 (NNSS Core Library), aseptically crushed, extracted with 5 mL boiling water, concentrated, and analyzed on HPLC, did not contain detectable levels of fumarate (data not shown). It is more likely that DRI-13^T is cryptically biodegrading the waste products or endogenous decay derived from other members of the microbial community (Béranger et al., 2006). Since DRI-13^T does not seem to be a dominant microbial community member (**Supplementary Figure S1**), it is possible that its relatively low representation is the result of occupying a narrow niche focusing on fumarate respiration or is a relic from a period after drilling when fumarate might have been present.

Assembly of the DRI-13^T draft genome from a single library prep resulted in 105 contigs. Complete coverage of the genome failed in regions where repetitive intergenic sequences (mobile elements), hypothetical proteins, or clustered regularly interspaced short palindromic repeats (CRISPR) arrays were present. The estimated genome size is 3,649,665 with a G + C content of 45%. This is comparable to close relatives with

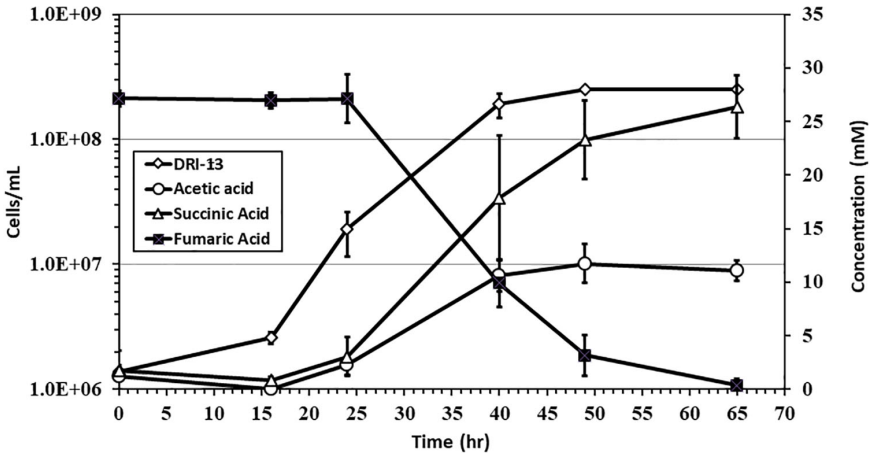

FIGURE 5 | Growth of DRI-13^T on 30 mM fumarate and metabolic end products: open diamonds, cell density; filled squares, fumarate depletion; filled triangles, succinate production; filled circles, acetate production. Each data point is an average of triplicate samples with standard deviation error bars.

sequenced genomes such as *D. gibsonia* (4.85 Mbp) and *P. thermopropionicum* (3.02 Mbp). Distribution of nucleotides and genes across the 105 contigs range from 1,045 to 193,268 bases (average 34,759 bases per contig), with 2 to 203 annotated genes (average 36 genes per contig). The JGI/IMG annotation gene calling algorithms predict 3,749 genes in DRI-13^T with 77% of them functionally assigned (**Supplementary Table S1**). Analysis of the metabolic capability of the DRI-13^T genome indicates core genes for glycolysis/gluconeogenesis, fatty acid biosynthesis, and amino acid metabolism. Homologs for assimilatory or dissimilatory sulfate and sulfite reduction (*dsrA*, *dsrB*, and *dsrD*) are present. However, sulfide production was never detected when sulfate was present in the media. Amino acid analysis of the *dsr* genes show an identity of 84% to 99% similarity to *Desulfitobacter alkalitolerans*, which was isolated from a Danish geothermal heating system, a site where an uncultured 16S rRNA gene with exact homology to DRI-13^T had been sequenced (Nielsen et al., 2006; Kjeldsen et al., 2007).

Examination of the anaerobic fumarate respiration pathway revealed that core fumarate catabolic and related genes are present within the genome. Some of the genes for fumarate respiration have undergone duplication generating paralogs (**Supplementary Table S2**). The metabolic pathway for fumarate respiration converts three fumarate molecules to one acetate and two succinate molecules (**Supplementary Figures S3A,B**). The gene for the enzyme fumarase is present in the genome and can reversibly convert fumarate by hydration to malate or malate to fumarate by dehydration. The decarboxylation of the malate molecule to pyruvate is completed by NADP dependent malate dehydrogenase (oxaloacetate-decarboxylating), generating carbon dioxide and reductive potential. The further oxidation of pyruvate to acetyl-CoA is accomplished by pyruvate ferredoxin oxidoreductase, generating carbon dioxide and reduced ferredoxin (Thauer et al., 1977). The final reduction of acetyl-CoA with succinate to acetate occurs by succinyl-CoA:acetate CoA-transferase. Concurrently, two molecules of fumarate can be reduced to succinate by succinate dehydrogenase which was also annotated. Generation of ATP by coupling substrate-level phosphorylation is achieved by succinyl-CoA synthetase. DRI-13^T generates a proton motive force for ATP synthesis through a NADH ubiquinone-oxidoreductase (Nuo Complex 1) and membrane bound Ni-Fe hydrogenase-4 (Marreiros et al., 2013; Schut et al., 2016; Yu et al., 2018). The FPO_F complex allows versatility of energy conservation among anaerobes and is perhaps a recent adaptation to environments rich in sulfide and at an interface with oxygen (e.g., buoyancy), similar to water chemistry conditions found in monitoring well U-3cn#5 (Schut et al., 2016). It is not known what molecule transports electrons to the hydrogenase-4 Ni-Fe complex. Interestingly, seven copies of electron transfer flavoprotein (EtfAB) and quinone oxidoreductase (FixC) were annotated within the genomes, suggesting capacity for high potential electron transfers in bifurcating energy conservation (Costas et al., 2017).

Secondary transporters dependent on substrate binding are ubiquitous in prokaryotes yet poorly characterized. Tripartite ATP-independent periplasmic (TRAP) transporters manage the passive transport of hydrocarbon molecules across the membrane for the cell to use as a source of carbon, electrons, and energy. Isolate DRI-13^T has fourteen TRAP 4TM/12TM genes present in its genome, six of which have fused transmembrane subsunits (**Supplementary Table S2**). TRAP transporters are proposed to be 'ancient' secondary transporters that are anchored in the membrane, taking advantage of sodium ion gradients to co-transport 4 carbon molecules from outside the cell wall into the cytoplasm (Rabus et al., 1999; Kelly and Thomas, 2001; Mulligan et al., 2011). The TRAP transporter's DctP subunit is seemingly specific to particular solutes (Fischer et al., 2015). DRI-13^T's almost exclusive utilization of the dicarboxylate molecule fumarate seems complimentary to the TRAP transport system. It has been demonstrated that the psychrophilic microorganism *Psychrobacter arcticus* 273-4, exhibited lower growth rates when its TRAP genes were genetically knocked out and afterward fed fumarate (Bakermans et al., 2009). DRI-13^T has 41

TABLE 3 | Cellular fatty acid composition (%) of strain DRI-13^T compared with its closest phylogenetic neighbors.

Fatty Acid	DRI-13^T	SI^T [1]	JT^T [2]	LR7.2^T [3]	GrolI^T [4]
$C_{11:0}$	–	–	–	–	1.9
Anteiso-$C_{13:0}$	2.1	–	–	–	–
$C_{13:0}$	1.3	–	–	–	–
iso-$C_{14:0}$	–	–	–	–	1.6
$C_{14:0}$	**11.6**	3.2	26	5.8	2.6
iso-$C_{15:1}$ F	2.9	–	–	–	–
*iso-$C_{15:1}$ H/$C_{13:0}$ 3OH	1.2	–	–	–	–
iso-$C_{15:0}$	**22.8**	**76.4**	**28.7**	**13.7**	5.4
anteiso-$C_{15:0}$	2.5	–	9.2	**18.9**	–
$C_{15:1}\omega 8c$	2.1	–	–	–	–
$C_{15:1}\omega 7c$	–	–	–	–	2.7
$C_{15:1}\omega 6c$	1.5	–	–	–	–
$C_{16:0}$ alde	–	–	–	–	2.2
$C_{15:0}$	15	–	–	3.5	–
$C_{15:0}$ dma	–	–	–	–	1.7
iso-$C_{16:0}$	–	–	–	7.5	–
$C_{16:1}\omega 7c$	–	–	–	–	3.3
$C_{16:1}\omega 9c$	1.1	–	–	**13.7**	**15.1**
$C_{16:1}\omega 11c$	–	–	–	–	3.6
*$C_{16:1}\omega 7c$/$C_{16:1}\omega 6c$	5.8	–	–	–	–
$C_{16:0}$	12	**10.7**	**16.7**	**12.5**	9.6
$C_{16:1}\omega 9c$ dma	–	–	–	–	4.6
$C_{16:0}$ dma	–	–	–	–	6.7
iso-$C_{17:1}$ $\omega 7c$	–	–	–	–	4.8
iso-$C_{17:1}$ $\omega 9c$	4.9	2.9	–	–	–
$C_{17:0}$ cyclo	–	–	–	–	2.7
iso-$C_{17:0}$	1.8	–	–	5.7	–
anteiso-$C_{17:0}$	–	–	–	7.3	–
$C_{17:1}\omega 8c$	1.5	–	–	–	–
$C_{17:0}$	1	–	–	–	–
$C_{18:1}\omega 9c$	–	–	–	4.6	2
$C_{18:1}\omega 11c$	–	–	–	–	3.3
$C_{18:1}\omega 13c$	–	–	–	–	2.8
$C_{18:0}$	3.6	6.7	7.1	4.2	5.6
$C_{18:1}\omega 11c$ dma	–	–	–	–	1.5

*Only fatty acids that represent ≥ 1% of the total fatty acids of at least one strain are shown. *Summed features represent groups of two FAs not separated by MIDI system. alde, aldehyde; dma, dimethyl acetal; cyclo, cyclopropane. [1]Pelotomaculum thermopropionicum strain SI^T. [2]Pelotomaculum terephthalicicum strain JT^T. [3]Cryptanaerobacter phenolicus strain LR7.2^T. [4]Desulfotomaculum gibsoniae strain GrolI^T. Bold values indicate major FA that are >10%.*

TRAP annotated transporter genes, compared with only three TRAP genes found in *P. thermopropionicum*. As for annotated genes, 10.4% of DRI-13^T genome fall under the category of transporter (390/3749 genes) as compared to 8.6% (259/3018) for *P. thermopropionicum*. Three of the fusion TRAP proteins in DRI-13^T genome (WP_034425417.1, WP_051965735.1, and WP_51966221.1) have 41-47% amino acid identity to homologs in the deep subsurface bacterium *Ca.* D. audaxviator (Chivian et al., 2008). The 'investment' of DRI-13^T genome with ATP independent secondary transporters potentially reveals a methodology of how subsurface microbes manage minimal energy metabolic activities in order to survive in oligotrophic environments. This is seemingly true for *Alphaproteobacteria* SAR11 that were sequenced from the Sargasso Sea, where TRAP transporters were found to be abundant (Morris et al., 2002; Mulligan et al., 2011).

Spore formation and germination genes were annotated in the genome as well (Brown et al., 1994; Browne et al., 2016). Isolate DRI-13^T appears to have 37 spore-related genes (**Supplementary Table S2**), as compared to microorganisms whose closest amino acid similarities to the *GerA* gene are *Bacillus camelliae*, which possesses 77 spore-related genes, and *Desulfonispora thiosulfatigenes*, which has 29 spore-annotated genes. Interestingly, the number of spore-related genes does not appear to differentiate microorganisms originating from surface and subsurface environments. For example, subsurface microorganisms such as *Desulfotomaculum putei* (26 spore-related genes), *Ca.* D. audaxviator (8 spore-related genes), and *Bacillus subterraneus* (64 spore-related genes) can be compared to surface microorganisms such as *Caldicellulosiruptor obsidiansis* (11 spore-related genes), and *Clostridium difficile* BI1 (17 spore related genes).

CONCLUSION

The thermophilic, anaerobic, fumarate-respiring bacterium DRI-13^T was successfully isolated from geothermal water from the Lower Carbonate Aquifer (LCA) of the Death Valley Regional Flow System (DVRFS) collected from fractures at 863 – 923 mbls. Physiological and molecular analysis of strain DRI-13^T revealed it to be a new species within a novel genus of the Family *Peptococcaceae*. Microbial community analysis via 16S rRNA gene libraries of *Archaea* and *Bacteria* reveal a community consistent with other anoxic, rock-hosted subsurface aquifers. However, DRI-13^T was not present in these samples as a major community member. This study represents one of the first descriptions of indigenous life from the LCA of the DVRFS, and DRI-13^T is the first characterized microorganism from this deep subsurface extensional zone habitat. The apparent obligate reliance upon fumarate by this organism is relatively unusual and of uncertain significance in a deep biosphere context. Here we introduce DRI-13^T as a representative microorganism from the terrestrial deep biosphere and propose the name *Thermoanaerosceptrum fracticalcis* DRI-13^T gen. nov. sp. nov.

Description of *Thermoanaerosceptrum* gen. nov.

Thermoanaerosceptrum gen. nov. (Ther.mo.an.a.e.ro.scep'trum. Gr. adj. *thermos*, hot; Gr. prefix an-, not; Gr. n. *aer* air; Gr. neut. n. *skeptron* staff; N.L. neut. n. *Thermoanaerosceptrum* a hot anaerobic staff).

Cells are rod-shaped. Cell wall is Gram-positive type. Central endospores are observed. Thermophilic. Obligate anaerobic chemoorganoheterotroph. Fermentation end products are succinate and acetate. The major fatty acids (>10%) were iso-$C_{15:0}$, $C_{15:0}$, $C_{16:0}$ and $C_{14:0}$.

The type species is *Thermoanaerosceptrum fracticalcis*.

Description of *Thermoanaerosceptrum fracticalcis* sp. nov.

(frac.ti.cal'cis. L. part. adj. *fractus*, broken; L. n. *calx*, -cis, limestone; N.L. gen. n. *fracticalcis*, of broken limestone, referring to the origin of the type strain).

Cells are long, straight rods averaging 6 μm long and 0.5 μm wide, occurring singly. The cell wall is Gram-positive type, with central endospores observed. Optimal growth temperature is 55°C, with a maximum of 65°C and minimum of 35°C. Optimal pH is 8.0 with a range of 7.0–8.5. Obligate anaerobic chemoorganoheterotroph that utilizes fumarate as a sole carbon source and electron donor/acceptor for growth. Glucose, casamino acids, peptone, and yeast extract can be weakly utilized as electron/carbon donors. Fermentation end products are succinate and acetate. The estimated genome size of DRI-13^T is 3,649,665 bp, of which 87.3% are coding regions. The major fatty acids (>10%) were iso-$C_{15:0}$, $C_{15:0}$, $C_{16:0}$ and $C_{14:0}$.

The type strain is DRI-13^T (DSM 100382^T = ATCC TSD-12^T), which was isolated from a terrestrial deep biosphere aquifer located in the US Great Basin. The DNA G + C content of the type strain is 45.2 mol%.

DATA AVAILABILITY STATEMENT

The datasets generated for this study can be found in the JGI/IMG and NCBI.

AUTHOR CONTRIBUTIONS

SH-B designed the research project, organized the contributions of all other authors, conducted the experiments, collected the data, and led the writing effort. LS screened the first enrichments and initiated the isolation of microorganism. MZ, TO, and BL provided the geochemical data on U-3cn#5. MC and PL performed and interpreted the lipid analysis. JG and IN performed HPLC and submitted the Illumina genome sequencing analysis. CR contributed to the experimental design and provided the hydrogeological and NNSS logistical expertise. DM secured the site access, collected the samples, secured the major funding, and co-wrote the manuscript.

FUNDING

This work was supported by the Department of Energy grant #DE-PS02-09ER09-07, NASA Astrobiology Institute Cooperative Agreement NNA13AA92A, U.S. National Science Foundation grant DEB-1441717, startup funds for SH-B from Southern Illinois University Carbondale, and JGI Project 'Genome analyses of microbes integral to the cycling of sulfate and iron' IDs: Gs0014904 and Gp0046988. Work at Lawrence Livermore National Laboratory (LLNL) was supported by the Subsurface Biogeochemical Research Program of the U.S. Department of Energy's Office of Biological and Environmental Research (SCW1053).

ACKNOWLEDGMENTS

We thank Russ Shelton, David Finnegan, Jeff Wurtz, and others associated with the DOE UGTA program for logistical support and Bill Wilborn for site access. Special thanks to Brenna R. Hardtner from Henderson Foothill High School for providing the founding scientific name for DRI-13^T, and to Craig Rosen from DRI's Green Power Project for facilitating the interaction with Southern Nevada High Schools. Thanks to Dr. John Shields from the University of Georgia for the SEM and TEM images, Dr. Bernhard Schink from the University of Konstanz for assisting with the proper Greek and Latin name description, Dr. Gerti Schut for the insightful discussions about hydrogenases, and Jenny C. Fisher for assisting with the collection of the U-3cn#5 samples. We also thank Beverly Parker and the reviewers at DOE for the editorial advice and document clearance. Thanks to an undergraduate student David Lynn from the University of Nevada, Las Vegas, NV, United States for the seemingly endless centrifugation for genomic DNA. Work by MZ was prepared by LLNL under contract DE-AC52-07NA27344.

SUPPLEMENTARY MATERIAL

The Supplementary Material for this article can be found online at: https://www.frontiersin.org/articles/10.3389/fmicb.2019.02224/full#supplementary-material

REFERENCES

Amy, P., Haldeman, D., Ringelberg, D., Hall, D., and Russell, C. (1992). Comparison of identification systems for classification of bacteria isolated from water and endolithic habitats within the deep subsurface. *Appl. Environ. Microbiol.* 58, 3367–3373.

Baito, K., Imai, S., Matsushita, M., Otani, M., Sato, Y., and Kimura, H. (2015). Biogas production using anaerobic groundwater containing a subterranean microbial community associated with the accretionary prism. *Microb. Biotechnol.* 8, 837–845. doi: 10.1111/1751-7915.12179

Bakermans, C., Sloup, R. E., Zarka, D. G., Tiedje, J. M., and Thomashow, M. F. (2009). Development and use of genetic system to identify genes required for efficient low-temperature growth of *Psychrobacter arcticus* 273-4. *Extremophiles* 13, 21–30. doi: 10.1007/s00792-008-0193-3

Bangerter, R. M., and Giblin, M. O. (1998). *Recompletion Report for BILBY. Nevada Environmental Restoration Project*. Springfield, VA: National Technical Information Service.

Bastin, E. S., and Greer, F. E. (1930). Additional data on sulphate-reducing bacteria in soils and waters of Illinois oil fields. *AAPG Bull.* 14, 153–159.

Belcher, W. R., Bedinger, M. S., Back, J. T., and Sweetkind, D. S. (2009). Interbasin flow in the great basin with special reference to the southern funeral mountains and the source of furnace creek springs, Death Valley, California, U.S. *J. Hydrol.* 369, 30–43. doi: 10.1016/j.jhydrol.2009.02.048

Belcher, W. R., Sweetkind, D. S., and Elliott, P. E. (2002). Probability distributions of hydraulic conductivity for the hydrogeologic units of the Death Valley regional ground-water flow system, Nevada and California. *Water Resour. Investig. Rep.* 2:4212.

Béranger, S. C., Sleep, B. E., Sherwood Lollar, B., and Brown, A. J. (2006). Isotopic fractionation of tetrachloroethene undergoing biodegradation supported by endogenous decay. *J. Environ. Eng.* 132, 725–735. doi: 10.1061/(asce)0733-9372(2006)132:7(725)

Boone, D. R., Liu, Y., Zhao, Z.-J., Balkwill, D. L., Drake, G. R., Stevens, T. O., et al. (1995). *Bacillus infernus* sp. nov., an Fe (III)-and Mn (IV)-reducing anaerobe from the deep terrestrial subsurface. *Int. J. Syst. Bacteriol.* 45, 441–448. doi: 10.1099/00207713-45-3-441

Borchardt, J. K. (1989). *Chemicals Used in Oil-Field Operations*. Houston, TX: Westhollow Research Center, Shell Development Company.

Bowen, S., Finnegan, D., Thompson, J., Miller, C., Baca, P., Olivas, L., et al. (2001). *Nevada Test Site Radionuclide Inventory, 1951-1992*. Los Alamos, NM: Los Alamos National Laboratory.

Brown, D. P., Ganova-Raeva, L., Green, B. D., Wilkinson, S. R., Young, M., and Youngman, P. (1994). Characterization of spo0A homologues in diverse *Bacillus* and Clostridium species identifies a probable DNA-binding domain. *Mol. Microbiol.* 14, 411–426. doi: 10.1111/j.1365-2958.1994.tb02176.x

Browne, H. P., Forster, S. C., Anonye, B. O., Kumar, N., Neville, B. A., Stares, M. D., et al. (2016). Culturing of 'unculturable'human microbiota reveals novel taxa and extensive sporulation. *Nature* 533:543. doi: 10.1038/nature17645

Bushmann, M., Nelson, S. T., Tingeya, D., and Eggett, D. (2010). Regional groundwater flow in structurally-complex extended terranes: an evaluation of the sources of discharge at Ash Meadows, Nevada. *J. Hydrol.* 386, 118–129. doi: 10.1016/j.jhydrol.2010.03.013

Chapelle, F. H., O'Neill, K., Bradley, P. M., Methé, B. A., Ciufo, S. A., Knobel, L. L., et al. (2002). A hydrogen-based subsurface microbial community dominated by methanogens. *Nature* 415, 312–315. doi: 10.1038/415312a

Chivian, D., Brodie, E. L., Alm, E. J., Culley, D. E., Dehal, P. S., Desantis, T. Z., et al. (2008). Environmental genomics reveals a single-species ecosystem deep within Earth. *Science* 322, 275–278. doi: 10.1126/science.1155495

Colwell, F. S., Onstott, T. C., Delwiche, M. E., Chandler, D., Fredrickson, J. K., Yao, Q. J., et al. (1997). Microorganisms from deep, high temperature sandstones: constraints on microbial colonization. *FEMS Microbiol. Rev.* 20, 425–435. doi: 10.1016/s0168-6445(97)00024-7

Costas, A. M. G., Poudel, S., Miller, A.-F., Schut, G. J., Ledbetter, R. N., Fixen, K. R., et al. (2017). Defining electron bifurcation in the electron transferring flavoprotein family. *J. Bacteriol.* 199:e0440-7. doi: 10.1128/JB.00440-17

D'Agnese, F. A., Faunt, C. C., Turner, A. K., and Hill, M. C. (1997). *Hydrogeologic Evaluation and Numerical Simulation of the Death Valley Regional Ground-Water Flow System, Nevada and California*. Denver, CO: U.S. Geological Survey.

Daumas, S., Cord-Ruwisch, R., and Garcia, J.-L. (1988). Desulfotomaculum geothermicum sp. nov., a thermophilic, fatty acid-degrading, sulfate-reducing bacterium isolated with H2 from geothermal ground water. *Antonie Van Leeuwenhoek* 54, 165–178. doi: 10.1007/bf00419203

Dorn, M., Andreesen, J., and Gottschalk, G. (1978). Fermentation of fumarate and L-malate by *Clostridium formicoaceticum*. *J. Bacteriol.* 133, 26–32.

Farnleitner, A. H., Wilhartitz, I., Ryzinska, G., Kirschner, A. K., Stadler, H., Burtscher, M. M., et al. (2005). Bacterial dynamics in spring water of alpine karst aquifers indicates the presence of stable autochthonous microbial endokarst communities. *Environ. Microbiol.* 7, 1248–1259. doi: 10.1111/j.1462-2920.2005.00810.x

Fischer, M., Hopkins, A. P., Severi, E., Hawkhead, J., Bawdon, D., Watts, A. G., et al. (2015). Tripartite ATP-independent periplasmic (TRAP) transporters use an arginine-mediated selectivity filter for high affinity substrate binding. *J. Biol. Chem.* 290, 27113–27123. doi: 10.1074/jbc.M115.656603

Fredrickson, J. K., McKinley, J. P., Bjornstad, B. N., Long, P. E., Ringelberg, D. B., White, D. C., et al. (1997). Pore-size constraints on the activity and survival of subsurface bacteria in a late Cretaceous shale-sandstone sequence, northwestern New Mexico. *Geomicrobiol. J.* 14, 183–202. doi: 10.1080/01490459709378043

Garber, M. S., and Johnson, R. H. (1967). *A Summary of Lithologic Data, Aquifer Tests, and Contruction of Hydraulic Test Well U-3cn#5, Nevada Test Site*. Denver, CO: United States Department of the Interior, Geological Survey.

Gihring, T., Moser, D., Lin, L.-H., Davidson, M., Onstott, T., Morgan, L., et al. (2006). The distribution of microbial taxa in the subsurface water of the Kalahari Shield, South Africa. *Geomicrobiol. J.* 23, 415–430. doi: 10.1080/01490450600875696

Glöckner, F. O., Yilmaz, P., Quast, C., Gerken, J., Beccati, A., Ciuprina, A., et al. (2017). 25 years of serving the community with ribosomal RNA gene reference databases and tools. *J. Biotechnol.* 261, 169–176. doi: 10.1016/j.jbiotec.2017.06.1198

Gold, T. (1992). The deep, hot biosphere. *Proc. Natl. Acad. Sci. U.S.A.* 89, 6045–6049.

Grayson, D. K. (2011). *The Great Basin: A Natural Prehistory*. Berkeley, CA: University of California Press.

Haldeman, D., and Amy, P. (1993). Bacterial heterogeneity in deep subsurface tunnels at Rainier Mesa, Nevada Test Site. *Microb. Ecol.* 25, 183–194. doi: 10.1007/BF00177194

Haldeman, D. L., Amy, P. S., Ringelberg, D., and White, D. C. (1993). Characterization of the microbiology within a 21 m 3 section of rock from the deep subsurface. *Microb. Ecol.* 26, 145–159. doi: 10.1007/BF00177049

Hohnstock-Ashe, A., Plummer, S., Yager, R., Baveye, P., and Madsen, E. (2001). Further biogeochemical characterization of a trichloroethene-contaminated fractured dolomite aquifer: electron source and microbial communities involved in reductive dechlorination. *Environ. Sci. Technol.* 35, 4449–4456. doi: 10.1021/es0110067

Imachi, H., Sakai, S., Ohashi, A., Harada, H., Hanada, S., Kamagata, Y., et al. (2007). *Pelotomaculum propionicicum* sp nov., an anaerobic, mesophilic, obligately syntrophic propionate-oxidizing bacterium. *Int. J. Syst. Evol. Microbiol.* 57, 1487–1492. doi: 10.1099/ijs.0.64925-0

Imachi, H., Sekiguchi, Y., Kamagata, Y., Hanada, S., Ohashi, A., and Harada, H. (2002). *Pelotomaculum thermopropionicum* gen. nov., sp nov., an anaerobic, thermophilic, syntrophic propionate-oxidizing bacterium. Int. J. Syst. Evol. Microbiol. 52, 1729–1735. doi: 10.1099/ijs.0.02212-0

Jorgensen, B. B. (2012). Shrinking majority of the deep biosphere. *Proc. Natl. Acad. Sci. U.S.A.* 109, 15976–15977. doi: 10.1073/pnas.1213639109

Juteau, P., Côté, V., Duckett, M.-F., Beaudet, R., Lépine, F., Villemur, R., et al. (2005). *Cryptanaerobacter phenolicus* gen. nov., sp. nov., an anaerobe that transforms phenol into benzoate via 4-hydroxybenzoate. *Int. J. Syst. Evol. Microbiol.* 55, 245–250. doi: 10.1099/ijs.0.02914-0

Kampfer, P., and Kroppenstedt, R. M. (1996). Numerical analysis of fatty acid patterns of coryneform bacteria and related taxa. *Can. J. Microbiol.* 42, 989–1005. doi: 10.1139/m96-128

Kang, M., and Jackson, R. B. (2016). Salinity of deep groundwater in California: water quantity, quality, and protection. *Proc. Natl. Acad. Sci. U.S.A.* 113, 7768–7773. doi: 10.1073/pnas.1600400113

Kelly, D. J., and Thomas, G. H. (2001). The tripartite ATP-independent periplasmic (TRAP) transporters of bacteria and archaea. *FEMS Microbiol. Rev.* 25, 405–424. doi: 10.1016/s0168-6445(01)00061-4

Kieft, T. L., Kovacik, W., Ringelberg, D. B., White, D. C., Haldeman, D. L., Amy, P. S., et al. (1997). Factors limiting microbial growth and activity at a proposed high-level nuclear repository, yucca mountain, nevada. *Appl. Environ. Microbiol.* 63, 3128–3133.

Kjeldsen, K. U., Kjellerup, B. V., Egli, K., Frolund, B., Nielsen, P. H., and Ingvorsen, K. (2007). Phylogenetic and functional diversity of bacteria in biofilms from metal surfaces of an alkaline district heating system. *FEMS Microbiol. Ecol.* 61, 384–397. doi: 10.1111/j.1574-6941.2006.00255.x

Kotelnikova, S., and Pedersen, K. (1997). Evidence for methanogenic Archaea and homoacetogenic Bacteria in deep granitic rock aquifers. *FEMS Microbiol. Rev.* 20, 339–349. doi: 10.1016/s0168-6445(97)00016-8

Krumholz, L. R., McKinley, J. P., Ulrich, G. A., and Suflita, J. M. (1997). Confined subsurface microbial communities in Cretaceous rock. *Nature* 386, 64–66. doi: 10.1038/386064a0

Kuever, J., Rainey, F. A., and Hippe, H. (1999). Description of *Desulfotomaculum* sp Groll as Desulfotomaculum gibsoniae sp nov. *Int. J. Syst. Bacteriol.* 49, 1801–1808. doi: 10.1099/00207713-49-4-1801

Lane, D. J. (1991). "16S/23S rRNA Sequencing," in *Nucleic Acid Techniques in Bacterial Systematics*, eds E. Stackebrandt, and M. Goodfellow, (Hoboken, NJ: John Wiley and Sons).

Lau, M. C., Cameron, C., Magnabosco, C., Brown, C. T., Schilkey, F., Grim, S., et al. (2014). Phylogeny and phylogeography of functional genes shared among seven terrestrial subsurface metagenomes reveal N-cycling and microbial evolutionary relationships. *Front. Microbiol.* 5:531. doi: 10.3389/fmicb.2014.00531

Lehman, R. M., Roberto, F. F., Earley, D., Bruhn, D. F., Brink, S. E., O'Connell, S. P., et al. (2001). Attached and unattached bacterial communities in a 120-meter corehole in an acidic, crystalline rock aquifer. *Appl. Environ. Microbiol.* 67, 2095–2106. doi: 10.1128/aem.67.5.2095-2106.2001

Lin, L.-H., Hall, J., Onstott, T., Gihring, T., Lollar, B. S., Boice, E., et al. (2006). Planktonic microbial communities associated with fracture-derived groundwater in a deep gold mine of South Africa. *Geomicrobiol. J.* 23, 475–497. doi: 10.1080/01490450600875829

Magnabosco, C., Lin, L.-H., Dong, H., Bomberg, M., Ghiorse, W., Stan-Lotter, H., et al. (2018). The biomass and biodiversity of the continental subsurface. *Nat. Geosci.* 11, 707–717. doi: 10.1038/s41561-018-0221-6

Markowitz, V. M., Chen, I. M., Palaniappan, K., Chu, K., Szeto, E., Pillay, M., et al. (2014). IMG 4 version of the integrated microbial genomes comparative analysis system. *Nucleic Acids Res.* 42, D560–D567. doi: 10.1093/nar/gkt963

Marreiros, B. C., Batista, A. P., Duarte, A. M., and Pereira, M. M. (2013). A missing link between complex I and group 4 membrane-bound [NiFe] hydrogenases. *Biochim. Biophys. Acta* 1827, 198–209. doi: 10.1016/j.bbabio.2012.09.012

McMahon, S., and Parnell, J. (2014). Weighing the deep continental biosphere. *FEMS Microbiol. Ecol.* 87, 113–120. doi: 10.1111/1574-6941.12196

Miller, T. L., and Wolin, M. J. (1974). A serum bottle modification of the Hungate technique for cultivating obligate anaerobes. *Appl. Microbiol.* 27, 985–987.

Morris, R. M., Rappé, M. S., Connon, S. A., Vergin, K. L., Siebold, W. A., Carlson, C. A., et al. (2002). SAR11 clade dominates ocean surface bacterioplankton communities. *Nature* 420, 806–810. doi: 10.1038/nature01240

Moser, D. P., Gihring, T. M., Brockman, F. J., Fredrickson, J. K., Balkwill, D. L., Dollhopf, M. E., et al. (2005). *Desulfotomaculum* and *Methanobacterium* spp. *dominate* a 4- to 5-kilometer-deep fault. *Appl. Environ. Microbiol.* 71, 8773–8783.

Mulligan, C., Fischer, M., and Thomas, G. H. (2011). Tripartite ATP-independent periplasmic (TRAP) transporters in bacteria and archaea. *FEMS Microbiol. Rev.* 35, 68–86. doi: 10.1111/j.1574-6976.2010.00236.x

Nielsen, M. B., Kjeldsen, K. U., and Ingvorsen, K. (2006). *Desulfitibacter alkalitolerans* gen. nov., sp nov., an anaerobic, alkalitolerant, sulfite-reducing bacterium isolated from a district heating plant. *Int. J. Syst. Evol. Microbiol.* 56, 2831–2836. doi: 10.1099/ijs.0.64356-0

Nilsen, R. K., Torsvik, T., and Lien, T. (1996). Desulfotomaculum thermocisternum sp. nov., a sulfate reducer isolated from a hot North Sea oil reservoir. *Int. J. Syst. Bacteriol.* 46, 397–402. doi: 10.1099/00207713-46-2-397

Nisman, B. (1954). The stickland reaction. *Bacteriol. Rev.* 18:16.

Osburn, M. R., LaRowe, D. E., Momper, L. M., and Amend, J. P. (2014). Chemolithotrophy in the continental deep subsurface: sanford underground research facility (SURF), USA. *Front. Microbiol.* 5:610. doi: 10.3389/fmicb.2014.00610

Park, J., Sanford, R. A., and Bethke, C. M. (2009). Microbial activity and chemical weathering in the Middendorf aquifer, South Carolina. *Chem. Geol.* 258, 232–241. doi: 10.1016/j.chemgeo.2008.10.011

Pedersen, K., and Ekendahl, S. (1990). Distribution and activity of bacteria in deep granitic groundwaters of southeastern Sweden. *Microb. Ecol.* 20, 37–52. doi: 10.1007/BF02543865

Pfiffner, S. M., Cantu, J. M., Smithgall, A., Peacock, A. D., White, D. C., Moser, D. P., et al. (2006). Deep subsurface microbial biomass and community structure in Witwatersrand Basin mines. *Geomicrobiol. J.* 23, 431–442. doi: 10.1080/01490450600875712

Puspita, I. D., Kamagata, Y., Tanaka, M., Asano, K., and Nakatsu, C. H. (2012). Are uncultivated bacteria really uncultivable? *Microbes Environ.* 27, 356–366. doi: 10.1264/jsme2.me12092

Qiu, Y.-L., Sekiguchi, Y., Hanada, S., Imachi, H., Tseng, I.-C., Cheng, S.-S., et al. (2006). *Pelotomaculum terephthalicum* sp. nov. and *Pelotomaculum isophthalicum* sp. nov.: two anaerobic bacteria that degrade phthalate isomers in syntrophic association with hydrogenotrophic methanogens. *Arch. Microbiol.* 185, 172–182. doi: 10.1007/s00203-005-0081-5

Rabus, R., Jack, D. L., Kelly, D. J., and Saier, M. H. Jr. (1999). TRAP transporters: an ancient family of extracytoplasmic solute-receptor-dependent secondary active transporters. *Microbiology* 145, 3431–3445. doi: 10.1099/00221287-145-12-3431

Ravot, G., Magot, M., Fardeau, M.-L., Patel, B., Prensier, G., Egan, A., et al. (1995). *Thermotoga elfii* sp. nov., a novel thermophilic bacterium from an African oil-producing well. *Int. J. Syst. Bacteriol.* 45, 308–314. doi: 10.1099/00207713-45-2-308

Sackett, J. D. (2018). *Prokaryotic Diversity and Aqueous Geochemistry of Subsurface Environments of the Death Valley Regional Flow System*. Ph.D. thesis, University of Nevada Las Vegas, Nevada.

Sambrook, J., and Russell, D. W. (2001). *Molecular Cloning: A Laboratory Manual*. Cold Spring Harbor, NY: Cold Spring Harbor Laboratory Press.

Sasser, M. (2001). *MIDI Technical Note #101: Bacterial Identification by Gas Chromatographic Analysis of Fatty Acids Methyl Esters (GC-FAME)*. Newark, DE: MIDI, Inc.

Schut, G. J., Zadvornyy, O., Wu, C.-H., Peters, J. W., Boyd, E. S., and Adams, M. W. (2016). The role of geochemistry and energetics in the evolution of modern respiratory complexes from a proton-reducing ancestor. *Biochim. Biophys. Acta* 1857, 958–970. doi: 10.1016/j.bbabio.2016.01.010

Stevens, T. O., and McKinley, J. P. (1995). Lithoautotrophic microbial ecosystems in deep basalt aquifers. *Science* 270, 450–455. doi: 10.1038/s41467-017-01288-8

Takai, K., Moser, D. P., DeFlaun, M., Onstott, T. C., and Fredrickson, J. K. (2001). Archaeal diversity in waters from deep South African gold mines. *Appl. Environ. Microbiol.* 67, 5750–5760. doi: 10.1128/aem.67.21.5750-5760.2001

Tamura, K., Peterson, D., Peterson, N., Stecher, G., Nei, M., and Kumar, S. (2011). MEGA5: molecular evolutionary genetics analysis using maximum likelihood, evolutionary distance, and maximum parsimony methods. *Mol. Biol. Evol.* 28, 2731–2739. doi: 10.1093/molbev/msr121

Thauer, R. K., Jungermann, K., and Decker, K. (1977). Energy conservation in chemotrophic anaerobic bacteria. *Bacteriol. Rev.* 41, 100–180.

Thomas, J. M., Moser, D. P., Fisher, J. C., Reihle, J., Wheatley, A., Hershey, R. L., et al. (2013). Using water chemistry, isotopes and microbiology to evaluate groundwater sources, flow paths and geochemical reactions in the death valley flow system, USA. *Proc. Earth Planet. Sci.* 7, 842–845. doi: 10.1016/j.proeps.2013.03.033

Thompson, J. (1999). *Laboratory and Field Studies Related to Radionuclide Migration at the Nevada Test Site*. Los Alamos, MN: Los Alamos National Laboratory.

Weisburg, W. G., Barns, S. M., Pelletier, D. A., and Lane, D. J. (1991). 16s ribosomal DNA amplification for phylogenetic study. *J. Bacteriol.* 173, 697–703. doi: 10.1128/jb.173.2.697-703.1991

Whitman, W. B., Coleman, D. C., and Wiebe, W. J. (1998). Prokaryotes: the unseen majority. *Proc. Natl. Acad. Sci. U.S.A.* 95, 6578–6583. doi: 10.1073/pnas.95.12.6578

Winograd, I. J., Fridrich, C. J., Sweetkind, D., Belcher, W. R., and Thomas, J. M. (2005). Comment on testing the interbasin flow hypothesis at Death Valley, California. *EOS Trans. Am. Geophys. Union* 86, 295–296.

Winograd, I. J., and Pearson, F. (1976). Major carbon 14 anomaly in a regional carbonate aquifer: possible evidence for megascale channeling, south central Great Basin. *Water Resour. Res.* 12, 1125–1143. doi: 10.1029/wr012i006p01125

Winograd, I. J., and Thordarson, W. (1975). *Hydrogeologic and Hydrochemical Framework, South-Central Great Basin, Nevada-California, With Special Reference to the Nevada Test Site*, USGS Professional Paper 712-C.

Yarza, P., Yilmaz, P., Pruesse, E., Glockner, F. O., Ludwig, W., Schleifer, K. H., et al. (2014). Uniting the classification of cultured and uncultured bacteria

and archaea using 16S rRNA gene sequences. *Nat. Rev. Microbiol.* 12, 635–645. doi: 10.1038/nrmicro3330

Ye, M., Pohlmann, K. F., and Chapman, J. B. (2008). Expert elicitation of recharge model probabilities for the Death Valley regional flow system. *J. Hydrol.* 354, 102–115. doi: 10.1016/j.jhydrol.2008.03.001

Yu, H., Wu, C.-H., Schut, G. J., Haja, D. K., Zhao, G., Peters, J. W., et al. (2018). Structure of an ancient respiratory system. *Cell* 173, 1636–1649.e16. doi: 10.1016/j.cell.2018.03.071

Zavarin, M. (2014). *Yields and Cavity Radii of Underground Nuclear Tests with Specified Yields Reported in DOE/NV–209-REV 15 (2000)*. Livermore, CA: Lawrence Livermore National Laboratory.

Conflict of Interest: The authors declare that the research was conducted in the absence of any commercial or financial relationships that could be construed as a potential conflict of interest.

frontiers in Microbiology

ORIGINAL RESEARCH
published: 11 October 2019
doi: 10.3389/fmicb.2019.02312

Over-Expression of UV-Damage DNA Repair Genes and Ribonucleic Acid Persistence Contribute to the Resilience of Dried Biofilms of the Desert Cyanobacetrium *Chroococcidiopsis* Exposed to Mars-Like UV Flux and Long-Term Desiccation

*Claudia Mosca[1], Lynn J. Rothschild[2], Alessandro Napoli[1], Fabrizio Ferré[3], Marco Pietrosanto[1], Claudia Fagliarone[1], Mickael Baqué[4], Elke Rabbow[5], Petra Rettberg[5] and Daniela Billi[1]**

[1]Department of Biology, University of Rome Tor Vergata, Rome, Italy, [2]Earth Sciences Division, NASA Ames Research Center, Mountain View, CA, United States, [3]Department of Pharmacy and Biotechnology, University of Bologna Alma Mater, Bologna, Italy, [4]Astrobiological Laboratories Research Group, German Aerospace Center, Institute of Planetary Research, Management and Infrastructure, Berlin, Germany, [5]German Aerospace Center, Institute of Aerospace Medicine, Cologne, Germany

The survival limits of the desert cyanobacterium *Chroococcidiopsis* were challenged by rewetting dried biofilms and dried biofilms exposed to 1.5 × 10^3 kJ/m^2 of a Mars-like UV, after 7 years of air-dried storage. PCR-stop assays revealed the presence of DNA lesions in dried biofilms and an increased accumulation in dried-UV-irradiated biofilms. Different types and/or amounts of DNA lesions were highlighted by a different expression of *uvrA, uvrB, uvrC, phrA,* and *uvsE* genes in dried-rewetted biofilms and dried-UV-irradiated-rewetted biofilms, after rehydration for 30 and 60 min. The up-regulation in dried-rewetted biofilms of *uvsE* gene encoding an UV damage endonuclease, suggested that UV-damage DNA repair contributed to the repair of desiccation-induced damage. While the *phrA* gene encoding a photolyase was up-regulated only in dried-UV-irradiated-rewetted biofilms. Nucleotide excision repair genes were over-expressed in dried-rewetted biofilms and dried-UV-irradiated-rewetted biofilms, with *uvrC* gene showing the highest increase in dried-UV-irradiated-rewetted biofilms. Dried biofilms preserved intact mRNAs (at least of the investigated genes) and 16S ribosomal RNA that the persistence of the ribosome machinery and mRNAs might have played a key role in the early phase recovery. Results have implications for the search of extra-terrestrial life by contributing to the definition of habitability of astrobiologically relevant targets such as Mars or planets orbiting around other stars.

Keywords: habitability and astrobiology, anhydrobiosis, desert cyanobacteria, Mars UV simulation, DNA repair

OPEN ACCESS

Edited by:
Akihiko Yamagishi, Tokyo University of Pharmacy and Life Sciences, Japan

Reviewed by:
Issay Narumi, Toyo University, Japan
Tatiana A. Vishnivetskaya, The University of Tennessee, Knoxville, United States
Virginia Helena Albarracín, Center for Electron Microscopy (CIME), Argentina

****Correspondence:***
Daniela Billi
billi@uniroma2.it

Specialty section:
This article was submitted to Extreme Microbiology, a section of the journal Frontiers in Microbiology

Received: *10 March 2019*
Accepted: *23 September 2019*
Published: *11 October 2019*

Citation:
Mosca C, Rothschild LJ, Napoli A, Ferré F, Pietrosanto M, Fagliarone C, Baqué M, Rabbow E, Rettberg P and Billi D (2019) Over-Expression of UV-Damage DNA Repair Genes and Ribonucleic Acid Persistence Contribute to the Resilience of Dried Biofilms of the Desert Cyanobacetrium Chroococcidiopsis Exposed to Mars-Like UV Flux and Long-Term Desiccation. Front. Microbiol. 10:2312. doi: 10.3389/fmicb.2019.02312

INTRODUCTION

Our knowledge of the limit of life's adaptability to extreme environments is mandatory for identifying habitable planets and moons in the Solar System and planetary systems orbiting around other stars (Schulze-Makuch et al., 2017). Dryness is one of the main factors threatening life since water removal causes membrane phase transition and production of reactive oxygen species that cause lipid peroxidation; this leads to protein oxidation and DNA damage, which are lethal to the majority of the organisms (França et al., 2007). Nevertheless, a few organisms called anhydrobiotes, survive desiccation by stabilizing their sub-cellular structures and entering a metabolic dormancy until water is available again (Crowe et al., 1992). As a by-product of desiccation tolerance, anhydrobiotes are also radiation tolerant, being able to cope with high doses of UV and ionizing radiation that are not present in nature (Cox and Battista, 2005).

Despite the interest in anhydrobiotes, it is not yet known how long they can persist in the air-dried state and which levels of radiation doses they can experience without dying. Knowing their desiccation endurance threshold is relevant to understanding not only the limits of life on Earth but also to assessing the potential habitability of astrobiologically relevant targets such as Mars and rocky exoplanets with transient availability of liquid water (Wilhelm et al., 2018). In addition, the identification of their UV resistance threshold has implications when tackling the surface habitability of rocky planets with elevated UV radiation fluxes (O'Malley-James and Kaltenegger, 2017).

Anhydrobiotic cyanobacteria of the genus *Chroococcidiopsis* possess a remarkable resistance to desiccation and radiation that has extended the limits of life, as we know it, in several new directions. *Chroococcidiopsis* sp. CCMEE 029 isolated from the Negev Desert survived 4 years of air-drying on the top of polycarbonate filters or spotted on Petri dishes (Billi, 2009; Fagliarone et al., 2017) and 13 years on desiccated agar (Cockell et al., 2017). When dried, *Chroococcidiopsis* sp. CCMEE 029 withstood up to 24 kGy of γ-radiation (Verseux et al., 2017), whereas dried monolayers could cope with 15 kJ/m^2 of a Mars-like UV flux (Cockell et al., 2005). This resistance was further extended by the survival of dried biofilms exposed to 1.5×10^3 kJ/m^2 of a Mars-like UV flux (Baqué et al., 2013). The exposure of microbial biofilms to Mars-like conditions was carried out during ground-based simulations performed in the context of the Biofilm Organisms Surfing Space (BOSS) project. This project aimed to assess whether biofilms are better suited than planktonic counterparts to cope with space and Mars-like conditions by taking advantage of the exposure to low Earth orbit conditions outside the International Space Station (Rabbow et al., 2017). The survival of dried *Chroococcidiopsis* biofilms exposed to 1.5×10^3 kJ/m^2 of a Mars-like flux was previously ascribed to the shielding provided to the bottom-layer cells by the top-layer cells, killed by the UV radiation, and to abundant extracellular *exopolysaccharides* (Baqué et al., 2013).

However, several aspects of the desiccation and radiation tolerance of desert strains of *Chroococcidiopsis* remain poorly characterized. For instance, it is not known whether dried cells irradiated with high radiation doses can recover when rewetted after prolonged desiccation. The survival of dried biofilms of *Chroococcidiopsis* sp. CCMEE 029 exposed to 1.5×10^3 kJ/m^2 of a Mars-like UV flux was reported soon after the ground-based simulation (Baqué et al., 2013); while their survival after exposure to Mars-like simulations in low Earth orbit was assessed on 2.5-year-old samples, due to the EXPOSE-R2 space mission duration, e.g., about 900 days from launch to sample return to the lab (Billi et al., 2019a).

In the present work, the survival limits of *Chroococcidiopsis* sp. CCMEE 029 were challenged by rewetting dried biofilms and dried biofilms exposed to 1.5×10^3 kJ/m^2 of a Mars-like UV after 7 years of air-dried storage. The presence of DNA lesions was evaluated by means of polymerase chain reaction (PCR)-stop assay. Viability was tested by assessing the capability of entering cell division and by staining with a redox dye after rehydration. An *in silico* survey of the genome was performed to search for genes encoding proteins involved in photoreactivation, nucleotide excision repair, and UV damage endonuclease (UvsE)-dependent excision repair, that are known to be associated with UV-induced DNA damage repair (Goosen and Moolenaar, 2008). The role of the identified UV-damage repair genes in the early phase recovery of dried-UV-irradiated biofilms and dried biofilms was investigated by real-time quantitative polymerase chain reaction (RT-qPCR) performed after 30 and 60 min of rehydration.

MATERIALS AND METHODS

Organism and Culture Conditions

Chroococcidiopsis sp. CCMEE 029 (hereafter *Chroococcidiopsis*) was isolated by Roseli Ocampo-Friedmann from cryptoendolithic growth in sandstone in the Negev Desert (Israel) and is now maintained at the University of Rome Tor Vergata, as part of the Culture Collection of Microorganisms from Extreme Environments (CCMEE) established by E. Imre Friedmann. *Chroococcidiopsis* sp. CCMEE 029 was reported to be not axenic (Billi et al., 1998), although routinely, colony transfers reduced the bacterial contamination to about 0.0001% (Billi et al., 2019b). Cultures were routinely grown in BG-11 medium (Rippka et al., 1979) at 25°C, under a photon flux density of 40 μmol/m^2 s^1 provided by fluorescent cool-white bulbs.

Desiccation, Mars-Like UV Irradiation, and Rehydration

Biofilms were obtained by growing *Chroococcidiopsis* cells on top of BG-11 agarized medium in Petri dishes sealed with Parafilm. After 2 months of growth, the Parafilm was removed and biofilms were allowed to air-dry for about 15 days. Finally 12-mm-in-diameter disks were cut out of biofilms and shipped to the Planetary and Space Simulation facilities (PSI) at the Radiation Biology Department of the Institute of Aerospace Medicine/Microgravity User Support Center (DLR Cologne, Germany). Samples in triplicates were integrated in the DLR 16-well aluminum sample carriers and exposed to solar simulator SOL2000 with a fluence of 1,370 W/m^2 in the 200- to 400-nm wavelength range (Rabbow et al., 2016). Dried biofilms were

irradiated with a dose of 1.5×10^3 kJ/m^2 obtained in 18 min of exposure, and then kept in the dark at room temperature until sent back to Tor Vergata University for analysis. Part of these samples were previously analyzed in the context of the Biofilm Organisms Surfing Space experiment (Baqué et al., 2013), the remaining samples were stored in the laboratory sealed in plastic envelopes, in the dark and at room temperature.

After 7 years of air-dried storage, the following analyses were performed: (1) cell morphology of dried biofilms and dried-UV-irradiated biofilms was evaluated by confocal laser scanning microscopy (CLSM), using liquid cultures as control; (2) viability of dried biofilms and dried-UV-irradiated biofilms was tested by assessing their capability of entering cell division and by staining with a redox dye after rewetting; (3) gene expression was evaluated in dried-rewetted biofilms after 30 and 60 min of rehydration, by using dried biofilms (0-min recovery) as control; (4) gene expression was evaluated in dried-UV-irradiated biofilms after 30 and 60 min of rehydration, by using as control dried-rewetted biofilms at the same rehydration time; and (5) DNA damage was quantified in dried biofilms and dried-UV-irradiated biofilms by performing PCR-stop assays; liquid cultures were used a control. A schematic experimental plan is shown in **Figure 1**.

Cell Morphology and Viability

Cells from dried biofilms and dried-UV-irradiated biofilms were observed with a CLSM (Olympus Fluoview 1,000 Confocal Laser Scanning System). Images were taken using a 60× objective and photosynthetic pigment autofluorescence was investigated by exciting the cells with a 543- and a 635-nm laser and collecting the emission from 645-nm, or from 553-nm, to 800-nm emission range.

Viability was assessed: (1) by inoculating biofilm fragments (about 25 mm^2) into 2 ml of liquid BG-11 medium and measuring cell densities with a spectrophotometer after 3 months of growth under routine conditions and (2) by staining with 2-(4-Iodophenyl)-3-(4-nitrophenyl)-5-phenyl tetrazolium chloride (Sigma Aldrich, Saint Louis, MO, USA) after rehydration for 30 min, 60 min, and 72 h, as previously reported (Billi, 2009).

Genomic DNA Extraction and Damage Evaluation by Polymerase Chain Reaction-Stop Assay

Genomic DNA was extracted by using a method developed to reduce bacterial contamination and based on lysozyme treatment, osmotic shock, and DNase I treatment, while *Chroococcidiopsis* lysis, due to its lysozyme resistance, is achieved by adding hot phenol and glass beads (Billi et al., 1998). Here lysozyme and DNase I steps were avoided because PCR-stop assays were performed by using *Chroococcidiopsis*-specific primers.

The extracted DNA was quantified by using the NanoDrop Lite Spectrophotometer (Thermo Fisher Scientific, Waltham, MA, USA) and 6 ng were used in 12-µl PCR reaction mixtures as follows:

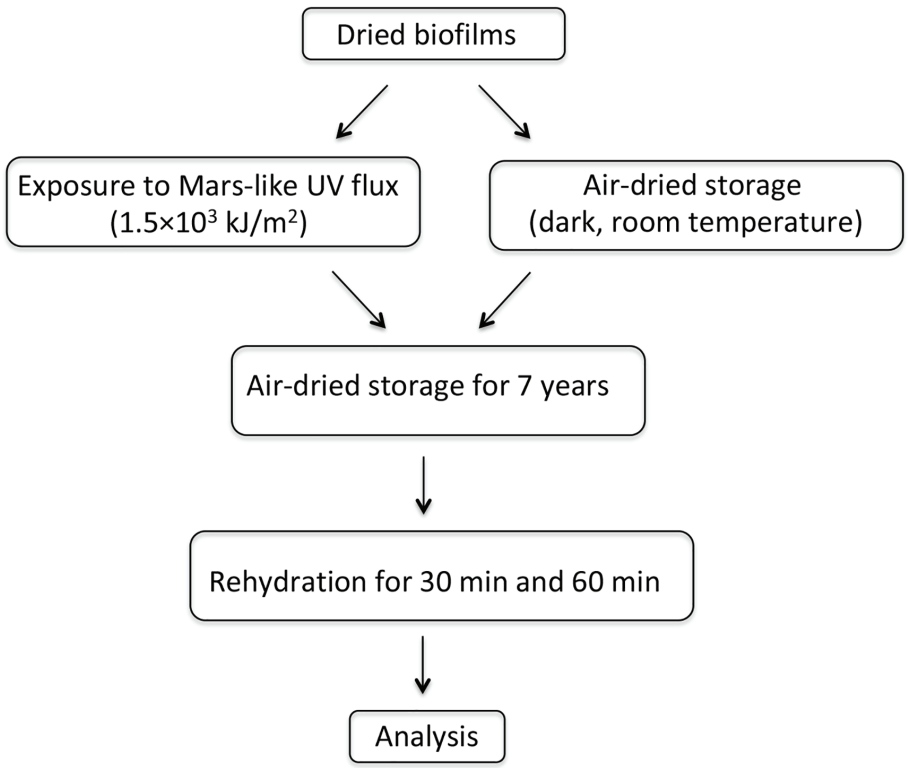

FIGURE 1 | Experimental scheme.

Short-Fragment Polymerase Chain Reaction Amplification

A 1,027-bp fragment of the 16S rRNA gene was amplified by using 0.5 μM each (final concentration) of primers CYA-359F (5′-GGGGAATTTTCCGCAATGG-3′) and CRev (5′-ACGGGCGGTGTGTAC-3′), and 6 μl of MyTaq™ Red Mix (Bioline Meridian Life Science, Memphis, TN, USA). PCR conditions were as follows: 94°C for 3 min; 35 cycles of 94°C for 1 min, 45°C for 1 min, and 72°C for 3 min; and 7 min at 72°C.

Long-Fragment Polymerase Chain Reaction Amplification

A 4-kbp genome fragment was amplified using 0.5 μM each (final concentration) of primers Chroo-4 K-2-F (5′-GCTAC TCGTTGCTTTGCGTC-3′) and Chroo-4 K-2-R (5′-TTCCCCAT ACTTTGCTTCCCA-3′), and 6 μl of High-Fidelity Master Mix (Thermo Fisher Scientific, Waltham, MA, USA). PCR conditions were as follows: 98°C for 3 min; 30 cycles of 98°C for 30 s, 65°C for 1 min, and 72°C for 2 min; and 7 min at 72°C.

Each one of the 12-μl PCR reaction mixtures was loaded onto 1.5% agarose gel containing 0.5 mg/ml ethidium bromide, subjected to electrophoresis for about 1 h at 90 V, and visualized with a trans-illuminator.

Real-Time Quantitative Polymerase Chain Reaction

A 1,027-bp fragment of the 16S rRNA was amplified in 25-μl reaction mixtures containing DNA template (5 ng), 12.5 μl of qPCR cocktail (iQ SYBR Green Supermix, Bio-Rad Laboratories, Hercules, CA, USA), and 0.5 μM (final concentration) of primers 16SF (5′-GGGGAATTTTCCGCAATGGGCG AAAGCCTGACG GAG-3′) and 16SR (5′-CGGGCGGTGTGTACAAGGCCCGGG AACGTATTCACC-3′). A real-time PCR detection system (iQ5, Bio-Rad Laboratories, Hercules, CA, USA) was programmed to operate as described (Baqué et al., 2013). PCR protocols were carried out performing $n \geq 3$ replicates.

Identification UV-Induced DNA Repair Genes

Genomic DNA extracted from liquid cultures as previously described (Billi et al., 1998) was sequenced by using Illumina Solexa technology (CD Genomics NY USA), obtaining around 1.7 M 300×2 paired-end reads. After quality control (by using FastQC, https://www.bioinformatics.babraham.ac.uk/projects/fastqc/), reads were trimmed and adapter sequences removed, by using Trimmomatic (Bolger et al., 2014) with parameters LEADING:20, TRAILING:20, AVGQUAL:28, MINLEN:25. Then, trimmed reads were checked for contaminants by using BLAST against the NCBI nt database, and discarding all reads having a significant match (coverage > 80%, e-value < 10^{-4}) with species other than Cyanobacteria. Surviving reads were assembled using Velvet version 1.2.10, a *de novo* assembler for next-generation sequencing data that employ de Bruijn graphs, with the following parameters: K-mer length 181, expected coverage (exp_cov) 8, and coverage cutoff (cov_cutoff) 7. The obtained contig genomic sequences were annotated using Prokka (Seemann, 2014), a prokaryotic gene annotator, using the interface provided by the Galaxy-based framework Orione (Cuccuru et al., 2014)[1], by setting the following parameters: similarity e-value cutoff 1e-06, minimum contig size 200, and using the pre-set for improving gene predictions for highly fragmented genomes.

RNA Extraction and Real-Time Quantitative Polymerase Chain Reaction

Total RNA was extracted by using 1 ml of TRI Reagent (Sigma Aldrich, Saint Louis, MO, USA) and treatment with RQ1 RNase-Free DNase I (Promega Corporation, Madison, WI, USA) according to the manufacturer's instructions. Then, 0.5 μg of total RNA extracted from each sample was retrotranscribed to single strand cDNA by using the SensiFAST™ cDNA Synthesis Kit (Bioline Meridian Life Science, Memphis, TN, USA). Real-time reactions were performed in a total volume of 20 μl, including 1 μg of cDNA template, 400 nM of appropriate primer (**Table 1**), and 10 μl of iTaqTM Universal SYBR Green Supermix (BioRad Laboratories, Hercules, CA, USA). PCR cycling conditions were performed in a LightCycler 480 (Roche Diagnostics International, Rotkreuz, Switzerland) as follows: a cycle of 95°C for 30 s, then 45 cycles of 95°C for 5 s, and 60°C for 30 s, followed by a ramp from 60 to 95°C for melting curve stage. For each gene target, $n \geq 3$ qPCR reactions were conducted, each reaction in duplicate.

Relative mRNA levels were calculated by the comparative Ct method. Primer specificity was confirmed by melting curve analysis. 16S rRNA (GenBank accession number AF279107) was used as reference gene (Pinto et al., 2012). For dried-rewetted biofilms, levels of gene expression of DNA repair genes were measured after 30 and 60 min of rehydration, while 0-min recovery control was obtained from dried biofilms incubated in ice and resuspended in 1 ml of TRI Reagent (Sigma Aldrich, Saint Louis, MO, USA), as reported above. Values obtained for dried biofilms at 0-min recovery were set as 1. For dried-UV-irradiated-rewetted biofilms, levels of gene expression of DNA repair genes were measured after 30 min and 60 of rehydration, and the corresponding values of dried-rewetted biofilms were set as 1. Values were considered to be up-regulated (>1) or down-regulated (<1).

[1]https://orione.crs4.it

TABLE 1 | Primers used for RT-qPCR.

Gene	PCR primers	Sequence (5′-3′)	PCR product size (bp)
16S	chr16S-F	TACTACAATGCTACGGACAA	83
	chr16S-R	CCTGCAATCTGAACTGAG	
uvrA	chruvrA-F	ACTTAGATGTGATTCGTTGT	102
	chruvrA-R	CTACTTGCTCTGGTGTTC	
uvrB	chruvrB-F	CGATTACTATCAACCAGAAG	91
	chruvrB-R	CCGTAGCATATCAATCTCA	
uvrC	chruvrC-F	ACGGATACAGAAGCAGAA	81
	chruvrC-R	CTTGAGCAGCACATTGAA	
uvsE	chruvsE-F	TGTCCTTAGTTCTGATTCG	90
	chruvsE-R	GGTAAGCCTAACAAGTCA	
phrA	chrphrA-F	TTGGAGTAATTGGCATTCG	83

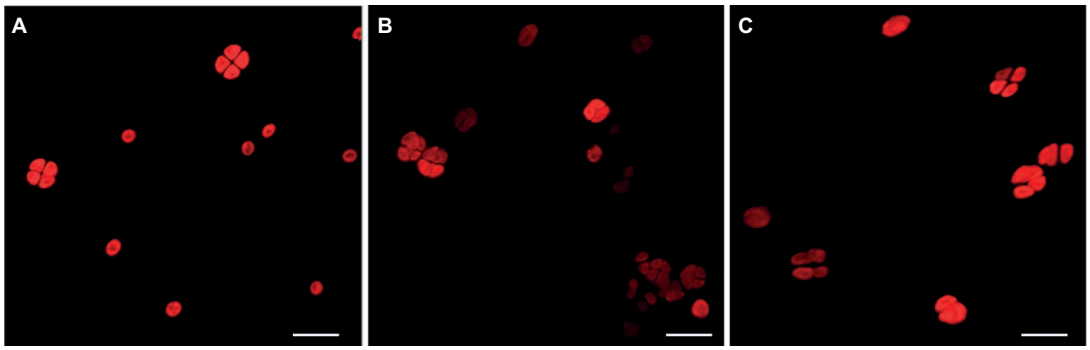

FIGURE 2 | CLSM images of photosynthetic pigment autofluorescence. Cells from liquid cultures **(A)**; dried biofilms **(B)**; and dried-UV-irradiated biofilms **(C)**. Scale bar: 10 μm.

RESULTS

Survivors Among Dried Biofilms and Dried-UV-Irradiated Biofilms

After 7 years of air-dried storage, the morphology of dried biofilms and dried-UV-irradiated biofilms (exposed to 1.5×10^3 kJ/m^2 of a Mars-like UV flux) was evaluated at the CLSM and compared to that of cells form liquid cultures used as control (**Figure 2A**). In dried biofilms (**Figure 2B**) as well as in UV-irradiated biofilms (**Figure 2C**), cells with an intense photosynthetic pigment autofluorescence (due to chlorophyll *a* and phycobiliproteins) occurred among bleached cells.

Dried-rewetted biofilms and dried-UV-irradiated-rewetted biofilms were tested for respiration by monitoring the INT reduction by dehydrogenases after 72 h of rehydration. The INT staining revealed 30 and 10% of alive cells with insoluble red formazan spots in the cytoplasm of dried-rewetted biofilms and dried-UV-irradiated-rewetted biofilms, respectively, (**Figure 3**). On the contrary, INT reduction was undetectable after 30 and 60 min of rehydration (not shown).

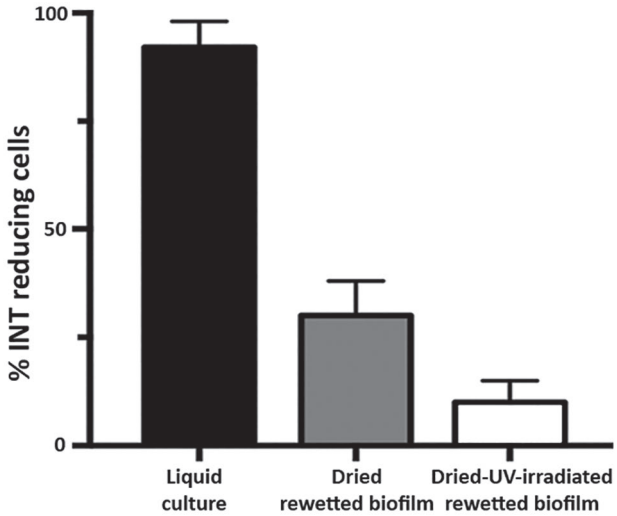

FIGURE 3 | Alive cells in dried biofilms and dried-UV-irradiated biofilms as revealed by INT reduction after 72 h of rewetting.

Increased DNA Damage in Dried-UV-Irradiated Biofilms Compared to Dried Biofilms

The presence of DNA damage in dried biofilms and in dried-UV-irradiated biofilms (exposed to 1.5×10^3 kJ/m^2 of a Mars-like UV flux) was qualitatively evaluated after 7 years of air-dried storage, by testing the genomic DNA suitability as template in PCR amplifications of short and long targets.

In dried biofilms, the 1,027-bp amplification yielded a PCR amplicon of reduced intensity (**Figure 4A**, lane 3) compared to cells from liquid cultures (**Figure 4A**, lane 2). In dried-UV-irradiated biofilms, no additional decrease in the band intensity was detected with 1,027-bp amplification (**Figure 4A**, lane 4).

The amplification of a 4-kbp fragment yielded an amplicon of reduced intensity in dried biofilms (**Figure 4B**, lane 3) compared to cells form liquid cultures (**Figure 4B**, lane 2). While the intensity of the 4-kbp amplicon from dried-UV-irradiated biofilms was slightly reduced compared to dried biofilms (**Figure 4B**, lane 4).

When genomic DNA damage was quantified by means of qPCR, by using the 1,027-bp fragment as target, a significant reduction in the amplified copy number occurred in dried biofilms compared to cells form liquid culture, while no additional reduction was detected in dried-UV-irradiated biofilms (**Figure 4C**).

Identification of UV-Damage DNA Repair Genes

The *in silico* analysis of *Chroococcidiopsis* genome identified sequences homologous to genes involved in three repair pathways of UV-induced DNA damage, namely photoreactivation, nucleotide excision repair, and UV damage endonuclease (UvsE)-dependent excision repair (**Table 2**).

The *phrA* gene has a length of 1,434 bp with the highest similarity (BlastN output: query cover 89%, e-value 0.0, total score 791, and identity 78%) to the homolog in *Scytonema* sp. HK-05 (Genbank accession number AP018194.1; 7105541-7106989), encoding a deoxyribodipyrimidine photolyase.

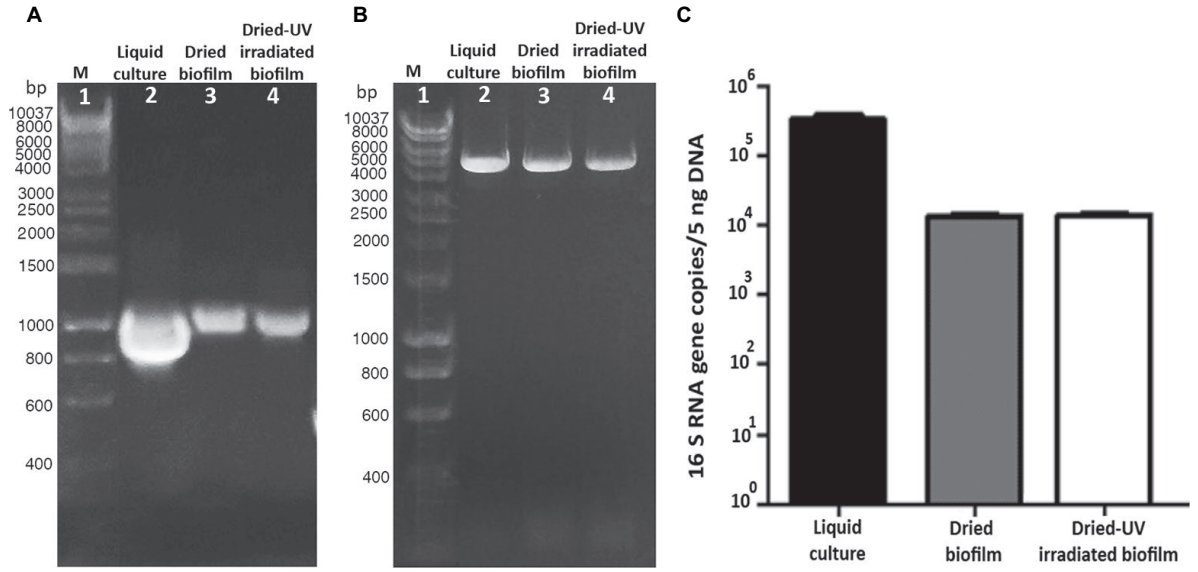

FIGURE 4 | Assessment of DNA damage in cells from liquid culture, dried-biofilm, and dried-UV-irradiated biofilm. PCR amplification of 1,027-bp fragment of the16S rRNA gene **(A)** and 4-kbp genomic fragment **(B)**; lane 2: control cells from liquid culture; lane 3: dried biofilm; lane 4: dried-UV-irradiated biofilm; lane 1: Hyperladder 1 kbp (Bioline Meridian Life Science, Memphis, TN, USA). qPCR by using as target gene a 1,027-bp fragment of the 16S rRNA gene **(C)**.

TABLE 2 | UV-induced DNA damage repair genes of *Chroococcidiopsis* sp. CCMEE 029 investigated in this study.

Gene name	Protein function	Gene length (nt)	Genbank accession number
phrA	deoxyribodipyrimidine photolyase	1,434	MK135046
uvsE	UV-damage endonuclease	981	MK135047
uvrA	UvrA, excinuclease ABC subunit A	3,033	MK135048
uvrB	UvrB, excinuclease ABC subunit B	2,004	MK135049
uvrC	UvrC, excinuclease ABC subunit C	1,923	MK135050

The *uvsE* gene with a length of 981 bp showed the highest similarity (BlastN output: query cover 87%, e-value 2e-84, total score 326, and identity 74%) to the UV endonuclease *uvdE* gene of *Cylindrospermum* sp. NIES-4074 (Genbank accession number AP018269.1), encoding a UV damage endonuclease.

The *uvrA*, *uvrB*, and *uvrC* genes of *Chroococcidiopsis* have a length of 3,033; 2,004; and 1,923 bp, respectively. The *uvrA* gene shared the highest similarity (BlastN output: query cover 52%, e-value 0.0, total score 933 and identity 77%) with the homolog in *Nostoc* sp. PCC 7524 (Genbank accession number CP003552.1), encoding the excinuclease ABC subunit A. The *uvrB* gene showed the highest similarity (BlastN output: query cover 98%, e-value 0.0, total score 1,369 and identity 79%) to the homolog in *Nostoc commune* HK-02 (Genbank accession number AP018326.1; 7094877-7096874), encoding the excinuclease ABC subunit B. The *uvrC* gene shared the highest similarity (BlastN output: query cover 96%, e-value 0.0, total score 1,062 and identity 77%) to the homolog in *Fremyella diplosiphon* NIES-3275 (Genbank accession number AP018233.1; 1447846-1449714), encoding the excinuclease ABC subunit C.

Different Expression of UV-Damage DNA Repair Genes in Dried-Rewetted Biofilms and Dried-UV-Irradiated-Rewetted Biofilms

In order to evaluate the expression of the investigated DNA repair genes in the recovery of dried-rewetted biofilms, transcript levels detected in dried biofilms (0-min recovery) were set as 1 (**Figure 5**). The *uvsE* gene was up-regulated by 2.71- and 2.91-fold after 30 and 60 min of rewetting, whereas the *phrA* gene was not up-regulated (**Figure 5A**). The *uvrA*, *uvrB*, and *uvrC* genes were up-regulated: after 30 min of rewetting, the *uvrA* and *uvrC* genes were up-regulated by 1.84- and 1.74-fold, respectively, while the *uvrB* gene was up-regulated by 2.56-fold. After 60 min of rewetting, the *uvrA*, *uvrB*, and *uvrC* genes were up-regulated by 2.63-, 5.30-, and 2.91-fold, respectively, compared to dried biofilms (0-min recovery) (**Figure 5B**).

In order to evaluate the expression of the investigated DNA repair genes in the recovery of dried-UV-irradiated-rewetted biofilms, transcript levels detected in dried-rewetted biofilms, rehydrated for the same period of time, were set as 1 (**Figure 6**). The *uvsE* gene was not up-regulated in dried-UV-irradiated-rewetted biofilms; whereas the *phrA* gene was up-regulated by 5.19- and 9.98-fold after 30 and 60 min of rewetting, respectively (**Figure 6A**). Nucleotide excision repair genes were up-regulated after 30 and 60 min of rewetting, with the highest expression of the *uvrC* gene compared to *uvrA* and *uvrB* genes. In particular, after 30 min of recovery, the *uvrA* and *uvrB* genes were up-regulated by 3.61- and 2.85-fold, respectively; these expression levels remained almost the same after 60 min of recovery (3.72- and 2.59-fold, respectively). Whereas, the *uvrC* gene was over-expressed by 4.26- and 11.12-fold after 30 and 60 min of recovery compared to dried-rewetted biofilms, at the same recovery points (**Figure 6B**).

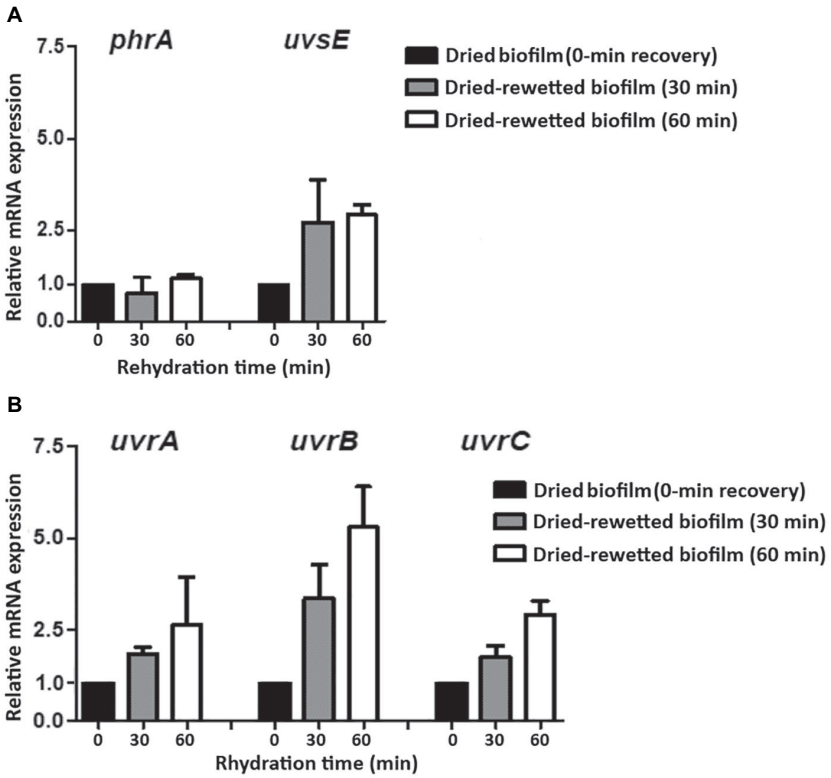

FIGURE 5 | Expression of DNA repair genes in dried-rewetted biofilm after 30 and 60 min of rehydration. Expression of the *phrA* and *uvsE* genes **(A)** and of *uvrA, uvrB*, and *uvrC* genes **(B)**. Values from dried biofilms (0-min rewetting) were considered as control values set to 1. Subsequent samples were compared in terms of fold regulation to control values.

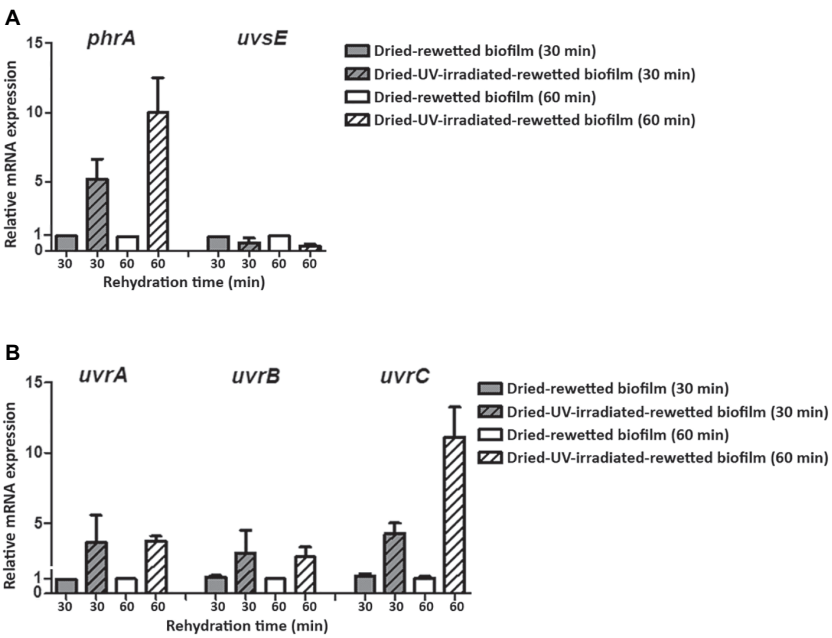

FIGURE 6 | Expression of DNA repair genes in dried-UV-irradiated-rewetted biofilm after 30 and 60 min of rehydration. Expression of *phrA* and *uvsE* gene **(A)** and of *uvrA, uvrB*, and *uvrC* genes **(B)**. Values of dried-rewetted biofilms after 30 and 60 min of rehydration were considered as control values and set to 1. Subsequent samples were compared in terms of fold regulation to control values.

DISCUSSION

Here, the desiccation and UV tolerance limits of *Chroococcidiopsis* sp. CCMEE 029 were stretched further by the recovery capability of dried biofilms and dried-UV-irradiated biofilms (exposed to 1.5×10^3 kJ/m^2 of a Mars-like UV flux) after 7 years of air-dried storage. This astonishing performance extends our knowledge of biofilm endurance, already recognized as the most successful life forms on Earth (Flemming and Wingender, 2010).

In order to unravel the mechanisms underlying such endurance, the role of both protection mechanisms taking place upon desiccation and repair mechanisms triggered upon rehydration must be taken into consideration. In fact, although *Chroococcidiopsis* adopts efficient countermeasures to avoid the otherwise lethal effects of water removal, its endurance when air-dried can be limited by the oxidative damage accumulated even in the absence of metabolic activity (Billi, 2009). In *Chroococcidiopsis* sp. CCMEE 029, the avoidance of protein oxidative damage was identified as a first line of defense against desiccation and ionizing radiation (Fagliarone et al., 2017). Indeed the degree of bacterial resistance to desiccation and radiation depends on the level of oxidative damage to proteins, including those needed to repair extensive DNA damage that prevents transcription and translation (Slade and Radman, 2011). In addition, during UV irradiation, dried cells accumulated DNA lesions, such us cyclobutane pyrimidine dimers and pyrimidine-pyrimidone (6–4) photoproducts and 8-oxo-7, 8-dihydroguanine cyclobutane pyrimidine (Goosen and Moolenaar, 2008), all of which must be repaired upon rehydration.

In the present work, the presence of DNA damage in dried biofilms and dried-UV-irradiated biofilms was evaluated after 7 years of desiccation, by testing the genome suitability as template in PCR-stop assays by using short and long PCR targets. The principle is that DNA damage inhibits PCR by impairing DNA polymerase progression (Kumar et al., 2004), while PCR targets of different lengths affect the likelihood of encountering a DNA damage, short amplicons having a lower likelihood than long amplicons (Rudi et al., 2010). The presence of DNA lesions in dried biofilms compared to cells from liquid cultures was revealed by a reduced intensity of the 1,027-bp and 4-kbp PCR band. No further reduction of the 1,027-bp PCR band intensity was detected in dried-UV-irradiated biofilms when using PCR-stop assay with the 1,027-bp target. Also, qPCR using the 1,027-bp target did not reveal any increase of the DNA damage in dried-UV-irradiated biofilms compared to dried biofilms. However, the reduced intensity of the 4,000-bp PCR band suggested an increased accumulation of DNA lesions in dried-UV-irradiated biofilms compared to dried biofilms. Anyway, the possibility to perform PCR amplifications is in agreement with the lack of genome degradation, previously reported for this cyanobacterium after 4 years of air-drying (Billi, 2009).

After 7 years of air-drying, *Chroococcidiopsis* not only avoided genome degradation but preserved at least a sub-set of mRNAs and 16S ribosomal RNA. This persistence is relevant if compared to that of desiccation-tolerant cyanobacteria dried for shorter periods. The absence of RNA fragmentation was reported for the desert cyanobacterium *Gloeocapsopsis* AAB1 desiccated for 13 days (Azua-Bustos et al., 2014), and the stable maintenance of mRNAs through dormancy was reported for Microcoleus vaginatus (Rajeev et al., 2013). Detectable ribosomal RNA and mRNAs, including abundant *sodF* mRNA, occurred in the cyanobacterium Nostoc commune dried for 3 years (Shirkey et al., 2000), while *in vitro* translation failed when using mRNA of Nostoc commune dried for 5 years (Jäger and Potts, 1988). Remarkably, a desiccation-sensitive cyanobacterium such as *Synechocystis* sp. PCC 6803 could not survive 3 months of air-dried storage (Fagliarone et al., 2017).

The presence of ribosome machinery is considered an indicator of cell viability and of a potential capability of a rapid response in a new environment conditions (Emerson et al., 2017). Alive 16S rRNA-containing cells were detected in dried biofilms of *Deinococcus geothermalis* (Frösler et al., 2017). Nucleic acid accumulation has been considered a requirement for cyanobacterial dormancy and germination (Kaplan-Levy et al., 2010). For example, *Aphanizomenon ovalisporum* akinetes showed a 10-fold increase in the volumetric ribosome content compared to vegetative cells (Sukenik et al., 2012).

In the present work, the occurrence of survivors in dried biofilms and dried-UV-irradiated biofilms was proved by growth after transfer into liquid BG-11 medium (not shown) and by INT reduction after 72 h of rewetting. These cells showed an intense autofluorescence of the photosynthetic pigments that were unable of INT reduction. Indeed after long-term (years of) desiccation, *Chroococcidiopsis* survivors were scored among dead cells that had bleached photosynthetic pigments, fragmented DNA, and degenerated ultrastructural features (Grilli Caiola, et al., 1993; Billi, 2009).

In the present work, a single-cell evaluation of the RNA content was not performed; nevertheless, the persistence of intact ribosome machinery and mRNAs might have contributed to *Chroococcidiopsis* biofilms' resuscitation from prolonged dormancy, when respiration should have already started (Scherer et al., 1984; Higo et al., 2007). Further investigation into the presence of a "dormant transcriptome" in dried *Chroococcidiopsis* should be carried out under mRNA *de novo* synthesis arrest. A synergic role might have been played by the presence in dried *Chroococcidiopsis* cells of a proteome, including DNA repair proteins, that was protected against oxidative damage (Fagliarone et al., 2017). Indeed during the first hour of *Deinococcus radiodurans*'s recovery from ionizing radiation and desiccation, most DNA repair genes were not over-expressed, possibly due to a constitutive expression, sufficient to repair DNA damage, or due to proteins of unknown function (Tanaka et al., 2004).

In *Chroococcidiopsis*, the different up-regulation of the investigated DNA repair genes during the early phase recovery of dried biofilms and dried-UV-irradiated biofilms highlighted the accumulation of different types and/or amounts of DNA lesions. It also suggested that genes involved in the repair of UV-induced damage played a key role in the recovery from desiccation.

The *phrA* gene was markedly over-expressed during the recovery of dried-UV-irradiated biofilms, supporting the relevance of the codified photolyase in repairing cyclobutane pyrimidine dimers.

By contrast, the *uvsE* gene, encoding a putative UV damage endonuclease, showed the highest over-expression during the recovery of dried biofilms. The UvsE-dependent excision repair is not common in cyanobacteria (Goosen and Moolenaar, 2008; Cassier-Chauvat et al., 2016), although its role in repairing UV-induced DNA damage was reported for *Deinococcus radiodurans* (Tanaka et al., 2005). However, since UvsE recognizes also non-UV-induced DNA damage such as abasic sites, nicks, and gaps (Meulenbroek et al., 2013), it might be involved in *Chroococcidiopsis* in repairing desiccation-induced DNA damage rather than UV-induced damage, thus reflecting a redundancy in order to counteract desiccation-induced DNA damage.

Dried-rewetted biofilms showed the up-regulation of the nucleotide excision repair genes encoding UvrA and UvrB, both involved in damage recognition and UvrC for the incision on either side of the lesions (Goosen and Moolenaar, 2008). Also, dried-UV-irradiated rewetted biofilms showed an increased expression of these genes, *uvrC* showing the highest value. A higher *uvrC* gene expression was reported for *Halococcus hamelinensis* during the first hour of UV-induced damage repair and it was suggested that *uvrA* and *uvrB* genes were constitutively expressed due to their having other roles in addition to that of DNA repair (Leuko et al., 2011). The role of the nucleotide excision repair in desiccation tolerance was highlighted in *Sinorhizobium meliloti* in which the inactivation of the *uvrA*, *uvrB*, and *uvrC* genes resulted in desiccation-sensitive mutants (Humann et al., 2009). Moreover, during the first hour of *Deinococcus radiodurans*'s recovery from ionizing radiation and desiccation *uvrA*, and *uvrB* genes were included in the 32 foci over-expressed (Tanaka et al., 2004).

The high similarity between the investigated DNA repair genes of *Chroococcidiopsis* sp. CCMEE 029 and homologs in filamentous, heterocystous cyanobacteria is in agreement with the phylogenetic analysis reporting that the unicellular non-heterocyst-differentiating genus *Chroococcidiopsis* and the filamentous heterocyst-differentiating cyanobacteria are each other's closest living relatives (Fewer et al., 2002). Moreover, among the strains with the highest sequence similarities occurred isolates from extreme environments such as *Scytonema* sp. HK-05 (genebank synonym *Scytonema* sp. NIES-2130) from a hot spring (Rippka et al., 1979) and *Nostoc* sp. HK-01 from natural cyanobacterial crusts (Katoh et al., 2012).

In the present work, the genome sequencing of *Chroococcidiopsis* sp. CCMEE 029 was undertaken; when the bioinformatics analysis will be completed and the genome resealed, key signatures for its desiccation and radiation tolerance will be identified, as recently reported for *Gloeocapsopsis* sp. UTEX B3054 (Urrejola et al., 2019). Preliminary bioinformatics analysis (not shown) pointed out that unlike other cyanobacteria (Cassier-Chauvat et al., 2016) and similar to *Deinococcus radiodurans* (Timmins and Moe, 2016), the genome of *Chroococcidiopsis* sp. CCMEE 029 lacks *recB* and *recC* genes that are involved in the homologous recombination (Spies and Kowalczykowski, 2005). Hence further investigations are needed to unravel additional pathways involved in the repair of DNA damage induced by UV irradiation and desiccation.

Reshaping the boundaries of *Chroococcidiopsis* desiccation and UV tolerance has implications in the search for extra-terrestrial life since it contributes to defining the habitability of Mars and planets orbiting other stars. In fact, the UV dose used here corresponds to that of a few hours at Mars's equator (Cockell et al., 2000). Hence, considering that survivors occurred in the bottom layers of the biofilms (Baqué et al., 2013), it might be hypothesized that if a biofilm life form ever appeared during Mars's climatic history, it might have been transported in a dried state under UV radiation, from niches that had become unfavorable to niches that were inhabitable (Westall et al., 2013). The reported survival also suggests that intense UV radiation fluxes would not prevent the presence of phototrophic biofilms or their colonizing of the landmass of other planets.

DATA AVAILABILITY STATEMENT

The raw data supporting the conclusions of this manuscript will be made available by the authors, without undue reservation, to any qualified researcher.

AUTHOR CONTRIBUTIONS

DB and LR supervised the study. CM performed the experiments, CF and MB contributed to the materials and analysis tool. ER and PR conceived and performed the martian UV radiation simulation. AN, FF and MP carried out the bioinformatic analyses. DB wrote the manuscript. All authors read and approved the final manuscript.

FUNDING

This research was supported by the Italian Space Agency (grant 2018-15-UO to DB) and Regione Lazio (grant Torno Subito 2017 to AN).

ACKNOWLEDGMENTS

AN acknowledges Regione Lazio for supporting the internship at NASA (call Torno Subito 2017). The authors thank CINECA for granting computer time (Application Code HP10CKZEGT) and Elena Romano, Centre of Advanced Microscopy "P.B. Albertano," University of Rome Tor Vergata, for her skillful assistance in using the confocal laser scanning microscope.

REFERENCES

Azua-Bustos, A., Zúñiga, J., Arenas-Fajardo, C., Orellana, M., Salas, L., and Rafael, V. (2014). *Gloeocapsopsis* AAB1, an extremely desiccation-tolerant cyanobacterium isolated from the Atacama Desert. *Extremophiles* 18, 61–74. doi: 10.1007/s00792-013-0592-y

Baqué, M., Scalzi, G., Rabbow, E., Rettberg, P., and Billi, D. (2013). Biofilm and planktonic lifestyles differently support the resistance of the desert

cyanobacterium *Chroococcidiopsis* under space and Martian simulations. *Orig. Life Evol. Biosph.* 43, 377–389. doi: 10.1007/s11084-013-9341-6

Billi, D. (2009). Subcellular integrities in *Chroococcidiopsis* sp. CCMEE 029 survivors after prolonged desiccation revealed by molecular probes and genome stability assays. *Extremophiles* 13, 49–57. doi: 10.1007/s00792-008-0196-0

Billi, D., Grilli-Caiola, M., Paolozzi, L., and Ghelardini, P. (1998). A method for DNA extraction from the desert cyanobacterium *Chroococcidiopsis* and its application to identification of *ftsZ*. *Appl. Environ. Microbiol.* 64, 4053–4056.

Billi, D., Staibano, C., Verseux, C., Fagliarone, C., Mosca, C., Baqué, M., et al. (2019a). Dried biofilms of desert strains of *Chroococcidiopsis* survived prolonged exposure to space and Mars-like conditions in low earth orbit. *Astrobiology* 19, 1008–1017. doi: 10.1089/ast.2018.1900

Billi, D., Verseux, C., Fagliarone, C., Napoli, A., Baqué, M., and de Vera, J.-P. (2019b). A desert cyanobacterium under simulated Mars-like conditions in low earth orbit: implications for the habitability of Mars. *Astrobiology* 19, 158–169. doi: 10.1089/ast.2017.1807

Bolger, A. M., Lohse, M., and Usadel, B. (2014). Trimmomatic: a flexible trimmer for Illumina sequence data. *Bioinformatics* 30, 2114–2120. doi: 10.1093/bioinformatics/btu170

Cassier-Chauvat, C., Veaudor, T., and Chauvat, F. (2016). Comparative genomics of DNA recombination and repair in cyanobacteria: biotechnological implications. *Front. Microbiol.* 7:1809. doi: 10.3389/fmicb.2016.01809

Cockell, C. S., Brown, S., Landenmark, H., Samuels, T., Siddall, R., and Wadsworth, J. (2017). Liquid water restricts habitability in extreme deserts. *Astrobiology* 17, 309–318. doi: 10.1089/ast.2016.1580

Cockell, C. S., Catling, D. C., Davis, W. L., Snook, K., Kepner, R. L., Lee, P., et al. (2000). The ultraviolet environment of Mars: biological implications past, present, and future. *Icarus* 146, 343–359. doi: 10.1006/icar.2000.6393

Cockell, C. S., Schuerger, A. C., Billi, D., Friedmann, E. I., and Panitz, C. (2005). Effects of a simulated martian UV flux on the cyanobacterium, *Chroococcidiopsis* sp. 029. *Astrobiology* 5, 127–140. doi: 10.1089/ast.2005.5.127

Cox, M. M., and Battista, J. R. (2005). *Deinococcus radiodurans*—the consummate survivor. *Nat. Rev. Microbiol.* 3, 882–892. doi: 10.1038/nrmicro1264

Crowe, J. H., Hoekstra, F. A., and Crowe, L. M. (1992). Anhydrobiosis. *Annu. Rev. Physiol.* 54, 579–599. doi: 10.1146/annurev.ph.54.030192.003051

Cuccuru, G., Orsini, M., Pinna, A., Sbardellati, A., Soranzo, N., Travaglione, A., et al. (2014). Orione, a web-based framework for NGS analysis in microbiology. *Bioinformatics* 30, 1928–1929. doi: 10.1093/bioinformatics/btu135

Emerson, J. B., Adams, R. I., Román, C. M. B., Brooks, B., Coil, D. A., Dahlhausen, K., et al. (2017). Schrödinger's microbes: tools for distinguishing the living from the dead in microbial ecosystems. *Microbiome* 5:86. doi: 10.1186/s40168-017-0285-3

Fagliarone, C., Mosca, C., Ubaldi, I., Verseux, C., Baqué, M., Wilmotte, A., et al. (2017). Avoidance of protein oxidation correlates with the desiccation and radiation resistance of hot and cold desert strains of the cyanobacterium *Chroococcidiopsis*. *Extremophiles* 21, 981–991. doi: 10.1007/s00792-017-0957-8

Fewer, D., Friedl, T., and Büdel, B. (2002). *Chroococcidiopsis* and heterocyst-differentiating cyanobacteria are each other's closest living relatives. *Mol. Phylogenet. Evol.* 23, 82–90. doi: 10.1006/mpev.2001.1075

Flemming, H. C., and Wingender, J. (2010). The biofilm matrix. *Nat. Rev. Microbiol.* 8, 623–633. doi: 10.1038/nrmicro2415

França, M. B., Panek, A. D., and Eleutherio, E. C. (2007). Oxidative stress and its effects during dehydration. *Comp. Biochem. Physiol. A Mol. Integr. Physiol.* 146, 621–631. doi: 10.1016/j.cbpa.2006.02.030

Frösler, J., Panitz, C., Wingender, J., Flemming, H. C., and Rettberg, P. (2017). Survival of *Deinococcus geothermalis* in biofilms under desiccation and simulated space and martian conditions. *Astrobiology* 17, 431–447. doi: 10.1089/ast.2015.1431

Goosen, N., and Moolenaar, G. F. (2008). Repair of UV damage in bacteria. *DNA Repair* 7, 353–379. doi: 10.1016/j.dnarep.2007.09.002

Grilli Caiola, M., Ocampo-Friedmann, R., and Friedmann, E. I. (1993). Cytology of long-term desiccation in the cyanobacterium *Chroococcidiopsis* (Chroococcales). *Phycologia* 32, 315–322. doi: 10.2216/i0031-8884-32-5-315.1

Higo, A., Suzuki, T., Ikeuchi, M., and Ohmori, M. (2007). Dynamic transcriptional changes in response to rehydration in *Anabaena*. *Microbiology* 153, 3685–3694. doi: 10.1099/mic.0.2007/009233-0

Humann, J. L., Ziemkiewicz, H. T., Yurgel, S. N., and Kahn, M. L. (2009). Regulatory and DNA repair genes contribute to the desiccation resistance of *Sinorhizobium meliloti* Rm1021. *Appl. Environ. Microbiol.* 75, 446–453. doi: 10.1128/AEM.02207-08

Jäger, K., and Potts, M. (1988). *In vitro* translation of mRNA from *Nostoc commune* (cyanobacteria). *Arch. Microbiol.* 149, 225–231. doi: 10.1007/BF00422009

Kaplan-Levy, R. N., Hadas, O., Summers, M. L., Rücker, J., and Sukenik, A. (2010). "Akinetes: dormant cells of cyanobacteria" in *Dormancy and resistance in harsh environments. Topics in current genetics*. eds. E. Lubzens, J. Cerda, and M. Clark (Berlin: Springer), 5–27.

Katoh, H., Furukawa, J., Tomita-Yokotani, K., and Nishi, Y. (2012). Isolation and purification of an axenic diazotrophic drought-tolerant cyanobacterium, *Nostoc commune*, from and its utilization for field research on soils polluted with radioisotopes. *Biochim. Biophys. Acta* 1817, 1499–1505. doi: 10.1016/j.bbabio.2012.02.039

Kumar, A., Tyagi, M. B., and Jha, P. N. (2004). Evidences showing ultraviolet-B radiation-induced damage of DNA in cyanobacteria and its detection by PCR assay. *Mol. Cell Biol. Res. Commun.* 318, 1025–1035. doi: 10.1016/j.bbrc.2004.04.129

Leuko, S., Neilan, B. A., Burns, B. P., Walter, M. R., and Rothschild, L. J. (2011). Molecular assessment of UVC radiation-induced DNA damage repair in the stromatolitic halophilic archaeon, *Halococcus hamelinensis*. *J. Photochem. Photobiol. B* 102, 140–145. doi: 10.1016/j.jphotobiol.2010.10.002

Meulenbroek, E. M., Peron Cane, C., Jala, I., Iwai, S., Moolenaar, G. F., Goosen, N., et al. (2013). UV damage endonuclease employs a novel dual-dinucleotide flipping mechanism to recognize different DNA lesions. *Nucleic Acids Res.* 41, 1363–1371. doi: 10.1093/nar/gks1127

O'Malley-James, J. T., and Kaltenegger, L. (2017). UV surface habitability of the TRAPPIST-1 system. *Mon. Not. R. Astron. Soc.: Lett.* 469, 26–30. doi: 10.1093/mnrasl/slx047

Pinto, F., Pacheco, C. C., Ferreira, D., Moradas-Ferreira, P., and Tamagnini, P. (2012). Selection of suitable reference genes for RT-qPCR analyses in cyanobacteria. *PLoS One* 7:e34983. doi: 10.1371/journal.pone.0034983

Rabbow, E., Parpart, A., and Reitz, G. (2016). The planetary and space simulation facilities at DLR Cologne. *Microgravity Sci. Technol.* 28, 215–229. doi: 10.1007/s12217-015-9448-7

Rabbow, E., Rettberg, P., Parpart, A., Panitz, C., Schulte, W., Molter, F., et al. (2017). EXPOSE-R2: the astrobiological ESA mission on board of the International Space Station. *Front. Microbiol.* 8:1533. doi: 10.3389/fmicb.2017.01533

Rajeev, L., da Rocha, U. N., Klitgord, N., Luning, E. G., Fortney, J., Axen, S. D., et al. (2013). Dynamic cyanobacterial response to hydration and dehydration in a desert biological soil crust. *ISME J.* 7, 2178–2191. doi: 10.1038/ismej.2013.83

Rippka, R., Deruelles, J., Waterbury, J. B., Herdman, M., and Stanier, R. Y. (1979). Generic assignments, strain histories and properties of pure cultures of cyanobacteria. *J. Gen. Microbiol.* 111, l–61. doi: 10.1099/00221287-111-1-1

Rudi, K., Hagen, I., Johnsrud, B. C., Skjefstad, G., and Tryland, I. (2010). Different length (DL) qPCR for quantification of cell killing by UV-induced DNAdamage. *Int. J. Environ. Res. Public Health* 7, 3376–3381. doi: 10.3390/ijerph7093376

Scherer, S., Ernst, A., Chen, T. W., and Böger, P. (1984). Rewetting of drought-resistant blue-green algae: time course of water uptake and reappearance of respiration, photosynthesis, and nitrogen fixation. *Oecologia* 62, 418–423. doi: 10.1007/BF00384277

Schulze-Makuch, D., Airo, A., and Schirmack, J. (2017). The adaptability of life on earth and the diversity of extraterrestrial habitats. *Front. Microbiol.* 8:2011. doi: 10.3389/fmicb.2017.02011

Seemann, T. (2014). Prokka: rapid prokaryotic genome annotation. *Bioinformatics* 30, 2068–2206. doi: 10.1093/bioinformatics/btu153

Shirkey, B., Kovarcik, D. P., Wright, D. J., Wilmoth, G., Prickett, T. F., Helm, R. F., et al. (2000). Active Fe-containing superoxide dismutase and abundant sodF mRNA in *Nostoc commune* (cyanobacteria) after years of desiccation. *J. Bacteriol.* 182, 189–197. doi: 10.1128/JB.182.1.189-197.2000

Slade, D., and Radman, M. (2011). Oxidative stress resistance in *Deinococcus radiodurans*. *Microbiol. Mol. Biol. Rev.* 75, 133–191. doi: 10.1128/MMBR.00015-10

Spies, M., and Kowalczykowski, S. C. (2005). "Homologous recombination by RecBCD and RecF pathways" in *The bacterial chromosome*. ed. N. P. Higgins (Washington, D.C: ASM Press), 389–403.

Sukenik, A., Kaplan-Levy, R. N., Welch, J. M., and Post, A. F. (2012). Massive multiplication of genome and ribosomes in dormant cells (akinetes) of *Aphanizomenon ovalisporum* (cyanobacteria). *ISME J.* 6, 670–679. doi: 10.1038/ismej.2011.128

Tanaka, M., Earl, A. M., Howell, H. A., Park, M. J., Eisen, J. A., Peterson, S. N., et al. (2004). Analysis of *Deinococcus radiodurans*'s transcriptional response to ionizing radiation and desiccation reveals novel proteins that contribute to extreme radioresistance. *Genetics* 168, 21–33. doi: 10.1534/genetics.104.029249

Tanaka, M., Narumi, I., Funayama, T., Kikuchi, M., Watanabe, H., Matsunaga, T., et al. (2005). Characterization of pathways dependent on the *uvsE, uvrA1*, or *uvrA2* gene product for UV resistance in *Deinococcus radiodurans*. *J. Bacteriol.* 187, 3693–3697. doi: 10.1128/JB.187.11.3693-3697.2005

Timmins, J., and Moe, E. (2016). A decade of biochemical and structural studies of the DNA repair machinery of *Deinococcus radiodurans*: major findings, functional and mechanistic insight and challenges. *Comput. Struct. Biotechnol. J.* 14, 168–176. doi: 10.1016/j.csbj.2016.04.001

Urrejola, C., Alcorta, J., Salas, L., Vásquez, M., Polz, M. F., Vicuña, R., et al. (2019). Genomic features for desiccation tolerance and sugar biosynthesis in the extremophile *Gloeocapsopsis* sp. UTEX B3054. *Front. Microbiol.* 10:950. doi: 10.3389/fmicb.2019.00950

Verseux, C., Baqué, M., Cifariello, R., Fagliarone, C., Raguse, M., Moeller, R., et al. (2017). Evaluation of the resistance of *Chroococcidiopsis* spp. to sparsely and densely ionizing irradiation. *Astrobiology* 17, 118–125. doi: 10.1089/ast.2015.1450

Westall, F., Loizeau, D., Foucher, F., Bost, N., Betrand, M., Vago, J., et al. (2013). Habitability on Mars from a microbial point of view. *Astrobiology* 13, 887–897. doi: 10.1089/ast.2013.1000

Wilhelm, M. B., Davila, A. F., Parenteau, M. N., Jahnke, L. L., Abate, M., Cooper, G., et al. (2018). Constraints on the metabolic activity of microorganisms in Atacama surface soils inferred from refractory biomarkers: implications for martian habitability and biomarker detection. *Astrobiology* 18, 955–966. doi: 10.1089/ast.2017.1705

Conflict of Interest: The authors declare that the research was conducted in the absence of any commercial or financial relationships that could be construed as a potential conflict of interest.

frontiers in Microbiology

ORIGINAL RESEARCH
published: 12 November 2019
doi: 10.3389/fmicb.2019.02595

Subsurface Microbial Ecology at Sediment-Groundwater Interface in Sulfate-Rich Playa; White Sands National Monument, New Mexico

Mihaela Glamoclija[1†], Steven Ramirez[1†], Kosala Sirisena[1,2,3] and Inoka Widanagamage[1,4]*

[1] Department of Earth and Environmental Sciences, Rutgers University, Newark, NJ, United States, [2] Geophysical Laboratory, Carnegie Institution of Washington, Washington, DC, United States, [3] Department of Environmental Technology, Faculty of Technology, University of Colombo, Colombo, Sri Lanka, [4] Department of Geology and Geological Engineering, The University of Mississippi, Oxford, MS, United States

The hypersaline sediment and groundwater of playa lake, Lake Lucero, at the White Sands National Monument in New Mexico were examined for microbial community composition, geochemical gradients, and mineralogy during the dry season along a meter and a half depth profile of the sediment *vs.* the groundwater interface. Lake Lucero is a highly dynamic environment, strongly characterized by the capillary action of the groundwater, the extreme seasonality of the climate, and the hypersalinity. Sediments are predominantly composed of gypsum with minor quartz, thenardite, halite, quartz, epsomite, celestine, and clays. Geochemical analysis has revealed the predominance of nitrates over ammonium in all of the analyzed samples, indicating oxygenated conditions throughout the sediment column and in groundwater. Conversely, the microbial communities are primarily aerobic, gram-negative, and are largely characterized by their survival adaptations. Halophiles and oligotrophs are ubiquitous for all the samples. The very diverse communities contain methanogens, phototrophs, heterotrophs, saprophytes, ammonia-oxidizers, sulfur-oxidizers, sulfate-reducers, iron-reducers, and nitrifiers. The microbial diversity varied significantly between groundwater and sediment samples as their temperature adaptation inferences that revealed potential psychrophiles inhabiting the groundwater and thermophiles and mesophiles being present in the sediment. The dynamism of this environment manifests in the relatively even character of the sediment hosted microbial communities, where significant taxonomic distinctions were observed. Therefore, sediment and groundwater substrates are considered as separate ecological entities. We hope that the variety of the discussed playa environments and the microorganisms may be considered a useful terrestrial analog providing valuable information to aid future astrobiological explorations.

Keywords: microbial ecology, playa, subsurface, groundwater, sulfates

OPEN ACCESS

Edited by:
Akihiko Yamagishi, Tokyo University of Pharmacy and Life Sciences, Japan

Reviewed by:
Mark Alexander Lever, ETH Zürich, Switzerland
Anirban Chakraborty, University of Calgary, Canada

****Correspondence:***
Mihaela Glamoclija
m.glamoclija@rutgers.edu

† These authors have contributed equally to this work

Specialty section:
This article was submitted to Microbiological Chemistry and Geomicrobiology, a section of the journal Frontiers in Microbiology

Received: *24 July 2019*
Accepted: *25 October 2019*
Published: *12 November 2019*

Citation:
Glamoclija M, Ramirez S, Sirisena K and Widanagamage I (2019) Subsurface Microbial Ecology at Sediment-Groundwater Interface in Sulfate-Rich Playa; White Sands National Monument, New Mexico. Front. Microbiol. 10:2595. doi: 10.3389/fmicb.2019.02595

INTRODUCTION

Hypersaline environments harbor very diverse ecosystems that may range from soda lakes, saltpans, salars, hypersaline springs, playas, and ancient salt deposits (Friedman and Krumbein, 1985; Reynolds et al., 2007; Oren et al., 2009). Consequently, the ecology of hypersaline environments has been extensively investigated, especially the surface water column of playas, and the sediments

after the wet seasons, which is the period when organisms flourish (Sorenson et al., 2004, 2005; Mesbah et al., 2007; Costa et al., 2008; Navarro et al., 2009; Oren et al., 2009; Makhdoumi-Kakhki et al., 2011). Many among the studies had focused on different ecological and chemical aspects of the stratification of microbial mats living in wet hypersaline sediments (Sorenson et al., 2004, 2005; Oren et al., 2009; Vogel et al., 2009) while sediments and/or groundwater were subject of the fewer investigations (Schulze-Makuch, 2002; Navarro et al., 2009; Pen-Mouratov et al., 2011; Sirisena et al., 2018). Therefore, to fully understand the microbial ecology of playa setting it is crucial to explore the microbial communities living in different substrates of playa (i.e., sediments and groundwater) during the drought period, characterized by these particularly harsh weather conditions.

Playas are intracontinental basins in which drought periods exceed wet periods that are characterized by precipitation and water inflow (Cooke et al., 1993). Due to the ephemeral nature of these environments, the microbial population is composed of organisms that can survive drought, as well as, temporary freshwater to saline and hypersaline conditions that alternate throughout the year (Ventosa et al., 2008). Previous studies have revealed diverse microbial communities living at similar saline environments with the phyla *Bacteroidetes*, *Firmicutes*, *Actinobacteria*, *Proteobacteria*, and *Euryarchaeota* generally being the most common (Mesbah et al., 2007; Costa et al., 2008; Navarro et al., 2009; Makhdoumi-Kakhki et al., 2011; Babavalian et al., 2013). Furthermore, halophilic microbes have been found as particularly abundant (Babavalian et al., 2013). The objective of this study is to investigate the composition of microbial communities living in the playa ecosystem at the WSNM during the dry season in exclusively hypersaline settings along the steep subsurface environmental gradients.

The study area is the White Sands National Monument (WSNM) in New Mexico (U.S.), the site that contains the world's largest gypsum dune field. To the west of the dunes, stretches the Alkali Flat. That is a large, flat, and mostly unvegetated space that hosts about 20 playas, including Lake Lucero (**Figure 1**). Lake Lucero is the largest among the playas, and it occupies the southern part of the Monument (Langford, 2003; Kocurek et al., 2007). Since Lake Lucero is the lowest topographic point at WSNM, evaporites accumulate here and build thick deposits that create a hypersaline environment (Kocurek et al., 2007). Previous studies, including the analysis of the nearby WSNM dune deposits, have indicated the presence of *Cyanobacteria* as primary producers and as a diverse microbial community capable of cycling nitrogen and sulfur compounds (Glamoclija et al., 2012). Only a few studies have examined the microbial ecology of Lake Lucero's sediments and groundwater specifically (e.g., Schulze-Makuch, 2002; Sirisena et al., 2018). Lake Lucero is a wet playa with the groundwater table relatively close to the surface; during the dry season, surface moisture is provided by capillary action (Cooke et al., 1993; Reynolds et al., 2007; Szynkiewicz et al., 2010; Newton and Allen, 2014). This process provides much-needed water to microbial communities on the playa surface, as well as a geochemically active environment on the surface and subsurface that organisms may take advantage of Cooke et al. (1993), Glamoclija et al. (2012). Lake Lucero's groundwater is influenced by a regional groundwater system more so than the rest of the WSNM, which further contributes to the salinity (Newton and Allen, 2014). The seasonal variations in water availability, wind erosion, and the hypersalinity pose potential challenges for life in this environment (Anton et al., 2008; Newton and Allen, 2014).

Desert environments and geomorphology of the WSNM have been discussed as terrestrial analog to Martian sedimentary sequences (Grotzinger et al., 2005; Szynkiewicz et al., 2010; Glamoclija et al., 2012). Sedimentary beds produced by past playa settings have been inferred to exist on Mars, and considering Martian geological history the historic increase in desertification and presence of evaporitic processes may mark some of the last habitats on the red planet (e.g., Andrews Hanna et al., 2010). In the light of Mars 2020 mission flying to past fresh water lake that may hold lacustrine and post-lacustrine lithologies, it is crucial for us to understand where life proliferates in ephemeral lake settings, such as this of Lake Lucero, and which strata may or may not hold the evidence of extinct or present life.

This study aims to evaluate variations in the microbial ecology along the 1.25 m depth profile, geochemical gradients, changes in mineralogy, and substrate (sediment vs. groundwater). Our sampling provides a snapshot of ecology during the dry season, and the sampled depth profile reached groundwater table that coincides with the hard crust of coarse gypsum that we could not sample using auger drilling method. We intend to answer how environmental parameters such as the presence of shallow groundwater table, solar radiation, and geochemistry may influence the distribution of the organisms and to inquire as to which settings are essential and will condition the community structure in these sediments. Furthermore, we have investigated whether groundwater and sediments represent separate ecological entities.

MATERIALS AND METHODS

Sampling Procedures

Sediment and groundwater samples were collected in March 2013 from three locations at the WSNM (**Figure 1**). The sediment sampling strategy was designed to assess the depth profile of playa deposits to capture different evaporation lithologies formed at Lake Lucero. The sampling location (N 32° 41.111′; W 106° 24.093′ ± 3 m) is an approximate topographic low within Lake Lucero where the lake surface water has had the opportunity to last longer time than in other areas of the playa, and the microbial communities had the most opportunity to colonize and diversify within the evaporitic sediments. Our initial attempt to manually drill had failed due to sediment characteristics (too hard and sticky). Instead, we sampled a 125 cm deep lithological profile using an auger device. The auger device was pre-cleaned to prevent contamination (Eigenbrode et al., 2009). Within this profile, we had subsampled 14 lithologically different samples (**Figure 2**), which were divided by depth as consistently as possible and then placed in Falcon tubes and sterile plastic bags. We discovered that the water table was located at 125 cm depth (**Figures 1**, **2**). The coarse gypsum at the bottom of the hole

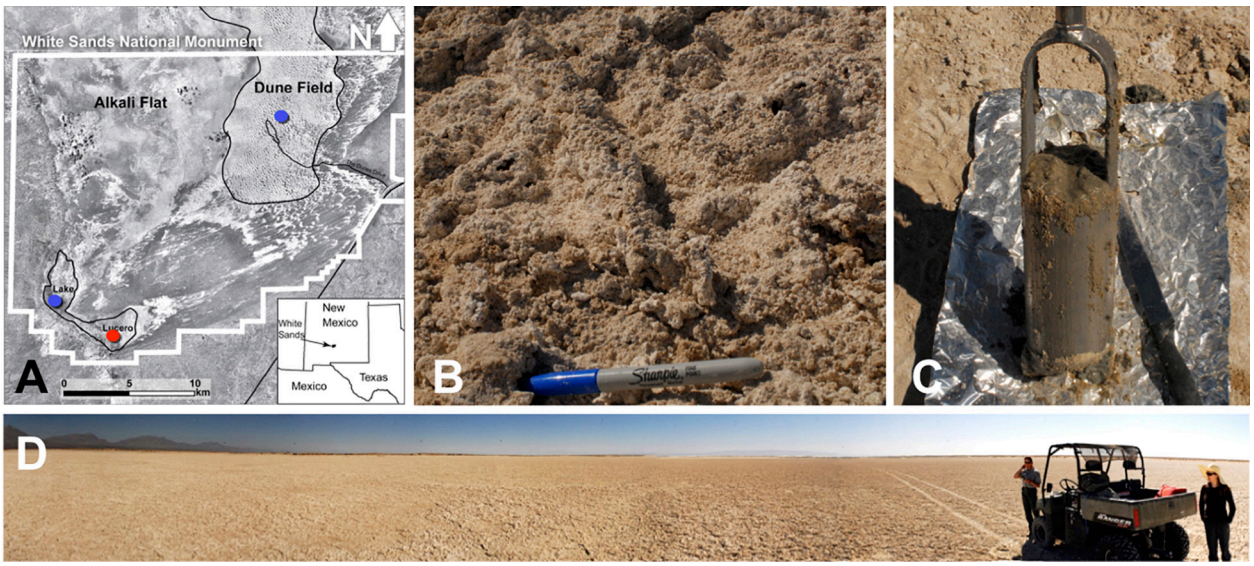

FIGURE 1 | (A) A map showing the WSNM area and the sampling points. The red dot denotes the location where the sediment (1–14) and one groundwater sample (GW-1) were collected. The blue dots indicate the location of groundwater samples in Lake Lucero (bottom blue dot, GW-2) and the dune field (upper blue dot, GW-3 and GW-4). **(B)** The surface salt crust at the sampling area. **(C)** A sample of sediment groundwater interface sampled at about 1 m depth. **(D)** The sampling location at the central area of Lake Lucero playa.

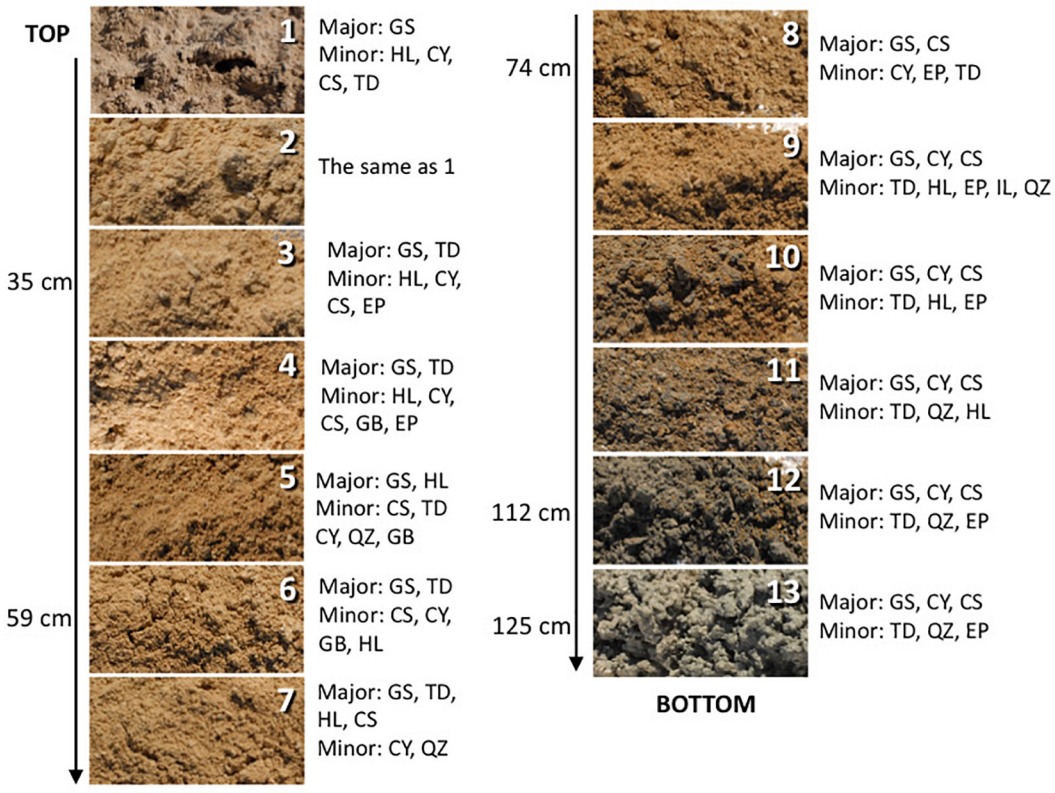

FIGURE 2 | The depth profile displaying changes in sediment appearance (texture and color) as the depth increases. Next to the photo of the sample are listed major and minor mineral compositions. Sample 14 is not pictured and shown here as it is mineralogically the same as sample 13 but it was more liquid due to higher mixture with groundwater. The letter symbols for minerals are: GS, gypsum; HL, halite; CY, clay; CS, celestine; TD, thenardite; EP, epsomite; GB, glauberite; QZ, quartz.

was too hard to auger through, and our sampling ended at this level. The groundwater within the drilled hole was left to settle until the next day and collected into a pre-cleaned, 4 L carboy using a manual vacuum pump (GW-1). Three other groundwater samples were collected from previously installed piezometers: one from a southernmost location in Lake Lucero (N 32° 42.167′; W 106° 26.960′ ± 3 m) (GW-2), and two from the dune field (N 32° 49.721′; W 106° 15.972′ ± 3 m). Dune field piezometers were installed for monitoring of shallow and deep aquifers, as clarified by WSNM park management. The shallow aquifer sample primarily contained meteoric water (GW-4), whereas the deep aquifer sample was the brines (GW-3) (see **Table 1**). The groundwater samples were filtered (4 L for each sample) using 0.22 μ membrane filters within a few hours of the collection. Filters were placed in sterile tubes, and all samples were held at 4°C in a refrigerator during the fieldwork and the transportation back to the laboratory, where they were stored in the freezer at −20 and −80°C until further processing.

Mineral Assemblages

Main mineral phases were identified by X-ray diffraction of powdered dry and dump wet samples using a Bruker D8 Advance Eco, equipped with a Cu-Kα radiation source and a LynxEye XE detector. Samples were afterward analyzed using EVA software. Scanning Electron Microscope (SEM) with Energy Dispersive X-ray Spectroscopy (EDS) Hitachi S-4800 was used to search for the presence of microbial morphologies or biofilm and to analyze their elemental composition and minor mineral phases and precipitates. All samples were subsampled three times for the SEM-EDS analysis. Once dried, the samples were coated with Iridium and analyzed using 25.0 and 15.0 kV voltage, 20 μA under standard vacuum, and working distance ranged from 9 to 13 mm.

Geochemistry

All of the collected samples were analyzed for Mg, Sr, Fe, Na, K, and Ti concentrations using ICP-OES. One gram (dry weight) of the sample was mixed with repeated additions of nitric acid (20%) up to 10 ml (following acid digestion of soils) for 4 days with periodic sample shaking and heating. Samples were filtered, and the filtrates were diluted with deionized water and volumes brought up to 30 ml and adjusted total acid to 3–5% (v/v) for ICP-OES analyses. The analytical reproducibility was calculated as standard deviation and was within a range of 0.1459 to 8.0000 for more abundant cation concentrations, on average 3.53 for all the analyzed samples.

The ammonium (NH_4^+) and nitrate + nitrite ($NO_3^- + NO_2^-$) concentrations from the deposits were assessed using colorimetric methods. One gram of sample was mixed with 10 ml of 2N potassium chloride (KCl) and left in the solution for 24 h at room temperature while shaking periodically. The supernatant was decanted into clean Falcon tubes. A range of 0, 5, 10, 25, 50, and 100 μM solutions were prepared for ammonium sulfate [$(NH_4^+)_2SO_4$] and sodium nitrate ($NaNO_3$) solutions to be used as standards. The absorbance of each sample was measured at least in triplicates using a GENESYS 10Bio spectrophotometer; 640 nm was used for ammonium and 540 nm for nitrate. The NH_4^+ concentration of the extracts was determined by the alkaline hypochlorite/phenol nitroprusside method, after the addition of sodium citrate to prevent the precipitation of calcium and magnesium salts (Solorzano, 1969). The analytical reproducibility for NH_4^+ measurements was calculated as standard deviation and was within a range of 0.001 to 0.033, on average 0.014 for all the analyzed samples. The $NO_3^- + NO_2^-$ concentrations were measured using the Nitrate Test kit (LaMotte, MD, United States) according to the manufacturer's instructions. This method does not allow for separate NO_2^- detection, and therefore the results are reported as a sum of NO_3^- and minor NO_2^-, which will henceforth be referred to as Nitrates NO_3^-. The analytical reproducibility for NO_3^- measurements was calculated as standard deviation and was within a range of 0.032 to 0.147, on average 0.076 for all the analyzed samples.

Nucleic Acid Extraction and Polymerase Chain Reaction

Sediment DNA extractions were carried out from approximately 0.5 g of powdered sediment sample, using Qiagen DNeasy® PowerSoil DNA Isolation Kit. Modifications to the manufacturer's protocol were made as described in Sirisena et al. (2018) to improve the extraction efficiency. The powdered sample was incubated at 70°C for 30 min in a Bead Tube that contained a bead solution from the kit. The incubated mixture was vortexed for 5 min and centrifuged for 30 s at 10,000 × *g*. This modification helps to mechanically separate microbial cells from the mineral substrate and eliminate most of the inhibitors to the DNA extraction (clays, gypsum, halite, and other salts) (Glamoclija et al., 2012). The supernatant was used as the starting material for the DNA extraction that was carried out according to the manufacturer's instructions. DNA extractions from all the samples were conducted at least in triplicates to account for sample heterogeneity. Negative (no sample) and positive (garden topsoil) extraction controls were used to ensure the extraction quality. Filters containing particles from groundwater samples were cut in small pieces using a sterile knife. The pieces

TABLE 1 | Groundwater field measurements.

Sample location	Lake Lucero – central (GW-1)	Lake Lucero – south (GW-2)	Dune field – deep aquifer (GW-3)	Dune field – shallow aquifer (GW-4)
Temperature (°C)	17.7	15.0	17.5–18.5	16.8–18.2
pH	7.09	7.84	7.02	7.40
Conductivity (mS)	59.0	139.9	37	11.98

were placed in the bead-beating tube using sterile tweezers and processed in the same way as other samples. The recovered DNA was stored at −20°C until further processing.

Microbial genomic DNA extraction from all three domains (archaea, eubacteria, and eukayota) was verified by polymerase chain reaction (PCR) using domain-specific 16S- and 18S- rRNA gene primers (Eubacterial B27-F and 1429-R (DeLong, 1992; Madden et al., 2007), Archaeal 8A-F and 1513U-R (Eder et al., 1999; Huber et al., 2002), and Eukaryal Euk1-F and Euk-R2 (Potvin and Lovejoy, 2008).

Illumina MiSeq 16S and 18S Amplicon Sequencing

A pair of universal primers: 515F (5′ GTG CCA GCM GCC GCG GTA A 3′) and 806R (5′ GGA CTA CHV GGG TWT CTA AT 3′) (Caporaso et al., 2012; Itoh et al., 2014; Pylro et al., 2014; Wu et al., 2015) was used to sequence the variable region V4 of the prokaryotic 16S rRNA gene for the detection of bacteria and archaea. Similarly, an another pair of universal primers: Euk7F (5′ AAC CTG GTT GAT CCT GCC AGT 3′) (Medlin et al., 1988; Auld et al., 2016) and Euk570R (5′ GCT ATT GGA GCT GGA ATT AC 3′) (Weekers et al., 1994; Auld et al., 2016) was used to sequence the variable region V1–V3 of the eukaryotic 18S rRNA gene to explore the eukaryotic microbial communities in the samples. Initial PCR amplification was conducted using approximately 15 ng of microbial genomic DNA from each sample using a forward primer with a unique barcode. PCR conditions comprised of an initial denaturation at 94°C for 3 min, 30 cycles of denaturation at 94°C for 30 s, annealing at 53°C for 40 s and elongation at 72°C for 1 min each, followed by a final elongation at 72°C for 5 min. After amplification, PCR products were checked in 2% agarose gel to determine the success of amplification. Then the PCR products with unique barcode for each sample were pooled together in equal proportions based on their molecular weight and DNA concentrations. Pooled samples were purified using calibrated Agencourt AMPure XP beads. This pooled and purified PCR product was used to prepare Illumina MiSeq DNA library according to the manufacturer's guidelines. The targeted variable regions of the 16S and 18S genes were sequenced on Illumina MiSeq platform (Caporaso et al., 2012; Garcia-Mazcorro et al., 2016).

Bioinformatics and Statistical Analysis

The two FASTQ files (R1 and R2) resulted from paired-end sequencing contained forward and reverse reads, respectively. The quality filtering and downstream sequence analysis were performed using Mothur v1.37.2 program (Schloss et al., 2009), according to the Standard Operating Procedure (SOP) outlined on https://www.mothur.org/wiki/MiSeq_SOP and customized as described by Sirisena et al. (2018). Briefly, the forward and reverse paired-end reads in R1 and R2 FASTQ files were merged to create consensus reads (contigs).

The following quality parameters were applied to eliminate low quality reads: (1) reads of a total quality score less than 25 were discarded; (2) reads with more than 2 bp mismatches in primers and more than one base pair mismatch in barcodes were eliminated. The barcodes and forward and reverse sequencing primers were trimmed from the contigs. The unique sequences were aligned to the SILVA reference alignment (release 123) (Quast et al., 2013). The detection and removal of Chimeric sequences were done using the UCHIME program within Mothur (Edgar et al., 2011). The unique sequences were classified to taxonomic levels using SILVA reference database (release 123) (Quast et al., 2013) with a cut-off of 80% of the bootstrap value. This enabled us to remove sequences related to "Chloroplast, Mitochondria, Eukaryota and Unknown" taxonomic lineages from bacteria and archaea analysis, and "Chloroplast, Mitochondria, Bacteria, Archaea and Unknown" lineages from for eukaryotic analysis. Subsequently, quality-filtered bacterial and archaeal unique sequences were clustered into operational taxonomic units (OTUs) at 97% similarity cut-off level using the average neighbor algorithm. For eukaryotic analysis, the quality-filtered unique sequences were clustered into "phylotypes" based on their taxonomy as opposed to the percentage similarity among sequences used in the OTU approach. Then, the abundances of OTUs/phylotypes in each sample were computed with the taxonomic identity up to the genus level for each OTU. The OTUs and phylotypes that were not classified up to lower taxonomic ranks (i.e., genus level) were further identified by manual BLASTn search in the NCBI Genomic Survey Sequences database. The singleton OTUs and phylotypes were not considered for subsequent diversity analyses.

The number of OTUs, the diversity indices: Shannon and Simpson; evenness indices: Shannon and Simpson; estimated richness: Chao 1 and ACE, and Good's coverage for each sample were calculated separately for bacteria and archaea using Mothur v1.37.2. PRIMER-7 software package was used to analyze changes in microbial community structure with ANOSIM and SIMPER analyses (Clarke and Gorley, 2015). ANOSIM tests the null hypothesis that the average rank similarity between objects within a group and objects from different groups is the same by producing a p-value and a test statistic (R) between −1 and 1, where 0 indicates the null hypothesis is true, and 1 shows a high degree of dissimilarity (Rees et al., 2004). SIMPER analysis facilitates the identification of OTUs that are responsible for contributing to community structure difference between individual samples and groups of samples (Rees et al., 2004).

The bacterial and archaeal community composition patterns across depth gradients as well as between sediment and groundwater were investigated by hierarchical cluster analysis using PRIMER-7 package (Clarke and Gorley, 2015). Briefly, the OTU abundances in each sample were standardized to the sum of the sample, and a similarity matrix between samples was constructed based on the Bray–Curtis similarity matric. A hierarchical cluster analysis was performed using the group average linkage method.

Metabolic Inference From 16S Taxonomic Data

The predicted metabolic functions of bacterial and archaeal communities in samples were determined using METAGENassist

web server tool (Arndt et al., 2012). Briefly, the OTUs with same taxonomic assignment were combined. Metabolic inference was conducted considering the taxonomic information available to lowest specified taxonomic rank. The dendrograms and heatmaps were constructed using Spearman distance and Ward linkage algorithm to explore the metabolic profile pattern of the prokaryotic microbial communities in each sample.

RESULTS

Mineralogy

The sediments analyzed for this study are predominantly composed of gypsum ($CaSO_4 \cdot 2H_2O$). Additionally, the surface crust contains thenardite (Na_2SO_4), halite (NaCl), and a minor amount of clay minerals. Along the profile relatively minor amounts of epsomite ($MgSO_4 \cdot 7H_2O$), glauberite [$Na_2Ca(SO_4)_2$], celestine ($SrSO_4$), and quartz (SiO_2) are detected too. Below the surface, a light brown mixture of gypsum and clay are identified, at about 60 cm deep the reddish clays, rich in iron oxides, were detected, and at about 1-m deep dark gray clay occurs, and it becomes thick and sticky just above the coarse gypsum strata (**Figure 2**). The bottom two samples are coarse gypsum and minor dark colored clay. The mineralogical observations reported here are mostly consistent with those previously reported (e.g., Langford, 2003). No obvious microbial morphologies or biofilms were observed in the samples using SEM technique, indicating very low biomass in the analyzed samples. Also, there is a possibility that microorganisms were included in the salt minerals and therefore invisible to SEM technique.

Geochemistry

The NH_4^+ and NO_3^- concentrations revealed that all of the samples had more NO_3^- than NH_4^+ (**Figure 3** and **Table 2**), indicating the presence of aerobic conditions throughout the depth profile and the potential presence of nitrifying organisms. The NO_3^- concentrations increased between the surface (23.06 ppm) and 60 cm depth, where it reached its highest value of 53.90 ppm (sample 6) after which the concentrations declined to about 16 ppm. The NH_4^+ levels are much less varying (1.50 to 2.59 ppm), increase with the depth, and it appears that they might be also influenced by lithology too (e.g., NO_3^- increased in the presence of clays).

The concentrations of the examined ions throughout the sediment column (**Figure 3** and **Table 2**) revealed specific patterns. Sodium and magnesium concentrations generally decrease with depth, which directly reflects the variety and contribution of salts other than gypsum to the examined lithologies. Sodium and magnesium derive mostly from halite, thenardite, epsomite, and glauberite. The prevalence of salt is generally consistent with the expectation that evaporitic action would result in higher salinity at the surface (Cooke et al., 1993). Iron concentrations generally increased in deeper sediments, and the same is true for titanium concentrations. The increase of Fe and Ti with depth may be related to the diagenetic processes and the presence of different clays (reddish, dark gray). For example, the change in concentrations of K, Mg, Na, and NO_3^- within horizons corresponding to samples 6 and 12 are characterized by the presence of sticky clays. Sticky clays result in high concentrations of monovalent cations (e.g., Na), which generate large hydration shells which reduce pore space and thus inhibit microbial transport, water flow, and soil aeration (Maier et al., 2009). Therefore, sticky clays can alter local geochemical conditions and microbial ecology. The K concentrations were relatively low and exhibited a trend similar to that of Fe, Mg, and Ti (**Figure 3**). The general changes in cation concentrations noted here are consistent with the observations made in SEM/EDS. Strontium in the samples is related to the presence of the mineral celestine ($SrSO_4$), the detected concentrations are consistent with SEM/EDS observations as celestine is observed as a minor mineral component in the samples. Strontium concentrations would likely be higher during the wet season due to increased dissolution (Ichikuni and Musha, 1978). Additionally, the strontium component in these samples likely derives from the local groundwater brines that increase the salinity of this playa.

Taxonomy

After the quality filtration, a total of 7627 OTUs for bacteria, 541 OTUs for archaea, and 34 phylotypes for eukaryota are obtained from the 14 sediment samples and four groundwater samples. Based on the number of OTUs, raw sequences, and diversity analysis, bacteria were the dominant and a diverse domain, especially within the sediment column (**Figures 4**, **5**).

Based on bacterial taxonomic composition, *Proteobacteria, Acidobacteria, Actinobacteria, Bacteroidetes, Firmicutes,* and *Gemmatimonadetes* are the most dominant phyla (**Figure 5**). The most dominant *Proteobacteria* accounted for 45% of all bacterial OTUs, and the most dominant within this phylum are *Gammaproteobacteria* (55% of *Proteobacteria* OTUs) and *Alphaproteobacteria* (27%). Archaea are less diverse than the bacteria, and the most dominant archaeal phyla are *Euryarchaeota* and *Thaumarchaeota* (**Figure 6**). *Euryarchaeota* constitutes approximately 72% of the archaeal OTUs. Eukaryota is identified in three sediment samples and all the groundwater samples, with the most prevalent *Viridiplantae* and *Fungi* (**Figure 7**). The eukaryotic communities showed very low diversity (**Figure 7**).

The dendrogram was utilized to segregate the samples based on the microbial community structure (OTU abundances). Bacterial clustering revealed that playa groundwater (GW-1 and GW-2) and dune groundwater (GW-3 and GW-4) were different from each other and in general groundwater clustered separately from the sediments (**Figure 8**). The SIMPER analysis indicates that sample 1 had a higher abundance of OTUs than other sediment samples. A high number of OTUs belongs to genera *Staphylococcus* and *Pseudomonas*. Overall sediment and groundwater were found to be significantly different (SIMPER indicates about 94% the lowest dissimilarity value among any two samples). The ANOSIM analysis confirms the clustering pattern by producing a sample statistic (R)

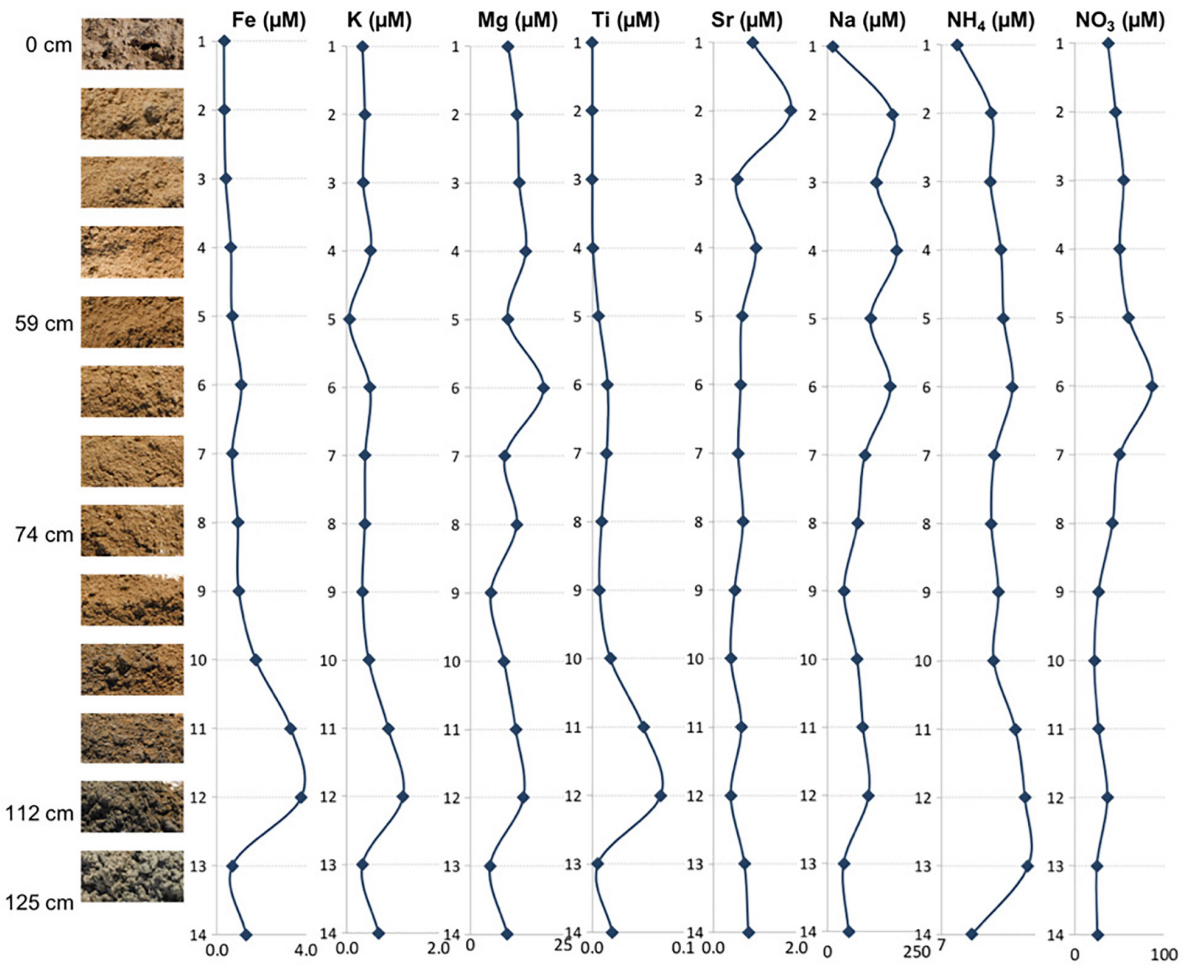

FIGURE 3 | Depth profile illustrating relationships between the mineral assemblages and concentrations of elemental ions, ammonium, and nitrates.

TABLE 2 | Cation concentrations for the soil samples from White Sand Monument.

Sample	Fe (μM)	K (μM)	Mg (μM)	Ti (μM)	Sr (μM)	Na (μM)	NH_4^+ (μM)	NO_3^- (μM)
1	0.31	0.34	10.17	BDL	0.95	15.04	8.34	37.19
2	0.33	0.39	12.51	BDL	1.87	182.92	11.26	45.93
3	0.39	0.35	13.08	BDL	0.57	137.94	11.16	54.47
4	0.63	0.52	14.85	BDL	1.03	195.05	12.06	50.53
5	0.68	0.05	10.02	0.01	0.69	120.57	12.31	60.50
6	1.10	0.50	19.58	0.02	0.66	176.42	13.07	86.93
7	0.69	0.40	9.27	0.02	0.60	105.56	11.53	50.46
8	0.93	0.39	12.38	0.01	0.72	85.04	11.25	42.48
9	0.98	0.34	5.42	0.01	0.51	47.33	11.85	26.86
10	1.74	0.47	8.96	0.02	0.43	83.36	11.45	22.05
11	3.32	0.90	12.15	0.06	0.68	99.93	13.31	27.12
12	3.79	1.22	14.18	0.08	0.42	115.25	14.13	36.47
13	0.69	0.34	5.22	0.01	0.75	46.36	14.40	24.94
14	1.31	0.69	9.91	0.02	0.84	59.40	9.58	25.42

The higher numbered samples are at greater depths (i.e., 1 is from the surface, 14 is from the groundwater). "BDL" stands for Below Detection Limit.

value of 0.99 with a p-value < 0.001, which indicates that playa sediments, playa groundwater, and dune groundwater are very different from each based on bacterial community structure. The SIMPER within-group similarities suggest that there is low similarity within the groups; 21.36% for sediments, 8.99% for the dune groundwater (GW-3 and GW-4), and 6.16% for the playa groundwater (GW-1 and GW-2). Based on SIMPER clustering, we can observe that different types of substrates host three differentiated clusters of Bacterial organisms as visible in the dendrogram, **Figure 8**. Additionally, it appears that samples adjacent to each other (e.g., samples 1 and 2, or samples 4 and 5) are more similar to each other than samples that are physically distant (e.g., samples 1 and 2 are more similar to each other than to sample 14 or sample 13). This style of clustering may indicate that the sediment lithology, geochemistry, or depth may influence the clustering and, therefore, the composition of the organisms within the sediment column. The sediment group was differentiated from the other groups mainly by OTUs classified as *Acidimicrobiales* OM1 clade, *Pseudomonas*, uncultured Sva0071 (*Gammaproteobacteria*), *Delftia* (*Betaproteobacteria*), unclassified *Gammaproteobacteria*, and unclassified *Actinobacteria*. The dune groundwater was differentiated mostly by OTUs classified as *Pseudomonas*, *Sphingobium* (*Alphaproteobacteria*), unclassified *Rhodobacteraceae* (*Alphaproteobacteria*), unclassified JG30-KF-CM66 (*Chloroflexi*), *Seohaeicola* (*Alpharoteobacteria*), and *Methylotenera* (*Betaproteobacteria*). The playa groundwater was differentiated by OTUs classified as *Halomonas* (*Gammaproteobacteria*), *Marinobacter* (*Gammaproteobacteria*), *Thiomicrospira* (*Gammaproteobacteria*), *Sediminimonas* (*Alphaproteobacteria*), uncultured E6AC02 (*Bacteroidetes*), unclassified *Gammaproteobacteria*.

Similar to bacteria, the archaeal communities clustered in three separate groups too. The ANOSIM indicate R of 0.62 with a p-value < 0.01, implying that the sample groups are moderately different among each other. However, this result may result from significant separation within the sediment group; since group-to-group comparisons in SIMPER showed that archaeal communities differed greatly between three different habitats just as the bacterial communities do (the lowest dissimilarity value between any two groups is about 97%). Within-group similarities were low: 22.61% for sediments and 11.42% for the playa groundwater. The sediment group was differentiated from the others mainly by OTUs classified as unclassified *Thermoplasmatales* (*Euryarchaeota*), *Marine Group I* (*Thaumarchaeota*), and *Halapricum* (*Euryarchaeota*). The deep dune aquifer sample was differentiated due to OTUs classified as *Marine Group I* (*Thaumarchaeota*), unclassified *Woesarchaeota,* and an unclassified archaean. The playa groundwater was differentiated by OTUs representing unclassified *ST-12K10A* (*Methanomicrobia*), genus *Candidatus Halonobonum* (*Euryarchaeota*), and an unclassified archaean.

The eukaryotes exhibit very limited distribution as they were only observed in three shallow sediment samples and all the groundwater samples. The most prevalent eukaryotic phyla were *Viridiplantae* and *Fungi* (**Figure 7**). The low quantity of eukaryotic sequences and their absence from many samples makes it unfeasible to examine trends in the community composition in detail.

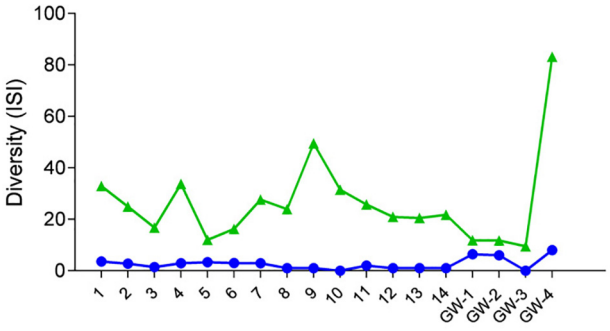

FIGURE 4 | Diversity of samples based on the Inverse Simpson Index (ISI), green triangles represent bacteria, and blue dots represent archaea.

Metabolic inferences of prokaryotic communities further indicate that microorganisms had colonized the subsurface sediments and groundwater taking advantage of diverse micro-environmental conditions (**Figures 9–11**).

DISCUSSION

Desert microbial communities strategically inhabit near-surface environments where they have the availability of sunlight and evaporation triggered chemical disequilibria; at the same time, they remain protected from the desiccation and UV radiation by a thin layer of sediment (e.g., Madigan et al., 2015). Our results show that overall near-surface samples contain more bacterial species that the bottom samples (**Table 3**). However, the diversity indices suggest that in general, the microbial diversity is relatively low and that diversity varies, and it seems to be increased at 50 cm (sample 4) and 90 cm (sample 9) depths. This suggested that near-surface samples contained diverse species, but with few dominate species that are well-adapted to the extreme conditions in this environment. Furthermore, this study shows that there are layers of sediments, possibly with similar geochemistry or similar physical conditions (comprised of two or more samples: Samples 1 and 2; Samples 4 and 5) that poses similar microbial communities (**Figures 9–11**). This observation is in accord with results of Sirisena et al. (2018), where they showed that similar microbial communities are present in sediments with similar geochemistry characterized by depth profiles at Lake Lucero ecosystem. The taxonomic, metabolic, and temperature inferences indicate that aerobic organisms are likely the dominant constituent of the microbial communities, although anaerobes and microaerophiles are also present throughout the sediment column and groundwater samples and that organisms have adapted to different temperature regimes that exist in groundwater (presence of psychrophiles) and sediment column (thermophiles and mesophiles). Based on the predominance of NO_3^- over NH_4^+ and the taxonomic data analyzed it appears that the environment is oxygenated throughout the depth column.

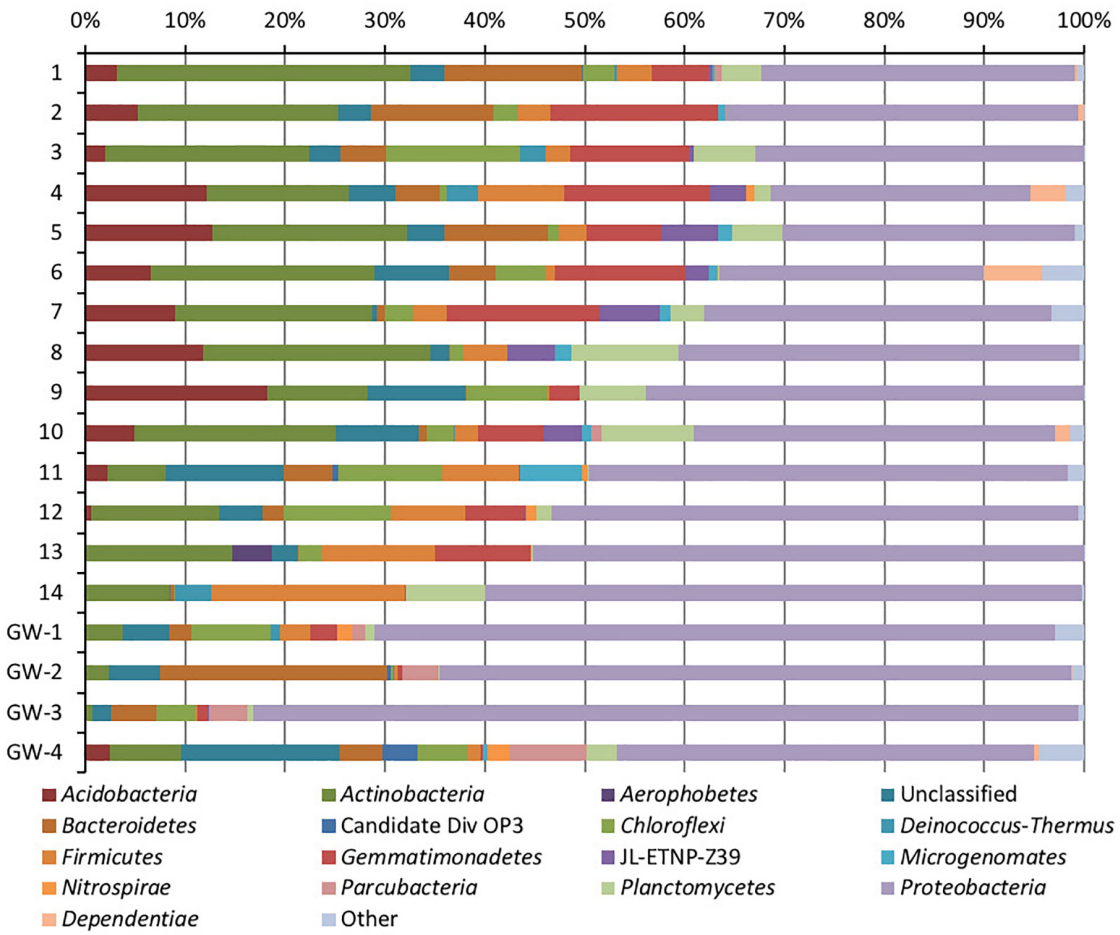

FIGURE 5 | Phylum-level distribution of bacteria in sediments (1 to 14, the numbers increase with the depth) and groundwater (GW-1: on the bottom of the drilled hole; GW-2: piezometer in Lake Lucero and GW-3 and -4: dune deep and shallow groundwater respectively).

Overall, the organisms observed here are generally consistent with those found in other playas and hypersaline environments (Mesbah et al., 2007; Costa et al., 2008; Oren, 2008; Navarro et al., 2009; Makhdoumi-Kakhki et al., 2012; Babavalian et al., 2013).

Groundwater

The analysis of groundwater samples shows that the microbial communities at WSNM differ greatly based on their playa or dune field location (**Figure 8**). Furthermore, groundwater samples varied significantly even within the same site (e.g., the two dune groundwater samples had low similarity) indicating a highly contained nature of these communities. The microbial communities of the dune groundwater samples are largely differentiated from each other by the presence of *Pseudomonas*, *Sphingobium*, and the class *Rhodobacteraceae,* which are significantly more abundant in the deep aquifer (GW-4). *Pseudomonas* specific OTUs are the only group with a significant presence in both samples (>10,000 sequences). *Sphingobium* and *Tepidimonas* are genera of obligate aerobes, so their high abundances may indicate that both aquifers are aerobic (Moreira et al., 2000; Chen et al., 2013). *Seohaeicola* contains aerobic and anaerobic species, as well as moderate halophiles (Yoon et al., 2009; Xie et al., 2014). All of the genera noted here are gram-negative. Archaeal data are not available for the shallow aquifer (GW-3); however, the deep aquifer contains more *Thaumarchaeota* and *Woesarcheota* than playa groundwater or the sediment; which may be indicative of ammonia oxidation at this location. The dune groundwater revealed the predominant presence of eukaryotic clade *Viridiplantae*, which are photosynthetic green algae adapted to live in extreme environments of desert soil (e.g., Lewis and Lewis, 2005) to deep marine water environments (Zechman et al., 2010).

Similar to the dune groundwater, in general, the playa groundwater samples differ from each other but are more similar to each other than to dune groundwater samples (see **Figure 8**). The groundwater below the sediment column (GW-1) has a higher abundance of the genera *Halomonas*, *Marinobacter*, and *Thiomicrospira* while the groundwater in southern Lake Lucero (GW-2) is more abundant in *Sediminimonas*, *Halobacteria*, *Methanomicrobia*, and the uncultured E6ACO2 (*Bacteroidetes*). The only OTU abundant at both locations denotes an unclassified *Gammaproteobacteria*. Similarly to the dune groundwater,

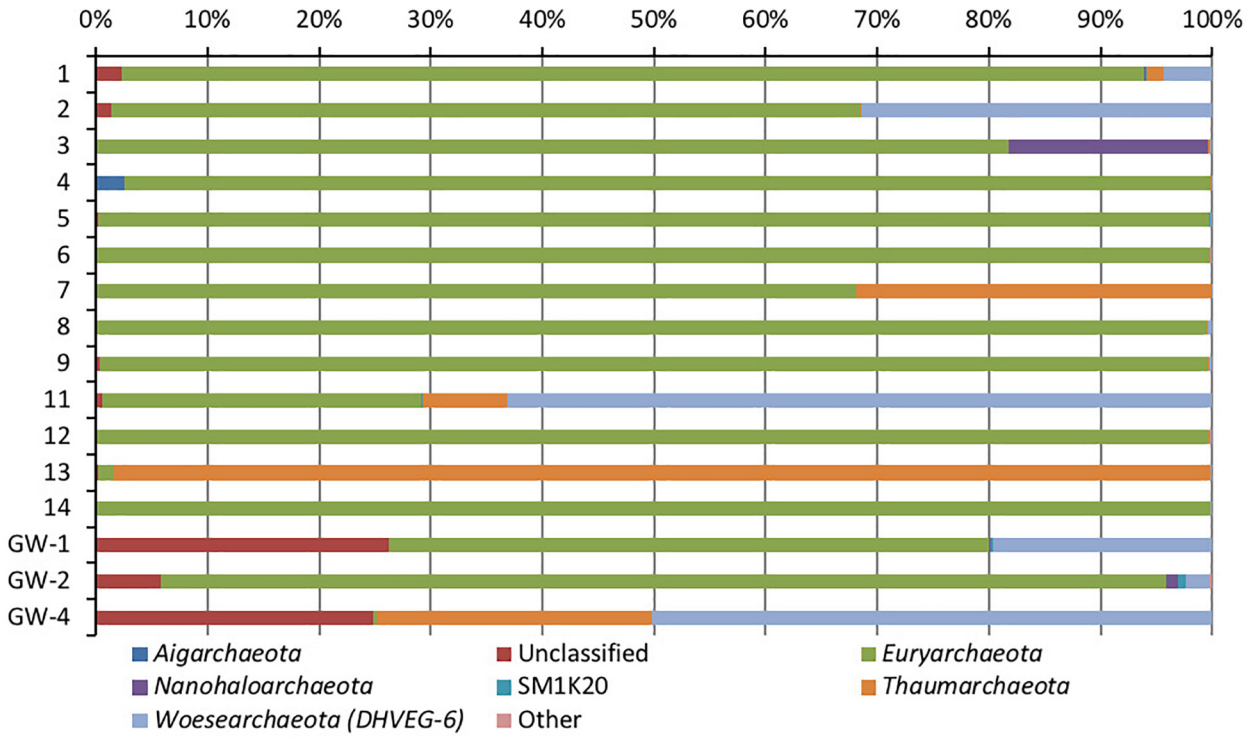

FIGURE 6 | Phylum-level distribution of archaea, in sediments (1 to 14, the numbers increase with the depth) and groundwater (GW-1: on the bottom of the drilled hole; GW-2: piezometer in Lake Lucero and GW-3 and -4: dune deep and shallow groundwater respectively). Samples that contained no archaeal DNA are excluded.

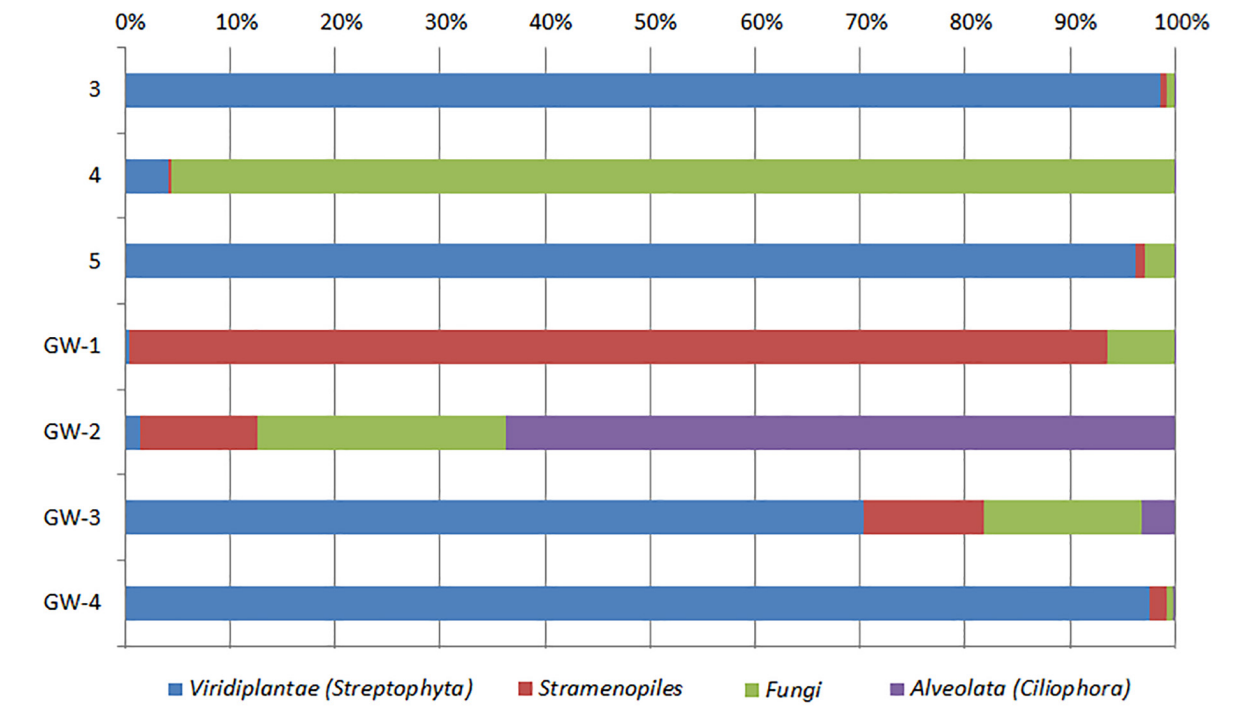

FIGURE 7 | Distribution of eukaryotic groups in sediments (1 to 14, the numbers increase with the depth) and groundwater (GW-1: on the bottom of the drilled hole; GW-2: piezometer in Lake Lucero and GW-3 and -4: dune deep and shallow groundwater respectively). Samples that contained no eukaryotic DNA are excluded.

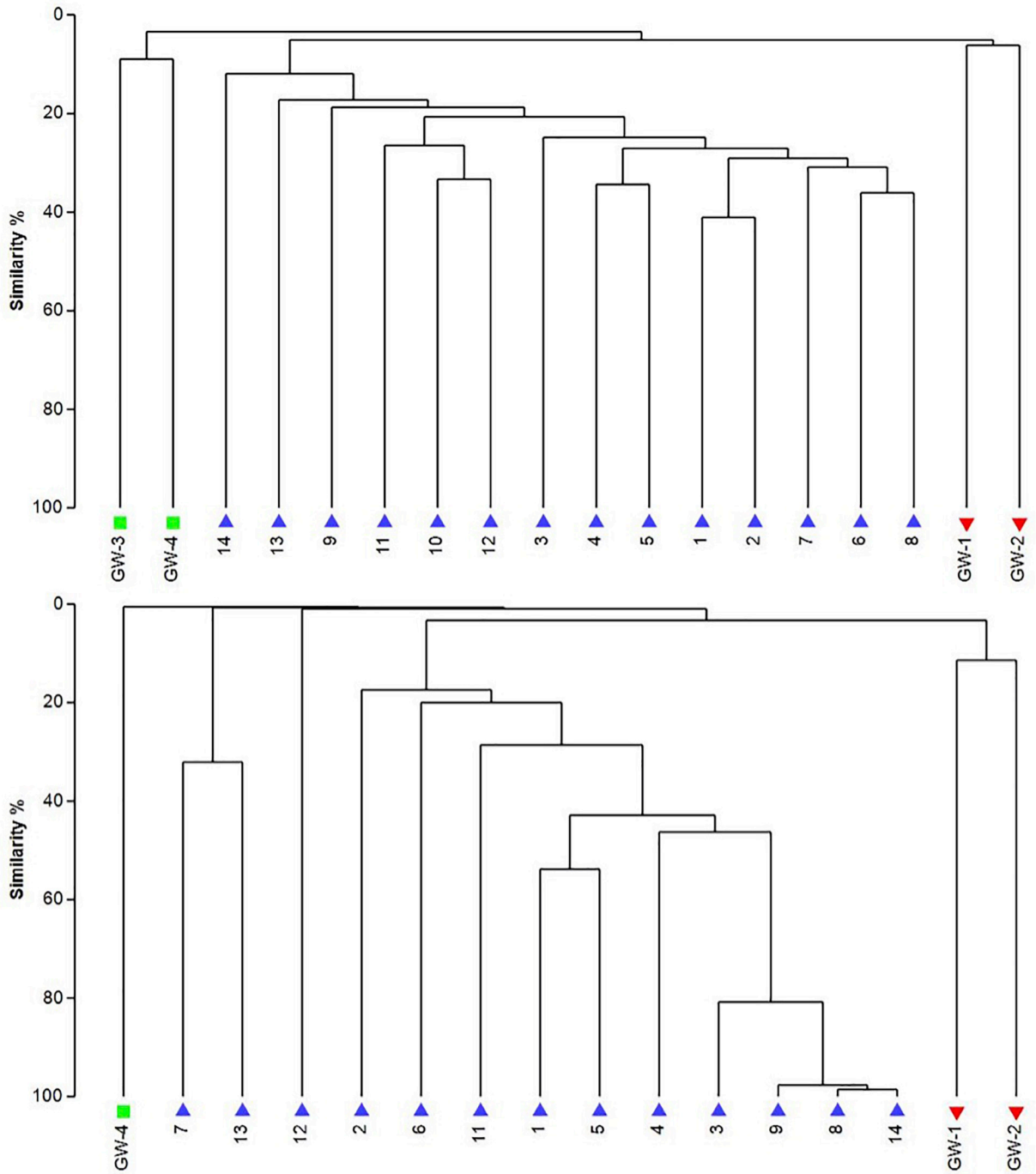

FIGURE 8 | The UPGMA dendrograms of bacteria **(top)** and archaea **(bottom)** based on OTU abundance. The blue triangle is for sediment (1 to 14), the red inverted triangle is for playa groundwater (GW-1, GW-2), and the green square is for dune groundwater (GW-3, GW-4).

gram-negative and aerobic microbes are prominent. Halophile (*Halobacteria*) have a more substantial presence in GW-2 (southern edge of the playa), implying higher salinity at this location (Jeong et al., 2013; Madigan et al., 2015; Zhong et al., 2015), which is confirmed by our conductivity measurements where GW-1 measured 59 μS and GW-2 139.9 μS (**Table 1**). The abundances of *Thiomicrospira* and *Sediminimonas* imply that both locations are primarily oxidizing environments with readily available reduced compounds (Wang et al., 2009; Madigan et al., 2015). Based on metabolic inferences, playa groundwater prokaryotes have a high potential for aerobic metabolic pathways (oxidize iron and sulfur, fix nitrogen to degrade various

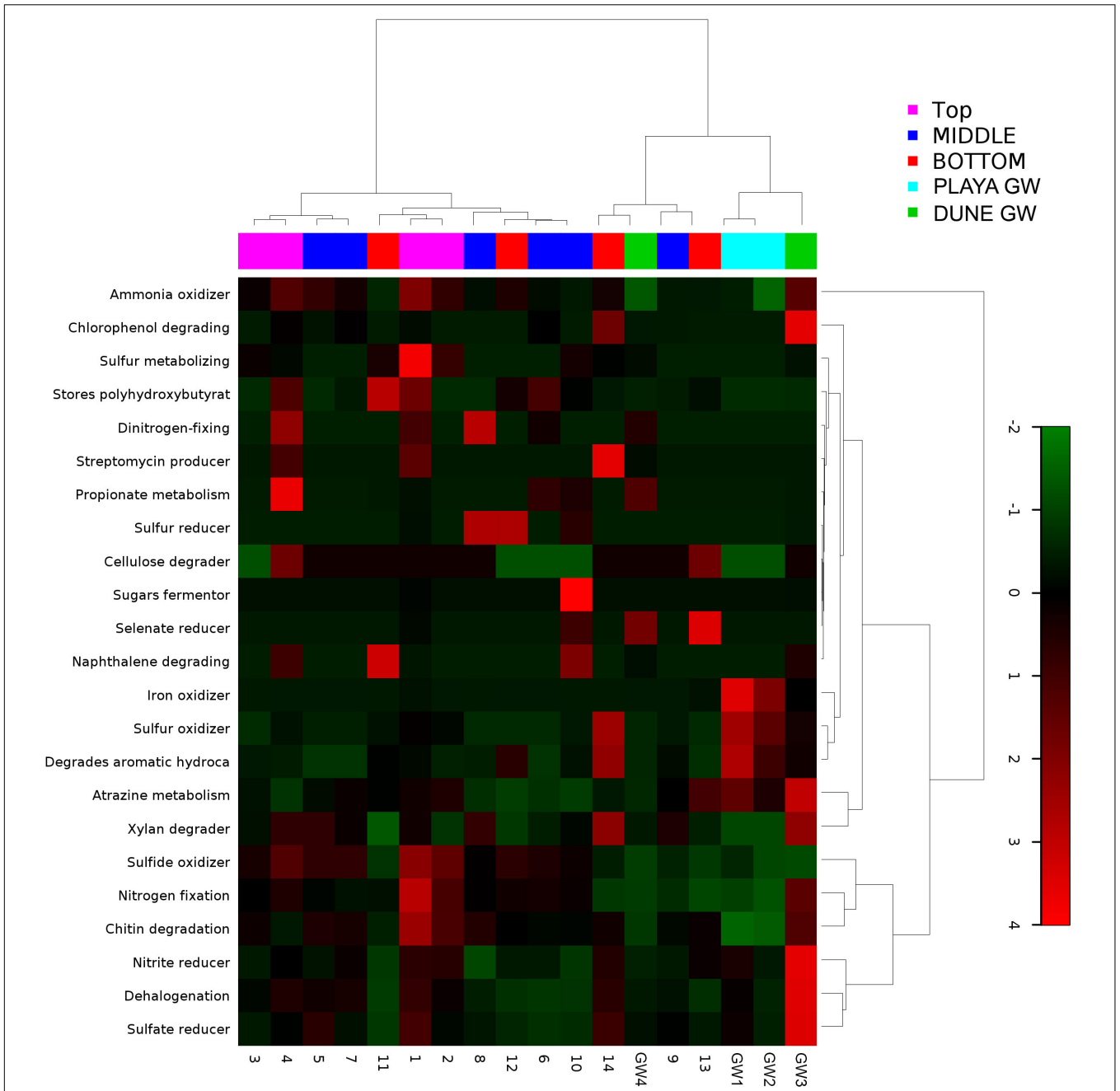

FIGURE 9 | Heatmap of 23 bacterial metabolic potentials constructed from 16S rRNA-based taxonomic identities. The color scale represents relative intensity of each metabolic pathway, with red being the highest and the green the lowest.

organic compounds), however, some organisms with sulfate and nitrate reducing metabolic potentials are available too (**Figures 9**, **10**). Bacterial temperature adaptation inferences indicate that groundwater community is adapted to daily and seasonal extreme temperature changes as organisms with the highest intensity indices belong to psychrophiles (**Figure 11**). Unclassified eukaryotic phyla dominate groundwater sample GW-1, while *Alveolata* and *Stramenopiles* are next relevant groups in GW-2 and GW-1. *Stramenopiles* are mostly represented as diatoms with flagella that would facilitate life in groundwater (Madigan et al., 2015).

A moderate number of methanogenic archaea are observed in the uncultured order STK1210A of the class *Methanomicrobia* (5,000–10,000 sequences) (Madigan et al., 2015). The vast majority of these are present in playa GW-2; methanogens have previously been reported in the groundwater of Lake Lucero (Schulze-Makuch, 2002) and subsurface sediments (Sirisena et al., 2018). Previous work

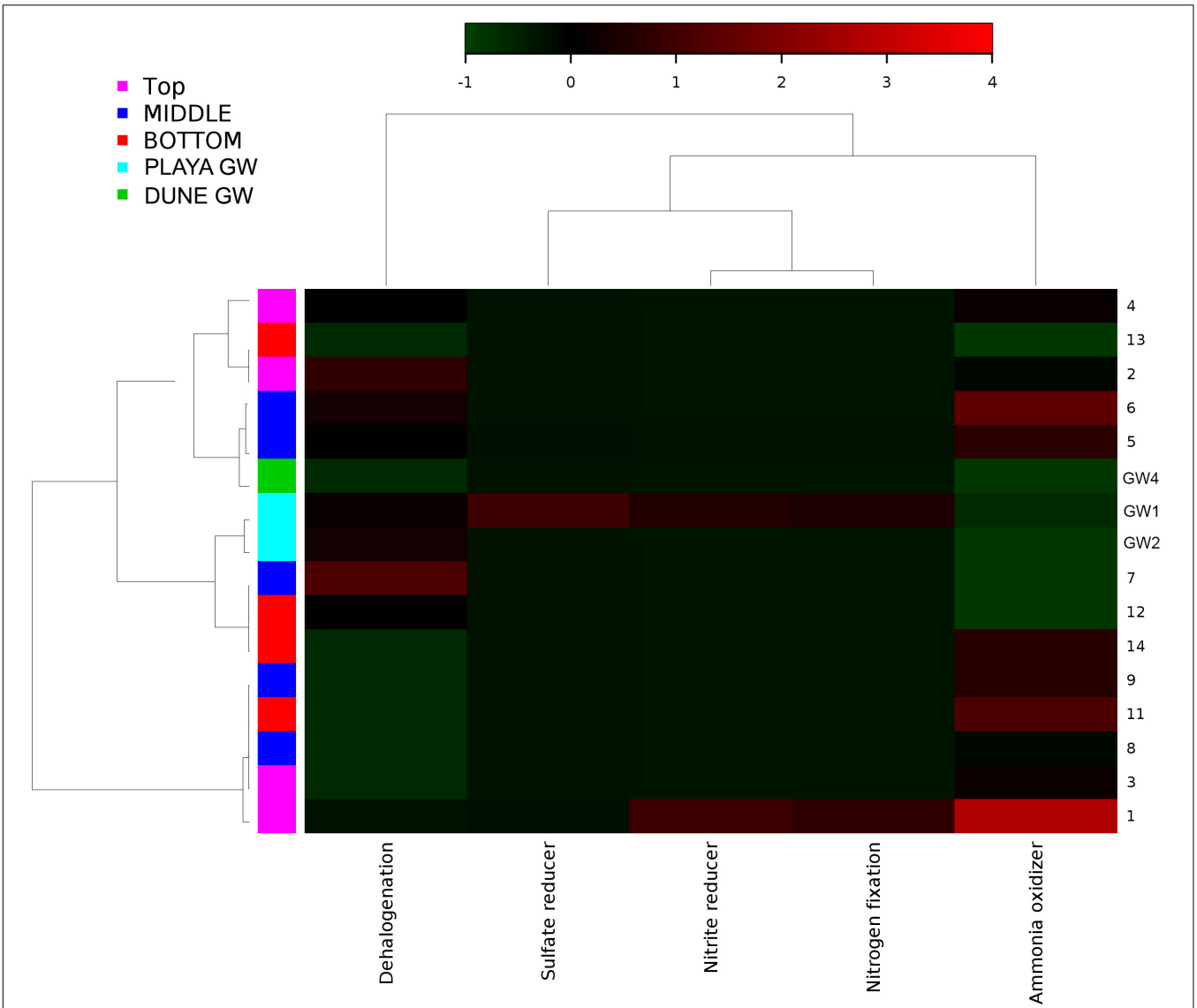

FIGURE 10 | Heatmap of archaeal metabolic potentials constructed from 16S rRNA-based taxonomic identities. The color scale represents relative intensity of each metabolic pathway, with red being the highest and the green the lowest.

has shown that hydrogenotrophic methanogens (such as the *Methanomicrobia*) tend to be inhibited in the presence of sulfate-reducing bacteria, as these microbes consume acetate and H_2 needed by the methanogens (Smith et al., 2008; Garcia-Maldonado et al., 2015).

Sediment and Groundwater Interactions

The mixing effect generated by the capillary action of a very shallow groundwater table makes the subsurface of Lake Lucero a very dynamic environment that intermittently receives moisture from the groundwater even when the surface gets very dry. This dynamism plays a significant role in structuring microbial communities. Although the composition of microbial communities identified within the sediments and groundwater differ significantly (**Figure 7**), it seems that the capillary action of the groundwater causes a limited redistribution of microbes throughout the column preventing microbial segregation by depth, in which some of the microbes appear to be displaced. For example, the presence of purple phototrophic bacteria deep in the sediment column, where they would have limited or no access to sunlight, they can survive under these conditions but cannot grow optimally (Casamayor et al., 2008). It is important to note that, in general, the playa's groundwater microbial community is more similar to the sediment community than that of the dune groundwater, although the similarity percentage is low. The stable stratification seen in microbial mats in wetter settings cannot be maintained under these dry and occasionally moistened conditions, and thus the community composition in Lake Lucero seems to be different from that seen in environments with a salt crust

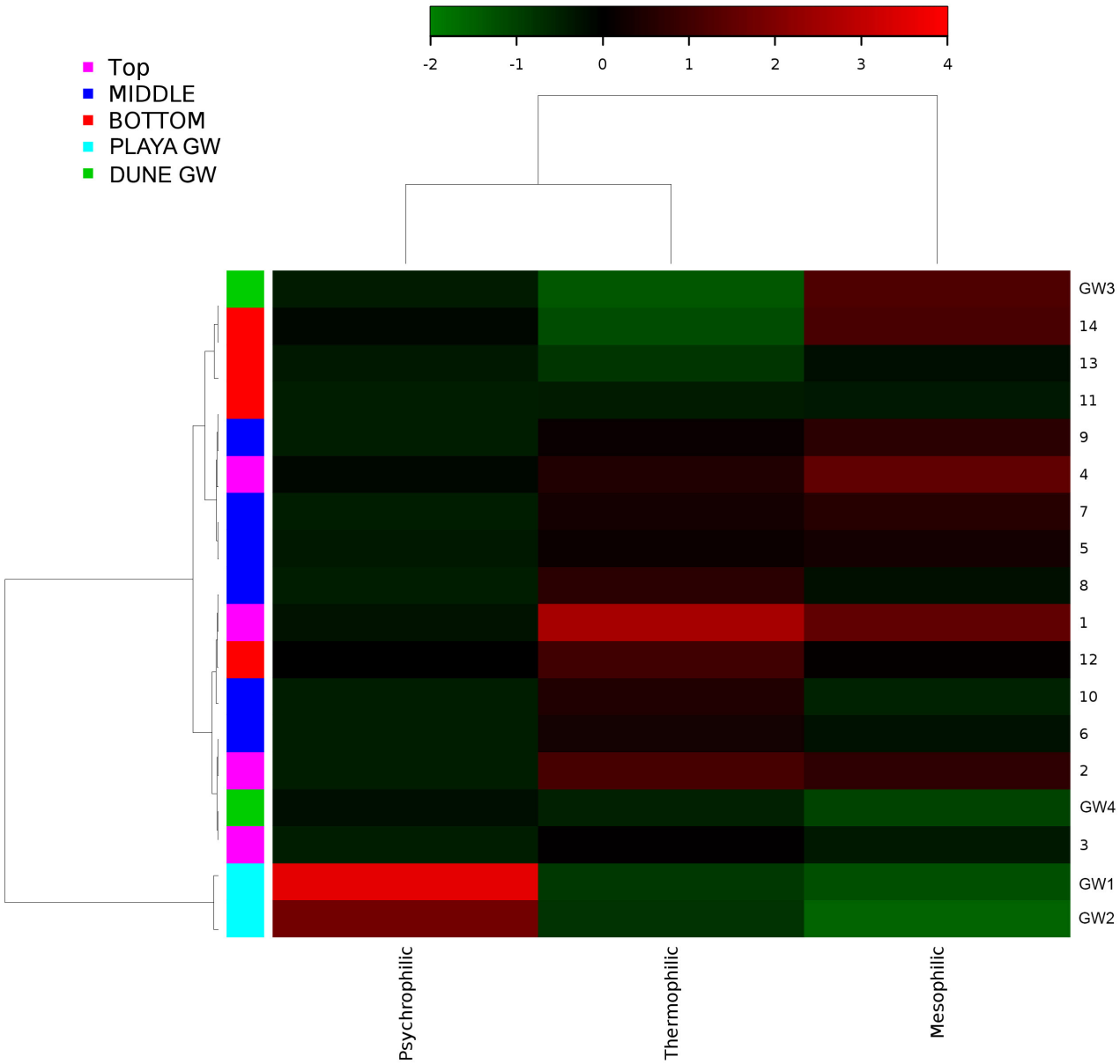

FIGURE 11 | Heatmap of bacterial temperature adaptation inferences constructed from 16S rRNA-based taxonomic identities. The color scale represents relative intensity of each metabolic pathway, with red being the highest and the green the lowest.

and microbial build-ups. Similarly, Canfora et al. (2014) show that the presence or absence of such crust is a significant differentiating factor amongst the microbial communities of saline environments.

Similarly, to more stable wet settings, the dry environments that maintain somewhat continuous environmental conditions will exhibit microbial stratification too (Sirisena et al., 2018). Sirisena et al. (2018) have observed microbial stratification at the edge of the Lake Lucero. The difference in this and their sampling points is that the lake edge dries sooner than the center (topographic low) and the groundwater table is deeper at the edge (they were not able to reach the groundwater table during the sampling), so the sediment was dry throughout the sampled profile. The lack of groundwater allowed for the development of anoxic communities on the bottom of the sampling site, and this is not the case in this central part of the playa where the oxidizing groundwater and associated capillary action are influencing community structure and environmental chemistry. Surprisingly groundwater and sediment contain communities with dramatically different adaptations to temperature regime. The groundwater may get easily cooled close to freezing during the winter time when the night temperatures get bellow the freezing point, and the organisms living in the water consist of psychrophiles

TABLE 3 | Diversity metrics from bacterial and archaeal 16S rRNA gene Illumina Miseq sequencing.

Sample	No. of reads	No. of OTUs	Diversity indices		Evenness indices		Estimated richness		Coverage
			Simpson	Shannon	Simpson	Shannon	Chao 1	ACE	Good
Bacteria[a]									
1	132,470	1,515	19.061178	4.718459	0.07429	0.747621	743.732058	967.250947	0.993249
2	79,517	812	21.988785	3.738441	0.250134	0.780696	397.041124	799.701548	0.994271
3	99,017	782	19.956364	3.619609	0.232723	0.759208	389.72082	896.242879	0.994169
4	117,298	899	36.639509	4.198392	0.349154	0.842351	398.779234	595.293092	0.99463
5	69,815	897	23.519454	3.980187	0.245591	0.804175	406.277957	806.39352	0.993948
6	66,297	770	23.111976	3.786453	0.220272	0.779215	388.356512	1239.246434	0.993596
7	105,162	706	16.867009	3.541933	0.214934	0.76288	308.724164	676.405993	0.994505
8	99,196	666	18.440478	3.5071	0.239623	0.768525	294.563452	609.696937	0.993955
9	118,886	697	19.739544	3.462572	0.240779	0.747145	332.211666	871.631594	0.994041
10	109,096	765	21.695474	4.107581	0.166903	0.807015	299.639737	303.734827	0.993275
11	81,756	711	14.023681	3.32267	0.225944	0.737564	425.100165	960.777085	0.994471
12	96,591	972	22.88627	4.085189	0.240819	0.813293	381.884719	637.456159	0.99393
13	83,903	548	11.454561	3.044709	0.145956	0.671205	229.294937	440.621694	0.994713
14	85,670	479	15.926822	3.120422	0.243184	0.728504	257.006363	748.584071	0.995031
GW-1	110,430	933	8.370894	3.560572	0.095972	0.709815	373.632901	787.195774	0.993874
GW-2	49,781	746	11.784472	3.546838	0.066229	0.662226	315.290841	335.071847	0.992447
GW-3	146,284	1,409	5.417147	3.736143	0.055545	0.664866	565.168842	1000.074716	0.993102
GW-4	83,477	1,311	71.262153	5.389618	0.208565	0.873887	554.577184	507.720065	0.991274
Archaea[b]									
1	13,946	130	3.594778	1.760895	0.413368	0.709585	16.5885	34.675379	0.996917
2	10,694	48	2.762361	1.149301	0.469699	0.642542	6.435833	12.567437	0.997569
3	3,204	34	1.48348	0.175187	0.69195	0.54049	2.165	0.082	0.99407
4	5,244	31	2.945836	1.296066	0.676964	0.796717	5.676667	9.24569	0.996758
5	6,190	77	3.340255	1.52502	0.611924	0.774539	9.48275	22.716393	0.993215
6	9,213	50	3.07368	1.393258	0.642189	0.798194	6.08	7.495332	0.997069
7	10,204	33	2.962945	0.888007	0.695001	0.740935	3.9525	1.730232	0.998138
8	1,781	23	1.036928	0.139464	0.737398	0.592432	1.8585	0.019	0.991016
9	3,525	40	1.057984	0.218579	0.638017	0.481737	2.5715	0.081111	0.992908
11	17,291	58	2.064032	0.183981	0.67752	0.521257	2.2265	0.082	0.997687
12	2,658	29	1.037109	0.322761	0.513639	0.347212	3.342333	0.598285	0.992476
13	5,404	34	1.039981	2.416355	0.522688	0.816609	27.70005	56.4991	0.995929
14	3,674	22	1.019328	0.07938	0.843008	0.747722	1.464	0.006	0.996189
GW-1	11,395	120	6.497753	2.134756	0.699867	0.860418	15.07845	16.888131	0.994208
GW-2	50,788	299	6.001275	2.517272	0.474777	0.809518	29.270993	56.417967	0.996909
GW-4	8,385	68	8.062561	1.714997	0.536062	0.775391	10.50305	14.292014	0.995587

[a] *Samples were rarefied to the smallest sample size (49781 reads) for the diversity, evenness, richness, and coverage calculations.* [b] *Samples were rarefied to the smallest sample size (1781 reads) for the diversity, evenness, richness, and coverage calculations. Samples 10 and GW-3 contain very low number of Archaeal reads (42 and 59 respectively). Therefore, these two samples were eliminated from subsequent analyses: diversity, cluster, and metabolic inference analysis.*

(**Figure 11**). The sediments may get hot during the day and the organisms living in the sediments are mostly represented by thermophilic and mesophilic forms. Additionally, we had hypothesized that the longer presence of readily available water at the center of the lake may influence the increase in diversity when compared to other, drier, parts of the playa (such as the location described at the edge of the lake in Sirisena et al., 2018). When comparing the diversity indices among the data, Simpson indices are showing overall higher values for the central location, and Shannon indices are about the same; which may be indicative of some increase in diversity at the center of the lake vs. the edge of the lake.

Distribution of Organisms Along the Sediment Profile

Although the capillary action of groundwater causes mixing of microbial organisms, we have observed some trends too. The deepest part of the sediment column contains sticky clays, a slight increase in NH_4^+ concentrations, lower NO_3^- concentrations, and the presence of saprophytes. However, NO_3^- levels are still higher

than NH_4^+ and saprophytes are low in abundance, and samples 12 to 14 metabolic potential (**Figure 9**) is the highest for NH_4^+ and sulfide oxidation, and Chitin degradation indicating that even at this depth, the playa sediments may still remain aerobic.

Proteobacteria were present in all samples and became more abundant with the depth. They were also more prevalent in groundwater, except the deep dune groundwater (GW-3); in the shallow dune groundwater, this phylum composed more than 80% of the bacterial OTUs. Such high presence of *Proteobacteria* may be due to the gram-negative nature of the *Proteobacteria*; their cell walls would make them less susceptible to osmotic lysis caused by sudden influxes of water during the wet season (Madigan et al., 2015). The *Gammaproteobacteria* genus *Pseudomonas* has a large presence throughout all samples, especially in the sediment (Madigan et al., 2015). SIMPER analysis showed that OTUs identified as *Pseudomonas* were significant differentiating factors for sample 14 and the dune groundwater samples. However, without species-level identification of the OTUs and more in-depth analysis (e.g., mRNA analysis), it is difficult to understand this distribution. Conversely, *Acidobacteria* and *Gemmatimonadetes* were abundant in most sediment samples but mostly absent from groundwater samples.

Bacteroidetes are significantly more abundant in the upper half of the sediment column than the bottom part, possibly due to the increased availability of cellulose and chitin closer to the surface (**Figure 5**). *Bacteroidetes* are typically saccharolytic (specializing in the degradation of complex polysaccharides such as cellulose and chitin) (Madigan et al., 2015), and polysaccharides could be available at WSNM from the plants and arthropods that have been seen on and near the surface (Stroud, 1950; Muldavin et al., 2000). The *Actinobacteria* are similarly less abundant in deeper sediment samples, and even less abundant in groundwater samples. The most significant of these are the family *Acidimicrobiales*, in particular, the OM1 clade; the single largest OTU in the dataset belongs to this class (approximately 102,000 sequences). They are more abundant in samples 1–13 of the sediment column than in sample 14 or the groundwater, as was shown via SIMPER analysis. This uncultured group of *Actinobacteria* has been observed often in freshwater and marine environments and is thought to be oligotrophic and planktonic (Morris et al., 2012; Ghai et al., 2013; Mizuno et al., 2015). In contrary, the *Firmicutes* are generally more abundant in deeper sediment samples and have a marginal presence in the groundwater samples.

Another example of localized distribution within community structure is bacterial phylum *Chloroflexi*, which is mostly present in samples 11–13 and the groundwater beneath the sediment column. Their distribution in the sediment correlates with the increase in the concentrations of Fe, K, Mg, and Ti ions in samples 11–13, the change in lithology (presence of sticky dark brown to black clay), and direct exposure to groundwater capillary action. This correlation may indicate that groundwater capillary action may provide higher availability of nutrients at this depth. Aside from the already mentioned green non-sulfur bacteria, the most abundant classes of the *Chloroflexi* are uncultured groups (JG30-KF-CM66 and S085) and unclassified OTUs. The unknown OTUs and JG30-KF-CM66 drive the *Chloroflexi* abundance in samples 11 to 13.

In comparison to groundwater, the sediment samples are more consistent in their microbial communities. The most distinct is sample 14, which is a relative outlier from the rest of the sediment column due to negligible presence of *Acidimicrobiales* OM1 in sample 14 as opposed to its high abundance in the rest of the sediment. These planktonic bacteria flourish during the wet season and lay dormant during the dry season, in our case they are the most abundant at the surface and seem to be redistributed throughout the sediment column most likely via capillary action (Morris et al., 2012; Ghai et al., 2013; Mizuno et al., 2015). Additionally, sample 14 contains a much higher abundance of *Acinetobacter*, a diverse bacterial genus with most free-living soil species that are saprophytes (Doughari et al., 2011). Only *Pseudomonas* is identified as being consistently abundant throughout the sediment column. The archaeal communities were less consistent than the bacterial, the sample 12 was isolated, and samples 7 and 13 were paired while the rest of the samples grouped in a dendrogram (**Figure 7**). Samples 7, 12, and 13 all had a negligible abundance of *Thermoplasmatales*, while the other samples had them in high abundance. The samples 7 and 13 also had a uniquely higher abundance of *Thaumarchaeota* (ammonia oxidizers), while 12 was unique for its high abundance of the halophilic genus *Halapricum* (Campbell et al., 2011; Song et al., 2014). Although the clustering of the *Halapricum* population in sample 12 is curious, it implies that the communities in this sample are not too different from 7 to 13 since halophiles are ubiquitous in all samples and *Halapricum* is not significantly different from other *Halobacteria* genera; additionally, 7 has a high abundance of unclassified *Halobacteria* (Song et al., 2014). Therefore, it seems that the main difference between the archaeal communities of samples 7, 12, and 13, and the rest of the sediment is the abundance of *Thermoplasmatales*. Considering that the metabolic inferences do not reveal any taxonomic grouping based on metabolic potential (**Figure 10**), it seems that differences within the archaeal communities derive from the fact that most of the Archaeal OTUs were not classified up to Genus level when compared to bacterial OTUs. Further, the upper levels of the sediment (samples 3, 4, and 5) show the presence of fungi and *Viridiplantae*, which may be organismal remnants of the ephemeral lake that withdrew their presence to the last near surface hydrated habitats. Fungi are mostly represented by the subphyla *Pezizomycotina* (phylum *Ascomycota*), a highly diverse group that includes saprophytes, plants, and mutualists (Kumar et al., 2012).

Halophiles and Oligotrophs

The hypersalinity is one of the most dominant characteristics of Lake Lucero environment, and halophiles have a substantial presence in the examined population. The identified archaeal OTUs are from the classes *Halobacteria* and *Methanomicobia* (unclassified halophile ST-12K10A), and the phylum *Nanohaloarchaeota*; which are common for hypersaline environments (Sorenson et al., 2005; Falb et al., 2008; Oren et al., 2009; Barton and Northup, 2011; Garcia-Maldonado et al., 2015;

Madigan et al., 2015; Di Meglio et al., 2016). The uncultured groups of order *Thermoplasmatales* are identified with a significant presence in the sediments; some of these uncultured groups have been previously reported in the saline environments (Siam et al., 2012; Madigan et al., 2015).

Halophiles are present in all the dominant bacterial phyla: *Proteobacteria, Actinobacteria, Firmicutes, Chloroflexi,* and *Bacteroidetes* (Madigan et al., 2015). The purple sulfur bacteria order *Chromatiales* (*Proteobacteria*) contains some of the most extreme bacterial halophiles and has been observed in similar hypersaline environments (Sorenson et al., 2005). A highly abundant (>10,000 sequences) halophile is the nitrite and nitrate-reducing genus *Sediminimonas* in the groundwater of southern Lake Lucero (Wang et al., 2009). Halophiles observed in moderate abundance (5,000–10,000 sequences) include the genera *Salinibacter*, *Staphylococcus*, *Streptococcus*, and *Nitriliruptor* (Mesbah et al., 2007; Anton et al., 2008; Makhdoumi-Kakhki et al., 2012; Madigan et al., 2015). *Nitriliruptor* is alkaliphilic (Sorokin et al., 2009). Low abundance (1,000–5,000 sequences) halophiles include the genera *Rothia*, *Kocuria*, and *Truepera* (Albuquerque et al., 2005; Chou et al., 2008; Tang et al., 2009).

The halophiles observed are diverse, and they include extreme (*Chromatiales)*, moderate (e.g., *Nitriliruptor*) and slightly (e.g., *Truepera*) halophilic groups (Albuquerque et al., 2005; Sorokin et al., 2009). The distribution of halophiles is relatively uniform, which implies that there is no significant salinity gradient within the sediment column. This observation is consistent with relatively uniform concentrations of Na in these samples. Additionally, the detected halophiles are predominantly aerobic (Costa et al., 2008; Navarro et al., 2009; Makhdoumi-Kakhki et al., 2012; Babavalian et al., 2013; Canfora et al., 2014).

The genus *Ralstonia* is observed in abundance, at the sediment surface (samples 1 and 2), the groundwater and the sediment interface (samples GW-1 and14), this genus contains oligotrophic organisms (such as *R. pickettii*) that are common in water and soil (Ryan et al., 2007). Another oligotrophic phylum, *Gemmatimonadetes* is highly abundant (Fawaz, 2013). These organisms are commonly observed in arid soils and are well-adapted to living in low moisture conditions, but they are not known to be well-adapted to wet-dry cycles of playa environment; therefore in here, they are present in lower abundance at the surface and very low abundance in the groundwater (Fawaz, 2013). The previously mentioned *Acidibacteriales* OM1 is also oligotrophic (Mizuno et al., 2015). The deficiency in available nutrients in Lake Lucero makes this a natural habitat for oligotrophs, so their abundance and wide distribution in this environment are anticipated (Madigan et al., 2015).

Photosynthetic Organisms

A moderate amount of green non-sulfur bacteria (anoxygenic phototrophs found in a wide range of environments) and purple sulfur bacteria were observed but the phylum *Chlorobi*, which consists of green sulfur bacteria, is present in very low abundance (Madigan et al., 2015). *Cyanobacteria* are observed in very low abundance. It is possible that the mixing effect of the groundwater capillary action limits the growth of phototrophs since it prevents the segregation of microbial communities, which would allow for stabilization in the most favorable position. This mixing would also have the potential to redistribute phototrophs to deeper levels of the sediment where they could be living in a state of dormancy (Jones and Lennon, 2010).

Nitrogen Cycle

Portions of the nitrogen cycle at Lake Lucero were assessed through the concentrations of NH_4^+, NO_3^-, and the OTU abundance data. The NO_3^- concentrations are 5.97 to 22.94 times higher than the NH_4^+ in analyzed samples, indicating the oxidizing environment and nitrogen oxidation as a possibly important microbial process. Organisms that possess capabilities to contribute to nitrogen cycling have been identified in the samples (**Figures 9**, **10**). However, based on our data, we cannot say with certainty whether they used these capacities and in what measure. Metabolic potential map indicates that bacterial and archaeal organisms have potential for nitrogen and dinitrogen fixation, ammonia oxidation and nitrate reduction (**Figure 9**), making them capable of utilizing and cycling available NH_4^+ and NO_3^- compounds. A moderate amount of green phototrophic bacteria capable of nitrogen fixation are observed in samples 11–13 (Wahlund and Madigan, 1993). A small amount of nitrogen-fixing purple phototrophic bacteria are observed, predominantly at the surface (sample 1). Additionally, they were found in samples 8, 11, 12, and the deep aquifer (GW-3) sampled at the dune field (Wahlund and Madigan, 1993). No other known nitrogen-fixing microbes are explicitly identified. These coincides with the mapped nitrogen fixing pathways (**Figures 9**, **10**) in prokaryotes from samples 1, 2, 4, 8, and 12 as well as GW-3. Nitrate reduction has been inferred in top most samples 1 and 2 and in groundwater samples GW-1 and 3 and for sample 14, at the bottom of the sampled interval. A very small amount of anaerobic ammonium oxidizing (anammox) bacteria of the order *Brocardiales* are observed, only in the deep aquifer of the dune groundwater (Jetten et al., 2009). Rhizobial genera are identified in large amounts (mostly *Bradyrhizobium*) and are well-distributed throughout the sediment column but with comparatively low abundance in groundwater (Madigan et al., 2015). The absence of observed plants here indicates that rhizobia likely live freely in the soil, in which state they cannot fix nitrogen (Madigan et al., 2015).

The distribution of green and purple bacteria in the sediment profile implies that nitrogen fixation is possible at the surface; additionally, the input of nitrogen into the system is likely augmented by atmospheric deposition too (Fenn et al., 2003). In our samples, the distribution of potential ammonia-oxidizers generally mirrors that of the potential nitrogen fixers. The small number of nitrifying microbes is distributed throughout the sediment column. These observations, as well as a large difference in NH_4^+ and NO_3^- concentrations, indicate that the environment along the depth profile is aerobic and that nitrification processes could be important in this system. The dune groundwater seems to have a predominant presence of organisms capable of nitrification, although the brine-based groundwater is differentiated by the presence of anammox bacteria. Both, NO_3^- and NH_4^+ concentrations are generally low,

as is typical in arid environments (Madigan et al., 2015). The slight increase in NH_4^+ concentrations at the bottom of the sediment profile implies the possible presence of the decaying organics or denitrification and DRNA (dissimilative reduction of nitrate to ammonium) that may occur here. Further, a moderate abundance of *Petrimonas* in sample 11 (contains the species *P. sulfuriphila* which reduces elemental sulfur and nitrate and is a mesophilic anaerobe) correlates with the darker coloration of sediments at this depth, which additionally suggests the presence of decaying organic matter (Grabowski et al., 2005). *Coryneform* bacteria are aerobic saprophytes that are also present in low abundance at this depth; by degrading organic matter, they release ammonium into the soil (Madigan et al., 2015). However, even in this part of the sediment column, NO_3^- concentrations are still 7.03 times higher than NH_4^+ concentration.

Sulfur Cycle

All of the WSNM environments are sulfur dominated, so it is interesting to inquire whether these resources are available and potentially used by microbial organisms inhabiting the area. From our work, we are only aware of the mineral substrates rich in sulfur element, as gasses or water composition had not been analyzed. The purple sulfur bacteria may use H_2S as an electron donor (or elemental sulfur if H_2S is limited) and often rely on sulfate-reducing and/or sulfur-reducing microbes to produce H_2S (Madigan et al., 2015). Their occurrence in samples 11 and 12 coincides with the presence of the sulfur-reducing *Petrimonas* detected in sample 11 (Grabowski et al., 2005). Despite the abundance of gypsum and other sulfur-bearing minerals in this environment, only a small number of sulfate-reducers and sulfur-reducers are observed, although the highly abundant genus *Pseudomonas* contains species that are capable of sulfur-reduction (such as *P. mendocina*) (Madigan et al., 2015). Inferred sulfur reducing metabolic pathways were observed in samples 8, 12, 10, while sulfate reducers were observed in samples 1, 5, 14 and in dune groundwater (GW-3). The low abundance of sulfate-reducing microbes is likely due to the predominantly aerobic environmental setting, and the samples are not rich in organic matter to use as electron donors (Madigan et al., 2015). We have not observed any living plants near our sampling site; no biofilm or decaying plants were detected in any of our samples by eye or using SEM/EDS. Possible carbon sources would include chitin from the exoskeletons of arthropods, and the phototrophic microbes observed in the sediment (Madigan et al., 2015).

Thiomicrospira is the only sulfur-oxidizing genus observed, but it is highly abundant and mostly distributed in sample GW-1 (at the bottom of the sampled sediment profile), with a minor presence at the surface (Sorokin et al., 2006a,b; Madigan et al., 2015). This coincides with the metabolic inferences heatmap where GW-1, GW-2, and sample 14 were mapped with the highest intensity for sulfur oxidation. The relative lack of sulfur oxidizers in the sediment column implies that most of the sediment has a low amount of reduced sulfur compounds compared to the groundwater, as would be likely in a primarily aerobic setting with a large number of sulfate minerals. The presence of *Chromatiales* and *Thiomicrospira* at the surface suggests that there is a source of reduced sulfur in this environment. The minor presence of purple sulfur bacteria in the dune groundwater implies the same at that location. Nonetheless, it seems that oxidative processes would dominate the sulfur cycle in Lake Lucero sediments, which would be consistent with the assessment of the nitrogen cycle and the microbial populations. Overall, the organisms with the metabolic potential of sulfur cycling are not abundant in this environment even though sulfur dominates the chemistry of mineral substrate, which seems not to be bioavailable.

CONCLUSION

The sediment and groundwater of Lake Lucero are highly dynamic environments, strongly characterized by the extreme seasonality of the climate, the capillary action of the groundwater, and the hypersalinity. This extreme environment harbors microbial communities that are primarily aerobic, gram-negative, and are largely characterized by their survival adaptations.

Halophiles and oligotrophs are extremely common throughout all samples, as anticipated. The observed communities are very diverse and contain organisms capable of different metabolic pathways: methanogens, phototrophs, heterotrophs, saprophytes, ammonia-oxidizers, sulfur-oxidizers, sulfate-reducers, iron-reducers, nitrifiers, and denitrifiers.

The microbial diversity varied significantly between groundwater and sediment samples. The dynamism of this environment manifests in the relatively consistent character of the sediment hosted microbial communities, where significant distinctions are more taxonomic than phenotypic. Taxonomically, the dune and playa groundwater organisms will group separately from each other and separately from sediment. Temperature adaptation inferences revealed that organisms living in the groundwater are likely psychrophiles, while organisms inhabiting the sediment column consist of thermophiles and mesophiles that can withstand elevated temperature regime. Additional ecological partition is observed as a change in the deepest part of the column as the communities are affected by the presence of sticky clays, higher concentrations of various cations, and potentially decaying organic material. Saprophytes and *Chloroflexi* are more abundant in these lithologies. The salinity appears to be lower, as indicated by the decrease in Na concentration, and a lower abundance of extreme halophiles relative to the rest of the sediment profile.

Complex ecosystems as such as the one of Lake Lucero may have existed on Mars in the past and we have demonstrated in this paper and in Sirisena et al. (2018), that subsurface of desert environment may host very diverse organisms and diverse environments. We hope that the variety of the discussed environments may inform future astrobiological explorations.

DATA AVAILABILITY STATEMENT

Raw Illumina sequencing data was archived in SRA (Sequence Read Archive) at NCBI under the BioProject number: PRJNA558907.

AUTHOR CONTRIBUTIONS

All authors contributed to the intellectual input and assistance on this project, and approved the final version of the manuscript. SR, MG, and IW collected the data. SR, KS, and MG contributed to the data processing and analysis. MG collected the samples. SR and MG wrote the manuscript.

FUNDING

This work was supported by a NASA-ASTEP NNX14AT28G grant to MG. Undergraduate interns working on this project MZ and SP were funded by NSF LSAMP 1400780 to PI Alexander Gates (Rutgers University – Newark).

ACKNOWLEDGMENTS

We thank Kimberly Wirtz and David Bustos (NPS White Sands) and Verena Starke (Geophysical Laboratory, Carnegie Institution of Washington) for their invaluable help during the field season. We also thank Mousa Ziedan and Steven Potochniak (undergraduate researchers) who had helped with XRD analyses and SEM/EDS observations.

REFERENCES

Albuquerque, L., Simoes, C., Nobre, M. F., Pino, N. M., Battista, J. R., Silva, M. T., et al. (2005). *Truepera radiovictrix* gen. nov., sp. nov., a new radiation resistant species and the proposal of *Trueperaceae fam*. nov. *FEMS Microbiol. Lett.* 247, 161–169. doi: 10.1016/j.femsle.2005.05.002

Andrews Hanna, J. C., Zuber, M. T., Arvidson, R. E., and Wiseman, S. M. (2010). Early Mars hydrology: Meridiani playa deposits and the sedimentary record of Arabia Terra. *J. Geophys. Res. Planet*. 115:E06002.

Anton, J., Pena, A., Santos, F., Martinez-Garcia, M., Schmitt-Kopplin, P., and Rossello-Mora, R. (2008). Distribution, abundance and diversity of the extremely halophilic bacterium *Salinibacter ruber*. *Salin. Syst.* 4:15. doi: 10.1186/1746-1448-4-15

Arndt, D., Xia, J., Liu, Y., Zhou, Y., Guo, A. C., Cruz, J. A., et al. (2012). METAGENassist: a comprehensive web server for comparative metagenomics. *Nucleic. Acid. Res.* 40, W88–W95. doi: 10.1093/nar/gks497

Auld, R. R., Mykytczuk, N. C., Leduc, L. G., and Merritt, T. J. (2016). Seasonal variation in an acid mine drainage microbial community. *Can. J. Microb.* 63, 137–152. doi: 10.1139/cjm-2016-2215

Babavalian, H., Amoozegar, M. A., Pourbabaee, A. A., Moghaddam, M. M., and Shakeri, F. (2013). Isolation and identification of moderately halophilic bacteria producing hydrolytic enzymes from the largest hypersaline playa in Iran. *Microbiol.* 82, 464–474. doi: 10.1134/S002626171304 0176

Barton, L. L., and Northup, D. E. (2011). *Microbial Ecology*. Hoboken, NJ: Wiley and Sons, 420.

Campbell, M. A., Chain, P. S. G., Dang, H., El Sheikh, A. F., Norton, J. M., Ward, N. L., et al. (2011). Nitrosococcuswatsonii sp. nov., a new species of marine obligate ammonia-oxidizing bacteria that is not omnipresent in the world's oceans: calls to validate the names '*Nitrosococcus halophilus*'and '*Nitrosomonas mobilis*. *FEMS Microbiol. Ecol.* 76, 39–48. doi: 10.1111/j.1574-6941.2010.01027.x

Canfora, L., Bacci, G., Pinzari, F., Lo, Papa G, Dazzi, C., and Benedetti, A. (2014). Salinity and bacterial diversity: to what extent does the concentration of salt affect the bacterial community in a saline soil? *PLoS One* 9:e106662. doi: 10.1371/journal.pone.0106662

Caporaso, J. G., Lauber, C. L., Walters, W. A., Berg-Lyons, D., Huntley, J., Fierer, N., et al. (2012). Ultra-high-throughput microbial community analysis on the Illumina HiSeq and MiSeq platforms. *ISME J.* 6, 1621–1624. doi: 10.1038/ismej.2012.8

Casamayor, E. O., Garcia-Cantizano, J., and Pedros-Alios, C. (2008). Carbon dioxide fixation in the dark by photosynthetic bacteria in sulfide-rich stratified lakes with oxic–anoxic interfaces. *Limnol. Oceanogr.* 53, 1193–1203. doi: 10.4319/lo.2008.53.4.1193

Chen, H., Jogler, M., Rohde, M., Klenk, H., Busse, H., Tindall, B. J., et al. (2013). *Sphingobium limneticum* sp. nov. and *Sphingobium boeckii* sp. nov., two freshwater planktonic members of the family *Sphingomonadaceae*, and reclassification of *Sphingomonas suberifaciens* as *Sphingobium suberifaciens* comb. nov. *Int. J. Syst. Evol. Microbiol.* 63, 735–743. doi: 10.1099/ijs.0.040105-0

Chou, Y., Chou, J., Lin, K., Lin, M., Wei, Y., Arun, A. B., et al. (2008). *Rothia terrae* sp. nov. isolated from soil in Taiwan. *Int. J. Syst. Evol. Microbiol.* 58, 84–88. doi: 10.1099/ijs.0.65172-0

Clarke, K. R., and Gorley, R. N. (2015). *PRIMER v7: User Manual/Tutorial*. Plymouth: PRIMER-E.

Cooke, R. U., Warren, A., and Goudie, S. A. (1993). *Desert Geomorphology*. London: UCL Press Limited.

Costa, K. C., Hallmark, J., Navarro, J. B., and Hedund, B. P. (2008). Geomicrobiological changes in two ephemeral desert playa lakes in the Western United States. *Geomicrobiol. J.* 25, 250–259. doi: 10.1080/01490450802153033

DeLong, E. F. (1992). Archaea in coastal marine environments. *Proc. Natl. Acad. Sci. U.S.A.* 89, 5685–5689. doi: 10.1073/pnas.89.12.5685

Di Meglio, L., Santos, F., Gomariz, M., Almansa, C., Lopez, C., Anton, J., et al. (2016). Seasonal dynamics of extremely halophilic microbial communities in three Argentinian salterns. *FEMS Microbiol. Ecol.* 92:fiw184. doi: 10.1093/femsec/fiw184

Doughari, H. M., Ndakidemi, P. A., Human, I. S., and Benade, S. (2011). The ecology, biology and pathogenesis of *Acinetobacter* spp.: an overview. *Microbes. Environ.* 26, 101–112. doi: 10.1264/jsme2.me10179

Eder, W., Ludwig, W., and Huber, R. (1999). Novel 16S rRna gene sequences retrieved from highly saline brine sediments of Kebrit Deep, Red Sea. *Arch. Microbiol.* 172, 213–218. doi: 10.1007/s002030050762

Edgar, R. C., Haas, B. J., Clemente, J. C., Quince, C., and Knight, R. (2011). UCHIME improves sensitivity and speed of chimera detection. *Bioinformatics* 27, 2194–2200. doi: 10.1093/bioinformatics/btr381

Eigenbrode, J., Benning, L. G., Maule, J., Wainwright, N., Steele, A., and Amundsen, H. E. (2009). A field-based cleaning protocol for sampling devices used in life-detection studies. *Astrobiology* 9, 455–465. doi: 10.1089/ast.2008.0275

Falb, M., Muller, K., Konigsmaier, L., Oberwinkler, T., Horn, P., Von Gronau, S., et al. (2008). Metabolism of *Halophilic archaea*. *Extremophiles* 12, 177–196. doi: 10.1007/s00792-008-0138-x

Fawaz, M. N. (2013). *Revealing the Ecological Role of Gemmatimonadetes through Cultivation and Molecular Analysis of Agricultural Soils*. Master's thesis, University of Tennessee, Knoxville, TN.

Fenn, M. E., Haeuber, R., Tonnesen, G. S., Baron, J. S., Grossman-Clarke, S., Hope, D., et al. (2003). Nitrogen emissions, deposition, and monitoring in the western United States. *Bioscience* 53, 391–403.

Friedman, G. M., and Krumbein, W. E. (1985). *Hypersaline Ecosystems: The Gavish Sabkha*. Heidelberg: Springer.

Garcia-Maldonado, J. Q., Bebout, B. M., Everroad, R. C., and Lopez-Cortes, A. (2015). Evidence of novel phylogenetic lineages of methanogenic archaea from hypersaline microbial mats. *Microb. Ecol.* 69, 106–117. doi: 10.1007/s00248-014-0473-7

Garcia-Mazcorro, J. F., Mills, D., and Noratto, G. (2016). Molecular exploration of fecal microbiome in quinoa-supplemented obese mice. *FEMS Microb. Ecol.* 92:fiw089. doi: 10.1093/femsec/fiw089

Ghai, R., Mizuno, C. M., Picazo, A., Camacho, A., and Rodriguez-Valera, F. (2013). Metagenomics uncovers a new group of low GC and ultra-small marine actinobacteria. *Nat. Sci. Rep.* 3:2471. doi: 10.1038/srep02471

Glamoclija, M., Fogel, M. L., Steele, A., and Kish, A. (2012). Microbial nitrogen and sulfur cycles at the gypsum dunes of white sands national monument,

New Mexico. *Geomicrobiol. J.* 29, 733–751. doi: 10.1080/01490451.2011.608111

Grabowski, A., Tindall, B. J., Bardin, V., Blanchet, D., and Jeanthon, C. (2005). *Petrimonas sulfuriphila* gen. nov., sp. nov., a mesophilic fermentative bacterium isolated from a biodegraded oil reservoir. *Int. J. Syst. Evol. Microbiol.* 55, 1113–1121. doi: 10.1099/ijs.0.63426-0

Grotzinger, J. P., Arvidson, R., Bell, J., Calvin, W., Clark, B., Fike, D., et al. (2005). Stratigraphy and sedimentology of a dry to wet eolian depositional system, Burns formation, Meridiani Planum, Mars. *Earth Planet. Sci. Lett.* 240, 11–72. doi: 10.1016/j.epsl.2005.09.039

Huber, H., Hohn, M. J., Rachel, R., Fuchs, T., Wimmer, V. C., and Stetter, K. O. (2002). A new phylum of Archaea represented by a nanosized hypothermophilic symbiont. *Nature* 417, 63–67. doi: 10.1038/417063a

Ichikuni, M., and Musha, S. (1978). Partition of strontium between gypsum and solution. *Chem. Geol.* 21, 359–363. doi: 10.1016/0009-2541(78)90055-4

Itoh, H., Navarro, R., Takeshita, K., Tago, K., Hayatsu, M., Hori, T., et al. (2014). Bacterial population succession and adaptation affected by insecticide application and soil spraying history. *Front. Microbiol.* 5:457. doi: 10.3389/fmicb.2014.00457

Jeong, S. H., Lee, J. H., Jung, J. Y., Lee, S. H., Park, M. S., and Jeon, C. O. (2013). *Halomonas cibimaris* sp. nov., isolated from jeotgal, a traditional Korean fermented seafood. *Antonie Leeuwenhoek* 103, 503–512. doi: 10.1007/s10482-012-9832-x

Jetten, M. S. M., Van Niftrik, L., Strous, M., Kartal, B., Keltjens, J. T., and Op de Camp, H. J. M. (2009). Biochemistry and molecular biology of anammox bacteria. *Crit. Rev. Biochem. Mol. Biol.* 44, 65–84. doi: 10.1080/10409230902722783

Jones, S. E., and Lennon, J. T. (2010). Dormancy contributes to the maintenance of microbial diversity. *Proc. Natl. Acad. Sci. U.S.A.* 107, 5881–5886. doi: 10.1073/pnas.0912765107

Kocurek, G., Carr, M., Ewing, R., Havholm, K. G., Nagar, Y. C., and Singhvi, A. K. (2007). White Sands Dune Field, New Mexico: age, dune dynamics and recent accumulations. *Sediment. Geol.* 197, 313–331. doi: 10.1016/j.sedgeo.2006.10.006

Kumar, T. K. A., Healy, R., Spatafora, J. W., Blackwelll, M., and McLaughlin, D. J. (2012). Orbilia ultrastructure, character evolution and phylogeny of Pezizomycotina. *Mycologia* 104, 462–476. doi: 10.3852/11-213

Langford, R. P. (2003). The Holocene history of the White Sands dune field and influences on eolian deflation and playa lakes. *Quat. Int.* 104, 31–39. doi: 10.1016/s1040-6182(02)00133-7

Lewis, L. A., and Lewis, P. O. (2005). Unearthing the molecular phylodiversity of desert soil green algae (Chlorophyta). *Syst. Biol.* 54, 936–947. doi: 10.1080/10635150500354852

Madden, A. S., Smith, A. C., Balkwill, D. L., Fagan, L. A., and Phelps, T. J. (2007). Microbial uranium immobilization independent of nitrate reduction. *Environ. Microbiol.* 9, 2321–2330. doi: 10.1111/j.1462-2920.2007.01347.x

Madigan, M. T., Martinko, J. M., Bender, K. S., Buckley, D. H., and Stahl, D. A. (2015). *Brock Biology of Microorganisms*, 14th Edn. Glenview, IL: Pearson.

Maier, R. M., Pepper, I. L., and Gerba, C. P. (2009). *Environmental Microbiology*, 2nd Edn. Burlington, MA: Elsevier.

Makhdoumi-Kakhki, A., Amoozegar, M. A., Kazemi, B., Pasic, L., and Ventosa, A. (2011). Prokaryotic diversity in Aran-Bigdol Salt Lake, the largest hypersaline Playa in Iran. *Microb. Environ.* 27, 87–93. doi: 10.1264/jsme2.me11267

Makhdoumi-Kakhki, A., Amoozegar, M. A., and Ventosa, A. (2012). Salinibacter iranicus sp. nov. and *Salinibacter luteus* sp. nov., isolated from a salt lake, and emended descriptions of the genus *Salinibacter* and of *Salinibacter ruber*. *Int. J. Syst. Evol. Microbiol.* 62, 1521–1527. doi: 10.1099/ijs.0.031971-0

Medlin, L., Elwood, H. J., Stickel, S., and Sogin, M. L. (1988). The characterization of enzymatically amplified eukaryotic 16S-like rRNA-coding regions. *Gene* 71, 491–499. doi: 10.1016/0378-1119(88)90066-2

Mesbah, M. N., Abou-El-Ela, S. H., and Wiegel, J. (2007). Novel and unexpected prokaryotic diversity in water and sediments of the Alkaline, hypersaline Lakes of the Wadi An Natrun, Egypt. *Microb. Ecol.* 54, 598–617. doi: 10.1007/s00248-006-9193-y

Mizuno, C. M., Rodriguez-Valera, F., and Ghai, R. (2015). Genomes of Planktonic Acidimicrobiales: widening horizons for marine actinobacteria by metagenomics. *mBio* 6:e2083-14. doi: 10.1128/mBio.02083-2014

Moreira, C., Rainey, F. A., Nobre, M. F., da Silva, M. T., and da Costa, M. S. (2000). Tepidimonas ignava gen. nov., sp. nov., a new chemolithoheterotrophic and slightly thermophilic member of the β-*Proteobacteria*. *Int. J. Syst. Evol. Microbiol.* 50, 735–742. doi: 10.1099/00207713-50-2-735

Morris, R. M., Frazar, C. D., and Carlson, C. A. (2012). Basin-scale patterns in the abundance of SAR11 subclades, marine Actinobacteria (OM1), members of the *Roseobacter clade* and OCS116 in the South Atlantic. *Environ. Microbiol.* 14, 1133–1144. doi: 10.1111/j.1462-2920.2011.02694.x

Muldavin, E., Harper, G., Neville, P., and Chauvin, Y. (2000). *The Vegetation of White Sands Missile Range, New Mexico*, Vol. II. Albuquerque, NM: New Mexico Natural Heritage Program.

Navarro, J. B., Moser, P. D., Flores, A., Ross, C., Rosen, M. R., Dong, H., et al. (2009). Bacterial succession within an ephemeral hypereutrophic Mojave Desert playa lake. *Microb. Ecol.* 57, 307–320. doi: 10.1007/s00248-008-9426-3

Newton, B. T., and Allen, B. (2014). *Hydrological Investigation at White Sands National Monument*, Open-File Report 559. Socorro, NM: New Mexico Bureau of Geology and Mineral Resources.

Oren, A. (2008). Microbial life at high salt concentrations: phylogenetic and metabolic diversity. *Saline Syst.* 4:2. doi: 10.1186/1746-1448-4-2

Oren, A., Sorenson, K. B., Canfield, D. E., Teske, A. P., Ionescu, D., Lipski, A., et al. (2009). Microbial communities and processes within a hypersaline gypsum crust in a saltern evaporation pond (Eilat, Israel). *Hydrobiology* 66, 15–26. doi: 10.1007/s10750-009-9734-8

Pen-Mouratov, S., Hu, C., and Hindin, E. (2011). Soil microbial activity and a free living nematode community in the playa and in the sandy biological crust of the Negev Desert. *Biol. Fertil. Soil.* 47, 363–375. doi: 10.1007/s00374-011-0540-x

Potvin, M., and Lovejoy, C. (2008). PCR-based estimates of artificial and environmental 18S rRNA gene libraries. *J. Eukaryot. Microbiol.* 56, 174–181. doi: 10.1111/j.1550-7408.2008.00386.x

Pylro, V. S., Roesch, L. F. W., Morais, D. K., Clark, I. M., Hirsch, P. R., and Tótola, M. R. (2014). Data analysis for 16S microbial profiling from different benchtop sequencing platforms. *J. Microbiol. Method* 107, 30–37. doi: 10.1016/j.mimet.2014.08.018

Quast, C., Pruesse, E., Yilmaz, P., Gerken, J., Schweer, T., Yarza, P., et al. (2013). The SILVA ribosomal RNA gene database project: improved data processing and web-based tools. *Nucleic Acid. Res.* 41, D590–D596. doi: 10.1093/nar/gks1219

Rees, N. G., Baldwin, D. S., Watson, G. O., Perryman, S., and Nielsen, D. L. (2004). Ordination and significance testing of microbial community composition derived from terminal restriction fragment length polymorphisms: application of multivariate statistics. *Antonie Leeuwenhoek* 86, 339–347. doi: 10.1007/s10482-005-0498-5

Reynolds, R. L., Yount, J. C., Reheis, M., Goldstein, H., Chavez, P., Fulton, R., et al. (2007). Dust emission from wet and dry playas in the Mojave Desert, USA. *Earth Surf. Process. Landf.* 32, 1811–1827. doi: 10.1002/esp.1515

Ryan, M. P., Pembroke, J. T., and Adley, C. C. (2007). *Ralstonia pickettii* in environmental biotechnology: potential and applications. *J. Appl. Microbiol.* 103, 754–764. doi: 10.1111/j.1365-2672.2007.03361.x

Schloss, P. D., Westcott, S. L., Ryabin, T., Hall, J. R., Hartmann, M., Hollister, E. B., et al. (2009). Introducing mothur: open-source, platform- independent, community-supported software for describing and comparing microbial communities. *Appl. Environ. Microbiol.* 75, 7537–7541. doi: 10.1128/AEM.01541-09

Schulze-Makuch, D. (2002). "Evidence of the discharge of hydrothermal water into Lake Lucero, White Sands National Monument, southern New Mexico," in *Proceedings of the Geology of White Sands, New Mexico Geological Society Fifty-third Annual Field Conference*, eds V. W. Lueth, K. A. Giles, S. G. Lucas, B. S. Kues, R. Myers, and D. S. Ulmer-Scholle, Socorro, 325–329.

Siam, R., Mustafa, G. A., Sharaf, H., Moustafa, A., Ramadan, A. R., Antunes, A., et al. (2012). Unique prokaryotic consortia in geochemically distinct sediments from Red Sea Atlantis II and discovery deep brine pools. *PLoS One* 7:e42872. doi: 10.1371/journal.pone.0042872

Sirisena, K. A., Ramirez, S., Steele, A., and Glamoclija, M. (2018). microbial diversity of hypersaline sediments from Lake Lucero Playa in white sands national monument, New Mexico, USA. *Microb. Ecol.* 76, 404–418. doi: 10.1007/s00248-018-1142-z

Smith, J. M., Green, S. J., Kelley, C. A., Prefurt-Bebout, L., and Bebout, B. M. (2008). Shifts in methanogen community structure and function associated with

long-term manipulation of sulfate and salinity in a hypersaline microbial mat. *Environ. Microbiol.* 10, 386–394. doi: 10.1111/j.1462-2920.2007.01459.x

Solórzano, L. (1969). Determination of ammonia in natural waters by the phenolhypochlorite method. *Limnol. Ocean.* 14, 799–801.

Song, H. S., Cha, I. T., Yim, K. J., Lee, H. W., Hyun, D. W., Lee, S. J., et al. (2014). *Halapricum salinum* gen. nov., sp. nov., an extremely halophilic archaeon isolated from non-purified solar salt. *Antonie Leeuwenhoek* 105, 979–986. doi: 10.1007/s10482-014-0156-x

Sorenson, K. B., Canfield, D. E., and Oren, A. (2004). Salinity responses of benthic microbial communities in a solar saltern (Eilat, Israel). *Appl. Environ. Microbiol.* 70, 1608–1616. doi: 10.1128/aem.70.3.1608-1616.2004

Sorenson, K. B., Canfield, D. E., Teske, A. P., and Oren, A. (2005). Community composition of a hypersaline endoevaporitic microbial mat. *Appl. Environ. Microbiol.* 71, 7352–7365. doi: 10.1128/aem.71.11.7352-7365.2005

Sorokin, D. Y., Tourova, T. P., Kolganova, T. V., Spiridonova, E. M., Berg, I. A., and Muyzer, G. (2006a). *Thiomicrospira halophila* sp. nov., a moderately halophilic, obligately chemolithoautotrophic, sulfur-oxidizing bacterium from hypersaline lakes. *Int. J. Syst. Evol. Microbiol.* 56, 2375–2380. doi: 10.1099/ijs.0.64445-0

Sorokin, D. Y., Tourova, T. P., Lysenko, A. M., and Muyzer, G. (2006b). Diversity of culturable halophilic sulfur-oxidizing bacteria in hypersaline habitats. *Microbiology* 152, 3013–3023. doi: 10.1099/mic.0.29106-0

Sorokin, D. Y., Van Pelt, S., Tourova, T. P., and Evtushenko, L. I. (2009). *Nitriliruptor alkaliphilus* gen. nov., sp. nov., a deep-lineage haloalkaliphilic actinobacterium from soda lakes capable of growth on aliphatic nitriles, and proposal of *Nitriliruptoraceae* fam. nov. and *Nitriliruptorales* ord. nov. *Int. J. Syst. Evol. Microbiol.* 59, 248–253. doi: 10.1099/ijs.0.002204-0

Stroud, C. P. (1950). A survey of the insects of white sands national monument, Tularosa Basin, New Mexico. *Am. Midl. Nat.* 44, 659–677.

Szynkiewicz, A., Moore, C. H., Glamoclija, M., Bustos, D., and Pratt, L. M. (2010). Origin of coarsely crystalline gypsum domes in a saline playa environment at the White Sands National Monument, New Mexico. *J. Geophys. Res.* 115:F02021. doi: 10.1029/2009JF001592

Tang, S., Wang, Y., Lou, K., Mao, P., Xu, L., Jiang, C., et al. (2009). *Kocuria halotolerans* sp. nov., an actinobacterium isolated from a saline soil in China. *Int. J. Syst. Evol. Microbiol.* 59, 1316–1320. doi: 10.1099/ijs.0.006627-0

Ventosa, A., Mellado, E., Sanchez-Porro, C., and Marquez, M. C. (2008). "Halophilic and Halotolerant Micro-Organisms from Soils," in *Microbiology of Extreme Soils*, ed. P. Dion, (Heidelberg: Springer-Verlag), 87–115. doi: 10.1007/978-3-540-74231-9_5

Vogel, B. M., Des Marais, D. J., Turk, K. A., Parenteau, M. N., Jahnke, L. L., and Kubo, M. D. Y. (2009). The role of biofilms in the sedimentology of actively forming gypsum deposits at Guerrero Negro, Mexico. *Astrobiology* 9, 875–893. doi: 10.1089/ast.2008.0325

Wahlund, T. M., and Madigan, M. T. (1993). nitrogen fixation by the thermophilic green sulfur bacterium *Chlorobium tepidum*. *J. Bacteriol.* 175, 474–478. doi: 10.1128/jb.175.2.474-478.1993

Wang, Y., Wang, Z., Liu, J., Chen, Y., Zhang, X., Wen, M., et al. (2009). *Sediminimonas qiaohouensis* gen. nov., sp. nov., a member of the *Roseobacter clade* in the order *Rhodobacterales*. *Int. J. Syst. Evol. Microbiol.* 59, 1561–1567. doi: 10.1099/ijs.0.006965-0

Weekers, P., Gast, R. J., Fuerst, P. A., and Byers, T. J. (1994). Sequence variations in small-subunit ribosomal RNAs of Hartmannella Vermiformis and their phylogenetic implications. *Mol. Biol. Evol.* 11, 684–690.

Wu, L., Wen, C., Qin, Y., Yin, H., Tu, Q., Van Nostrand, J. D., et al. (2015). Phasing amplicon sequencing on Illumina Miseq for robust environmental microbial community analysis. *BMC Microbiol.* 15:125. doi: 10.1186/s12866-015-0450-4

Xie, B., Lv, X., Cai, M., Tang, Y., Wang, Y., Cui, H., et al. (2014). *Seohaeicola nanhaiensis* sp. nov., a moderately halophilic bacterium isolated from the benthic sediment of South China Sea. *Curr. Microbiol.* 69, 802–808. doi: 10.1007/s00284-014-0658-9

Yoon, J., Kang, S., Lee, S., Oh, K., and Oh, T. (2009). *Seohaeicola saemankumensis* gen. nov., sp. nov., isolated from a tidal flat. *Int. J. Syst. Evol. Microbiol.* 59, 2675–2679. doi: 10.1099/ijs.0.011312-0

Zechman, F. W., Verbuggen, H., Leliaert, F., Ashworth, M., Buchheim, M. A., and Fawley, M. W. (2010). An unrecognized ancient lineage of green plants persists in deep marine waters. *J. Phycol.* 46, 1288–1295. doi: 10.1111/j.1529-8817.2010.00900.x

Zhong, Z., Liu, Y., Liu, H., Wang, F., Zhou, Y., and Liu, Z. (2015). *Marinobacter halophilus* sp. nov., a halophilic bacterium isolated from a salt lake. *Int. J. Syst. Evol. Microbiol.* 65, 2838–2845. doi: 10.1099/ijs.0.000338

Conflict of Interest: The authors declare that the research was conducted in the absence of any commercial or financial relationships that could be construed as a potential conflict of interest.

frontiers in Microbiology

ORIGINAL RESEARCH
published: 05 December 2019
doi: 10.3389/fmicb.2019.02793

Deep Microbial Colonization in Saponite-Bearing Fractures in Aged Basaltic Crust: Implications for Subsurface Life on Mars

*Yuri Sueoka, Seiya Yamashita, Mariko Kouduka and Yohey Suzuki**

Department of Earth and Planetary Science, The University of Tokyo, Tokyo, Japan

One of the most promising planetary bodies that might harbor extraterrestrial life is Mars, given the presence of liquid water in the deep subsurface. The upper crust of Mars is mainly composed of >3.7-billion-year-old basaltic lava where heat-driven fluid circulation is negligible. The analogous crustal environment to the Martian subsurface is found in the Earth's oceanic crust composed of basaltic lava. The basaltic crust tends to cool down for 10–20-million-years after formation. However, microbial life in old cold basaltic lava is largely unknown even in the Earth's oceanic crust, because the lack of vigorous circulation prevents sampling of pristine crustal fluid from boreholes. Alternatively, it is important to investigate deep microbial life using pristine drill cores obtained from basaltic lava. We investigated a basaltic rock core sample with mineral-filled fractures drilled during Integral Ocean Drilling Project Expedition 329 that targeted 104-million-year-old oceanic crust. Mineralogical characterizations of fracture-infilling minerals revealed that fractures/veins were filled with Mg-rich smectite called saponite and calcium carbonate. The organic carbon content from the saponite-rich clay fraction in the core sample was 23 times higher than that from the bulk counterpart, which appears to be sufficient to supply energy and carbon sources to saponite-hosted life. Furthermore, a newly developed method to detect microbial cells in a thin-section of the saponite-bearing fracture revealed the dense colonization of SYBR-Green-I stained microbial cells spatially associated with saponite. These results suggest that the presence of saponite in old cold basaltic crust is favorable for microbial life. In addition to carbonaceous chondrite, saponite is a common product of low-temperature reactions between water and mafic minerals on Earth and Mars. It is therefore expected that deep saponite-bearing fractures could host extant life and/or the past life on Mars.

Keywords: water–rock interactions, rock-hosted life, Fe, Mg-smectite, basaltic basement, clay-catalyzed organic synthesis

OPEN ACCESS

Edited by:
Tetyana Milojevic,
University of Vienna, Austria

Reviewed by:
Shinsuke Kawagucci,
Japan Agency for Marine-Earth Science and Technology, Japan
Xinxu Zhang,
Shenzhen University, China

****Correspondence:***
Yohey Suzuki
yohey-suzuki@eps.s.u-tokyo.ac.jp

Specialty section:
This article was submitted to Extreme Microbiology, a section of the journal Frontiers in Microbiology

Received: *07 September 2019*
Accepted: *18 November 2019*
Published: *05 December 2019*

Citation:
Sueoka Y, Yamashita S, Kouduka M and Suzuki Y (2019) Deep Microbial Colonization in Saponite-Bearing Fractures in Aged Basaltic Crust: Implications for Subsurface Life on Mars. Front. Microbiol. 10:2793. doi: 10.3389/fmicb.2019.02793

INTRODUCTION

The surfaces of Earth-like planets are extensively covered with basaltic lava as a consequence of planetary differentiation (Hazen, 2012; De Pater and Lissauer, 2015). Mars retained active hydrologic systems at the near-surface settings until ∼3-billion-years ago (Ehlmann et al., 2011). Unlike on Earth, the organic and inorganic products of ancient basalt-water interactions are

known to be preserved under freeze-drying conditions without being altered by tectonic forces (Wordsworth, 2016). It is therefore expected that the signatures of life and/or biomolecules might be discovered from the Martian surface (Onstott et al., 2019). On Earth, old, tectonically undeformed basaltic lava is ubiquitously distributed in the upper oceanic crust (Heberling et al., 2010). The oceanic crust is 100-million-years old on average (Parsons, 1982), as a result of the tectonic recycling into the mantle (Jarrard, 2003). Understanding of microbial life in the old basaltic lava on Earth is important to constrain the habitability of basaltic lava on Mars.

Previously, basaltic lava underneath sediments called basaltic basement has been microbiologically investigated at 3.5- and 8-million-year-old ridge flank systems (Juan de Fuca: Cowen et al., 2003; North Pond: Orcutt et al., 2013). Recent genome-resolved metagenomics analysis of crustal fluid samples collected from 3.5- to 8-million-year-old basaltic basement revealed the metabolic potential that could support lithotrophic microbial life mediating the oxidation of H_2, Fe(II) compounds, ammonia and reduced S compounds coupled to the reduction of O_2, nitrate and sulfate (Tully et al., 2018; Smith et al., 2019). Metabolic activities of lithotrophic microbial life have been indicated by characterizing basaltic rocks drilled prior to crustal fluid sampling (Lever et al., 2013; Zhang et al., 2016a,b).

After 10-million-years after the formation of basaltic basement (10 Ma), the heat-driven circulation of crustal fluid becomes weak (Sclater et al., 1980; Hasterok et al., 2011), which causes the technical difficulty in sampling pristine crustal fluid from drilled boreholes. Hence, microbiological investigations need to be performed by using drilled rocks obtained from >10 Ma basaltic basement. Recently, we have investigated microbial life in old basaltic basement by drilling into 104-Ma oceanic crust, where basaltic lava is overlain by a 75-m thick sediment layer (Yamashita et al., 2019). At the site, low organic contents of the entire sediment column render the penetration of O_2 in seawater from the ocean floor down to the basaltic basement (D'Hondt et al., 2015). It is also important to note that the fluid circulation in basaltic basement is not detected by heat flow measurements at this site (Expedition 329 Scientists, 2011). By characterizing 110- and 122-m deep basaltic rock cores, it has been revealed that the basaltic basement is permeable and reactive with oxygenated seawater to produce a clay mineral structurally and compositionally similar to Fe-rich smectite called nontronite [$(CaO_{0.5},Na)_{0.3}Fe_2^{3+}(Si,Al)_4O_{10}(OH)_2{\cdot}nH_2O$]. As the formation of nontronite is associated with the oxidation of Fe(II) from basalt dissolution coupled to the reduction of O_2 from seawater, we infer that 104 Ma oceanic crust could sustain lithotrophic life under aerobic conditions (Yamashita et al., 2019).

Nontronite is widely observed on Mars as a result of oxic basalt-water interactions (Chevrier et al., 2007). Under oxygen-deprived conditions, it is considered that fractures/veins are filled with secondary minerals commonly found under anoxic conditions such as pyrite [FeS_2], Mg-rich smectite called saponite [$Ca_{0.17}Mg_3(Si, Al)_4O_{10}(OH)_2{\cdot}n(H_2O)]_5$ and calcium carbonate such as calcite [$CaCO_3$] (Teagle et al., 1996). Calcium carbonate is of particular importance, given that calcium carbonate is the prominent product of basalt-seawater interactions to seal fractures/veins in the oceanic crust on Earth (Müller and Dutkiewicz, 2018). Carbonate-bearing basaltic rocks are widely found on Mars (Murchie et al., 2009). In the 104 Ma oceanic crust where nontronite formation has been reported from the 110- and 122-m deep core samples (Yamashita et al., 2019), a 102-m deep basaltic rock core was associated with fractures/veins filled with calcium carbonate. In this study, we investigated mineralogical and microbiological characteristics of a fracture filled with calcium carbonate.

MATERIALS AND METHODS

Sample Collection

The basaltic rock core sample associated with fractures with calcium carbonate was collected at Site U1365 in the South Pacific Gyre during Integrated Ocean Drilling Program (IODP) Expedition 329 (October 9 through December 13, 2010). The 104 Ma basaltic basement is overlain by 75-m thick sediments found to contain an extremely low abundance of microbial cells (D'Hondt et al., 2015). As primary production near the seawater surface was also extremely low, the supply of detrital organic matter for the consumption of O_2 is very limited in sediments (D'Hondt et al., 2015).

For drilling into the basaltic basement, a rotary core barrel (RCB) coring system was used on the drilling research vessel JOIDES Resolution. After the core recovery, approximately 18 h passed until subsequent microbiological sampling of the rock sample in the cold room. The portion of the rock core sample was fixed overnight with 2% glutaraldehyde in a solution containing 100 mM Tris–HCl (pH 8) and stored in the Tris–HCl solution without glutaraldehyde at 4°C. For mineralogical characterizations, the portion of the rock core sample was ground and powdered on board as described below and stored at −80°C.

Contamination Check

Fluorescence microspheres (0.5-μm in diameter) were used to monitor contamination. Fluorescence microspheres in a bag placed on the core-catcher were released into drilling fluid upon the start of drilling. The presence of microspheres was inspected before and after cleaning and subsampling steps. First, the untreated exterior removed from the rock core sample using a flame-sterilized hammer and chisel was examined for contamination. Second, 3% NaCl solution was used to wash the rock core surface twice. Third, the rock core surface was slightly heated with a propane torch, and then the interior and exterior of the flamed rock pieces were separated by a flame-sterilized hammer and chisel. All rock pieces subsampled for contamination check were soaked in 25-mL 3% NaCl solution, from which 3-mL of the solutions with microspheres were filtered using 25 mm black polycarbonate filters (0.22-μm pore size) and examined under epifluorescence using an Olympus BX51 microscope (Olympus, Tokyo, Japan).

Preparation of a Thin Section and Light Microscopy

We prepared a thin section to clarify the mineral composition within rock fractures. A fracture-bearing rock piece was dehydrated twice in 100% ethanol for 5 min, followed by the infiltration of the rock piece with LR White resin (London Resin Co. Ltd., Aldermaston, England) for 30 min. The infiltrated rock piece was solidified in an oven at 50°C for 48 h. After trimming into a 100-μm thin section, the surface was polished with corundum powder and diamond paste. Mineralogical assemblages were observed using an optical microscope (BX51; Olympus) with a charge-coupled device (CCD) camera (DP71; Olympus).

Scanning Electron Microscopy (SEM)

Using a Hitachi field emission scanning electron microscopy (FE-SEM) S-4500 instrument (Tokyo, Japan), back-scattering electron images were obtained from the thin section coated with carbon. FE-SEM was operated at an emission current of 15 μA and an accelerating voltage of 15 kV. For chemical compositions of mineral phases, energy-dispersive X-ray spectroscopy (EDS) was used according to contrasts of the image corresponding to atomic density.

Analysis of X-Ray Diffraction (XRD) Pattern

The powder of the rock core was prepared with a flame-sterilized mortar and pestle. The clay-sized fraction in the powder sample was dispersed in distilled and deionized water, centrifuged at 3,000 rpm for 5 min, and then freeze-dried for storage. X-ray diffraction (XRD) pattern analysis was performed to identify phyllosilicate minerals using a RIGAKU RINT-ULTIMA-2100 (Tokyo, Japan) at an operation voltage of 40 kV and an operation current of 30 mA with monochromatized Cu-Kα radiation. To orient the sheet structure, the freeze-dried sample suspended in distilled and deionized water was mounted on a glass slide. The mounted samples were air-dried and treated with ethylene glycolate and subjected to X-ray scanning in a 2θ range of 2–10°. To determine the 060 reflection for clarifying the sheet structure, the randomly oriented sample was examined.

Organic Carbon Characterizations of the Clay Fraction

The powdered core sample was suspended in sterilized deionized water. The supernatant after centrifugation at 3,000 rpm for 5 min contained the clay fraction. The clay fraction was collected by centrifugation at 10,000 rpm for 10 min. We measured the organic carbon contents of the powdered core sample and the clay fraction using a mass spectrometer (Thermo Electron DELTAplus Advantage; Thermo Fisher Scientific Inc., Waltham, MA) connected to an elemental analyzer (EA1112, Thermo Electron DELTAplus Advantage) through a Conflo III interface. Before the measurement, the sample was heated at 100°C in 3% HCl to eliminate carbonate minerals, washed twice with distilled, deionized water, and dried.

Microbiological Characterizations of the Thin Section and the Clay Fraction

We developed a new method to clarify the mineral composition and microbial distribution within rock fractures by modifying a protocol established for the localization of endosymbiotic cells in chemosynthetic animals (Nussbaumer et al., 2006). Previously, hybridizations are performed for thin sections of biological tissues with fluorescently labeled oligonucleotide probes and 4′,6-diamidino-2-phenylindole (DAPI). In this study, microbial cells in the thin section of the rock piece were stained with SYBR Green I (TaKaRa). Prior to SEM-EDS analysis, the thin section was incubated in TE buffer containing SYBR Green I for 5 min. After rinsing with deionized water, the thin section was mounted with the antifade reagent VECTASHIELD (Vector Laboratories, Burlingame, CA, USA). SYBR-Green-I-stained microbial cells in the thin section were observed using an epifluorescence microscope (BX51; Olympus) equipped with a charge-coupled device (CCD) camera (DP71; Olympus). We used two ranges of fluorescence between 540 and 570 nm and 570 and 600 nm for the discrimination of microbial cells from mineral-specific fluorescence signals. For a positive control, *Shewanella oneidensis* (ATCC 700500) cultured aerobically in LB Broth (ATCC Mediun 1065) at 30°C was embedded in LR White resin as described above. A 100-μm thick thin section was prepared from the resin block embedded with *Shewanella* cells. For a negative control, a resin block without *Shewanella* cells was used to prepare a thin section. The thin sections for the positive and negative controls were stained with SYBR Green I and examined using the epifluorescence microscope. To visualize individual microbial cells associated with saponite, the portion of the clay fraction was embedded in LR White resin. Three micrometer thick thin sections were prepared using an ultramicrotome (Reichert Ultracut S; Leica, Wetzlar, Germany). The 3-μm thick thin sections were stained with SYBR Green I and examined using the epifluorescence microscope.

RESULTS

Rock Core Descriptions

We investigated the basaltic core sample (sample code: U1365E-7R2) at a depth of 102 m below the seafloor (mbsf). Microsphere enumeration revealed that microspheres indicative of microbial contamination from drilling fluid were not detected from the interior of the rock core sample (**Supplementary Table 1**). On-board visual characterizations of the rock core revealed calcite (white) and celadonite (dark green) were main fracture-infilling minerals (**Figure 1A**). In addition, small pyrite grains (gold) were visually observed on the opened fracture surface (**Figure 1B**).

Characterizations of Fracture-Infilling Minerals

We prepared and observed a thin section using optical microscopy to investigate the distribution of minerals in a fracture in U1365E-7R2. It was observed that the fracture hosted in phyrytic microcrystalline basaltic groundmass was associated with a white inner portion surrounded by a yellow-brownish

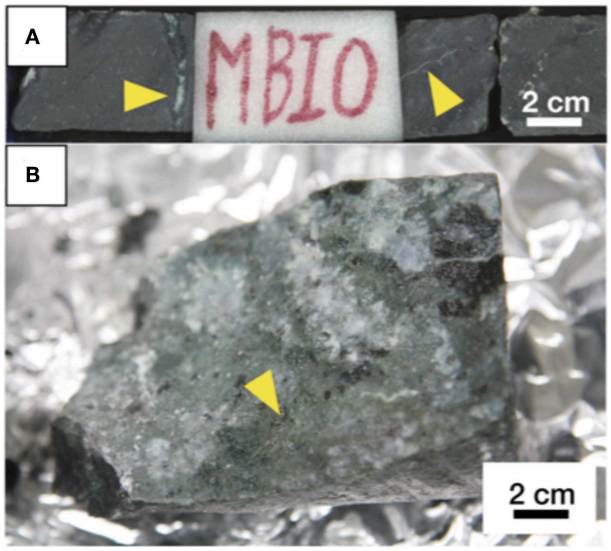

FIGURE 1 | Pictures of a basaltic core sample (U1365E-7R2). **(A)** A whole-round core including the sampling interval as labeled with MBIO. White fractures/veins pointed out by yellow arrows are filled with calcite. **(B)** Fracture surface after opening. A yellow arrow indicates the presence of pyrite grains.

outer portion (**Figure 2A**). We analyzed chemical compositions of the inner and outer portions by SEM-EDS (**Figure 2B**). As consistent with the on-board visual mineral identification, the white material is calcium carbonate (**Figure 2C**). From the outer yellow-brownish portion, Si, O, and Mg were detected as major elements, whereas Fe and Al were detected as relatively minor elements (**Figure 2D**). As a ratio of peak intensities of Si and Mg was ∼2:1, it is indicated that the yellow-brownish material is a 2:1 clay mineral.

Clay Fraction Characterizations of the Rock Core Sample

To identify the yellow-brownish material, a clay-sized fraction was separated from the powdered core sample. XRD analysis of crystallographically oriented clay minerals with and without intercalation using ethylene glycol revealed that based on the expansion of a basal spacing from 1.47 to 1.73 nm after the ethylene glycol treatment (**Figure 3A**), the clay fraction mainly contained a smectite mineral rather than other non-expandable clays such as mica and chlorite minerals (Moore and Reynolds, 1989). Furthermore, we unambiguously identified the sheet structure of the smectite mineral to be tri-octahedral, based on the 060 reflection (**Figure 3A**). To clarify the chemical composition of the tri-octahedral smectite, we performed SEM-EDS analysis of the clay fraction. A low-contrast phase characteristic of an EDS spectrum (**Figure 3B**) similar to that of the yellow-brownish material in the thin section (**Figure 2C**) was found to include fine grains with a relative high contrast (**Figure 3C**). EDS spectra obtained from relatively large grains with the same contrast (**Figure 3D**) as that of the fine grains in the low-contrast phase indicate Ca, Si, Al, and O to be major elements (**Figure 3E**). Given the presence of anorthite [$CaAl_2Si_2O_8$] revealed by XRD analysis of the clay fraction (**Supplementary Figure 1**), it is inferred that the high-contrast phase associated with the low-contrast phase was anorthite. This inference is supported by the fact that Al and Ca peak intensities relative to that of Si were higher in the low-contrast phase in the clay fraction (**Figure 3B**) than that of the yellow-brownish material in the thin section (**Figure 2C**). Taken together, the yellow-brownish material found in the fracture was identified to be sapointe, a tri-octahedral smectite mineral with Mg in the octahedral site (Meunier, 2005).

Organic Carbon Contents of the Bulk and Clay Fraction of the Core Sample

Recently, the abiotic synthesis of amino acids has been reported in saponite formed after serpentinization of olivine and pyroxene minerals at a depth of 173 mbsf in the Atlantis Massif (Ménez et al., 2018). As it is expected that saponite is also enriched in abiotic organic matter in the basaltic basement, we measured the organic carbon content of the clay fraction where saponite was dominantly identified. In comparison to the bulk counterpart before the separation of the clay fraction (an organic carbon content of 0.016 wt. %), the organic carbon content of the clay fraction was 0.363 wt. %. The 23-fold increase in organic carbon content from the saponite-dominated clay fraction is consistent with the localized concentration of amino acids in saponite after serpentinization (a bulk carbon content of 0.023 wt. %; Ménez et al., 2018).

Distributions of DNA-Stained Microbial Cells in the Mineral-Filled Fracture

We developed a new method to visualize microbial cells in the thin section of the basaltic rock sample by using hydrophilic resin. *S. oneidensis* cells embedded and stained with SYBR-Green I were clearly visualized from the background of resin (**Supplementary Figure 2**). Thereby, it is possible to correlate the distributions of microbial cells and minerals in fractures. As shown in **Figure 4**, fluorescence microscopic examination of the saponite-bearing fracture revealed densely colonized microbial cells, where SEM-EDS analysis revealed the presence of saponite near the basalt groundmass (**Figure 2C**). From these results, we infer that the organic matter enriched in the saponite-bearing fraction is derived, at least in part, from the cellular components of microorganisms. In contrast, DNA-stained microbial cells were not observed neither from basaltic groundmass nor calcium carbonate in the fracture. To demonstrate that microbial cells could be visually distinguishable from saponite, 3-μm thick thin sections of the clay fraction mainly composed of saponite were stained with SYBR-Green I and observed using the fluorescent microscope. As shown in **Figure 4C**, individual microbial cells with spherical and rod shapes were visualized from the background of saponite particles.

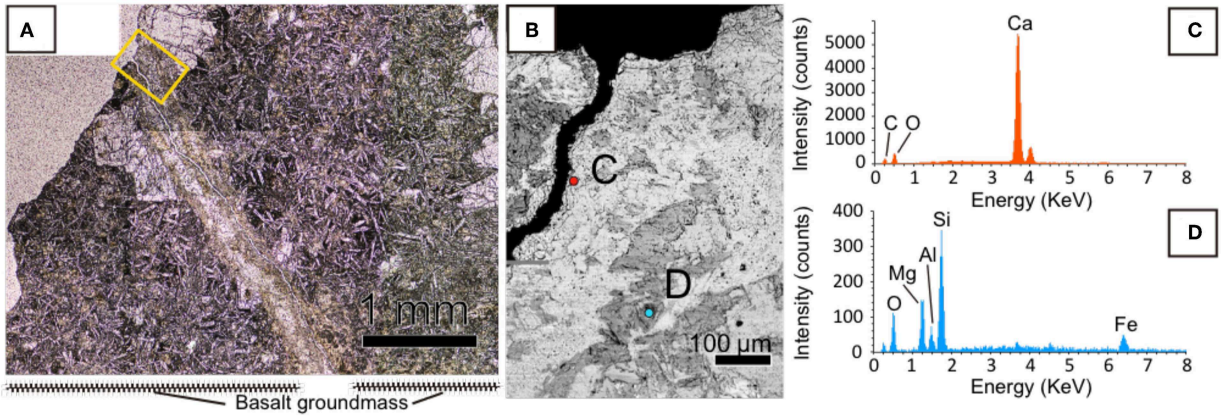

FIGURE 2 | Mineralogical characteristics of a fracture filled with calcium carbonate in U1365E-7R2. **(A)** Optical microscopic image of the fracture with a yellow rectangle indicating an enlarged area shown in **(B)**. **(B)** Back-scattered electron image of the fracture obtained by SEM. **(C,D)** EDS spectra with colors obtained from circles with the same colors in **(B)**.

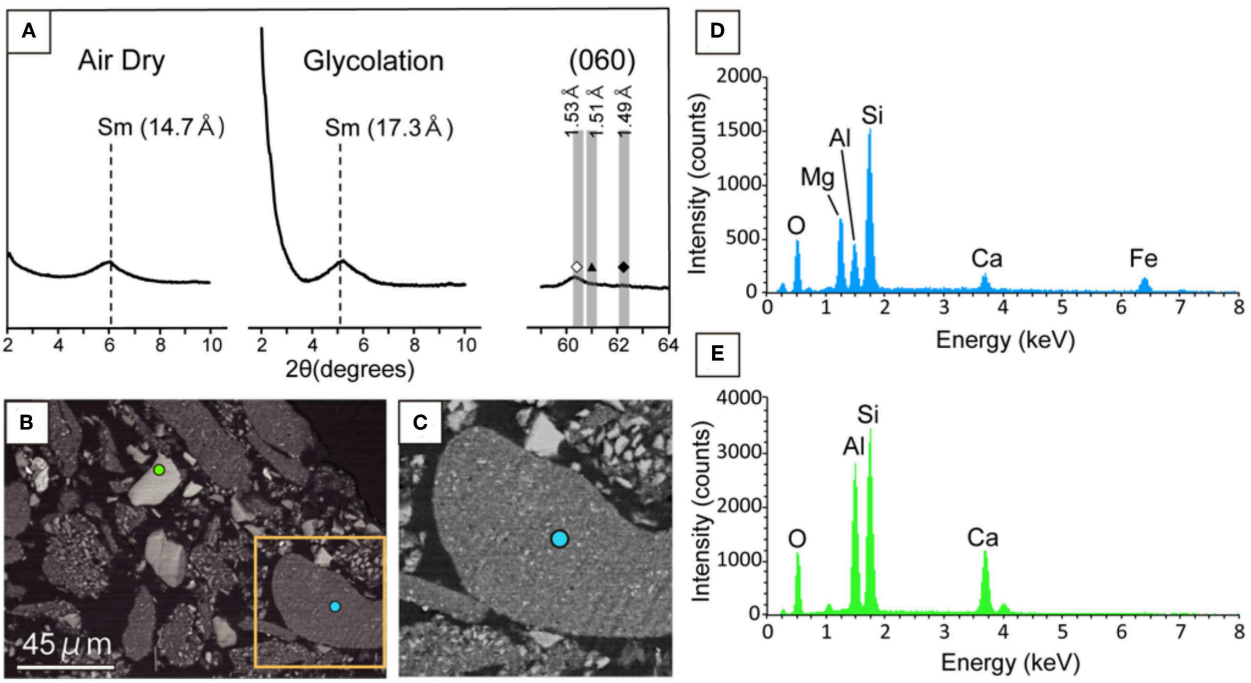

FIGURE 3 | Mineralogical characterization of the clay fraction separated from a powdered core sample in U1365E-7R2. **(A)** Low-angle XRD patterns (2θ: 2–10°) from air-dried and ethylene-glycolated samples vertically oriented to the c-axis of phyllosilicate minerals (left and middle). High angle XRD pattern (2θ: 59–64°) including 060 reflections from the randomly oriented sample (right). Sm indicates smectite. In the high-angle XRD pattern, vertical bands show 2θ ranges of 060 reflections from trioctahedral phyllosilicate minerals (left with open diamond), nontronite and celadonite (middle with filled triangle), and dioctahedral phyllosilicate minerals (right with filled diamond; Moslehuddin and Egashira, 1997). **(B)** Back-scattered electron image of the clay fraction with light blue and light green circles, from which EDS spectra were obtained for the low-contrast phase and the high contrast phase **(D,E)**. An orange rectangle indicates an enlarged area shown in **(C)**. **(C)** Back-scattered electron image of the enlarged area in **(B)**. **(D)** EDS spectra from light blue and light green circles in **(B)**.

DISCUSSION

Temporal and Spatial Variations in Mineral Formation in Basalt Fissures

On Earth, basaltic lava is erupted and solidified at mid-ocean ridges, where oxygenated seawater is vigorously circulated by the buoyance of heated fluid. It is generally known that hydrothermal alterations lead to the formation of secondary minerals such as a mica mineral called celadonite [$K(Mg, Fe^{2+})(Fe^{3+}, Al)(Si_4O_{10})(OH)_2$] and iron oxyhydroxides (Teagle et al., 1996; Bach and Edwards, 2003). On the ridge flank associated with the restricted circulation of oxygenated seawater

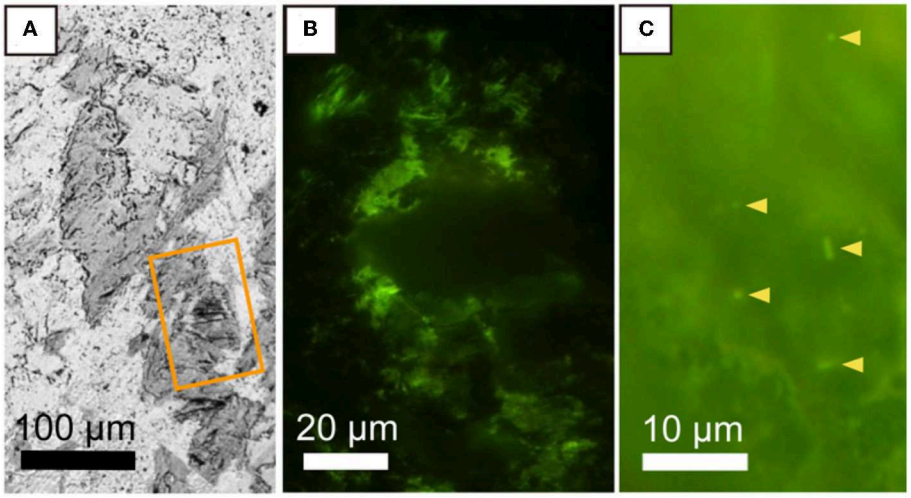

FIGURE 4 | Microbial distribution in a saponite-bearing locus near basaltic groundmass revealed by staining of a thin section with SYBR-Green I. **(A)** Back-scattered electron image of saponite aggregates enlarged from **Figure 2B**. An orange rectangle indicates the area shown in **(B)**. Fluorescence microscopy images of SYBR Green I-stained microbial cells associated with saponite in a 100-μm thin section of a rock piece **(B)** and in a 3-μm thin section of a clay fraction **(C)**.

(Lin et al., 2014), pyrite and saponite tend to form in fractures/veins (Teagle et al., 1996; Lever et al., 2013). After the cooling of the ridge flank, further infilling with calcium carbonate is generally considered to seal fractures/veins (Müller and Dutkiewicz, 2018). Recently, we revealed that subseafloor basaltic lava is percolated with oxygenated seawater through fractures/veins filled with celadonite and iron oxyhydroxides in cold oceanic crust aged 33 and 104 Ma (Yamashita et al., 2019). The product of basalt-water interactions under oxic conditions is nontronite associated with Fe(III) in the octahedral layer.

In U1365E-7R2, the formation of nontronite was not evident at the interface between saponite and basalt groundmass where nontronite has been found in the deeper basaltic core samples with fractures/veins filled with celadonite and iron oxyhydroxides (Yamashita et al., 2019). This result suggests that the oxygenated seawater is not intruded in the fracture through the interface adjacent to saponite. The persistence of pyrite in the calcite-filled fracture also supports the possibility that the oxygenated seawater is not permeable in the calcite-filled fracture. The mineral assemblage and texture observed in the fracture support the following mineralization order:

Stage 1: Celadonite formation from high-temperature crustal fluid around the mid-oceanic ridge (< ∼1 Ma).

Stage 2: The formation of saponite and pyrite from moderate-temperature crustal fluid under reducing conditions at the ridge flak (< ∼10 Ma).

Stage 3: The formation of calcite from low-temperature crustal fluid from the ridge flank to the abyssal plain (< ∼10–20 Ma).

Saponite-Hosted Organic Matter and Microbial Cells

DNA-stained microbial cells were densely observed where saponite was distributed in the fracture. This spatially limited occurrence excludes the possibility that contaminant microbial cells were attached during polishing the thin section. In addition to microspheres checked for microbial contamination (**Supplementary Table 1**), bentonite used in the drilling fluid was different from saponite (Yamashita et al., 2019). It is therefore unlikely that microbial cells were introduced into the fracture during drilling. The enrichment of organic matter in the saponite-bearing fraction is consistent with the dense colonization of DNA-stained cells with saponite. As saponite has the ability to effectively adsorb organic matter (Pinnavaia, 1983; Ménez et al., 2018), it is plausible to observe DNA-stained cells in the fracture-infilling saponite. The sources of organic matter and microbial cells might be explained by four cases:

Case 1: Organic matter and microbial cells on saponite are derived from seawater. In this case, both seem to originate from the photosynthetic biosphere.

Case 2: Organic matter on saponite is derived from seawater, and microbial cells are growing *in situ* by metabolizing the organic matter. In this case, microbes are dependent on photosynthetic organic matter.

Case 3: Organic matter and microbial cells are produced on saponite *in situ*. In this case, energy sources for lithoautotrophic metabolisms from saponite are unknown. One possibility could be H_2 derived from H_2O reacted with Fe(II) in saponite. This reaction has been demonstrated by Fe(II) in octahedral layers in Fe(II)-rich chlorites at high temperatures (Lempart et al., 2018).

Case 4: Organic matter is produced abiotically, and microbial cells metabolize the organic matter. In this case, abiotic organic synthesis appears to be catalyzed by Fe(II)-rich saponite with H_2 as the energy source (Ménez et al., 2018). H_2 might be derived from the moderate-temperature crustal fluid at the Stage 2.

There is the possibility that DNA-stained cells are the relics of microbial life metabolically active after the saponite formation and before the infilling of calcium carbonate (∼1 to ∼20 Ma).

This possibility seems to be supported by the tight sealing of the fracture with calcium carbonate and saponite, which might have prevented the hydrolysis of DNA in fossilized cells. However, the life time of DNA is the order of, at most, several million years in geological formations (Allentoft et al., 2012), and the persistence of DNA for ∼80 Ma is unlikely. Hence, it is plausible that microbial cells could survive under oxygen-deprived conditions by metabolizing inorganic and/or organic energy available around saponite.

Implications for Extant and Past Life in the Subsurface on Mars

The abundant and widespread occurrence of saponite has been found on the crater walls in ∼4-billion-year-old basaltic terrains. These findings lead to the inference that until ∼3-billion-years ago, there appears to have been near-neutral basalt-water interactions in the deep subsurface on Mars (Murchie et al., 2009; Ehlmann and Edwards, 2014). As the supply of atmospheric oxidant was periodically limited (Hurowitz et al., 2017), the deprival of O_2 by reacting with Fe(II) favors the production of saponite over nontronite in the ancient basaltic subsurface (Bach, 2016). The production of saponite is also expected in the modern basaltic crust where the persistence of rock-water interactions has been recently demonstrated (Wade et al., 2017; Orosei et al., 2018). Given the prevalence of organic matter associated with saponite in the Solar System (Pearson et al., 2002), it is indicated that saponite-bearing fractures/veins in the basaltic crust could host extant microbial life and/or signatures from past life on Mars.

CONCLUSION

We revealed that microbial cells were hosted in saponite-bearing fractures. Given the saponite-bearing fraction enriched with organic matter, it is likely that the dense colonization of microbial cells is supported by lithotrophy and/or heterotrophy. Given that low-temperature interactions between mafic minerals and water universally result in the assemblage of saponite and organic matter, extraterrestrial life could be found in the subsurface, where liquid water is disseminated in rock bodies containing mafic minerals.

DATA AVAILABILITY STATEMENT

All datasets generated for this study are included in the article/**Supplementary Material**.

AUTHOR CONTRIBUTIONS

YSue conducted SEM-EDS and microbial cell characterizations and wrote the manuscript. SY conducted optical microscopy and XRD. MK conducted microbial cell characterizations. YSuz initiated and planned the project, conducted sampling, and wrote the manuscript.

FUNDING

This research was partially supported by the Astrobiology Center of National Institutes of Natural Sciences (NINS) (Grant Number 190500000868).

ACKNOWLEDGMENTS

We acknowledge all crews, drilling team members, technical staff members, and shipboard scientists on the drilling vessel *JOIDES Resolution* for conducting core sampling during IODP Expedition 329. We are also grateful to Koji Ichimura for his technical assistance. Comments from reviewers significantly improved this manuscript.

SUPPLEMENTARY MATERIAL

The Supplementary Material for this article can be found online at: https://www.frontiersin.org/articles/10.3389/fmicb.2019.02793/full#supplementary-material

REFERENCES

Allentoft, M. E., Collins, M., Harker, D., Haile, J., Oskam, C. L., Hale, M. L., et al. (2012). The half-life of DNA in bone: measuring decay kinetics in 158 dated fossils. *Proc. R. Soc. B Biol. Sci.* 279, 4724–4733. doi: 10.1098/rspb.2012.1745

Bach, W. (2016). Some compositional and kinetic controls on the bioenergetic landscapes in oceanic basement. *Front. Microbiol.* 7:107. doi: 10.3389/fmicb.2016.00107

Bach, W., and Edwards, K. J. (2003). Iron and sulfide oxidation within the basaltic ocean crust: implications for chemolithoautotrophic microbial biomass production. *Geochim. Cosmochim. Acta.* 67, 3871–3887. doi: 10.1016/S0016-7037(03)00304-1

Chevrier, V., Poulet, F., and Bibring, J.-P. (2007). Early geochemical environment of Mars as determined from thermodynamics of phyllosilicates. *Nature* 448, 60–63. doi: 10.1038/nature05961

Cowen, J. P., Giovannoni, S. J., Kenig, F., Johnson, H. P., Butterfield, D., Rappé, M. S., et al. (2003). Fluids from aging ocean crust that support microbial life. *Science* 299, 120–123. doi: 10.1126/science.1075653

De Pater, I., and Lissauer, J. J. (2015). *Planetary Sciences*. Cambridge: Cambridge University Press.

D'Hondt, S., Inagaki, F., Zarikian, C. A., Abrams, L. J., Dubois, N., Engelhardt, T., et al. (2015). Presence of oxygen and aerobic communities from sea floor to basement in deep-sea sediments. *Nat. Geosci.* 8:299. doi: 10.1038/ngeo2387

Ehlmann, B. L., and Edwards, C. S. (2014). Mineralogy of the Martian surface. *Annu. Rev. Earth Planet. Sci.* 42, 291–315. doi: 10.1146/annurev-earth-060313-055024

Ehlmann, B. L., Mustard, J. F., Murchie, S. L., Bibring, J.-P., Meunier, A., Fraeman, A. A., et al. (2011). Subsurface water and clay mineral formation during the early history of Mars. *Nature* 479, 53–60. doi: 10.1038/nature10582

Hasterok, D., Chapman, D., and Davis, E. (2011). Oceanic heat flow: implications for global heat loss. *Earth Planet. Sci. Lett.* 311, 386–395. doi: 10.1016/j.epsl.2011.09.044

Hazen, R. M. (2012). "Geochemical origins of life," in *Fundamentals of Geobiology*, eds A. H. Knoll, D. E. Canfield, and K. O. Konhauser (Oxford: Blackwell Publishing Ltd.), 315–332.

Heberling, C., Lowell, R. P., Liu, L., and Fisk, M. R. (2010). Extent of the microbial biosphere in the oceanic crust. *Geochem. Geophys. Geosyst.* 11:Q08003. doi: 10.1029/2009GC002968

Hurowitz, J. A., Grotzinger, J. P., Fischer, W. W., McLennan, S. M., Milliken, R. E., Stein, N., et al. (2017). Redox stratification of an ancient lake in Gale crater, Mars. *Science* 356:eaah6849. doi: 10.1126/science.aah6849

Jarrard, R. D. (2003). Subduction fluxes of water, carbon dioxide, chlorine, and potassium. *Geochem. Geophys. Geosyst.* 4:8905. doi: 10.1029/2002GC000392

Lempart, M., Derkowski, A., Luberda-Durna,ś, K., Skiba, M., and Błachowski, A. (2018). Dehydrogenation and dehydroxylation as drivers of the thermal decomposition of Fe-chlorites. *Am. Mineral.* 103, 1837–1850. doi: 10.2138/am-2018-6541

Lever, M. A., Rouxel, O., Alt, J. C., Shimizu, N., Ono, S., Coggon, R. M., et al. (2013). Evidence for microbial carbon and sulfur cycling in deeply buried ridge flank basalt. *Science* 339, 1305–1308. doi: 10.1126/science.1229240

Lin, H.-T., Cowen, J. P., Olson, E. J., Lilley, M. D., Jungbluth, S. P., Wilson, S. T., et al. (2014). Dissolved hydrogen and methane in the oceanic basaltic biosphere. *Earth Planet. Sci. Lett.* 405, 62–73. doi: 10.1016/j.epsl.2014.07.037

Ménez, B., Pisapia, C., Andreani, M., Jamme, F., Vanbellingen, Q. P., Brunelle, A., et al. (2018). Abiotic synthesis of amino acids in the recesses of the oceanic lithosphere. *Nature* 564, 59–63. doi: 10.1038/s41586-018-0684-z

Meunier, A. (2005). *Clays.* New York, NY: Springer Science and Business Media.

Moore, D. M., and Reynolds, R. C. (1989). *X-Ray Diffraction and the Identification and Analysis of Clay Minerals.* New York, NY: Oxford University Press.

Moslehuddin, A. Z., and Egashira, K. (1997). Characterization of smectites found in Ganges Floodplain soils of Bangladesh. *Clay. Sci.* 10, 151–162. doi: 10.11362/jcssjclayscience1960.10.151

Müller, R. D., and Dutkiewicz, A. (2018). Oceanic crustal carbon cycle drives 26-million-year atmospheric carbon dioxide periodicities. *Sci. Adv.* 4:eaaq0500. doi: 10.1126/sciadv.aaq0500

Murchie, S. L., Mustard, J. F., Ehlmann, B. L., Milliken, R. E., Bishop, J. L., McKeown, N. K., et al. (2009). A synthesis of Martian aqueous mineralogy after 1 Mars year of observations from the Mars Reconnaissance Orbiter. *J. Geophys. Res.* 114:E00D06. doi: 10.1029/2009JE003342

Nussbaumer, A. D., Fisher, C. R., and Bright, M. (2006). Horizontal endosymbiont transmission in hydrothermal vent tubeworms. *Nature* 441, 345–348. doi: 10.1038/nature04793

Onstott, T., Ehlmann, B., Sapers, H., Coleman, M., Ivarsson, M., Marlow, J., et al. (2019). Paleo-rock-hosted life on earth and the search on mars: a review and strategy for exploration. *Astrobiology* 19, 1230–1262. doi: 10.1089/ast.2018.1960

Orcutt, B. N., Wheat, C. G., Rouxel, O., Hulme, S., Edwards, K. J., and Bach, W. (2013). Oxygen consumption rates in subseafloor basaltic crust derived from a reaction transport model. *Nat. Commun.* 4:2539. doi: 10.1038/ncomms3539

Orosei, R., Lauro, S. E., Pettinelli, E., Cicchetti, A., Coradini, M., Cosciotti, B., et al. (2018). Radar evidence of subglacial liquid water on Mars. *Science* 361, 490–493. doi: 10.1126/science.aar7268

Parsons, B. (1982). Causes and consequences of the relation between area and age of the ocean floor. *J. Geophys. Res.* 87, 289–302. doi: 10.1029/JB087iB01p00289

Pearson, V. K., Sephton, M. A., Kearsley, A. T., Bland, P. A., Franchi, I. A., and Gilmour, I. (2002). Clay mineral-organic matter relationships in the early solar system. *Meteorit. Planet. Sci.* 37, 1829–1833. doi: 10.1111/j.1945-5100.2002.tb01166.x

Pinnavaia, T. J. (1983). Intercalated clay catalysts. *Science* 220, 365–371. doi: 10.1126/science.220.4595.365

Sclater, J., Jaupart, C., and Galson, D. (1980). The heat flow through oceanic and continental crust and the heat loss of the Earth. *Rev. Geophys.* 18, 269–311. doi: 10.1029/RG018i001p00269

Smith, A. R., Kieft, B., Mueller, R., Fisk, M. R., Mason, O. U., Popa, R., et al. (2019). Carbon fixation and energy metabolisms of a subseafloor olivine biofilm. *ISME J.* 13, 1737–1749. doi: 10.1038/s41396-019-0385-0

Teagle, D. A., Alt, J. C., Bach, W., Halliday, A. N., and Erzinger, J. (1996). Alteration of upper ocean crust in a ridge-flank hydrothermal upflow zone: mineral, chemical, and isotopic constraints from Hole 896A. *Proc. ODP. Sci. Results* 148, 119–150. doi: 10.2973/odp.proc.sr.148.113.1996

Tully, B. J., Wheat, C. G., Glazer, B. T., and Huber, J. A. (2018). A dynamic microbial community with high functional redundancy inhabits the cold, oxic subseafloor aquifer. *ISME J.* 12, 1–16. doi: 10.1038/ismej.2017.187

Wade, J., Dyck, B., Palin, R. M., Moore, J. D., and Smye, A. J. (2017). The divergent fates of primitive hydrospheric water on Earth and Mars. *Nature* 552, 391–394. doi: 10.1038/nature25031

Wordsworth, R. D. (2016). The climate of early Mars. *Annu. Rev. Earth Planet. Sci.* 44, 381–408. doi: 10.1146/annurev-earth-060115-012355

Yamashita, S., Mukai, H., Tomioka, N., Kagi, H., and Suzuki, Y. (2019). iron-rich Smectite formation in Subseafloor Basaltic Lava in Aged oceanic crust. *Sci. Rep.* 9, 1–8. doi: 10.1038/s41598-019-47887-x

Zhang, X., Fang, J., Bach, W., Edwards, K. J., Orcutt, B. N., and Wang, F. (2016a). Nitrogen stimulates the growth of subsurface basalt-associated microorganisms at the western flank of the Mid-Atlantic Ridge. *Front. Microbiol.* 7:633. doi: 10.3389/fmicb.2016.00633

Zhang, X., Feng, X., and Wang, F. (2016b). Diversity and metabolic potentials of subsurface crustal microorganisms from the western flank of the Mid-Atlantic Ridge. *Front. Microbiol.* 7:363. doi: 10.3389/fmicb.2016.00363

Conflict of Interest: The authors declare that the research was conducted in the absence of any commercial or financial relationships that could be construed as a potential conflict of interest.

frontiers in Microbiology

ORIGINAL RESEARCH
published: 20 February 2020
doi: 10.3389/fmicb.2020.00229

Carbon Oxidation State in Microbial Polar Lipids Suggests Adaptation to Hot Spring Temperature and Redox Gradients

Grayson M. Boyer[1]*, *Florence Schubotz*[2], *Roger E. Summons*[3], *Jade Woods*[4] and *Everett L. Shock*[1,5]

[1] School of Earth and Space Exploration, Arizona State University, Tempe, AZ, United States, [2] MARUM and Department of Geosciences, University of Bremen, Bremen, Germany, [3] Department of Earth, Atmospheric and Planetary Science, Massachusetts Institute of Technology, Cambridge, MA, United States, [4] Department of Chemistry, University of Nebraska-Lincoln, Lincoln, NE, United States, [5] School of Molecular Sciences, Arizona State University, Tempe, AZ, United States

The influence of oxidation-reduction (redox) potential on the expression of biomolecules is a topic of ongoing exploration in geobiology. In this study, we investigate the novel possibility that structures and compositions of lipids produced by microbial communities are sensitive to environmental redox conditions. We extracted lipids from microbial biomass collected along the thermal and redox gradients of four alkaline hot springs in Yellowstone National Park (YNP) and investigated patterns in the average oxidation state of carbon (Z_C), a metric calculated from the chemical formulae of lipid structures. Carbon in intact polar lipids (IPLs) and their alkyl chains becomes more oxidized (higher Z_C) with increasing distance from each of the four hot spring sources. This coincides with decreased water temperature and increased concentrations of oxidized inorganic solutes, such as dissolved oxygen, sulfate, and nitrate. Carbon in IPLs is most reduced (lowest Z_C) in the hot, reduced conditions upstream, with abundance-weighted Z_C values between −1.68 and −1.56. These values increase gradually downstream to around −1.36 to −1.33 in microbial communities living between 29.0 and 38.1°C. This near-linear increase in Z_C can be attributed to a shift from ether-linked to ester-linked alkyl chains, a decrease in average aliphatic carbons per chain (nC), an increase in average degree of unsaturation per chain (nUnsat), and increased cyclization in tetraether lipids. The Z_C of lipid headgroups and backbones did not change significantly downstream. Expression of lipids with relatively reduced carbon under reduced conditions and oxidized lipids under oxidized conditions may indicate microbial adaptation across environmental gradients in temperature and electron donor/acceptor supply.

Keywords: geobiochemistry, intact polar lipid, redox gradient, hydrothermal system, microbial community, carbon oxidation state

OPEN ACCESS

Edited by:
Akihiko Yamagishi, Tokyo University of Pharmacy and Life Sciences, Japan

Reviewed by:
Jeremy Dodsworth, The California State University, United States
Zackary J. Jay, Montana State University, United States

***Correspondence:**
Grayson M. Boyer
gmboyer@asu.edu

Specialty section:
This article was submitted to Extreme Microbiology, a section of the journal Frontiers in Microbiology

Received: *05 May 2019*
Accepted: *31 January 2020*
Published: *20 February 2020*

Citation:
Boyer GM, Schubotz F, Summons RE, Woods J and Shock EL (2020) Carbon Oxidation State in Microbial Polar Lipids Suggests Adaptation to Hot Spring Temperature and Redox Gradients. Front. Microbiol. 11:229. doi: 10.3389/fmicb.2020.00229

1. INTRODUCTION

There is ongoing interest in how geochemistry influences lipid compositions expressed in living communities of microorganisms. Lipids can provide valuable information about the environmental conditions experienced by the microbes that produced them (Summons and Walter, 1990; Pearson and Ingalls, 2013; Schouten et al., 2013). Structural diversity, longevity, and potential traceability

have led to the extensive use of lipids in biogeoscience as biomarkers (Summons et al., 1999; Brocks and Pearson, 2005; Schouten et al., 2007a). However, interpreting lipid biomarkers can be challenging because they are often not specific to any single type of organism or set of geochemical conditions (Rashby et al., 2007; Pitcher et al., 2009; French et al., 2015). For this reason, it is useful to investigate how bulk lipid compositions change across a variety of natural systems and then look for patterns that are universally applicable.

Hot spring outflow channels provide particularly accessible locations for studying changes in lipid composition across strong temperature and chemical gradients. For instance, microbial communities in the submerged sediments and biofilms of boiling springs tend to express lipid compositions substantially different from those in a hot spring photosynthetic microbial mat downstream (Zeng et al., 1992; Schubotz et al., 2013). It is conceivable that temperature is not the only environmental stress governing distributions of lipid structural adaptations along a hot spring outflow channel. As is often the case in hydrothermal systems, temperature gradients coincide with gradients in water chemistry, such as pH, salinity, solute concentrations, and redox potential. Changes in lipid structures and compositions along these gradients likely reflect adaptation to the collective set of environmental conditions experienced by the microorganisms present.

Our goal was to identify patterns in the properties of microbial lipids that might be influenced by redox geochemistry. We decided to explore the average oxidation state of carbon (Z_C) in lipids. In general, lower values of Z_C in a molecule represent more reduced carbon (e.g., −4 in CH_4) while higher values indicate more oxidized carbon (e.g., +4 in CO_2). Z_C was chosen as a metric primarily because thermodynamic or kinetic relationships with redox potential have been implicated in a variety of natural processes. Examples include the predicted energetic favorability of amino acids biosynthesis in submarine hydrothermal vents (Amend and Shock, 1998), preservation and degradation of organic matter in sediments and soils (Likens, 2010; LaRowe and Van Cappellen, 2011; Boye et al., 2017), oxidation rates of atmospheric organic aerosols (Kroll et al., 2011, 2015), and evolutionary convergence on proteomes inferred from metagenomes of microbial communities in natural systems (Dick and Shock, 2011, 2013; Dick, 2014; Dick et al., 2019; Fones et al., 2019), in aerobic and anaerobic nitrogen-fixing bacteria and archaea (Poudel et al., 2018), and in human cancer tissue (Dick, 2016, 2017). Further, several of these studies have implicated Z_C as a useful proxy for biosynthetic costs predicted from redox geochemistry (Amend and Shock, 1998; Dick and Shock, 2013; Dick et al., 2019). Thermodynamic properties do not exist for the full suite of lipid structures found along a hot spring outflow channel, so a similar assessment is not yet possible. However, we reasoned that if patterns in Z_C were evident, this would provide impetus for an eventual thermodynamic analysis to quantify lipid energy costs along thermal and chemical gradients.

We calculated Z_C values for intact polar lipids (IPLs) from eighteen sediment and microbial biomass samples collected from the outflow channels of four alkaline YNP hot springs: Bison Pool, Mound Spring, Empress Pool, and Octopus Spring. Further, we calculated the Z_C of lipid headgroups, backbones, and alkyl chains to better understand how these components influence changes in the Z_C of IPLs. These Z_C values could then be correlated with the temperature, chemical composition, and redox state of the surrounding environment. We hypothesized that lipids sampled closest to the hot, reduced source of each spring would have the most reduced carbon on average, while the cool, oxidized conditions downstream would be characterized by lipids with more oxidized carbon. This general pattern aligns with observations of amino acid compositions inferred from metagenomes along the outflow channel of Bison Pool (Dick and Shock, 2011, 2013), and the strong correlations found between the Z_C of metagenomes and metatranscriptomes across natural redox gradients in a variety of microbial mats, terrestrial and marine hydrothermal systems, and hypersaline lakes (Dick et al., 2019). If compositions of microbial lipids display similar trends across a variety of natural systems, patterns in Z_C preserved in lipid biomarkers could potentially present a tantalizing target for inferring paleoredox.

2. METHODS

2.1. Water Chemistry

Temperature, conductivity, and pH were measured in the field as close to sampling locations as possible and before sample collection. Temperature and conductivity were measured with a YSI model 30 meter. Sample pH was measured with a WTW brand 3300i or 3110 model pH meter with WTW probe calibrated daily with pH 4, 7, and 10 buffer solutions at ambient temperature. Concentrations of dissolved oxygen and total sulfide were obtained from unfiltered water samples in the field using a Hach 2400 or 2800 portable spectrophotometer with Hach reagents and protocols. Water samples collected for laboratory analyses were filtered in the field with Supor^{TM} (Pall Corporation) 0.2 μm polyethersulfone (PES) syringe filters into 30 mL HDPE Nalgene bottles and stored at −20°C. Concentrations of total ammonium, nitrate, nitrite, and sulfate were obtained by ion chromatography on two Dionex DX-600 systems; one for the analysis of cations and the other for anions. Suppressor columns on both systems were regenerated with deionized water to improve the signal-to-noise ratio. The anion analysis system was equipped with a potassium hydroxide eluent generator, carbonate removal device, and AS11-HC/AG11-HC columns. Columns were equilibrated with 5 mM hydroxide for 10 min before each injection. The injection volume was 100 μL for anions. Using a constant flow rate of 1.0 mL/min, the eluent hydroxide concentration was held isocratically at 5 mM for 5 min, then increased over the course of 31 min with a non-linear gradient (Chromeleon curve 8). The cation analysis system was equipped with CS-16 and CG-16 columns. Cation samples were acidified with 6 N methanesulfonic acid (MSA) to 19 mM final concentration. The injection volume was 75 μL for cation analysis. The columns were eluted isocratically with 19 mM MSA and a flow rate of 0.5 mL/min. Ion concentrations were obtained by comparison to calibration curves created using mixed ion standards (Environmental Express, Charleston, SC, USA). Quantification accuracy was verified by the inclusion

of mixed ion-quality control standards (Thermo Scientific, Waltham, MA, USA) before, between, and after samples in each tray.

2.2. Sample Collection and Preparation

Samples for lipid analysis were collected with ethanol-cleaned spatulas or forceps into sterile 15 mL falcon tubes. Sediment and microbial mat samples were collected to ∼1 cm depth, while samples BP1, BP2, and OS1 were taken from streamer biofilm communities clinging to gravel below the surface of the outflow water. Samples were frozen on dry ice in the field before storage in a −80°C freezer. Frozen samples were freeze-dried and homogenized with a sterile mortar and pestle. Lipid extractions were carried out using a modified version of the Bligh and Dyer procedure (White and Ringelberg, 1998). Briefly, 0.5–2 g sediment or 200–800 mg biofilm was dissolved in a mixture of methanol (MeOH), dichloromethane (DCM), and 50 mM phosphate buffer at pH 7.4 (2:1:0.8 v/v). The mixture was sonicated for 10 min and then centrifuged for 10 min at 2,000 rpm. The supernatant was collected and the remaining sediment or biofilm underwent one more extraction with the same solvent proportions, followed by two more times with a mixture of MeOH, DCM, and 50 mM trichloroacetic acid buffer at pH 2 (2:1:0.8) to aid extraction of glycerol dialkyl glycerol tetraether (GDGT) lipids (Nishihara and Koga, 1987), and one more time with a mixture of 3:1 DCM:MeOH to account for less polar lipids. A liquid-liquid extraction was performed by adding equal volumes of water and DCM to the pooled supernatant, which was then mixed and allowed to separate into aqueous polar and organic non-polar phases. The non-polar organic phase was collected and the remaining aqueous phase was washed with equal parts DCM for two additional rounds of liquid-liquid extraction. The resulting total lipid extract (TLE) was dried under N_2 and redissolved in 9:1 DCM and MeOH for later analyses.

2.3. HPLC-MS

Aliquots of the TLE were chromatographically separated on an Agilent 1200 series high-performance liquid chromatograph (HPLC) equipped with a Waters Acquity Ultra Performance Liquid Chromatography ethylene bridge hybrid (BEH) amide column according to the hydrophilic interaction chromatography (HILIC) method described in Wörmer et al. (2013). Mobile phases included solvent A, a mixture of acetonitrile, DCM, formic acid, and ammonia (750:250:0.015:0.15 v/v) and solvent B, a mixture of MeOH, H_2O, formic acid, and ammonia (500:500:4:4). The initial eluent was 99% solvent A and 1% solvent B that was brought to 5% B with a linear gradient over 4 min. The gradient continued to 25% B over 18.5 min, then to 40% over 0.5 min and held isocratically for 3.5 min. The flow rate was held constant at 0.4 mL min^{-1} throughout each run. Mass spectral analysis of IPLs was performed in positive ion mode on an Agilent 6520 Accurate-Mass Quadrupole Time-of-Flight (Q-TOF) mass spectrometer equipped with an electrospray ionization source.

2.4. Interpretation of Mass Spectra

IPLs were identified by the exact mass (M) of their parent ion, i.e., the intact lipid molecule with either a proton adduct $[M + H]^+$ or ammonium ion adduct $[M + NH_4]^+$, and by comparing mass-to-charge (m/z) fragmentation patterns to previously published data as described in Sturt et al. (2004). **Table 1** summarizes references used for structural elucidation or mass spectral interpretation of IPLs. Structures exceeding the analytical window (m/z >2000) were not detected, potentially leading to the exclusion of some higher molecular weight lipids.

While headgroup moiety identities, number of chains, backbone-chain linkage types, unsaturations, and aliphatic chain carbons were inferred based on mass spectra, other structural information was not obtained, such as positions of double bonds in alkyl chains or glycosidic bonds linking sugar headgroup moieties. Branching in non-isoprenoidal chains, such as those found in iso- and anteiso fatty acids, could not be determined from their straight-chain counterparts, necessitating "number of aliphatic carbons per chain" as a metric of alkyl chain carbon content rather than "chain length," which implies distance spanned by straight or branching chains. Chain cyclizations in non-GDGT IPLs, such as cyclopropane fatty acids synthesized by certain bacteria (Grogan and Cronan, 1997), could not be discerned from unsaturations, as both types of chain modification have two fewer hydrogen atoms relative to a saturated straight chain. As such, these were counted as unsaturations. It is important to note that knowledge of the carbon positions of alkyl chain modifications, or whether a 2 Da loss is due to unsaturation or cyclization, and other fine details of molecular configuration are not required for the calculation of lipid Z_C. This is because Z_C depends solely on elemental abundances, oxidation states of non-carbon elements, and molecular charge. Additional discussion regarding IPLs potentially underrepresented in this study can be found in the **Supplementary Material**.

2.5. Lipid Quantification

IPLs were quantified based on manual peak integration of identified parent ions. The mole fraction of the ith IPL in a sample, x_i, was calculated using

$$x_i = \frac{I_i \cdot RF_i^{-1} \cdot mi_i^{-1}}{\sum_i \left(I_i \cdot RF_i^{-1} \cdot mi_i^{-1}\right)}, \quad (1)$$

where I_i stands for the manually integrated MS peak area, RF_i indicates the assigned analytical response factor, and mi_i designates the monoisotopic mass, all taken for the ith IPL parent ion.

Analytical response factors were applied in this study to partially account for differences in IPL ionization efficiency. Response factors were estimated by taking the linear slope of the injected masses vs. peak intensity for a small suite of co-analyzed commercially-available IPL standards. Because authentic standards are not available for every observed IPL structure, response factors were assigned based primarily on the similarity of headgroups to those of existing standards, under the assumption that headgroups are the chemical feature most likely responsible for differences in ionization efficiency among observed IPLs. For instance, Popendorf et al. (2013) found that response factors varied strongly between IPLs of

TABLE 1 | Observed polar lipids, headgroup formulae and their Z_C values, references used for identification, and assigned HPLC-MS quantification standards.

Headgroup			Backbone-chain linkage types*	Ref‡	RF§	Headgroup			Backbone-chain linkage types*	Ref‡	RF§
Abbreviation*	**Formula†**	**Z_C**				**Abbreviation***	**Formula†**	**Z_C**			
Glycolipids						**Phospholipids**					
1G	$C_6H_{11}O_5$	$-0.16\overline{6}$	DEG, AEG, DAG	a, b	1	APT	$C_5H_{13}NO_6P$	−0.600	DEG, AEG, DAG	a, b	3
			GDGT	b, c	2	DPG	$C_3H_8O_7P_2$	$-1.33\overline{3}$	DAG	a	7
			CER	a, d	3	PC	$C_5H_{14}NO_3P^+$	−1.800	DAG	a, b	3
2G	$C_{12}H_{21}O_{10}$	$-0.08\overline{3}$	DEG, AEG, DAG	a, b	4	PDME	$C_4H_{11}NO_3P$	−1.750	DAG	j	8
			GDGT	b, c	2	PE	$C_2H_7NO_3P$	−1.500	DAG, DEG, CER	a, c, d	9
3G	$C_{18}H_{31}O_{15}$	$-0.05\overline{5}$	DEG, DAG	a	4	PG	$C_3H_8O_5P$	−1.000	DAG	a, b	10
			GDGT	b, c	2	PME	$C_3H_9NO_3P$	$-1.66\overline{6}$	DAG	j	11
2G-NAcG-G	$C_{24}H_{41}NO_{19}$	0.000	DAG, DEG	b, e	3	PS	$C_3H_7NO_5P$	0.333	DAG	a	12
3G-NAcG-G	$C_{30}H_{51}NO_{24}$	0.000	DEG	f	3						
4G	$C_{24}H_{41}O_{20}$	−0.042	GDGT	b, c	2	**Aminolipids**					
GA	$C_6H_9O_6$	0.500	DAG	g	1	BL	$C_7H_{15}NO_2^+$	−1.000	DAG	b, k	13
G-GA	$C_{12}H_{19}O_{11}$	0.250	DAG	f	4	OL	$C_5H_{10}NO_2$	−0.600	FA-OH-FAm(-OH)	l, b, g	13
G-NG	$C_{12}H_{22}NO_9$	$-0.08\overline{3}$	DAG, DEG	h	3	TM-KL	$C_9H_{19}NO_2^+$	$-1.22\overline{2}$	FA-OH-FAm	f	13
NG-GA	$C_{12}H_{20}NO_{10}$	0.250	DAG, AEG, DEG	f	3	TM-OL	$C_8H_{17}NO_2^+$	−1.125	FA-OH-FAm(-OH)	m	13
SQ	$C_6H_{11}O_7S$	$-0.16\overline{6}$	DAG	b	5						
						Unidentified					
Glycophospholipids						"223"	$C_7H_{12}NO_6$	0.429	DAG	f	3
1G-P	$C_6H_{12}O_8P$	$-0.16\overline{6}$	GDGT	b, c	2						
2G-P	$C_{12}H_{22}O_{13}P$	$-0.08\overline{3}$	DEG	a, c	6	**Other**					
			GDGT	b, c	2	hydroxyl "H"	H	Special‖	GDGT	b, c	2
3G-P	$C_{18}H_{32}O_{18}P$	$-0.05\overline{5}$	GDGT	b, c	2						
G-MeNG-G-P	$C_{19}H_{35}NO_{17}P$	−0.158	DEG	f	3						
G-NG-G-P	$C_{18}H_{33}NO_{17}P$	$-0.05\overline{5}$	DEG	f	3						
MeNG-G-P	$C_{13}H_{25}NO_{12}P$	−0.231	DEG	f	3						
NAcG-P	$C_{12}H_{21}N_2O_{10}P$	0.000	DAG, DEG	b, i	3						
NG-G-P	$C_{12}H_{23}NO_{12}P$	$-0.08\overline{3}$	DEG	f	3						
PI	$C_6H_{12}O_8P$	$-0.16\overline{6}$	DAG, AEG, DEG	a, b	6						
			CER	a, b, d	3						

*See text for abbreviations.

†Formulae correspond to elemental abundances contained in headgroups according to the division scheme depicted in ***Figure 1*** and described in the methods.

‡References used for structural elucidation and/or mass spectral interpretation; a. Sturt et al. (2004); b. Schubotz et al. (2013); c. Yoshinaga et al. (2011); d. Karlsson et al. (1998); e. Ferreira et al. (1999); f. this work (see ***Supplementary Material*** for mass spectral interpretation); g. Diercks et al. (2015); h. Schubotz et al. (2015); i. Yang et al. (2006); j. Wang et al. (2015); k. Benning et al. (1995); l. Zhang et al. (2009); m. Moore et al. (2013).

§IPL standard used to determine analytical response factors. Numbers correspond to commercially-available standards reported in ***Table S1***.

‖This headgroup does not contain carbon and therefore does not have a Z_C value, though it still contributes to the Z_C calculated for all IPLs or headgroups in a sample.

different headgroups and less so from chain length during HPLC electrospray ionization.

Authentic standards and response factors are shown in **Table S1** and their assignments to observed IPLs are reported in **Table 1**. IPLs with headgroup analogs among standards include monoglycose (1G), diglycose (2G), sulfoquinovose (SQ), phosphatidylinositol (PI), diphosphatidyl glycerol (DPG), phosphatidylcholine (PC), phosphatidyl (N,N-dimethyl)ethanolamine (PDME), phosphatidylethanolamine (PE), phosphatidylglycerol (PG), phosphatidyl (N-methyl)ethanolamine (PME), and phosphatidylserine (PS). The rationale guiding response factor assignments for IPLs with no direct headgroup analog are briefly outlined below. IPLs with nitrogen-bearing groups, such as diglycosyl (N-acetyl)glycosaminyl glycose (2G-NAcG-G), triglycosyl (N-acetyl)glycosaminyl glycose (3G-NAcG-G), monoglycosyl (N)glycosamine (G-NG), (N)glycosaminyl glycoronic acid (NG-GA), glycosyl (N-methyl) glycosaminyl glycosyl phosphate (G-MeNG-G-P), glycosyl (N)glycosaminyl glycosyl phosphate (G-NG-G-P), (N-methyl)glycosaminyl glycosyl phosphate (MeNG-G-P), (N-acetyl)glycosaminyl phosphate (NAcG-P), (N)glycosaminyl monoglycosyl phosphate (NG-G-P), aminophosphopentanetetrol (APT), ceramide (CER) lipids, and lipids with an unidentified "223" headgroup (see **Figure S4**) were assigned the response factor obtained from C42:0 PC diacylglycerol (DAG), under the assumption that the nitrogen-bearing functional groups contained in these lipids might result in comparable ionization efficiencies. This assumption was

based on qualitative assessment of the differences in relative peak intensities of nitrogen-bearing and non-nitrogen bearing standards; the former had peak intensities that averaged about an order of magnitude greater than the latter (**Table S1**). Lipids with a glycoronic acid (GA) headgroup, a non-nitrogen-containing single-moiety glycosyl group, were assigned the response factor obtained from a 1G-DAG standard composed of a mixture of C34:2 and C34:3 chain lengths. Lipids with a monoglycosyl glycoronic acid (G-GA), triglycose (3G), or tetraglycose (4G) headgroup were assigned the response factor of the standard containing the closest number of non-nitrogen-bearing glycosyl moieties; a 2G-DAG standard mixture of C34:2, C34:3, and C36:6 chain lengths. Glycophospholipids with no nitrogen, such as monoglycosyl phosphate (1G-P), diglycosyl phosphate (2G-P) or triglycosyl phosphate (3G-P) headgroups, were assigned the response factor obtained from C32:0 PI-DAG. All GDGTs were assigned the response factor obtained from the 1G-GDGT-PG standard that included a mixture of H-shaped and non-H-shaped alkyl chains with 0-3 internal rings. All aminolipids, including ornithine lipids (OL), monohydroxylated ornithine lipids (OL-OH), trimethylornithine lipids (TM-OL), monohydroxylated trimethylornithine lipids (TM-OL-OH), trimethyllysine lipids (TM-KL) and betaine lipids (BL), were assigned the response factor obtained from C32:0 1,2-dipalmitoyl-sn-glycero-3-O-4′-[*N*,*N*,*N*-trimethyl(d9)]-homoserine (DGTS-d9) based on structural similarities of their amino acid headgroups.

2.6. IPL Structural Designations and Chemical Formulae

Headgroups, backbones, and alkyl chains serve as the three basic building blocks comprising IPL structure, each with its own set of observed structural variations. The schematic used to categorize divisions among observed headgroup-backbone-alkyl chain variation is shown in **Figure 1**, with green, blue, and orange portions indicating headgroup, backbone, and alkyl chain structures, respectively. When considering differences across

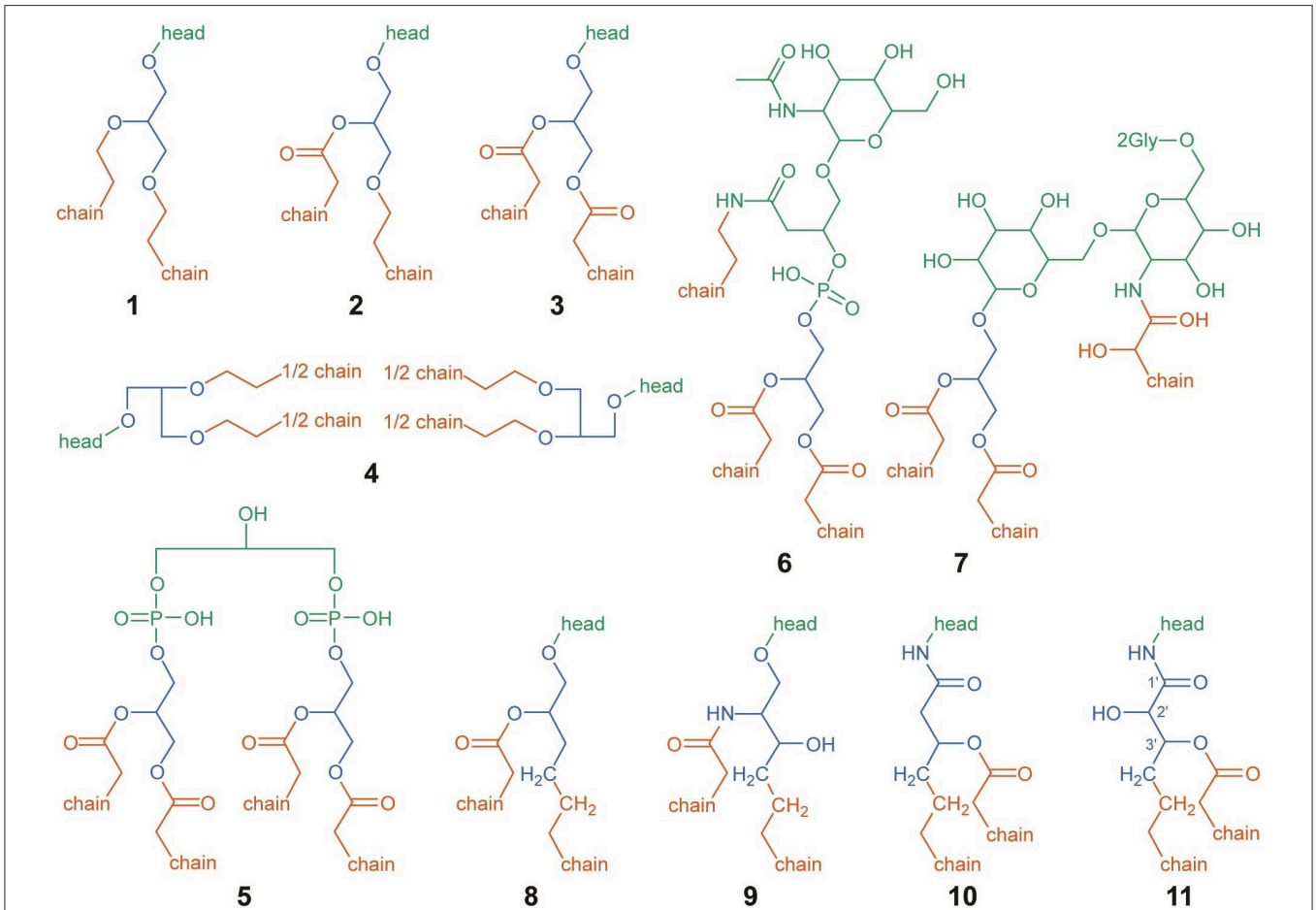

FIGURE 1 | Structural designations used for IPL headgroups (green), backbones (blue), and alkyl chains (orange), for the sake of calculating abundance-weighted average properties and chemical formulae. Structures are depicted for DEG **(1)**, AEG **(2)**, DAG **(3)**, GDGT **(4)**, DPG **(5)**, NAcG-P-DAG **(6)**, 2GNAcG-G-DAG **(7)**, 1,2-alkanediol **(8)**, CER **(9)**, FA-OH-FAm **(10)**, and FA-OH-FAm-OH **(11)**. Abbreviations are defined in the text. For structures **(1–4)** and **(8–11)**, the chemical structure of the headgroup is represented by "head." Putative headgroup structures are shown for **(6)** and **(7)**. Only the chemical structure of the first two carbons of each alkyl chain are shown; with "chain" representing the rest. In FA-OH-FAm-OH **(11)**, backbone-alkyl chain esterification may occur on either the 2′ or 3′ hydroxyl group (Diercks et al., 2015).

widely varying lipid structures, it is important to define strict boundaries between components for the sake of consistently comparing properties that depend on chemical formulae, such as Z_C or the number of aliphatic carbons in an alkyl chain. This is particularly important for comparing lipids with glycerol backbones to those without. Generalized lipid structures with glycerol backbones considered in this study include diether glycerol (DEG, **1**), mixed acyl/ether glycerol (AEG, **2**), diacyl glycerol (DAG, **3**), GDGT (**4**), DPG (**5**), and putative structures NAcG-P (**6**, DAG variant shown), 2GNAcG-G (**7**, DAG variant shown), and 3GNAcG-G-DEG (**Figure S7**). Structures that do not contain a glycerol backbone include 1,2-alkanediols (**8**), CER lipids (**9**), fatty acid esters of hydroxy fatty amides (FA-OH-FAm, **10**), and monohydroxylated FA-OH-FAm lipids (FA-OH-FAm-OH, **11**).

The headgroup of an IPL was structurally designated as one or more covalently bonded polar moieties linked to one or more backbones, represented by green structures in **Figure 1**. In some cases, the headgroup itself may be directly linked to one or more alkyl chains, such as in structures **6** and **7**. The chemical formulae of all headgroups reported in **Table 1** are assumed to be protonated to an extent that results in a neutrally-charged IPL, though it should be noted that Z_C is not affected by pH-dependent ionization. The +1 charge imparted by a quaternary ammonium functional group is not the result of pH-dependent ionization and therefore affects Z_C, which is why this charge is included in the chemical formulae of PC, TM-OL, TM-OL-OH, and TM-KL.

Most IPL structures observed in this study have one mole of headgroup per mole of lipid with the exception of GDGTs, which has two. It has been shown that sugar and phosphate moieties can be distributed between the two headgroups of a GDGT, resulting in a variety of possible isomers (Yoshinaga et al., 2011). In this study, we could determine the total number and type of moieties among the two headgroups of GDGTs but the analytical method did not allow us to determine headgroup positions. For instance, the two hexose moieties in 2G-GDGT may be clustered on one end of the lipid or evenly distributed among both ends. Our definition of an IPL headgroup was chosen to ensure consistency in headgroup chemical formulae regardless of position. All configurations of headgroup moieties in 2G-GDGT, for example, have the same total elemental abundance. A 2G-GDGT with two monoglycosyl headgroups, each with the formula $C_6H_{11}O_5$, has a total elemental abundance of $C_{12}H_{22}O_{10}$ among headgroups. If the 2G-GDGT has one diglycosyl headgroup with the formula $C_{12}H_{21}O_{10}$, then its other headgroup must be a single hydrogen atom to bring the total to $C_{12}H_{22}O_{10}$. In GDGTs with every headgroup moiety clustered on one side, this hydrogen atom is defined as belonging to the hydroxyl group on the opposite end of the GDGT, and is listed as its own headgroup in **Table 1**.

Lipid backbones are designated by the blue structures in **Figure 1**. Most IPLs observed in this study have one mole of backbone per mole of lipid. However, GDGT (**4**) and DPG (**5**) lipids were counted as having two moles of backbone per mole of lipid. IPL backbones were structurally designated according to two criteria chosen to promote consistency among observed IPL structures. First, the backbone must have a linear aliphatic chain of three carbons. Second, the backbone must include three "connector" functional groups that serve to anchor the headgroup and alkyl chains. In addition to these three connector groups, the three-carbon backbone may include modifications like hydroxylations or carbonyl groups. Various backbone-alkyl chain linkage types are shown in **Figure 2**, with backbone connector groups shown proximal to the R_1 group representing the rest of the backbone; a methylene group (CH_2) for a carbon-carbon (C–C) link **(12)**, an oxygen atom (–O–) for an ether link **(13–16)**, –NH– for an amide link **(17)**, or an oxygen atom (–O–) for an ester link **(18–21)**. Connector groups were included in the structure of the backbone rather than in the alkyl chain to maintain consistency when calculating nC in alkyl chains with C-C backbone-chain linkage relative to other chains. To demonstrate, consider the C-C linked alkyl chain **(12)** and the ether-linked alkyl chain **(13)** in **Figure 2**. Both are saturated and have approximately the same physical length. To ensure that both chains have the same value for nC, the connector groups proximal to R_1 must be categorized as part of the backbone. Structures **8** through **11** illustrate how the backbone contains one CH_2 group (in blue) and the alkyl chain contains the other (in orange) in a C-C link.

Alkyl chains are aliphatic hydrocarbon chains linked to the IPL backbone or in some cases, directly to the headgroup. Their designation is indicated by orange structures in **Figure 1**. Alkyl chains begin at the carbon atom directly after the backbone "connector" atom and continue to the distal methyl group that caps the end of the chain. Most of the IPL structures observed in this study had two moles of alkyl chains per mole of lipid **(1–3, 8–11)**, though some had three **(6–7)** or four **(4–5)**. Each GDGT had two membrane-spanning biphytanyl alkyl chains with forty carbons apiece. GDGT chains were conceptually divided into twenty-carbon half-chains to permit averaging of chain properties, such as Z_C and nC, between GDGTs and non-GDGT bilayer lipids. Therefore, one mole of GDGT was counted as having four moles of half-chains (see Structure **4**) so that they could be more directly compared to the alkyl chains of non-GDGTs. GDGT half-chains terminate in a methylene group (CH_2) that is covalently bonded to the methylene group of another GDGT half-chain within the membrane interior (e.g., Structures **15** or **16**).

2.7. Calculation of Average Lipid Properties and Elemental Composition

Abundance-weighted properties of IPL headgroups, backbones, and chains were calculated for each sample using the equation

$$\Xi = \frac{\sum_i \Xi_{ipl,i} \cdot x_i}{\sum_i n_{component,i} \cdot x_i}, \quad (2)$$

where Ξ indicates the average property of interest (e.g., average nC of IPLs in a sample), $\Xi_{ipl,i}$ represents the property summed across all components of the same type in the ith IPL (e.g., 32 carbons in the alkyl chains of a C32 IPL) with $n_{component,i}$ instances of the component in the IPL (e.g., 2 alkyl chains in

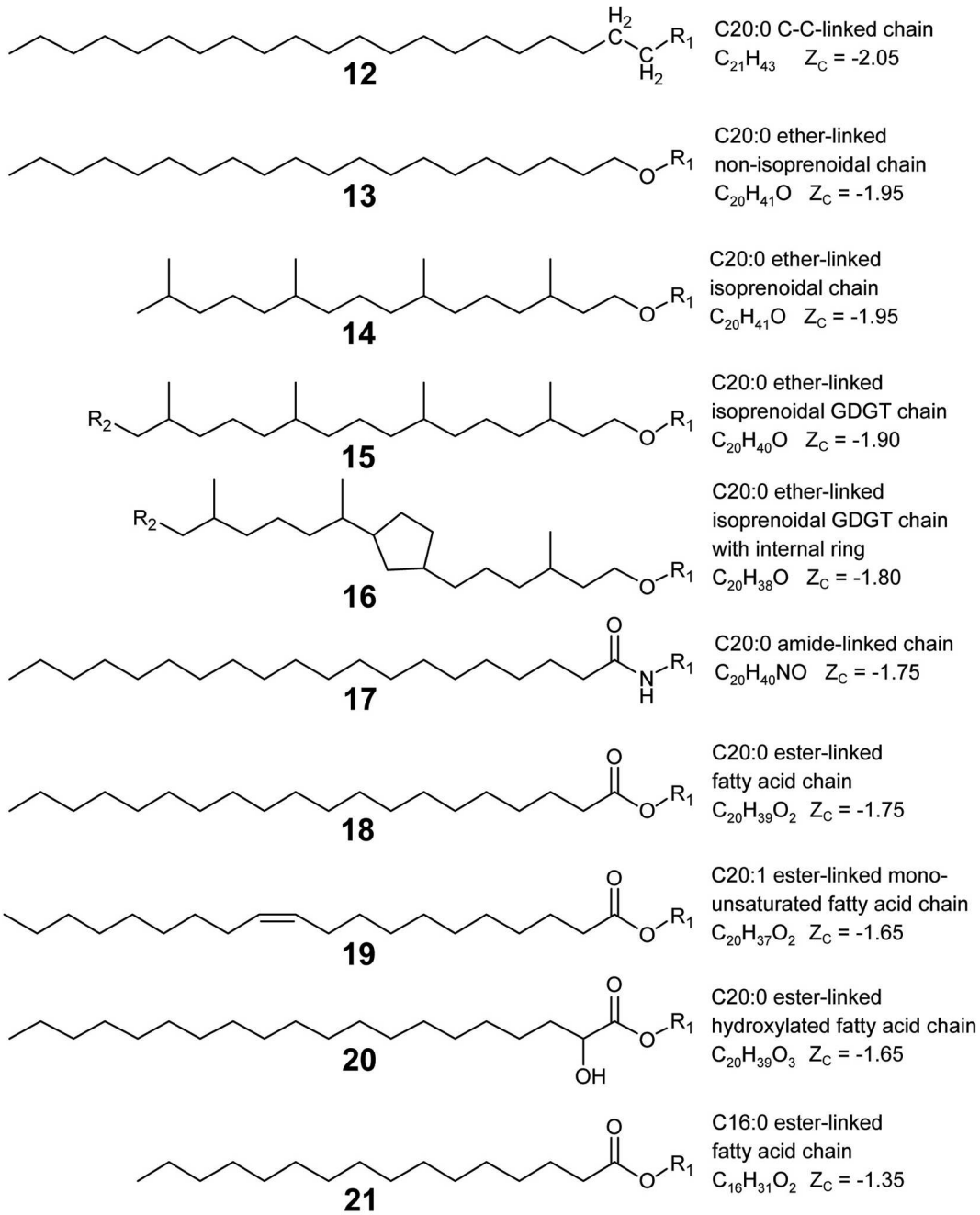

FIGURE 2 | Lipid alkyl chain modifications and backbone-chain linkage types organized by Z_C from reduced (top) to oxidized (bottom). Example structures were chosen to permit comparison of Z_C between various types of alkyl chain modifications: chain-backbone linkage type as C–C **(12)**, ether **(13)**, amide **(17)**, or ester **(18)**; non-branching and branching chains **(13, 14)**; isoprenoidal non-GDGT chains and GDGT half-chains **(14, 15)**; GDGT half-chains without and with an internal ring **(15, 16)**; saturated and unsaturated chains **(18, 19)**; non-hydroxylated and hydroxylated chains **(18, 20)**; and chains with a greater and lesser number of aliphatic carbons **(18, 21)**. R_1 represents a covalent bond to the rest of the lipid, and R_2 indicates a covalent bond with another GDGT half-chain.

a DAG IPL). Finally, x_i represents the mole fraction of the ith IPL. Abundance-weighted properties calculated in this way include nC, nUnsat, and the number of hydroxylations (nOH) per alkyl chain, the fraction of alkyl half-chains belonging to GDGT (x_{GDGT}), and the fraction backbone-alkyl chain linkage types with an ether (x_{ether}), ester (x_{ester}), amide (x_{amide}), or C-C (x_{C-C}) bond. The abundance-weighted number of internal rings per GDGT (not per alkyl chain) in a sample was also calculated using Equation (2) by setting x_i to the mole fraction of the ith GDGT (rather than the ith IPL), and setting $n_{component,i}$

equal to one, thereby producing a per-GDGT property and not a per-chain property.

Average chemical formulae of IPLs and their component parts were also calculated for each sample using Equation (2) by substituting $\Xi_{ipl,i}$ with charge and elemental abundances of carbon, hydrogen, nitrogen, oxygen, phosphorus, and sulfur atoms in the *i*th IPL. The value of $n_{component,i}$ was set to one when calculating average chemical formulae of full IPLs. Even when the structure of an IPL or component is unclear, its elemental composition is typically obtainable with high resolution accurate-mass mass spectrometry. This permits the inclusion of ambiguous structures when calculating average chemical formulae. For example, the unidentified "223" headgroup is suspected to have the chemical formula $C_7H_{12}NO_6$ based on mass spectral interpretation (**Figure S4**) and could therefore be included in the calculation of average chemical formulae of IPLs and headgroups.

2.8. Calculation of IPL Z_C

A step-by-step example illustrating how lipid Z_C can be calculated for a hypothetical sample is provided in the **Supplementary Material**. The Z_C of IPLs and their component parts were calculated using the equation

$$Z_C = \frac{2o + 3n - 5p - 4s - h + Z}{c}, \quad (3)$$

where *Z* stands for the net charge and *c*, *h*, *n*, *o*, *p*, and *s* represent the number of atoms of carbon, hydrogen, nitrogen, oxygen, phosphorus, and sulfur in the chemical formula of interest. Hydrogen, oxygen, and nitrogen were assigned oxidation states of +1, −2, and −3. Sulfur within the sulfonic acid group of SQDAG was assigned an oxidation state of +4. Phosphorus was assigned an oxidation state of +5 to be consistent with that of phosphorus within the phosphate ion. Charge gained or lost by pH-dependent protonation or deprotonation, as is common in many lipid headgroups, does not affect Z_C.

Equation (3) was used to determine the Z_C values of individual lipid structures, such as those reported in **Figure 2**. It was also used to calculate abundance-weighted Z_C values in each sample; in this case, using the abundance-weighted charge and carbon, hydrogen, nitrogen, oxygen, phosphorus, and sulfur atoms in the average chemical formulae of IPLs and their components.

2.9. Statistical Simulation of Analytical Uncertainty

We conducted a statistical analysis to check whether observed trends in Z_C were not an artifact of the methods chosen for IPL quantification. To do this, we employed an R script to carry out a Monte Carlo-style bootstrap sensitivity analysis in which manually integrated IPL HPLC-MS peak areas were allowed to vary randomly by up to 30% of their original value over 999 iterations. In addition, the analytical response factors applied to any headgroup-backbone combination listed in **Table 1** were allowed to vary by up two orders of magnitude higher and lower. Z_C for lipids and their components were re-calculated from average chemical formulae after each iteration.

3. RESULTS AND DISCUSSION

3.1. Hot Spring Sample Sites

Temperature, pH, and conductivity measurements are shown in **Table 2** for samples taken along the outflow channels of Bison Pool, Mound Spring, Empress Pool, and Octopus Spring. Upstream samples collected closest to the source pools of each spring ranged from circumneutral to alkaline (pH 5.78–8.81), with temperatures close to the boiling point of water (82.2–91.0°C) given their altitude in YNP (∼2,200 m above sea level at Bison Pool and Mound Spring, 2,250 m at Octopus Spring, and 2,300 m at Empress Pool). Water temperature decreased and pH increased with distance from the source, with the furthest samples downstream ranging between 29.0 and 59.8°C and pH 8.27 and 9.53. Trends in conductivity were typically non-linear and were not shared among hot springs.

Microbial communities inhabiting the sediment below the surface of the water changed visibly downstream. At Bison Pool and Octopus Spring, upstream samples contained white or pink streamer biofilm communities (SBCs) clinging to submerged pebbles or mineral protrusions. A study by Meyer-Dombard et al. (2011) found the bulk of the bacterial community in the pink streamers of Bison Pool belonged to *Aquificales* and *Thermatogales*, while most archaea were mainly comprised of *Crenarchaeota* and *Desulfurococcales*. SBCs were absent at Empress Pool and Mound Spring, despite the latter's proximity and apparent geochemical similarity to Bison Pool. Communities of photosynthetic microorganisms were visually identified in downstream samples by their pigmentation. At Bison Pool, Mound Spring, and Octopus Spring, the transition from chemotrophic to mixed photo/chemo-trophic microbial communities could be readily identified by the sharp onset of photosynthetic pigmentation over a span of a few centimeters. This transition at Empress Pool was not as distinct, and visual confirmation of samples with phototrophic communities relied on faint patches of pigmented microorganisms. The maximum temperature we observed for phototrophic organisms was at 73.3°C at BP3, which falls close to the maximum temperature limit observed for photosynthesis among alkaline YNP hot springs reported by Cox et al. (2011).

Downstream from the "photosynthetic fringe," laminated green/orange photosynthetic mats were present at Bison Pool, Mound Spring, and Octopus Spring. Previous work by Ward et al. (1987) at Octopus Spring and Meyer-Dombard et al. (2011) at Bison Pool and Mound Spring showed that *Synechococcus* cyanobacteria and *Chloroflexus* bacteria comprise the bulk of the community at these mats. Empress Pool did not have a massive laminar microbial mat, though green/orange photosynthetic communities were visually apparent along either side of the channel in broken patches downstream. Samples BP6 and MS5, taken from post-mat runoff zones of gray-beige flocculent matter, were identified as hosting photosynthetic microbes based on visual confirmation of green pigmentation within the floc.

Microbial mats like those found at Bison Pool, Mound Spring, and Octopus Spring are complex stratified ecosystems of interconnected metabolic cycles. The oxic conditions measured in the water column and upper mat give way to anoxia after

TABLE 2 | Selected geochemical and physical data from each sample site.

Site	Sample	12T UTM coordinates		Dist[a] (m)	Zone[b]	Temperature (°C)	pH	Conductivity[c] (μS/cm)
		Easting	Northing					
Bison	BP1	510710	4935155	2.9	C	89.0	7.23	1550
Pool	BP2	510715	4935156	8.2	C	80.9	7.34	1568
	BP3	510718	4935157	11.1	T	73.3	7.27	1540
	BP4	510719	4935159	13.4	P	63.1	8.09	–[d]
	BP5	510719	4935163	17.2	P	40.5	8.25	1508
	BP6	510724	4935165	22.6	P	29.0	9.01	1697
Mound	MS1	511114	4934621	3.6	C	91.0	8.81	1612
Spring	MS2	511108	4934624	12.7	C	77.3	8.65	1621
	MS3	511098	4934628	24.2	P	64.8	9.08	1617
	MS4	511083	4934621	38.7	P	53.0	9.22	1634
	MS5	511049	4934625	53	P	35.1	9.53	1660
Empress	EP1	0521589	4948280	2.2	C	82.2	5.78	1824
Pool	EP2	0521585	4948280	6.2	T	70.5	6.96	1832
	EP3	0521580	4948285	13.3	T	60.7	7.63	1840
	EP4	0521560	4948293	34.8	P	51.6	7.99	1860
	EP5	0521558	4948295	37.6	P	38.1	8.42	1664
Octopus	OS1	0516054	4931217	7.0	C	85.4	7.29	1622
Spring	OS2	0516016	4931212	38.3	P	59.8	8.27	1581

[a] *Distance from hot spring source.*

[b] *Major metabolic regime representative of the microbial community at the sample site, interpreted visually in the field based on the presence or absence of photosynthetic pigments; C, strictly chemosynthetic; T, transition to phototrophy; P, photosynthetic.*

[c] *Conductivity was normalized to 25 °C using the formula* $Cond_T/(1+\alpha(T-25))$*, where* $Cond_T$ *stands for the conductivity measured at the temperature of the sample site and* α *represents the temperature correction coefficient taken as 0.02 for freshwater.*

[d] *No data.*

only a few millimeters depth (Dupraz and Visscher, 2005; Franks and Stolz, 2009). Further, redox conditions in a microbial mat have been shown to undergo extreme fluctuations throughout a 24-h period (Fenchel, 1998; Visscher et al., 1998; Jonkers et al., 2003). The upper few millimeters of a mat are supersaturated with O_2 from cyanobacterial photosynthesis during the day and anoxic within minutes to hours of darkness. In this study, we strove to minimize the influence of sunlight availability, diel cycles, and other complicating factors arising from the passage of time by collecting samples at each outflow channel during light hours of the same day. In this way, we sought to capture a snapshot of water chemistry and lipid profiles from which to draw broad correlations. There is an intriguing possibility of steep biogeochemical gradients coinciding with substantial changes in lipid composition across a depth of millimeters, though these would have been interpreted as bulk averages according to our sampling method.

3.2. Water Chemistry

Measured concentrations of dissolved oxygen, nitrate, nitrite, sulfate, total ammonia, and total sulfide are given in **Table 3**. In all four outflow channels, concentrations of dissolved oxygen were lowest in samples closest to the source and increased downstream. This could be attributable to a combination of factors, such as extent of mixing with atmospheric O_2, input from microbial oxygenic photosynthesis, and concentration via evaporation. Sulfate concentrations also increased downstream and coincided with decreasing sulfide concentrations, as shown in **Figure 3**. A previous experiment by Cox et al. (2011) concluded that abiotic processes, such as degassing, oxidation by O_2 and hydrogen peroxide, and mineral precipitation were too slow to explain the downstream decrease in sulfide concentration at Bison Pool, and that oxidation of sulfide by outflow channel microorganisms was likely responsible. It is feasible that biological oxidation of sulfide may also be occurring in the outflow channels of Mound Spring, Empress Pool, and Octopus Spring given the parallels in geochemistry observed among these springs. In addition to sulfide and sulfate, we observed an inverse correlation between ammonia and nitrate concentrations, with the highest concentrations of ammonia closest to the source and decreasing downstream while nitrate concentrations steadily increase (**Table 3**). Oxidation of ammonia into nitrite and nitrate by microbial communities via nitrification is one possible explanation. However, previous phylogenetic and metagenomic studies of nitrogen-cycling genes in Bison Pool and Mound Spring microbial communities have found either an absence of genes involved in ammonia oxidation (Swingley et al., 2012), or limited presence with no active expression (Loiacono, 2013). Regardless of the cause, depletion of sulfide and ammonia coinciding with an increase in sulfate,

TABLE 3 | Concentrations of selected redox-sensitive dissolved chemical species[a].

Site	Sample	Oxidized				Reduced	
		O_2 (mg l^{-1})	NO_3^- (mg l^{-1})	NO_2^- (mg l^{-1})	$\sum SO_4^{2-}$ (mg l^{-1})	$\sum NH_4^+$ (mg l^{-1})	$\sum HS^-$ (μg l^{-1})
Bison Pool	BP1	0.2	0.01	0.02	13.11	0.07	230
	BP2	0.7	0.01	0.04	15.43	0.06	220
	BP3	1.1	0.02	0.01	16.81	0.04	bdl[b]
	BP4	2.3	0.03	0.02	16.50	0.02	6
	BP5	5.7	0.004	bdl	17.18	0.01	15
	BP6	3.3	0.07	bdl	18.32	0.02	10
Mound Spring	MS1	0.4	0.01	bdl	14.33	0.07	716
	MS2	2.2	0.01	bdl	15.03	0.01	758
	MS3	1.4	0.04	0.02	16.99	0.03	236
	MS4	3.6	0.02	0.01	17.56	0.02	70
	MS5	6.9	0.06	bdl	20.11	bdl	bdl
Empress Pool	EP1	0.4	0.01	0.08	106.87	0.42	260
	EP2	0.7	–[c]	–	–	–	97
	EP3	1.2	0.01	bdl	106.70	0.31	37
	EP4	1.3	0.03	0.03	111.70	0.39	31
	EP5	3.4	0.08	0.01	111.24	0.14	18
Octopus Spring	OS1	0.5	0.03	0.03	17.82	0.06	13
	OS2	3.3	0.03	0.02	18.76	0.02	12

[a] *Sulfide (HS^-), ammonium (NH_4^+), and sulfate (SO_4^{2-}) concentrations are summed for their respective pH-dependent protonated states.*
[b] *bdl: below detection limit.*
[c] *No data.*

nitrate, and dissolved oxygen suggests that water is most reduced at the source and becomes increasingly oxidized downstream along these hot spring outflow channels. This would agree with previous oxidation-reduction potential (ORP) Ag/AgCl electrode measurements that confirmed a downstream increase in Eh along the outflow channels of Bison Pool and Mound Spring (Dick and Shock, 2011).

3.3. IPL Headgroup and Backbone Distributions

Mole fractions of IPLs grouped according to their headgroup/backbone combinations and color-coded by their suspected source organisms are shown in **Figure 4**. Archaeally-derived GDGT and archaeol (AR) lipids (**Figure 4**, blue bars 1–5) were most abundant in samples collected closer to the source of each hot spring. MS1 and EP1 were the only two samples where archaeal lipids outnumbered those of non-archaea. Considering that one mole of GDGT is functionally equivalent to two moles of non-GDGTs in a membrane bilayer (in a general sense), it is unsurprising that archaeal membranes comprise the majority of lipids in the hottest upstream samples where Archaea are expected to thrive (Barns et al., 1994, 1996; Meyer-Dombard et al., 2005; Schouten et al., 2007b; Zhang et al., 2008). 1G-GDGT was found in >2% abundance in all but five samples and was always more abundant than any other archaeal lipid except for 2G-P-AR in sample OS1. Upstream samples were typically rich in lipids thought to be diagnostic of members of *Aquificae* bacteria (**Figure 4**, red bars 6–9), including PI-DEG/AEG and APT-DEG/AEG (Sturt et al., 2004; Schubotz et al., 2013). Indeed, previous phylogenetic analyses have confirmed the presence of *Aquificae* in the SBCs of Bison Pool and Octopus Spring, and in the high-temperature sediments of Mound Spring, and Empress Pool (Reysenbach et al., 1994; Meyer-Dombard et al., 2005, 2011; Spear et al., 2005; Swingley et al., 2012; Schubotz et al., 2013; Beam et al., 2016; Colman et al., 2016; Romero, 2018). SQ-DAG lipids found in the photosynthetic membranes of cyanobacteria and other phototrophs (Sato, 2004) were located in mid-to-downstream samples where green/orange pigments were visually confirmed in microbial communities (**Figure 4**, green bar 10). These sites also hosted an abundance of other lipids common in, but not specific to, phototrophic membranes, such as DAG lipids with 1G, 2G, and PG headgroups (Murata and Siegenthaler, 1998).

Glycolipids were abundant in every sample (**Figure 4**, yellow bars 11–22), with mole fractions ranging from 31% in OS2 to nearly 100% in MS1. Glycophospholipids (**Figure 4**, yellow bars 23–24), especially PI-DAG, were also abundant in nearly every sample and reached up to 63% in OS2. This preponderance of glyco(phospho)lipids is thought to confer heat tolerance via inter-lipid hydrogen bonding (Curatolo, 1987). Evidence to support this hypothesis comes from experiments by Adams et al. (1971), Ray et al. (1971), and Prado et al. (1988) demonstrating that higher growth temperatures result in a greater proportion of glycolipids to other membrane lipids in various thermophilic microorganisms.

Downstream samples collected from Bison Pool, Mound Spring, and Empress Pool featured many DAG phospholipids common to unspecific Bacteria and Eukaryotes (**Figure 4**, yellow bars 25–31), such as DPG, PC, PE, PG, PME, and PS (Kent, 1995; López-Lara and Geiger, 2017). These lipids were not abundant in Octopus Spring sample OS2, possibly because the temperature measured at this sample site, 59.8°C, roughly corresponds to the upper temperature limit of about 60°C reported for Eukaryotes (Tansey and Brock, 1972). Aminolipids (**Figure 4**, yellow bars 32–34) were less abundant upstream (typically <2%) than in downstream samples, where they reached up to 19% in sample EP5. IPLs bearing a headgroup with an exact mass consistent with the formula of $C_7H_{12}NO_6$, referred to here as "223-DAG" (**Figure 4**, purple bar 35), were most abundant (2–3%) in samples collected between 40 and 53°C. The structure and source of this lipid is unknown.

3.4. IPL Alkyl Chain Properties

Changes in abundance-weighted average properties of microbial IPL alkyl chains were observed downstream in all four outflow channels (**Table S2**). Patterns in chain-backbone linkage, aliphatic carbon number, degree of unsaturation and GDGT cyclization, and chain hydroxylations are described below.

3.4.1. Chain-Backbone Linkage

As shown in **Figure 5**, upstream samples from all four hot spring outflow channels are dominated by ether-linked alkyl chains

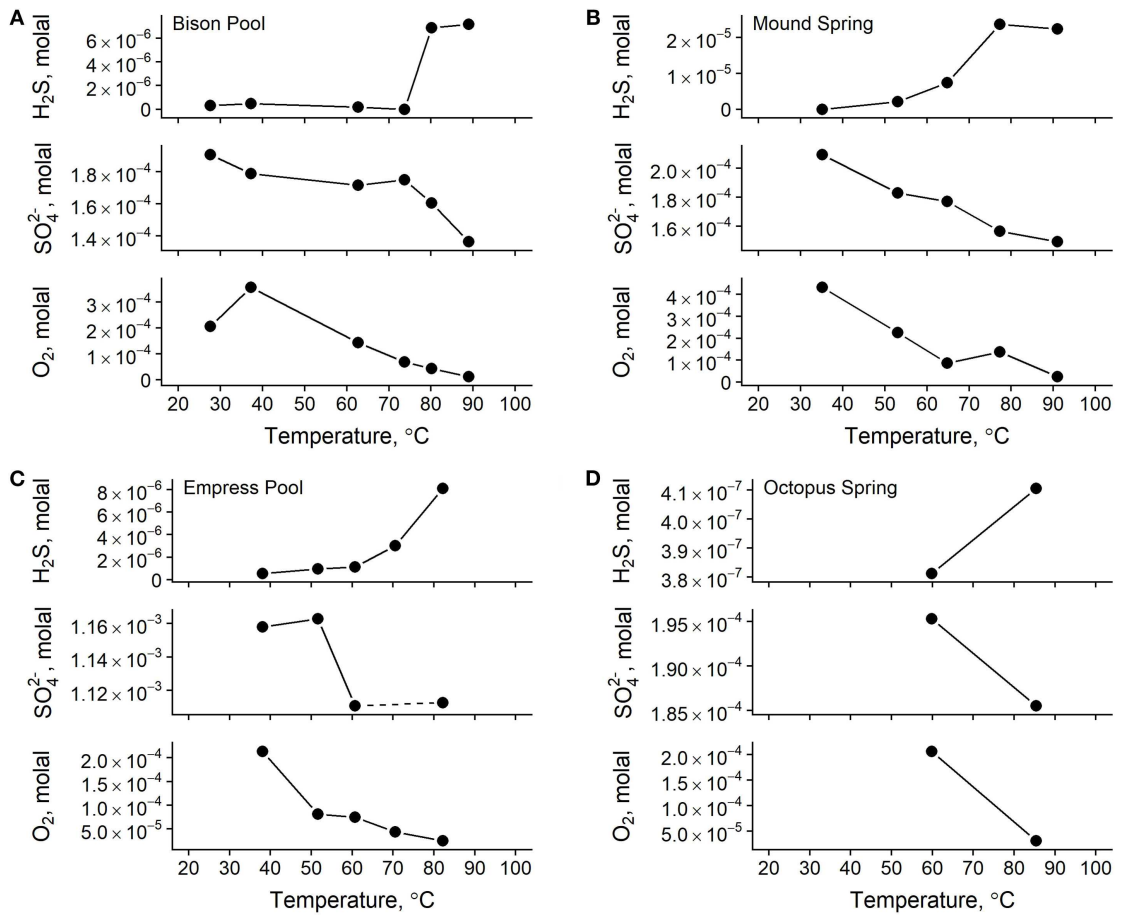

FIGURE 3 | Total concentrations of redox-sensitive aqueous chemical species in samples from Bison Pool **(A)**, Mound Spring **(B)**, Empress Pool **(C)**, and Octopus Spring **(D)**. Lines between points are meant to guide the eye between measurements only. A water sample was not collected for sulfate at Empress Pool site EP2 during the 2012 field season, indicated here by a dashed line between sulfate measurements for sites EP1 and EP3.

(70% mole fraction at BP1 to nearly 100% at MS1). Ether-linked alkyl chains are resistant to hydrolysis (Daniel and Cowan, 2000). The proportion of ether-linked chains decreases downstream from each hot spring source, giving rise to a growing proportion of ester-linked chains. The onset of photosynthetic communities coincides with a sharp increase in the proportion of ester-linked chains, comprising over 50% of alkyl chains in all samples containing visible photosynthetic pigmentation. Downstream samples have the highest abundance of ester-linked chains in each outflow channel (81–97% in samples below 40°C). Chains linked to the backbone via an amide or C–C bond are also present, though in relatively low abundance (<5% in any sample).

While ether lipids are the common chain-backbone linkage in archaea, they are a rare occurrence in bacteria. Bacterial ether lipids are predominantly reported from thermophilic bacteria (Huber et al., 1992; Jahnke et al., 2001). However, few mesophilic organisms are also able to synthesize these lipids in culture (Vinçon-Laugier et al., 2017). Contrasting these sparse culturing reports, bacterial ether lipids are abundantly found in the environment, typically under anoxic conditions, such as stratified water columns and marine sediments (Schubotz et al., 2009; Schröder, 2015; Evans et al., 2017). Based on these reports, temperature is not the only environmental variable influencing the distribution of bacterial ether lipids. Similarly, it is unclear whether pH plays an important factor. Some environments, such as marine sediments dominated by the process of anaerobic oxidation of methane where bacterial ether lipids are abundantly found, are more alkaline than their surrounding environment. However, the sediments and stratified water columns in these studies are relatively circumneutral. We therefore explore whether apart from temperature or pH, other variables, such as redox may influence backbone-chain linkage.

3.4.2. Number of Aliphatic Carbons, nC

As shown in **Figures 6A,B**, nC of alkyl chains tends to be greatest at the highest measured temperatures (above 80°C) and lowest dissolved oxygen concentration (around −5.0 log molal O_2). Values of nC approach 20 aliphatic carbons in samples furthest upstream, partly because these samples are rich in GDGTs with four 20-carbon half-chains. However, values of average nC approach 20 aliphatic carbons in upstream samples even after excluding contributions from GDGTs (empty symbols,

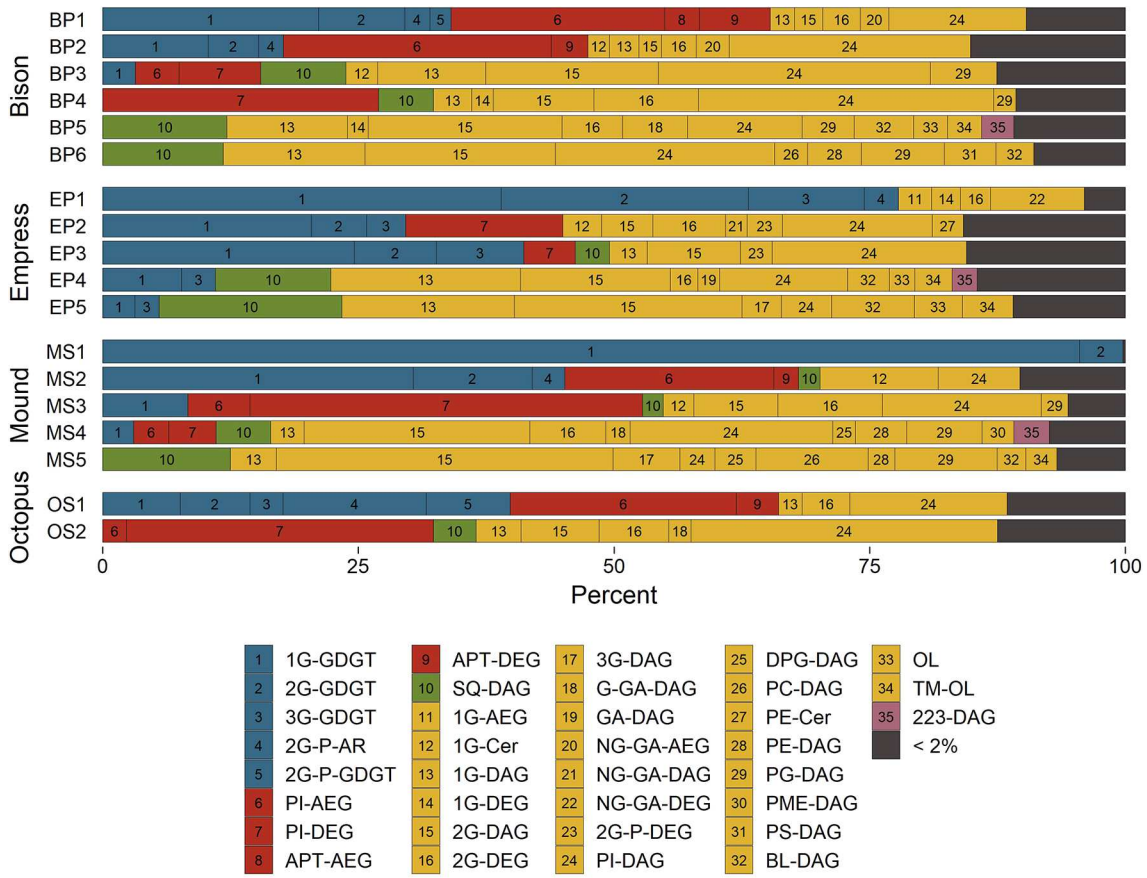

FIGURE 4 | Distributions of hot spring microbial IPLs classified by their headgroup-backbone-chain linkage. See text for abbreviations. Bar numbers reference indices in the legend. Bar colors represent suspected source organisms; unspecific Archaea (blue), *Aquificales* (red), phototrophs (green), unspecific Bacteria and Eukarya (yellow), and unknown (purple).

Figures 6A,B). Sample MS1 represents the only upstream sample where the weighted nC non-GDGT alkyl chains is anomalously small at 17.4 carbons, though it should be noted that non-GDGT chains comprise <1% of alkyl chains in this sample. Sample OS1 has the greatest weighted nC at 20.42 carbons because it was rich in C_{50} and C_{55} 2G-P-AR lipids that averaged 25 or 27.5 carbons per chain. Alkyl chain nC decreased with progressively cooler temperatures and oxidized conditions, reaching about 16.7–17 aliphatic carbons in samples furthest downstream. Overall, these trends in weighted nC agree with a plethora of studies demonstrating the capacity of microorganisms to adapt their membrane fluidity and permeability in response to temperature by adjusting the strength of hydrophobic interactions in the non-polar portion of their membranes (see reviews by Denich et al., 2003; van Meer et al., 2008; Siliakus et al., 2017).

3.4.3. Degree of Unsaturation, nUnsat

Average degree of unsaturation in IPL alkyl chains increased downstream in all four outflow channels, as shown in **Figures 6C,D**. Samples above 50°C or below -4.0 log molal O_2 had values of weighted nUnsat between 0 and 0.4 unsaturations and increased to 0.4–1 unsaturations in samples further downstream. This trend is especially prominent at Mound Spring and Empress Pool, where nUnsat is near-zero in MS1 and EP1 and gradually increases to about 0.7 and 1 unsaturation per chain in MS5 and EP5, respectively. Inverse correlations between temperature and average degree of unsaturation are well-documented in the literature (Marr and Ingraham, 1962; Siliakus et al., 2017). An unsaturation can either be in the *cis* and *trans* configuration; a *cis*-unsaturation is thought to increase membrane fluidity by introducing a "kink" in an alkyl chain that decreases chain packing and disrupts neighboring lipids in the membrane. Conversely, relatively straight *trans*-unsaturated fatty acids reduce membrane fluidity and have been correlated with microbial growth at higher temperatures and resistance to solvents and desiccation (Okuyama et al., 1990, 1991; Weber et al., 1994; Halverson and Firestone, 2000; Kiran et al., 2004, 2005). Determination of *cis* or *trans* configurations in unsaturated IPL alkyl chains was beyond the analytical scope of this study, though it should be emphasized that Z_C is not affected by isomerism.

3.4.4. Degree of GDGT Cyclization

The incorporation of one or more cycloalkyl rings into the alkyl chains of GDGTs (e.g., Structure **16**) has been proposed to enhance lipid packing while increasing fluidity in archaeal

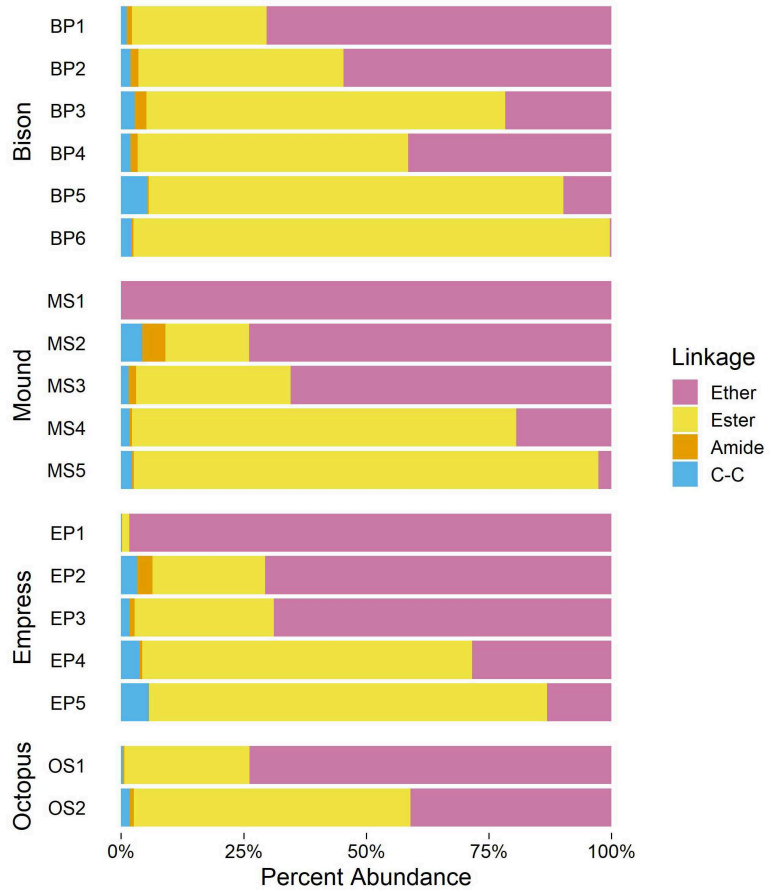

FIGURE 5 | Relative abundances of major backbone-alkyl chain linkage types in samples.

membranes (Gliozzi et al., 1983; Gabriel and Chong, 2000; Chong et al., 2012; Sollich et al., 2017). We observed a downstream increase in the number of internal rings in the GDGTs in the outflow channels of Bison Pool, Mound Spring, and Octopus Spring, as shown in **Figures 6E,F**. Between samples collected closest to each hot spring source and those furthest downstream, the average number of rings in GDGTs increased from 1.8 to 3.3 between BP1 and BP6, 2.5 to 3.5 between MS1 and MS5, and 1.1 to 2.5 between OS1 and OS2. Samples collected from the outflow channel of Empress Pool averaged between 2.1 and 2.5 rings and showed no clear correlation with temperature or dissolved oxygen concentration.

This downstream increase in the number of rings per GDGT agrees with a previous study by Schubotz et al. (2013) reporting a similar trend along the Bison Pool outflow channel. However, these results do not corroborate with studies by Schouten et al. (2002, 2007a) that propose a positive correlation between GDGT chain cyclization and temperature as the basis for the TEX_{86} paleothermometer (though TEX_{86} was originally calibrated for sea surface temperatures). Additionally, these observations do not match the results of laboratory growth experiments demonstrating increased chain cyclization with temperature in thermoacidophilic archaea (Boyd et al., 2011), marine *Crenarchaeota* (Wuchter et al., 2004), and *Thaumarchaeota* (Elling et al., 2015). Conflicting trends have also been reported in terrestrial hydrothermal systems. Kaur et al. (2015) observed an increase in GDGT ring abundance with temperature between a pH range of 5.5–7.2 in hot springs from the Taupo volcanic zone in New Zealand, though their low pH samples did not. Wu et al. (2013) studied GDGTs in Yunnan hot springs, China, and found that ring index increased with temperature in one statistical grouping and increased with acidity in the other.

Low pH has been observed to cause an increase in GDGT chain cyclization (Macalady et al., 2004; Boyd et al., 2013), which has been attributed to a denser packing of the cell membrane resulting in a higher tolerance toward large ion gradients (Gabriel and Chong, 2000). Studies on the influence of high pH on the incorporation of the number of rings, comparable to our systems, have not been systematically conducted, therefore it remains unclear whether the change in pH from alkaline to circumneutral plays an important role in the downstream increase in the number of rings. However, we find it conversely conceivable that the lower pH conditions upstream may cause the incorporation of more rings for a denser packing of the membrane, which is

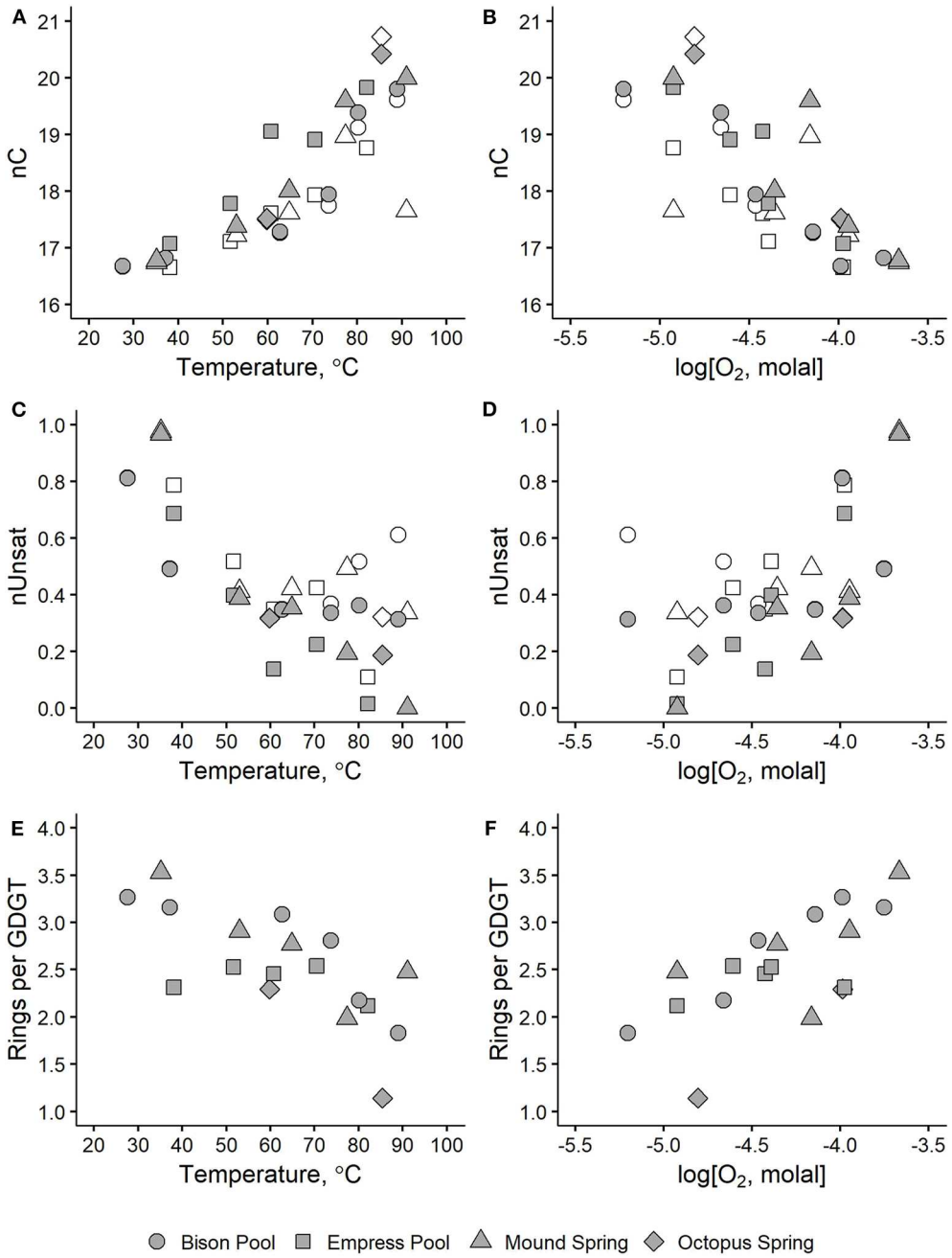

FIGURE 6 | Average alkyl chain properties in hot spring microbial IPLs plotted against temperature (left panels) and dissolved oxygen concentration (right panels) for number of aliphatic carbons, nC **(A,B)**, degree of unsaturation, nUnsat **(C,D)**, and internal rings per GDGT **(E,F)**. Shaded symbols indicate values that include all IPL alkyl chains. Values represented by empty symbols are calculated in the same way but exclude contributions from GDGTs.

not reflected in our data. Temperature and pH have been cited as competing variables in numerous studies of GDGT ring index in hydrothermal systems and thermophilic archaea (Pearson et al., 2008; Boyd et al., 2011, 2013). It is still unclear how combinations of geochemical variables influence the incorporation of rings into archaeal membranes in a predictable way, though we propose that environmental redox conditions may influence ring distributions in section 3.6.

3.4.5. Number of Hydroxylations, nOH

Alkyl chains bearing a secondary hydroxyl group (e.g., Structure **20**) comprised only a small portion (<1%) of total chains in our sample set (see **Table S2**). Even if the backbone hydroxylation of CER (**9**) and FA-OH-FAm-OH (**11**) are counted toward chain nOH, the total proportion of hydroxylated chains would only increase to a maximum of 4% in any sample.

3.5. Z_C of IPLs and Their Components

Downstream changes in IPLs and their component parts are reflected in their average chemical formulae (**Table S3**) and consequently, their Z_C values (**Table S4**). Trends in the Z_C of full IPLs and their headgroups, backbones, and alkyl chains are described below.

3.5.1. Full IPLs

Abundance-weighted Z_C values calculated for microbial IPLs collected from Bison Pool, Mound Spring, Empress Pool, and Octopus Spring are plotted against temperature and dissolved oxygen concentrations in **Figure 7**. It can be seen that decreasing temperature and increasingly oxidized conditions coincide with near-linear changes in the Z_C of IPLs. Carbon was most reduced in IPLs sampled closest to each hot spring source (Z_C between −1.68 and −1.56 in samples BP1, MS1, EP1, and OS1) where temperatures were highest (82.2–91.0°C) and oxidized inorganic species (nitrate, sulfate, and oxygen) had the lowest concentrations. In progressively downstream samples, carbon in IPLs became more oxidized, with Z_C between −1.36 and −1.33 for samples in between 29.0 and 38.1°C where measured concentrations of sulfate, nitrate, and oxygen tended to be highest.

Downstream trends remain intact after performing a statistical simulation of potential sources of analytical error, as shown in **Figure 7** by the black bars above and below the calculated values of Z_C. These bars indicate the standard deviation of Z_C values resulting from 999 iterations of the bootstrap sensitivity analysis. The standard deviations of IPL Z_C show little overlap between upstream and downstream samples after random variation of up to 30% for integrated HPLC-MS peak areas and up to two orders of magnitude for response factors.

3.5.2. Headgroups

Z_C values of IPL headgroups were most positive in mid-stream samples and most negative in samples furthest upstream and downstream (**Figure 7**). Upstream samples had relatively reduced headgroup carbon due to an abundance of 1G-GDGT lipids. These lipids have two headgroups according to our structural division scheme; a hexose and a hydrogen atom (e.g., the GDGT in **Figure S9**). This "hydrogen-only" headgroup drives down the Z_C of headgroups in upstream samples where 1G-GDGT is abundant. In downstream samples, phospholipids and aminolipids with relatively reduced headgroup carbon, such as PC, PE, PG, and TM-OL became more abundant and drove down the Z_C.

Glycolipid headgroups 1G ($Z_C = -0.16\overline{6}$) and 2G ($Z_C = -0.08\overline{3}$) were among the most abundant headgroups observed in all four springs regardless of temperature or redox state,

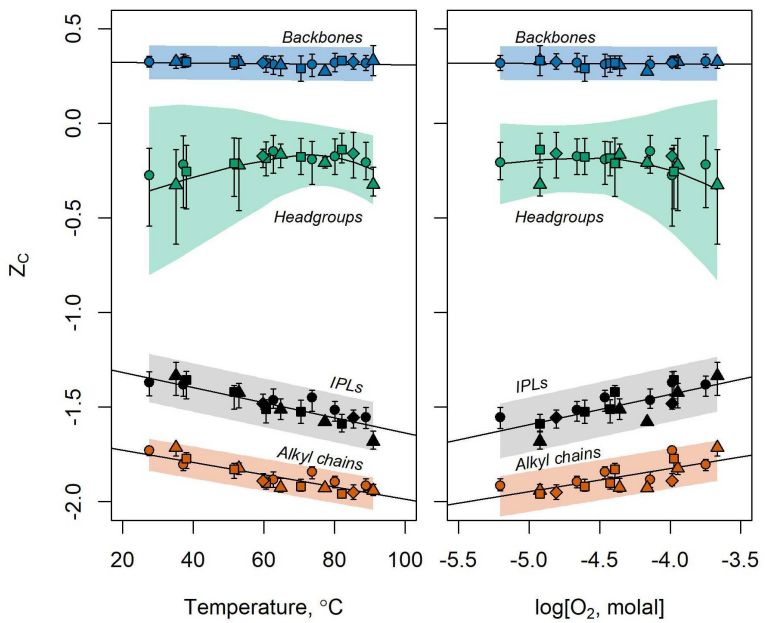

FIGURE 7 | Z_C of IPLs (black) and their headgroups (green), backbones (blue), alkyl chains (orange) sampled along the outflow channels of Bison Pool (circles), Mound Spring (triangles), Empress Pool (squares), and Octopus Spring (diamonds) with respect to temperature (left) and log molality of dissolved O_2 (right). Symbols designate the observed values of Z_C of extracted lipids and their components. Bars around the points show the standard deviation of 999 Z_C values resulting from the random variation of analytical peak areas and response factors during the bootstrap sensitivity analysis. Regression of these bootstrap values are indicated by fitted lines. Full lipids, backbones, and alkyl chains are fitted with linear regressions while headgroups are fit by local polynomial regression (LOESS). Shaded areas represent 95% prediction intervals for values of Z_C produced by the sensitivity analysis. LOESS regression was performed in R using the loess.sd function ("msir" package version 1.3.2) with parameters nsigma = 1.96 (for the 95% prediction interval) and span = 0.9 (for smoothing).

though they were most abundant, along with the glycolipid SQ ($Z_C = -0.16\overline{6}$) in samples where photosynthetic microorganisms are visually apparent. This agrees with observations that 1G, 2G, and SQ glycolipids are abundant in cyanobacterial (Wada and Murata, 2009) and algal (Guschina and Harwood, 2006) photosynthetic membranes.

Phosphate-bearing phospholipids and glycophospholipids, especially with PI headgroups, were more abundant downstream than upstream. However, the incorporation of phosphate itself into headgroups has no effect on abundance-weighted headgroup Z_C, as there is no difference in Z_C between analogous non-phosphorylated and phosphorylated headgroups (e.g., between 1G-P and 1G, or between 2G-P and 2G, *etc.*). The greatest abundance of lipids with an APT phospholipid headgroup ($Z_C = -0.6$) was observed in "pink streamer" thermophile communities sampled from the upstream chemosynthetic zones of Bison Pool and Octopus Spring; this result agrees with previous reports that this lipid is common in streamers with *Aquificales* bacteria (Sturt et al., 2004; Schubotz et al., 2013). However, after applying response factors, the abundance APT was low relative to other headgroups, even in streamer samples.

Values of Z_C for headgroups were substantially more sensitive to simulated sources of analytical uncertainty than those calculated for alkyl chains, backbones, or full IPLs. After 999 iterations of randomly adjusting response factors and HPLC-MS peak areas, the standard deviations in Z_C values (vertical bars in **Figure 7**) and the 95% prediction interval for future bootstrap calculations (shaded region) were greatest in magnitude for headgroups and overlapped for most samples. This calls into question the significance of downstream trends in headgroup Z_C, as they may be mere artifacts of the analytical method we used to quantify lipids.

3.5.3. Backbones

Backbones had the most oxidized carbon of any component owing to a high ratio of electronegative atoms (e.g., oxygen, nitrogen) to carbon. The Z_C of IPL backbones did not change significantly with temperature or redox state, as most observed backbones were composed of glycerol regardless of the sample location. A fully-linked glycerol backbone has a chemical formula of $C_3H_5O_3$ that corresponds to a Z_C of $0.33\overline{3}$. This is close to the average value in every sample, with little variation.

3.5.4. Alkyl Chains

Alkyl chains tend to have Z_C values ∼0.3–0.4 more negative than those of the full structure regardless of the sample. The Z_C values of alkyl chains were closest to those of the full lipid compared to either headgroups or backbones, indicating that alkyl chains are the main contributor to the oxidation state of carbon in full lipids. This is unsurprising, given that alkyl chains generally contain more carbon than any other IPL component. Since alkyl chains have a high hydrogen:carbon ratio to facilitate their hydrophobicity, the weighted Z_C of IPLs and their chains are significantly more negative than those of headgroups or backbones. Because alkyl chains contribute more to the average oxidation state of carbon in the full lipid than any other component, changes in alkyl chains are most responsible for the correlations observed between Z_C and temperature or dissolved oxygen in these hot spring outflow channels. Alkyl chain modifications with the most influence on Z_C were backbone-alkyl chain linkage chemistry, nC, nUnsat, and the number of internal rings per GDGT.

Changes in chain-backbone linkage chemistry correspond to a downstream increase in the Z_C of microbial IPLs stemming from the difference in chemical formulae between an ester and an ether bond. Carbon is more oxidized in an ester bond relative to an ether because it contains two fewer hydrogens and one more oxygen atom (compare Structures **13** and **18**). The number of aliphatic carbons in alkyl chains also has a great effect on Z_C. Each additional methylene group increases the chemical formula of a lipid by CH_2 for saturated chains, or by C_2H_4 for each methyl branch. Both of these groups have Z_C equal to -2, so as more aliphatic carbons are added, the Z_C of an alkyl chain is driven closer to this value. This effect can be seen in **Figure 7**, where the Z_C of alkyl chains approach -2 in upstream samples where average nC is highest. Unsaturated alkyl chains are more oxidized than their saturated counterparts. This is because an alkyl chain with a double bond has two fewer hydrogen atoms (e.g., compare Structures **19** and **18**). This is also true for a GDGT ring (e.g., compare Structures **15** and **16**). As such, increased degree of unsaturation and GDGT ring indices contributed to the downstream increase in Z_C for lipids and their alkyl chains. Other alkyl chain modifications did not notably impact Z_C, either because they were observed at very low abundance, such as chain hydroxylations, or did not substantially change lipid chemical formulae, such as the single hydrogen difference between GDGT half-chains and the isoprenoidal chains of non-GDGTs (e.g., Structure **15** compared to **14**).

As shown in **Figure 7**, trends involving Z_C are more resistant to simulated sources of analytical uncertainty in alkyl chains than in full lipids. Linear regression of Z_C values produced by the bootstrap sensitivity analysis results in a narrower 95% prediction interval band for alkyl chains than for full lipids. Further, the standard deviations for individual samples tend to have narrower ranges, and overlap less, in alkyl chains. Taken together, we interpret this as evidence that the downstream increase in the Z_C of alkyl chains is not an artifact of the analytical method used to quantify lipid abundance.

3.6. Redox and Lipid Composition

Thermodynamic analyses are needed to test how redox constraints influence the energetic favorability of lipid modifications, such as alkyl chain length, degree of unsaturation, ester and ether alkyl chain linkage, headgroup type, and so on. Several experiments have already yielded intriguing evidence that the expression of ringed GDGT alkyl chains is favorable under oxidized conditions. Following a laboratory study by Qin et al. (2015) that implicated O_2 limitation

as a confounding factor when interpreting TEX_{86}-derived temperatures, Hurley et al. (2016) showed an inverse correlation between ammonia oxidation rate and degree of ring cyclization in GDGTs of cultured ammonia oxidizing *Thaumarchaeota* and hypothesized that the supply of NH_4^+, provides the reduction potential necessary to drive saturation to GDGT-0 during lipid synthesis. Further evidence was provided by (Evans et al., 2018), who showed that ammonia oxidizing *Nitrosopumilus maritimus* produces GDGTs with fewer rings when grown in media containing excess NH_4^+. Zhou et al. (2019) found that GDGT cyclization from electron supply limitation also occurred in thermoacidophilic *Sulfolobus acidocaldarius* cultures. If sufficient reduction potential is necessary to saturate GDGTs, then an increasingly limited electron supply from ammonia, sulfide, and/or other electron donors may be responsible for the downstream increase in the average number of rings per GDGT found in Bison Pool, Mound Spring, and Octopus Spring. This may also explain why fewer GDGT rings were observed downstream in this study and in Schubotz et al. (2013), which is seemingly at odds with temperature-derived trends reported in various culture experiments (Wuchter et al., 2004; Boyd et al., 2011; Elling et al., 2015) and used in the TEX_{86} paleothermometer (Schouten et al., 2002, 2007a), though redox conditions were not the focus of these studies.

It is intriguing to consider that other lipid structural modifications, or even entire lipid compositions, may be sensitive to redox constraints. Lipid compositions produced by a microbial community might tend to be "electron-rich" (low Z_C) under reduced environmental conditions where electron supply is high, and "electron-poor" (high Z_C) under oxidized conditions where electron supply is low. If such a compositional advantage exists, then trends in lipid Z_C may be evident along other environmental redox gradients. For instance, studies of IPL distributions in the Black Sea have reported changes in alkyl chain structure along relatively isothermal redox gradients similar to those found along the hot spring outflow channels in this study; deeper sampling in the water column coincides with a pronounced shift in ester- to ether- linked alkyl chains, an increase in nC, a decrease in nUnsat, and an increase in the abundance of GDGTs and ARs (Schubotz et al., 2009; Schröder, 2015; Evans et al., 2017). Based on our approach, IPLs in the oxic zone of the Black Sea have relatively oxidized carbon, while deeper and more reduced conditions correspond to increasingly reduced carbon. This fits the general pattern observed in this study, and may indicate a biological drive for microbial communities to synthesize stable membranes within the redox constraints of their surroundings. If so, Z_C information preserved in lipid biomarker compositions could offer valuable insights into the geochemical paleoredox conditions experienced by source organisms. These hypotheses can be tested in a variety of natural systems by comparing the Z_C of IPLs produced by the microbial communities to concurrent redox measurements. Studies that strive for completeness and quantitative accuracy in their underlying lipid and geochemical datasets will be extraordinarily valuable for investigating these potential relationships.

4. CONCLUDING REMARKS

Lipids were extracted from microbial communities sampled spatially along the outflow channels of four alkaline hot springs in Yellowstone National Park. Chemical formulae and relative abundances of lipid structures interpreted from HPLC-MS/MS were used to calculate the average oxidation state of carbon, Z_C, for lipids in each sample. Values of Z_C were also calculated for lipid headgroups, backbones, and alkyl chains. We found that lipids extracted from microbial communities living under the hottest, most reduced conditions had the most reduced carbon (lowest Z_C). This is because lipids in upstream samples contained a greater number of modifications that increased their hydrogen-to-carbon ratio, including alkyl chains with a greater number of aliphatic carbons, fewer unsaturations, fewer GDGT rings, and linked to the backbone with a higher proportion of ether bonds. The Z_C of lipids increased (representing increasingly more oxidized carbon) with distance downstream, coinciding with more oxidized conditions and cooler temperatures. Lipids sampled furthest downstream had the most oxidized carbon (highest Z_C) resulting from an abundance of alkyl chain modifications that decreased their hydrogen-to-carbon ratio (fewer aliphatic carbons, higher degree of unsaturation, a greater number of GDGT rings, and a greater proportion of ester-linkage). These alkyl chain modifications permit membrane function in the microbial communities sampled across the extreme temperature gradients of Yellowstone outflow channels. The tendency to find oxidized lipid modifications under oxidized conditions and vice versa for reduced conditions may represent adaptation to limitations in available reduction potential imposed by concentrations of electron donors and acceptors in the surrounding water. If this pattern is widespread, the Z_C of bulk lipid compositions could become a useful metric for assessing prevailing redox across a variety of natural settings. Preserved in lipid biomarkers, these Z_C signatures could offer a window into redox conditions of the past.

DATA AVAILABILITY STATEMENT

The code and IPL abundance data used in this study can be found in the repository PolarLipidZC, https://gitlab.com/gmboyer/polarlipidzc.

AUTHOR CONTRIBUTIONS

GB and ES conceived the study. GB and JW performed the lipid extractions. GB and FS analyzed the HPLC-MS data. GB performed the calculations. All authors contributed to the writing and revision of this manuscript.

FUNDING

Research reported here was funded by NSF grants EAR-1123649 and EAR-1529963, and NASA Exobiology grant NNX16AJ61G. FS acknowledges funding from the Alexander from Humboldt society and the Central Research Development Fund of the University of Bremen. Financial support for

the lipid analyses conducted at MIT was provided by the NASA Astrobiology Institute NNA13AA90A, Foundations of Complex Life, Evolution, Preservation, and Detection on Earth and Beyond.

ACKNOWLEDGMENTS

We thank Kris Fecteau, Kirt Robinson, Brian St. Clair, Vince Debes, Kristin Johnson, Apar Prasad, and Alta Howells for their help in collecting and analyzing water geochemistry data. We also thank Jeff Dick for valuable discussions regarding the Z_C of biomolecules.

SUPPLEMENTARY MATERIAL

The Supplementary Material for this article can be found online at: https://www.frontiersin.org/articles/10.3389/fmicb.2020.00229/full#supplementary-material

REFERENCES

Adams, B. L., McMahon, V., and Seckbach, J. (1971). Fatty acids in the thermophilic alga, *Cyanidium caldarium*. *Biochem. Biophys. Res. Commun.* 42, 359–365.

Amend, J. P., and Shock, E. L. (1998). Energetics of amino acid synthesis in hydrothermal ecosystems. *Science* 281, 1659–1662.

Barns, S. M., Delwiche, C. F., Palmer, J. D., and Pace, N. R. (1996). Perspectives on archaeal diversity, thermophily and monophyly from environmental rRNA sequences. *Proc. Natl. Acad. Sci. U.S.A.* 93, 9188–9193.

Barns, S. M., Fundyga, R. E., Jeffries, M. W., and Pace, N. R. (1994). Remarkable archaeal diversity detected in a Yellowstone National Park hot spring environment. *Proc. Natl. Acad. Sci. U.S.A.* 91, 1609–1613.

Beam, J. P., Jay, Z. J., Schmid, M. C., Rusch, D. B., Romine, M. F., Jennings, Rde.M., et al. (2016). Ecophysiology of an uncultivated lineage of *Aigarchaeota* from an oxic, hot spring filamentous "streamer" community. *ISME J.* 10, 210–224. doi: 10.1038/ismej.2015.83

Benning, C., Huang, Z.-H., and Gage, D. A. (1995). Accumulation of a novel glycolipid and a betaine lipid in cells of Rhodobacter sphaeroides grown under phosphate limitation. *Arch. Biochem. Biophys.* 317, 103-111.

Boyd, E., Hamilton, T., Wang, J., He, L., and Zhang, C. (2013). The role of tetraether lipid composition in the adaptation of thermophilic archaea to acidity. *Front. Microbiol.* 4:62. doi: 10.3389/fmicb.2013.00062

Boyd, E. S., Pearson, A., Pi, Y., Li, W.-J., Zhang, Y. G., He, L., et al. (2011). Temperature and pH controls on glycerol dibiphytanyl glycerol tetraether lipid composition in the hyperthermophilic crenarchaeon *Acidilobus sulfurireducens*. *Extremophiles* 15, 59–65. doi: 10.1007/s00792-010-0339-y

Boye, K., Noël, V., Tfaily, M. M., Bone, S. E., Williams, K. H., Bargar, J. R., et al. (2017). Thermodynamically controlled preservation of organic carbon in floodplains. *Nat. Geosci.* 10:415. doi: 10.1038/ngeo2940

Brocks, J. J., and Pearson, A. (2005). Building the biomarker tree of life. *Rev. Mineral. Geochem.* 59, 233–258. doi: 10.2138/rmg.2005.59.10

Chong, P. L. G., Ayesa, U., Prakash Daswani, V., and Hur, E. C. (2012). On physical properties of tetraether lipid membranes: effects of cyclopentane rings. *Archaea* 2012:12. doi: 10.1155/2012/138439

Colman, D. R., Jay, Z. J., Inskeep, W. P., Jennings, Rde.M., Maas, K. R., Rusch, D. B., et al. (2016). Novel, deep-branching heterotrophic bacterial populations recovered from thermal spring metagenomes. *Front. Microbiol.* 7:304. doi: 10.3389/fmicb.2016.00304

Cox, A., Shock, E. L., and Havig, J. R. (2011). The transition to microbial photosynthesis in hot spring ecosystems. *Chem. Geol.* 280, 344–351. doi: 10.1016/j.chemgeo.2010.11.022

Curatolo, W. (1987). Glycolipid function. *Biochim. Biophys. Acta* 906, 137–160.

Daniel, R. M., and Cowan, D. A. (2000). Biomolecular stability and life at high temperatures. *Cell. Mol. Life Sci.* 57, 250–264. doi: 10.1007/PL00000688

Denich, T. J., Beaudette, L. A., Lee, H., and Trevors, J. T. (2003). Effect of selected environmental and physico-chemical factors on bacterial cytoplasmic membranes. *J. Microbiol. Methods* 52, 149–182. doi: 10.1016/S0167-7012(02)00155-0

Dick, J. M. (2014). Average oxidation state of carbon in proteins. *J. R. Soc. Interface* 11:20131095. doi: 10.1098/rsif.2013.1095

Dick, J. M. (2016). Proteomic indicators of oxidation and hydration state in colorectal cancer. *PeerJ* 4:e2238. doi: 10.7717/peerj.2238

Dick, J. M. (2017). Chemical composition and the potential for proteomic transformation in cancer, hypoxia, and hyperosmotic stress. *PeerJ* 5:e3421. doi: 10.7717/peerj.3421

Dick, J. M., and Shock, E. L. (2011). Calculation of the relative chemical stabilities of proteins as a function of temperature and redox chemistry in a hot spring. *Public Lib. Sci. One* 6:e22782. doi: 10.1371/journal.pone.0022782

Dick, J. M., and Shock, E. L. (2013). A metastable equilibrium model for the relative abundances of microbial phyla in a hot spring. *Public Lib. Sci. One* 8:e72395. doi: 10.1371/journal.pone.0072395

Dick, J. M., Yu, M., Tan, J., and Lu, A. (2019). Changes in carbon oxidation state of metagenomes along geochemical redox gradients. *Front. Microbiol.* 10:120. doi: 10.3389/fmicb.2019.00120

Diercks, H., Semeniuk, A., Gisch, N., Moll, H., Duda, K. A., and Hölzl, G. (2015). Accumulation of novel glycolipids and ornithine lipids in *Mesorhizobium loti* under phosphate deprivation. J. Bacteriol. 197, 497-509. doi: 10.1128/JB.02004-14

Dupraz, C., and Visscher, P. T. (2005). Microbial lithification in marine stromatolites and hypersaline mats. *Trends Microbiol.* 13, 429–438. doi: 10.1016/j.tim.2005.07.008

Elling, F. J., Könneke, M., Mußmann, M., Greve, A., and Hinrichs, K.-U. (2015). Influence of temperature, pH, and salinity on membrane lipid composition and TEX_{86} of marine planktonic thaumarchaeal isolates. *Geochim. Cosmochim. Acta* 171, 238–255. doi: 10.1016/j.gca.2015.09.004

Evans, T. W., Könneke, M., Lipp, J. S., Adhikari, R. R., Taubner, H., Elvert, M., et al. (2018). Lipid biosynthesis of *Nitrosopumilus maritimus* dissected by lipid specific radioisotope probing (lipid-RIP) under contrasting ammonium supply. *Geochim. Cosmochim. Acta* 242, 51–63. doi: 10.1016/j.gca.2018.09.001

Evans, T. W., Wörmer, L., Lever, M. A., Lipp, J. S., Lagostina, L., Lin, Y.-S., et al. (2017). Size and composition of subseafloor microbial community in the Benguela upwelling area examined from intact membrane lipid and DNA analysis. *Organ. Geochem.* 111, 86–100. doi: 10.1016/j.orggeochem.2017.06.008

Fenchel, T. (1998). Artificial cyanobacterial mats: cycling of C, O, and S. *Aquat. Microb. Ecol.* 14, 253–259.

Ferreira, A. M., Wait, R., Nobre, M. F., and da Costa, M. S. (1999). Characterization of glycolipids from Meiothermus spp. *Microbiology* 145, 1191-1199.

Fones, E. M., Colman, D. R., Kraus, E. A., Nothaft, D. B., Poudel, S., Rempfert, K. R., et al. (2019). Physiological adaptations to serpentinization in the Samail Ophiolite, Oman. *ISME J.* 13, 1750–1762. doi: 10.1038/s41396-019-0391-2

Franks, J., and Stolz, J. F. (2009). Flat laminated microbial mat communities. *Earth Sci. Rev.* 96, 163–172. doi: 10.1016/j.earscirev.2008.10.004

French, K. L., Hallmann, C., Hope, J. M., Schoon, P. L., Zumberge, J. A., Hoshino, Y., et al. (2015). Reappraisal of hydrocarbon biomarkers in Archean rocks. *Proc. Natl. Acad. Sci. U.S.A.* 112, 5915–5920. doi: 10.1073/pnas.1419563112

Gabriel, J. L., and Chong, P. L. G. (2000). Molecular modeling of archaebacterial bipolar tetraether lipid membranes. *Chem. Phys. Lipids* 105, 193–200. doi: 10.1016/S0009-3084(00)00126-2

Gliozzi, A., Paoli, G., De Rosa, M., and Gambacorta, A. (1983). Effect of isoprenoid cyclization on the transition temperature of lipids in thermophilic archaebacteria. *Biochim. Biophys. Acta* 735, 234–242.

Grogan, D. W., and Cronan, J. E. (1997). Cyclopropane ring formation in membrane lipids of bacteria. *Microbiol. Mol. Biol. Revi.* 61, 429–441.

Guschina, I. A., and Harwood, J. L. (2006). Lipids and lipid metabolism in eukaryotic algae. *Prog. Lipid Res.* 45, 160–186. doi: 10.1016/j.plipres.2006.01.001

Halverson, L. J., and Firestone, M. K. (2000). Differential effects of permeating and nonpermeating solutes on the fatty acid composition of *Pseudomonas putida*. *Appl. Environ. Microbiol.* 66, 2414–2421. doi: 10.1128/AEM.66.6.2414-2421.2000

Huber, R., Wilharm, T., Huber, D., Trincone, A., Burggraf, S., König, H., et al. (1992). *Aquifex pyrophilus* gen. nov. sp. nov., represents a novel group of marine hyperthermophilic hydrogen-oxidizing bacteria. *Syst. Appl. Microbiol.* 15, 340–351. doi: 10.1016/S0723-2020(11)80206-7

Hurley, S. J., Elling, F. J., Könneke, M., Buchwald, C., Wankel, S. D., Santoro, A. E., et al. (2016). Influence of ammonia oxidation rate on thaumarchaeal lipid composition and the TEX_{86} temperature proxy. *Proc. Natl. Acad. Sci. U.S.A.* 113, 7762–7767. doi: 10.1073/pnas.1518534113

Jahnke, L. L., Eder, W., Huber, R., Hope, J. M., Hinrichs, K.-U., Hayes, J. M., et al. (2001). Signature lipids and stable carbon isotope analyses of Octopus Spring hyperthermophilic communities compared with those of *Aquificales* representatives. *Appl. Environ. Microbiol.* 67, 5179–5189. doi: 10.1128/AEM.67.11.5179-5189.2001

Jonkers, H. M., Ludwig, R., De Wit, R., Pringault, O., Muyzer, G., Niemann, H., et al. (2003). Structural and functional analysis of a microbial mat ecosystem from a unique permanent hypersaline inland lake: "La Salada de Chiprana" (NE Spain). *FEMS Microbiol. Ecol.* 44, 175–189. doi: 10.1016/S0168-6496(02)00464-6

Karlsson, A. Å., Michélsen, P., and Odham, G. (1998). Molecular species of sphingomyelin: determination by high-performance liquid chromatography/mass spectrometry with electrospray and high-performance liquid chromatography/tandem mass spectrometry with atmospheric pressure chemical ionization. *J. Mass Spectr.* 33, 1192-1198.

Kaur, G., Mountain, B. W., Stott, M. B., Hopmans, E. C., and Pancost, R. D. (2015). Temperature and pH control on lipid composition of silica sinters from diverse hot springs in the Taupo Volcanic Zone, New Zealand. *Extremophiles* 19, 327–344. doi: 10.1007/s00792-014-0719-9

Kent, C. (1995). Eukaryotic phospholipid biosynthesis. *Annu. Rev. Biochem.* 64, 315–343.

Kiran, M., Prakash, J., Annapoorni, S., Dube, S., Kusano, T., Okuyama, H., et al. (2004). Psychrophilic *Pseudomonas syringae* requires *trans*-monounsaturated fatty acid for growth at higher temperature. *Extremophiles* 8, 401–410. doi: 10.1007/s00792-004-0401-8

Kiran, M. D., Annapoorni, S., Suzuki, I., Murata, N., and Shivaji, S. (2005). *Cis–trans* isomerase gene in psychrophilic *Pseudomonas syringae* is constitutively expressed during growth and under conditions of temperature and solvent stress. *Extremophiles* 9, 117–125. doi: 10.1007/s00792-005-0435-6

Kroll, J. H., Donahue, N. M., Jimenez, J. L., Kessler, S. H., Canagaratna, M. R., Wilson, K. R., et al. (2011). Carbon oxidation state as a metric for describing the chemistry of atmospheric organic aerosol. *Nat. Chem.* 3:133. doi: 10.1038/nchem.948

Kroll, J. H., Lim, C. Y., Kessler, S. H., and Wilson, K. R. (2015). Heterogeneous oxidation of atmospheric organic aerosol: kinetics of changes to the amount and oxidation state of particle-phase organic carbon. *J. Phys. Chem. A* 119, 10767–10783. doi: 10.1021/acs.jpca.5b06946

LaRowe, D. E., and Van Cappellen, P. (2011). Degradation of natural organic matter: a thermodynamic analysis. *Geochim. Cosmochim. Acta* 75, 2030–2042. doi: 10.1016/j.gca.2011.01.020

Likens, G. E. (Eds.). (2010). *Biogeochemistry of Inland Waters*. Millbrook, NY: Academic Press.

Loiacono, S. T. (2013). *Merging genomics, transcriptomics and geochemistry to assess nitrogen cycling in terrestrial hot springs* (MS thesis). University of Illinois at Chicago, Chicago, IL, United States.

López-Lara, I. M., and Geiger, O. (2017). Bacterial lipid diversity. *Biochim. Biophys. Acta* 1862, 1287–1299. doi: 10.1016/j.bbalip.2016.10.007

Macalady, J. L., Vestling, M. M., Baumler, D., Boekelheide, N., Kaspar, C. W., and Banfield, J. F. (2004). Tetraether-linked membrane monolayers in *Ferroplasma* spp: a key to survival in acid. *Extremophiles* 8, 411–419. doi: 10.1007/s00792-004-0404-5

Marr, A. G., and Ingraham, J. L. (1962). Effect of temperature on the composition of fatty acids in *Escherichia coli*. *J. Bacteriol.* 84, 1260–1267.

Meyer-Dombard, D. R., Shock, E. L., and Amend, J. P. (2005). Archaeal and bacterial communities in geochemically diverse hot springs of Yellowstone National Park, USA. *Geobiology* 3, 211–227. doi: 10.1111/j.1472-4669.2005.00052.x

Meyer-Dombard, D. R., Swingley, W., Raymond, J., Havig, J., Shock, E. L., and Summons, R. E. (2011). Hydrothermal ecotones and streamer biofilm communities in the Lower Geyser Basin, Yellowstone National Park. *Environ. Microbiol.* 13, 2216–2231. doi: 10.1111/j.1462-2920.2011.02476.x

Moore, E. K., Hopmans, E. C., Rijpstra, W. I. C., Villanueva, L., Dedysh, S. N., Kulichevskaya, I. S., et al. (2013). Novel mono-, di-, and trimethylornithine membrane lipids in northern wetland planctomycetes. *Appl. Environ. Microbiol.* 79, 6874-6884. doi: 10.1128/AEM.02169-13

Murata,N., and Siegenthaler, P.-A. (eds.). (1998). "Lipids in photosynthesis: an overview," in *Lipids in Photosynthesis: Structure, Function and Genetics* (Dordrecht: Kluwer Academic Publishers), 1–20.

Nishihara, M., and Koga, Y. (1987). Extraction and composition of polar lipids from the archaebacterium, *Methanobacterium thermoautotrophicum*: effective extraction of tetraether lipids by an acidified solvent. *J. Biochem.* 101, 997–1005.

Okuyama, H., Okajima, N., Sasaki, S., Higashi, S., and Murata, N. (1991). The *cis/trans* isomerization of the double bond of a fatty acid as a strategy for adaptation to changes in ambient temperature in the psychrophilic bacterium, *Vibrio* sp. strain ABE-1. *Biochim. Biophys. Acta* 1084, 13–20.

Okuyama, H., Sasaki, S., Higashi, S., and Murata, N. (1990). A *trans*-unsaturated fatty acid in a psychrophilic bacterium, *Vibrio* sp. strain ABE-1. *J. Bacteriol.* 172, 3515–3518.

Pearson, A., and Ingalls, A. E. (2013). Assessing the use of archaeal lipids as marine environmental proxies. *Annu. Rev. Earth Planet. Sci.* 41, 359–384. doi: 10.1146/annurev-earth-050212-123947

Pearson, A., Pi, Y., Zhao, W., Li, W., Li, Y., Inskeep, W., et al. (2008). Factors controlling the distribution of archaeal tetraethers in terrestrial hot springs. *Appl. Environ. Microbiol.* 74, 3523–3532. doi: 10.1128/AEM.02450-07

Pitcher, A., Schouten, S., and Damsté, J. S. S. (2009). In situ production of crenarchaeol in two California hot springs. *Appl. Environ. Microbiol.* 75, 4443–4451. doi: 10.1128/AEM.02591-08

Popendorf, K. J., Fredricks, H. F., and Van Mooy, B. A. (2013). Molecular ion-independent quantification of polar glycerolipid classes in marine plankton using triple quadrupole MS. *Lipids* 48, 185–195. doi: 10.1007/s11745-012-3748-0

Poudel, S., Colman, D. R., Fixen, K. R., Ledbetter, R. N., Zheng, Y., Pence, N., et al. (2018). Electron transfer to nitrogenase in different genomic and metabolic backgrounds. *J. Bacteriol.* 200:e00757-17. doi: 10.1128/JB.00757-17

Prado, A., Da Costa, M. S., and Madeira, V. M. (1988). Effect of growth temperature on the lipid composition of two strains of *Thermus* sp. *Microbiology* 134, 1653–1660.

Qin, W., Carlson, L. T., Armbrust, E. V., Devol, A. H., Moffett, J. W., Stahl, D. A., et al. (2015). Confounding effects of oxygen and temperature on the TEX_{86} signature of marine thaumarchaeota. *Proc. Natl. Acad. Sci. U.S.A.* 112, 10979–10984. doi: 10.1073/pnas.1501568112

Rashby, S. E., Sessions, A. L., Summons, R. E., and Newman, D. K. (2007). Biosynthesis of 2-methylbacteriohopanepolyols by an anoxygenic phototroph. *Proc. Natl. Acad. Sci. U.S.A.* 104, 15099–15104. doi: 10.1073/pnas.0704912104

Ray, P. H., White, D. C., and Brock, T. D. (1971). Effect of growth temperature on the lipid composition of *Thermus aquaticus*. *J. Bacteriol.* 108, 227–235.

Reysenbach, A.-L., Wickham, G. S., and Pace, N. R. (1994). Phylogenetic analysis of the hyperthermophilic pink filament community in Octopus Spring, Yellowstone National Park. *Appl. Environ. Microbiol.* 60, 2113–2119.

Romero, J. T. (2018). *Changes in microbial communities and geochemical energy supplies across the photosynthetic fringe of hot spring outflows in Yellowstone National Park* (MS thesis). Arizona State University Tempe, AZ, United States.

Sato, N. (2004). Roles of the acidic lipids sulfoquinovosyl diacylglycerol and phosphatidylglycerol in photosynthesis: their specificity and evolution. *J. Plant Res.* 117, 495–505. doi: 10.1007/s10265-004-0183-1

Schouten, S., Forster, A., Panoto, F. E., and Damsté, J. S. S. (2007a). Towards calibration of the TEX_{86} palaeothermometer for tropical sea surface temperatures in ancient greenhouse worlds. *Organ. Geochem.* 38, 1537–1546. doi: 10.1016/j.orggeochem.2007.05.014

Schouten, S., Hopmans, E. C., and Damsté, J. S. S. (2013). The organic geochemistry of glycerol dialkyl glycerol tetraether lipids: a review. *Organ. Geochem.* 54, 19–61. doi: 10.1016/j.orggeochem.2012.09.006

Schouten, S., Hopmans, E. C., Schefuß, E., and Damste, J. S. S. (2002). Distributional variations in marine crenarchaeotal membrane lipids: a new tool for reconstructing ancient sea water temperatures? *Earth Planet. Sci. Lett.* 204, 265–274. doi: 10.1016/S0012-821X(02)00979-2

Schouten, S., Meer, M., Hopmans, E., Rijpstra, W., Reysenbach, A., Ward, D., et al. (2007b). Archaeal and bacterial glycerol dialkyl glycerol tetraether lipids in hot springs of Yellowstone National Park. *Appl. Environ. Microbiol.* 73, 6181–6191. doi: 10.1128/AEM.00630-07

Schröder, J. M. (2015). *Intact polar lipids in marine sediments: improving analytical protocols and assessing planktonic and benthic sources* (Dissertation). Staats-und Universitätsbibliothek Bremen, Bremen, Germany.

Schubotz, F., Hays, L. E., Meyer-Dombard, D'R., Gillespie, A., Shock, E. L., and Summons, R. E. (2015). Stable isotope labeling confirms mixotrophic nature of streamer biofilm communities at alkaline hot springs. Front. Microbiol. 6:42. doi: 10.3389/fmicb.2015.00042

Schubotz, F., Meyer-Dombard, D., Bradley, A., Fredricks, H., Hinrichs, K., Shock, E., et al. (2013). Spatial and temporal variability of biomarkers and microbial diversity reveal metabolic and community flexibility in Streamer Biofilm Communities in the Lower Geyser Basin, Yellowstone National Park. *Geobiology* 11, 549–569. doi: 10.1111/gbi.12051

Schubotz, F., Wakeham, S. G., Lipp, J. S., Fredricks, H. F., and Hinrichs, K.-U. (2009). Detection of microbial biomass by intact polar membrane lipid analysis in the water column and surface sediments of the Black Sea. *Environ. Microbiol.* 11, 2720–2734. doi: 10.1111/j.1462-2920.2009.01999.x

Siliakus, M. F., van der Oost, J., and Kengen, S. W. (2017). Adaptations of archaeal and bacterial membranes to variations in temperature, pH and pressure. *Extremophiles* 21, 651–670. doi: 10.1007/s00792-017-0939-x

Sollich, M., Yoshinaga, M. Y., Häusler, S., Price, R. E., Hinrichs, K.-U., and Bühring, S. I. (2017). Heat stress dictates microbial lipid composition along a thermal gradient in marine sediments. *Front. Microbiol.* 8:1550. doi: 10.3389/fmicb.2017.01550

Spear, J. R., Walker, J. J., McCollom, T. M., and Pace, N. R. (2005). Hydrogen and bioenergetics in the Yellowstone geothermal ecosystem. *Proc. Natl. Acad. Sci. U.S.A.* 102, 2555–2560. doi: 10.1073/pnas.0409574102

Sturt, H. F., Summons, R. E., Smith, K., Elvert, M., and Hinrichs, K.-U. (2004). Intact polar membrane lipids in prokaryotes and sediments deciphered by high-performance liquid chromatography/electrospray ionization multistage mass spectrometry–new biomarkers for biogeochemistry and microbial ecology. *Rapid Commun. Mass Spectr.* 18, 617–628. doi: 10.1002/rcm.1378

Summons, R. E., Jahnke, L. L., Hope, J. M., and Logan, G. A. (1999). 2-Methylhopanoids as biomarkers for cyanobacterial oxygenic photosynthesis. *Nature* 400:554.

Summons, R. E., and Walter, M. R. (1990). Molecular fossils and microfossils of prokaryotes and protists from Proterozoic sediments. *Am. J. Sci.* 290, 212–244.

Swingley, W. D., D'Arcy, R., Shock, E. L., Alsop, E. B., Falenski, H. D., Havig, J. R., et al. (2012). Coordinating environmental genomics and geochemistry reveals metabolic transitions in a hot spring ecosystem. *PLoS ONE* 7:e38108. doi: 10.1371/journal.pone.0038108

Tansey, M. R., and Brock, T. D. (1972). The upper temperature limit for eukaryotic organisms. *Proc. Natl. Acad. Sci. U.S.A.* 69, 2426–2428.

van Meer, G., Voelker, D. R., and Feigenson, G. W. (2008). Membrane lipids: where they are and how they behave. *Nat. Rev. Mol. Cell Biol.* 9:112. doi: 10.1038/nrm2330

Vinçon-Laugier, A., Cravo-Laureau, C., Mitteau, I., and Grossi, V. (2017). Temperature-dependent alkyl glycerol ether lipid composition of mesophilic and thermophilic sulfate-reducing bacteria. *Front. Microbiol.* 8:1532. doi: 10.3389/fmicb.2017.01532

Visscher, P. T., Reid, R. P., Bebout, B. M., Hoeft, S. E., Macintyre, I. G., and Thompson, J. A. (1998). Formation of lithified micritic laminae in modern marine stromatolites (Bahamas): the role of sulfur cycling. *Am. Mineral.* 83, 1482–1493.

Wada, H., and Murata, N. (2009). "Lipids in thylakoid membranes and photosynthetic cells," in *Lipids in Photosynthesis*, eds H. Wada and N. Murata (Dordrecht: Springer), 1–9.

Wang, M., Kim, G. H., Wei, F., Chen, H., Altarejos, J., and Han, X. (2015). Improved method for quantitative analysis of methylated phosphatidylethanolamine species and its application for analysis of diabetic-mouse liver samples. *Anal. Bioanal. Chem.* 407, 5021-5032. doi: 10.1007/s00216-015-8534-4

Ward, D. M., Tayne, T. A., Anderson, K. L., and Bateson, M. M. (1987). "Community structure and interactions among community members in hot spring cyanobacterial mats," in *Symposia of the Society for General Microbiology* (Cambridge).

Weber, F. J., Isken, S., and De Bont, J. A. (1994). *Cis/trans* isomerization of fatty acids as a defence mechanism of *Pseudomonas putida* strains to toxic concentrations of toluene. *Microbiology* 140, 2013–2017.

White, D. C., and Ringelberg, D. B. (1998). "Signature lipid biomarker analysis," in *Techniques in Microbial Ecology*, Vol. 255, eds R. S. Burlage, R. Atlas, D. Stahl, G. Geesey, and G. Sayler (New York, NY: Oxford University Press), 255–272.

Wörmer, L., Lipp, J. S., Schröder, J. M., and Hinrichs, K.-U. (2013). Application of two new LC–ESI–MS methods for improved detection of intact polar lipids (IPLs) in environmental samples. *Organ. Geochem.* 59, 10–21. doi: 10.1016/j.orggeochem.2013.03.004

Wu, W., Zhang, C., Wang, H., He, L., Li, W., and Dong, H. (2013). Impacts of temperature and pH on the distribution of archaeal lipids in Yunnan hot springs, China. *Front. Microbiol.* 4:312. doi: 10.3389/fmicb.2013.00312

Wuchter, C., Schouten, S., Coolen, M. J., and Sinninghe Damsté, J. S. (2004). Temperature-dependent variation in the distribution of tetraether membrane lipids of marine Crenarchaeota: implications for TEX_{86} paleothermometry. *Paleoceanography* 19, 1–10. doi: 10.1029/2004PA001041

Yang, Y.-L., Yang, F.-L., Jao, S.-C., Chen, M.-Y., Tsay, S.-S., Zou, W., et al. (2006). Structural elucidation of phosphoglycolipids from strains of the bacterial thermophiles Thermus and Meiothermus. *J. Lipid Res.* 47, 1823-1832. doi: 10.1194/jlr.M600034-JLR200

Yoshinaga, M. Y., Kellermann, M. Y., Rossel, P. E., Schubotz, F., Lipp, J. S., and Hinrichs, K.-U. (2011). Systematic fragmentation patterns of archaeal intact polar lipids by high-performance liquid chromatography/electrospray ionization ion-trap mass spectrometry. *Rapid Commun. Mass Spectr.* 25, 3563–3574. doi: 10.1002/rcm.5251

Zeng, Y. B., Ward, D. M., Brassell, S. C., and Eglinton, G. (1992). Biogeochemistry of hot spring environments: 2. Lipid compositions of Yellowstone (Wyoming, USA) cyanobacterial and *Chloroflexus* mats. *Chem. Geol.* 95, 327–345.

Zhang, C. L., Ye, Q., Huang, Z., Li, W., Chen, J., Song, Z., et al. (2008). Global occurrence of archaeal amoA genes in terrestrial hot springs. *Appl. Environ. Microbiol.* 74, 6417–6426. doi: 10.1128/AEM.00843-08

Zhang, X., Ferguson-Miller, S. M., and Reid, G. E. (2009). Characterization of ornithine and glutamine lipids extracted from cell membranes of Rhodobacter sphaeroides. *J. Am. Soc. Mass Spectr.* 20, 198-212. doi: 10.1016/j.jasms.2008.08.017

Zhou, A., Chiu, B. K., Weber, Y., Elling, F. J., Cobban, A. B., Pearson, A., et al. (2019). Energy flux controls tetraether lipid cyclization in *Sulfolobus acidocaldarius*. *Environ. Microbiol.* 22, 343–353. doi: 10.1111/1462-2920.14851

Conflict of Interest: The authors declare that the research was conducted in the absence of any commercial or financial relationships that could be construed as a potential conflict of interest.

frontiers in Microbiology

REVIEW
published: 15 May 2020
doi: 10.3389/fmicb.2020.00923

Molecular Mechanisms of Microbial Survivability in Outer Space: A Systems Biology Approach

Tetyana Milojevic[1]* *and Wolfram Weckwerth*[2,3]

[1] *Extremophiles/Space Biochemistry Group, Department of Biophysical Chemistry, University of Vienna, Vienna, Austria,* [2] *Department of Ecogenomics and Systems Biology, University of Vienna, Vienna, Austria,* [3] *Vienna Metabolomics Center, University of Vienna, Vienna, Austria*

Since the dawn of space exploration, the survivability of terrestrial life in outer space conditions has attracted enormous attention. Space technology has enabled the development of advanced space exposure facilities to investigate *in situ* responses of microbial life to the stress conditions of space during interplanetary transfer. Significant progress has been made toward the understanding of the effects of space environmental factors, e.g., microgravity, vacuum and radiation, on microorganisms exposed to real and simulated space conditions. Of extreme importance is not only knowledge of survival potential of space-exposed microorganisms, but also the determination of mechanisms of survival and adaptation of predominant species to the extreme space environment, i.e., revealing the molecular machinery, which elicit microbial survivability and adaptation. Advanced technologies in –omics research have permitted genome-scale studies of molecular alterations of space-exposed microorganisms. A variety of reports show that microorganisms grown in the space environment exhibited global alterations in metabolic functions and gene expression at the transcriptional and translational levels. Proteomic, metabolomic and especially metabolic modeling approaches as essential instruments of space microbiology, synthetic biology and metabolic engineering are rather underrepresented. Here we summarized the molecular space-induced alterations of exposed microorganisms in terms of understanding the molecular mechanisms of microbial survival and adaptation to drastic outer space environment.

Keywords: microbes in space, space missions, –omics technology, extremophiles, outer space

OPEN ACCESS

Edited by:
André Antunes,
Macau University of Science and Technology, China

Reviewed by:
Felipe Gómez,
Centro de Astrobiología (CSIC-INTA), Spain
Alexander Josef Probst,
University of Duisburg-Essen, Germany

***Correspondence:**
Tetyana Milojevic
tetyana.milojevic@univie.ac.at

Specialty section:
This article was submitted to Extreme Microbiology, a section of the journal Frontiers in Microbiology

Received: *03 December 2019*
Accepted: *20 April 2020*
Published: *15 May 2020*

Citation:
Milojevic T and Weckwerth W (2020) Molecular Mechanisms of Microbial Survivability in Outer Space: A Systems Biology Approach. Front. Microbiol. 11:923. doi: 10.3389/fmicb.2020.00923

INTRODUCTION

The outer space environment, which is characterized by a high vacuum and an intense radiation, provides hostile conditions to any form of life. With the upcoming long-term space explorations, it is becoming increasingly important to understand the molecular mechanisms of survival in outer space. Remarkably, a few extremophilic microbial species have been shown to withstand the drastic influence of the outer space factors (Saffary et al., 2002; Sancho et al., 2007; Cockell et al., 2011; Wassmann et al., 2012; Kawaguchi et al., 2013; Selbmann et al., 2015), and numerous studies have significantly proved the possibility of microbial life transfer through space (Horneck et al., 2008; Nicholson, 2009). Considerable progress has been made toward the understanding of the effects of

space environmental factors, e.g., microgravity, vacuum and radiation, on microorganisms exposed to real and simulated space conditions. However, we still have been missing an explicit knowledge of molecular mechanisms permitting survival and adaptation in the outer space environment. Space parameters affect microorganisms by altering a variety of physiological features, including cell metabolism, proliferation rate, cell division, cell motility, virulence, and biofilm production (**Figure 1**). These physiological perturbations of space-exposed microorganisms are very poorly understood at the molecular level. In this context, omics-based analyses combined with classical phenotyping and physiological measurements provide the integrative suite of tools to functionally decipher the mechanisms of microbial survivability in outer space. Exploring the relevant mechanisms underlying metabolic and physiological changes which microorganisms experience during exposure to outer space, the omics-based approach integrates the different fragments of biological information to understand the flow of information from genomes, mRNA, proteins to metabolites (Weckwerth, 2011a; Ott et al., 2017, 2019b,a), and explains how the microorganisms adapt to this extreme environment.

Systems biology is an interdisciplinary field that incorporates the results of genome-scale molecular analysis–omics techniques–such as genomics, transcriptomics, proteomics, and metabolomics and genome-scale metabolic and regulatory biomathematical models to reveal complex molecular interactions underlying molecular evolution, functional and phenotypical diversity and molecular adaptation (Kitano, 2000; Ideker et al., 2001; Weckwerth, 2003, 2011a,b). The roots of systems biology go back to the development of the General System Theory by Ludwig von Bertalanffy in the early 30's of the 20th century. He published one of the first explicit articles about open systems, feedback regulation and self-organization in living systems and proposed the basic mathematical framework for systems biology (Bertalanffy, 1940, 1969; Weckwerth, 2016, 2019).

In this review we focus on molecular mechanisms of microbial survivability in the outer space environment revealed with the help of global and integrative –omics approaches of systems biology that have been recently used to study microorganisms exposed to real and simulated space conditions. The use of –omics in space life sciences potentially has a pivotal role in the understanding of the molecular machineries implicated by microorganisms to tolerate the harsh conditions of space.

METABOLIC CHANGES

Exposure to space environment strongly modifies the expression of genes and the abundance of proteins related to metabolism (**Table 1**). Space parameters primarily affect the genes involved

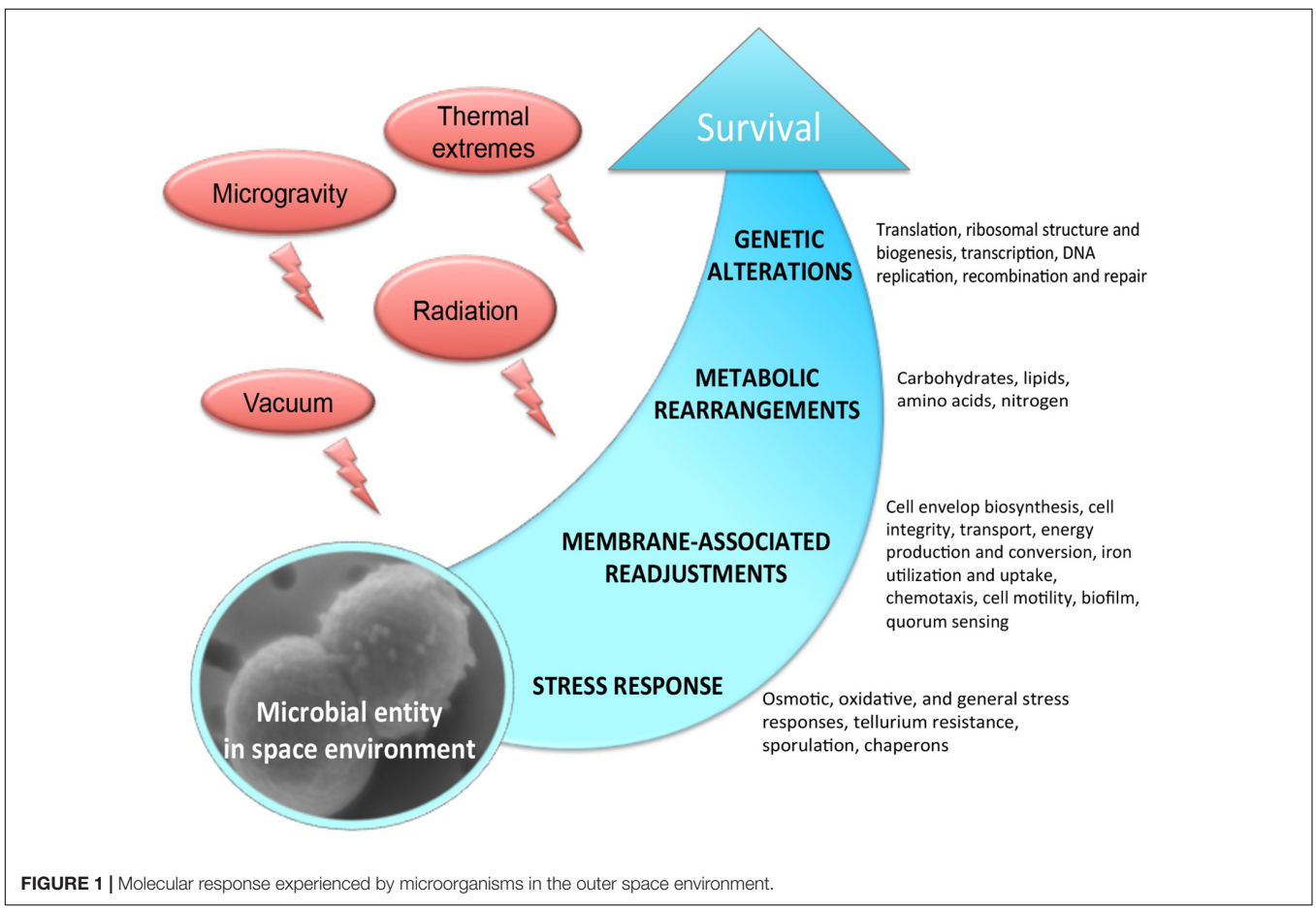

FIGURE 1 | Molecular response experienced by microorganisms in the outer space environment.

TABLE 1 | Omics studies of the microbial physiology in real and simulated outer space environment.

Microorganism studied	Exposure conditions	Research platform	Physiological effect	Molecular alterations	References
Aspergillusfumigatus, Cladosporium cladosporioides	UVC Simulated Martian Conditions	TMT (tandem mass tag) LC/MS Orbitrap Fusion Tribrid mass spectrometer	Differential abundance of proteins involved in ribosome biogenesis, translation, and carbohydrate metabolic processes was observed	Differential abundance of proteins involved in ribosome biogenesis, translation, and carbohydrate metabolic processes	Blachowicz et al., 2019
Candida albicans	Simulated microgravity	qRT-PCR	Increased filamentous forms, morphogenic switch consistent with enhanced pathogenicity	Gene expression changes related to budding, separation and yeast hyphal transition	Altenburg et al., 2008
Candida albicans	Cultivation aboard NASA Shuttle Atlantis STS-115	Microarray Agilent platform	Enhanced aggregation and random budding	Downregulation of ergosterol-encoding genes and genes involved in actin cytoskeleton; induction of ABC transporters and members of the major facilitator family; up-regulation of genes involved in oxidative stress resistance	Crabbé et al., 2013
Cupriavidus metallidurans strain CH34	Simulated microgravity	ICPL MudPIT MALDI-TOF-MS	A switch to anoxic or microoxic conditions	Differentially abundant universal stress proteins, cold shock proteins, nitrate reductase, and proteins involved in transport activity	Leroy et al., 2010
Bacillus cereus strains LCT-BC25 and LCT-BC235	398 h space flight (Tiangong-1 space station)	Illumina HiSeq 2000 sequencer 2D-LC-MS/MS ESI-MS/MS using the TripleTOF 5600 System	Significantly slower growth rate; significantly higher amikacin resistance level; changes in metabolism	Three polymorphic loci in the flight strains LCT-BC25 and LCT-BC235; differential expression of genes and abundance of proteins relevant to metabolism, structural function, gene expression modification and translation, and virulence	Su et al., 2014
Bacillus subtilis spores	559-day space mission (ISS) Simulated Martian conditions	Microarray Agilent platform	Broader and more severe stress response of spores exposed to space than spores exposed to simulated Martian conditions	Increased transcript levels of stress-related regulons responding to DNA damage (SOS response, SPbprophage induction), protein damage (CtsR/Clp system), oxidative stress (PerR regulon), and cell envelope stress (SigV regulon)	Nicholson et al., 2012
Bacillus subtilis	Spaceflight aboard the ISS (BRIC-21 and BRIC-23)	Illumina HiSeq 4000 platform	Differences in oxygen availability between flight and ground control samples, likely due to differences in cell sedimentation and the toroidal shape assumed by the liquid cultures in microgravity	Upregulated genes involved in biofilm formation, biotin and arginine biosynthesis, siderophores, manganese transport, toxin production and resistance, and sporulation inhibition	Morrison et al., 2019
Bacillus pumilus	18-month space mission (ISS) Simulated space conditions	Fluorescence two-dimensional difference gel electrophoresis (2D-DiGE) and mass spectrometry based proteomic analysis	Enhanced UVC resistance of "space-surviving" strains (spores and vegetative cells)	Differentially abundant proteins involved in menaquinone biosynthesis, electron transport, ribosome structure, transcription, spore thermostability, and oxidative stress response	Vaishampayan et al., 2012
Bacillus pumilus	18 months on-board the ISS	LC-MS/MS Orbitrap Fusion Tribrid	Enhanced resistance to UV irradiation and oxidative stress	Increased abundance of proteins related to survival, growth advantage, and stress response	Chiang et al., 2019
Escherichia coli	Spaceflight aboard the ISS	RNA-Seqwith Illumina platform	Adapted to grow at higher antibiotic concentrations in space compared to Earth	Specific responses related to oxidative stress and starvation response	Aunins et al., 2018

(Contined)

TABLE 1 | Continued

Microorganism studied	Exposure conditions	Research platform	Physiological effect	Molecular alterations	References
Escherichia coli strain K12 MG1655	Simulated microgravity	Microarray Affymetrix Analysis RT-PCR	The enhanced growth in simulated gravity conditions; glycerol supplementation of cultivation medium reduced multiple stress responses to microgravity	Up-regulation of genes encoding adaptation to stress (*sufE* and *ssrA*) and involved in DNA replication (*srmB*); down-regulation of genes encoding membrane transporters (*ompC*, *exbB*, *actP*, *mgtA*, *cysW* and nikB), carbohydrate catabolic processes (*ldcC*, *ptsA*, *rhaD* and *rhaS*) and nucleoside metabolism (*dfp*, *pyrD* and *spoT*)	Arunasri et al., 2013
Deinococcus radiodurans R1	Simulated UVC and vacuum conditions	Shotgun proteomics with HPLC nESI-MS/MS using Orbitrap Elite Metabolomics analysis with LECO Pegasus® 4D GC × GC-TOF spectrometer	Relative survival rate of 65% for UVC/vacuum exposed cells compared to control conditions; preserved cellular integrity, no detectable damage of cell surface and cell morphology	Differentially abundant proteins involved in TCA cycle, DNA damage response systems (PolA, PprA, GyrA/B, DdrB, DdrD, UvrB, recQ, ruvABC, MutT, MutS2, and Mrr restriction protein), ROS scavenging systems (pyridoxal 5′-phosphate synthase, peroxidase, sulfoxide reductase MsrA, thioredoxin reductase, PdxS and PdxT), and transcriptional regulators (DdrO and CRP regulon); up-regulation of protein functional categories of cysteine, methionine and tryptophan metabolism, RNA degradation, and aminoacyl-tRNA biosynthesis; significantly increased abundance of ethanolamine (cellular supply of reduced nitrogen and precursor for acetyl CoA), O-Palmytoyl-L-Carnitine chloride (quaternary amine and compatible solute which impacts bacterial survival in extreme conditions), and octadecanoic (stearic) acid (biofilm-associated compound)	Ott et al., 2017
Deinococcus radiodurans R1	Simulated vacuum conditions	Shotgun proteomics with HPLC nESI-MS/MS using Orbitrap Elite Metabolomics analysis with LECO Pegasus® 4D GC × GC-TOF spectrometer	After 90 days of high vacuum exposure, survival of *D. radiodurans* cells was 2.5-fold lower compared to control cells	Proteases, tRNA ligases, reactive oxygen species (ROS) scavenging proteins, nucleic acid repair proteins, TCA cycle proteins, and *S*-layer proteins are highly abundant after vacuum exposure. The overall abundance of amino acids and TCA cycle intermediates is reduced during the recovery phase of *D. radiodurans* as they are needed as carbon source; upregulation of Type III histidine kinases	Ott et al., 2019a
Deinococcus radiodurans R1	Simulated microgravity	Shotgun proteomics with HPLC nESI-MS/MS using Orbitrap Elite Metabolomics analysis with LECO Pegasus® 4D GC × GC-TOF spectrometer	Growth under simulated microgravity causes an increased demand for amino acids	Increased abundance of several proteins associated with processes involving DNA, such as DR_2410 (DnaX), DR_1707 (PolA), DNA ligase DR_2069 (LigA) and the transcription repair coupling factor DR_1532 (Mfd); increased abundance of cell envelope-associated proteins.	Ott et al., 2019b
Klebsiella pneumonia strain LCT-KP289	398 h space flight (Tiangong-1 space station)	Illumina HiSeq 2000 sequencer	A higher cotrimoxazole resistance level of flight strain	Differentially expressed genes and proteins involved in energy production and conversion, carbohydrate transport and metabolism, translation, ribosomal structure and biogenesis, posttranslational modification, protein turnover, and chaperone functions; synonymous mutation of the ytfG gene, which may influence fructose and mannose metabolic processes of flight strain.	Guo et al., 2015

(Continued)

TABLE 1 | Continued

Microorganism studied	Exposure conditions	Research platform	Physiological effect	Molecular alterations	References
Klebsiella pneumoniae strain ATCC BAA-2146	15-day space mission. Simulated space condition with microgravity	Illumina HiSeq 2000 sequencer RNA-Seq and comparative transcriptomics Quantitative RT-PCR	Strain-specific mutations, elongated forms, reduced hydrogen peroxide (H_2O_2) tolerance and increased biofilm formation ability of flight strain	Differentially expressed genes involved in amino acid transport and metabolism, and carbohydrate transport and metabolism; several differentially regulated non-coding RNAs (ncRNAs)	Li et al., 2014
Klebsiella pneumoniae	398 h space flight (Tiangong-1 station)	Illumina HiSeq 2000 sequencer	Increased strain diversity Acquired drug resistance	Large number of mutant genes related to transport and metabolism, including the gene encoding dihydroxyaceton kinase, which generates the ATP and NADH required for microbial growth	Guo et al., 2014
Pseudomonas aeruginosa PAO1	9-day spaceflight (ISS) Simulated microgravity	MudPIT via nano LC-MS/MS Microarray Affymetrix GeneChip analysis	Adaptation to an anaerobic mode of growth during spaceflight	Differentially expressed genes and differentially abundant proteins associated with growth under anaerobic conditions, virulence, nitrogen metabolism, purine and pyrimidine metabolism, fatty acid biosynthesis, oxidative phosphorylation, ribosome synthesis, and transcription with Hfq regulon as global transcriptional regulator involved	Crabbé et al., 2011
Rhodospirillum rubrum S1H	10 and 12-day space flights (ISS). Simulated microgravity and space-ionizing radiation.	Microarray platform High throughput gel-free proteomics with Isotope-Coded Protein Label (ICPL) technology Multi-Dimensional Protein Identification Technology (MudPIT)	Minimized effect of microgravity; increased sensitivity to ionizing radiation during space mission	Differential expression of genes and abundance of proteins associated with translation, transcription, ribosomal structure and biogenesis, energy production and conversion, putative oxidative and osmotic stress, tellurium resistance, solute transport and osmotic regulation	Mastroleo et al., 2009
Rhodospirillum rubrum S1H	Simulated microgravity	Microarray platform ICPL MudPIT LC-QqQLIT-MS liquid chromatography coupled to hybrid quadrupole-linear ion trap mass spectrometry	Higher pigmentation, no change in cell density and culture oxygenation	Elevated components of the N- acylhomoserine lactone (AHL)-type quorum sensing (QS)-system. Differentially expressed genes and differentially abundant proteins associated with membrane-bound photosynthetic apparatus, cell envelope biogenesis, ribosomal structure and biogenesis, transcription, lipid metabolism, amino acid and carbohydrate transport and metabolism, stress response, inorganic ion transport, chemotaxis	Mastroleo et al., 2013
Saccharomyces cerevisiae	12-day space flight (ISS)	2D-PAGE MALDI-TOF/TOF MS	Altered budding patterns; a switch toward more random budding	Increased protein degradation; ubiquitin presence in the microgravity samples indicating enhanced degradosome activity; changes in abundance for proteins involved in energy metabolism and in stress response (oxidative stress proteins and chaperones)	Van Mulders et al., 2011
Salmonella typhimurium	25 h space missions	MudPIT via LC-LC-MS/MS Microarray qRT-PCR	Increased virulence regulated by media composition	Differentially expressed genes involved in motility, energy production and conversion, iron utilization and uptake, ribosomal structure, and genes encoding small regulatory RNA molecules	Wilson et al., 2008
Salmonella typhimurium	9-day spaceflight (ISS) Simulated microgravity	Microarray Analysis Nano LC-MS/MS	Enhanced virulence in a murine infection model and extracellular matrix/biofilm accumulation	Differential expression of genes associated with ribosome structure, iron utilization/storage, periplasmic stress signalling, and biofilm formation;RNA-binding protein Hfq is identified as a global regulator involved in the response tospace environment	Wilson et al., 2007

(Contined)

TABLE 1 | Continued

Microorganism studied	Exposure conditions	Research platform	Physiological effect	Molecular alterations	Reference
Salmonella enterica	Simulated microgravity	Whole Genome Microarrays OmniGrid Array Maker, RT-PCR	Increased virulence	Differentially expressed transcriptional regulators, virulence factors, lipopolysaccharide biosynthetic enzymes, iron-utilization enzymes	Wilson et al., 2002
Serratiamarcescens strains LCT-SM166 and LCT-SM262	398 h space flight (Tiangong-1 space station)	Illumina HiSeq 2000 sequencer 2D-LC-MS/MS	No changes in the morphology, post-culture growth kinetics, hemolysis or antibiotic sensitivity; differences in carbon source utilization patterns	Differential expression of genes associated with glycolysis/gluconeogenesis, pyruvate metabolism, arginine and proline metabolism and the degradation of valine, leucine and isoleucine; up-regulation of genes associated with metabolism; down-regulation of *nudE* functionally associated with replication, recombination and repair; *PgaB* encoding the biofilm PGA synthesis lipoprotein; *FliE* encoding the flagellar hook-basal body complex protein; up regulation of FlgG, which encodes the flagellar basal-body rod protein	Wang et al., 2014
Streptomyces coelicolor A3(2)	16.5-day space mission (Tiangong-1 space station) Simulated microgravity	Microarray Agilent platform Real-time qRT-PCR analysis	Shortened life cycle; accelerated sporulation; altered secondary metabolism; increased biomass production; stronger bacteriostatic activity against *B. subtilis*	Differential expression of genes involved in morphological differentiation, aerial hyphae erection, sporulation, spore germination, cell wall structure, transport, spore structure, and development-associated secondary sigma factors; accumulation of gray spore pigment	Huang et al., 2015
Streptococcus mutants	Simulated microgravity	Illumina HiSeq 2500 platform	Increased killing by H_2O_2 compared to normal gravity control cultures	Altered expression of a number of genes located on extrachromosomal elements, as well as genes involved in carbohydrate metabolism, translation, and stress responses	Orsini et al., 2017
Staphylococcus aureus	Simulated microgravity	Transcriptional Affymetrix GeneChip microarray profiling	Slower growth; a novel biofilm/colonization phenotype with diminished virulence characteristics	Decreased carotenoid production, increased susceptibility to oxidative stress, and reduced survival in whole blood; alterations in metabolic pathways: carbohydrate, pyruvate, and arginine metabolism, and response to environmental stressors; down-regulation of RNA chaperone and transcriptional regulatorhfq	Castro et al., 2011
Vibrio fischeri *V. fischeri* Δhfq	Simulated microgravity	Illumina NextSeq500 platform	Changes of the growth phase transition between exponential and stationary phase	Overexpression of stress-associated genes; decrease in gene expression associated with translational activity; Δhfq mutants exhibited an increase of transcripts associated with flagellar assembly and transcriptional regulators	Duscher et al., 2018

in metabolism, raising further alterations of the microbial growth. However, energy and regenerative power are needed for the microbial cell to counteract the drastic effects of space exposure by launching a number of regenerative activities and repair mechanisms.

Carbohydrate Metabolism

The molecular mechanisms of adaptive reactions under stress conditions require additional energy and carbohydrate metabolism is crucial in generating that energy (Minic, 2015). Carbon source utilization by various microorganisms has been primarily affected during short- and long-term exposure to space conditions. In response to space environmental stress, microorganisms with great adaptability to survive successfully exhibit certain flexibility in carbon source utilization. Strains of *Serratia marcescens*, *Escherichia coli,* and *Klebsiella pneumoniae* after a long-term flight on-board of the SHENZHOU-8 spacecraft exhibited a difference in carbon source utilization (as suggested by multi-omics analysis), while their morphology or growth patterns were not affected (Li et al., 2014, 2015; Wang et al., 2014; Guo et al., 2015; Zhang et al., 2015). Strains of *S. marcescens* after spaceflight displayed a positive reaction in the sole-carbon-source utilization of D-Mannitol, D-Raffinose, and N-Acetyl neuraminic acid (Wang et al., 2014). Correspondingly, proteomic analysis showed up-regulation of the proteins of the glycolysis/gluconeogenesis pathway of *S. marcescens* grown during spaceflight, which was suggested to reflect adaptive changes of the strain aboard the spacecraft (Wang et al., 2014). The strain of *E. coli* after spaceflight showed increased carbon source utilization and 2,58-fold up-regulation of maltose regulon periplasmic protein malmM (shown in proteomic analysis), which can be explained by the increased demand for additional carbon substrates during stress adaptability to the space environment (Zhang et al., 2015). *Klebsiella pneumoniae* gained the ability to use D-Mannose after spaceflight, possibly reflecting an overall slowed down metabolism of this microorganism to better adapt to the space environment (Guo et al., 2015). Numerous *K. pneumoniae* genes differentially expressed after spaceflight were involved in carbohydrate transport and metabolism, as suggested by genomic and transcriptomic analyses (Li et al., 2014). Integrative proteotranscriptomic analysis of *Bacillus cereus* strain flown on-board of the SHENZHOU-8 spacecraft has shown that genes of glucose metabolism (*glpX* gene product, trehalose-6-phosphate hydrolase) were differentially expressed during spaceflight (transcriptomic analysis reported in Su et al., 2014). Glyceraldehyde-3-phosphate dehydrogenase (GAPDH) is one of the key enzymes in glycolytic pathway that serves to break down glucose for carbon molecules and energy. GAPDH provides an important source of NADH during glycolysis and contributes to the various regulatory functions (Sirover, 2012, 2014). Proteomic analysis showed that GAPDH was significantly up-regulated in *Bacillus pumilus* spores exposed to outer space (Vaishampayan et al., 2012). Apart from the differential expression of GAPDH under a variety of stress conditions (Nicholls et al., 2012; Hildebrandt et al., 2015), a microgravity induced up-regulation of this housekeeping protein together with pyruvate kinase and a subunit from pyruvate decarboxylase was observed in proteomic analysis of *Saccharomyces cerevisiae* after the 2-day trip on-board of the Soyuz TMA-9 vehicle (Van Mulders et al., 2011). RNAseq-based analysis of *Streptococcus* mutants displayed an alteration in early stationary-phase metabolism under the influence of simulated microgravity, and expression of phosphortransferase system genes associated with transport of carbohydrates (trehalose, mannose, glucose, mannitol, and cellobiose) was significantly increased (Orsini et al., 2017). Proteomic profiling of several fungal strains exposed to simulated Martian conditions revealed that carbohydrate metabolic functional category was among significantly over-represented biological processes (Blachowicz et al., 2019). A set of up-regulated proteins involved in carbohydrate metabolism included enzymes (e.g., isocitrate lyase AcuD, cellobiohydrolases, exo-polygalacturonase, and chitin deacetylases), which enable exposed fungal strains using an alternative carbon source and permit morphogenetic alterations in the course of growth and differentiation. The authors reported on adjustments in carbohydrate metabolism as an adaptive response to simulated Martian conditions (Blachowicz et al., 2019).

The analyzed –omics-assisted investigations indicate characteristic changes in carbohydrate metabolism of microorganisms cultivated during spaceflight and exposed to outer space. These changes are directed to restore energy balance in stress conditions and frequently serve to satisfy the increased demand in carbon source during adaptive reactions to the space environment.

Amino Acid Metabolism

Apart from their main contribution as substrates for protein synthesis, amino acids act as signaling molecules exerting regulatory functions (Sturme et al., 2002; Rinaldo et al., 2018), and serve as indirect carbon sources through citrate cycle. Frequently observed down-regulation of enzymes involved in amino acid transport and metabolism of space-exposed microorganisms is usually associated with their arrest in growth. Among all the genes of *K. pneumonia*, *E. coli* and *B. cereus* affected during spaceflight on-board of space vehicle, functional category of amino acid transport and metabolism was the most represented (Li et al., 2014, 2015; Su et al., 2014; Guo et al., 2015; Zhang et al., 2015). The strain of *K. pneumoniae* after spaceflight characterized by increased biofilm formation was suggested to use amino acids as an indirect carbon source through TCA cycle in stress-related space conditions (Li et al., 2014). Proteomic analysis showed that most key enzymes of the TCA cycle were more abundantly represented in *Deinococcus radiodurans* cells after the exposure to UVC/vacuum conditions (Ott et al., 2017). Proteomic analysis of *S. marcescens* and *K. pneumonia* revealed that proteins involved in arginine and proline metabolism, and degradation pathways of valine, leucine, and isoleucine were down regulated after spaceflight (Wang et al., 2014; Guo et al., 2015). However, another study by Morrison et al., 2019 reported that genes of arginine biosynthesis were up-regulated during spaceflight of *B. subtilis* aboard the ISS (based on the RNA-seq analysis). Such discrepancies between different reports can be very well stated by the experimental

set up of the studies. One group of the studies reported on molecular profiles during spaceflight, i.e., avoiding re-cultivation of returned samples (e.g., Morrison et al., 2019), while another group of investigations analyzed space-returned strains upon their recovery in liquid medium (e.g., Li et al., 2014). Serine hydroxymethyltransferase responsible for the enzymatic catalysis of the reversible conversion of L-serine to L-glycine was up-regulated in proteomic analysis of space-returned spores of *B. pumilus* (Vaishampayan et al., 2012). Proteomic analysis of spaceflight grown cells of *P. aeruginosa* indicated the down-regulation of ArcA, an enzyme associated with the fermentation of arginine (Crabbé et al., 2011). Proline and arginine metabolism implement in microbial mechanisms of stress survival (Zhao and Houry, 2010; Goh et al., 2011; Liang et al., 2013). Various studies have shown evidence that proline metabolism leads to increased production of endogenous reactive oxygen species (ROS) (Liang et al., 2013).

Experimental data obtained in the post-flight/post-exposure analysis suggest that amino acids metabolism is majorly down regulated in order to favor the suppressed microbial growth and proliferation. The observed suppression of proline metabolism in a number of space exposed bacterial strains can be considered as one of the microbial strategies to minimize the generation of endogenous metabolically produced ROS in order to cope efficiently with radiation-induced damage. The functional categories of cysteine and methionine metabolism, however, can be up-regulated in response to radiation component of the outer space environment (Ott et al., 2017). Methionine and cysteine are sulfur-containing amino acids, which significantly contribute to the antioxidant defense system of exposed microorganisms. Cysteine chemistry, i.e., cysteine-mediated redox signaling is important biochemical response against ROS damage (Paulsen and Carroll, 2013). Methionines located on the surface of protein structures act as effective endogenous antioxidants to defend functionally essential molecules against oxidative damage (Levine et al., 2000). In case with outer space-associated radiation exposure, activation of cysteine and methionine metabolism is one of the most obvious microbial responses to oxidative damage.

Lipid Metabolism

Microorganisms adapt their membrane lipid composition to stressful environmental conditions by adjusting the relative amounts of different types of lipids and the degree of unsaturation of fatty acyl residues. Strains of *Bacillus horneckiae* sp. isolated from the Phoenix spacecraft were characterized by altered lipid profiles based on the results of traditional biochemical lipid analyses (Vaishampayan et al., 2010). Radiation-induced elevated generation of ROS causes multiple disintegrative disorders, including oxidative changes in lipid metabolism. The genes involved in lipid biosynthesis (enoyl-CoA hydratase/isomerase with fatty acid synthase activity) and in fatty acid metabolism were down-regulated in RNAseq-based analysis of *B. cereus* and *K. pneumoniae* strains after spaceflight (Li et al., 2014; Su et al., 2014). The authors connect it with the detected reduced growth of *B. cereus* after spaceflight as an adaptive strategy that enable the survival and maintenance of the energy status. Transcriptomic analysis of space exposed *B. subtilis* spores and *Rhodospirillum rubrum* exposed to modeled microgravity in frames of the Micro-Ecological Life Support System Alternative (MELiSSA) project showed the down-regulation of genes encoding lipid biosynthetic enzymes (Nicholson et al., 2012; Mastroleo et al., 2013). Multi-omic analyses showed that metabolic pathways associated with fatty acid metabolism, phospholipid biosynthetic process, and cellular lipid biosynthetic processes were affected in *E. coli* and *Enterococcus faecium* strains after spaceflight (Chang et al., 2013a; Li et al., 2015).

Studies of microbial biochemistry in microgravity conditions generally suggest the up-regulation of genes encoding lipoproteins and lipopolysaccharide biosynthetic enzymes (Wilson et al., 2007; Leroy et al., 2010). Several of them are associated with bacterial biofilm formation, virulence, and pathogenicity. The gene encoding rhamnosyltransferase (*rhlA*) involved in surfactant biosynthesis was found among the major virulence-associated genes of *P. aeruginosa* stimulated in spaceflight along with the accumulation of rhamnolipids under simulated microgravity conditions, which might be connected to low shear liquid sensing (transcriptomic analysis in Crabbé et al., 2011).

In summary, many of changes in lipid metabolism observed under the space environmental conditions aim to adjust the energy status toward the slowed down growth of exposed microorganisms. However, the mobilization of certain microbial lipoproteins and lipopolysaccharides is activated in spaceflight and under simulated microgravity conditions to adapt cell-cell contacts and communication toward the low-shear growth environment.

MEMBRANE-ASSOCIATED PROCESSES

The destructive effect of space vacuum (10^{-7} to 10^{-4} Pa) triggers cellular integrity of space-exposed microorganisms, influencing numerous processes in membrane apparatus of microbial cell (Horneck et al., 2010). Among them are rearrangements of lipid bilayers, changes in membrane fluidity and permeability, and alteration of membrane bound enzymatic activities. Cell membrane that carries a function of physical barrier and protect the cell from extracellular environment can be affected in conditions of microgravity, causing the altered uptake or excretion rates.

Cell Envelope Biosynthesis and Maintenance

Microbiological and biochemical analysis of the survival and behavior of *C. metallidurans* in the MESSAGE-1 flight experiment by means of flow cytometry-assisted analysis of cell physiology and proteomic profiling revealed a minor damage of cell membrane; the remaining viable cells acquired a higher membrane potential than the ground control cells (Leys et al., 2009). The genes involved in the cell wall/membrane/envelope biogenesis of *E. faecium* were among the differentially expressed genes with the greatest change in expression after flight on the SHENZHOU-8 spacecraft, as suggested by comparative transcriptomic and proteomic analyses. Comparative genomic

analysis of returned after spaceflight *E. faecium* strain revealed mutation of the *arpU* gene associated with cell wall growth, which in turn may affect the expression of molecular players responsible for cell wall and membrane biogenesis of *E. faecium* (Chang et al., 2013a). The post-flight transcriptomic and proteomic studies of *E. coli* revealed the up-regulation of the envelope stress induced periplasmic protein Spy and the *yfbE* gene encoding predicted pyridoxal phosphate-dependent enzyme with regulatory functions in cell wall biogenesis (Li et al., 2015; Zhang et al., 2015). A number of differentially expressed genes involved in cell wall and spore structure were described microarray-based analysis of *Streptomyces coelicolor* during spaceflight and simulated microgravity (Huang et al., 2015). Modeled microgravity affected gene groups of *Salmonella* involved in type III secretion, lipopolysaccharides, and cell wall synthesis (microarray-based analysis in Wilson et al., 2002). Proteomic analysis showed that *D. radiodurans* grown in simulated microgravity showed an increased abundance of cell envelope-associated proteins (Ott et al., 2019a). Cell envelope biosynthesis and maintenance was triggered in multi-omics analysis of *R. rubrum* by spaceflight and simulated space environment (the top 20 of the most induced genes) (Mastroleo et al., 2009, 2013). Cell envelope of *B. subtilis* exposed to 1.5 years of simulated Martian and space conditions was massively affected as suggested by a comprehensive transcriptomic analysis with a number of up-regulated membrane and cell envelope stress proteins (SigV regulon) (Nicholson et al., 2012).

A number of spaceflight induced alterations associated with cell envelope, e.g., a thickened cell envelope and intensive vesiculation (Zea et al., 2017), are quick stress responses to enhance microbial adaptation rates and regulate the level of protein accumulation in the cell envelope. These autonomous stress responses are mediated by means of altered cell envelope protein machinery, allowing exposed cells to export stress products (e.g., damage or misfolded proteins) and to achieve alleviated stress response.

Transport

The effects of simulated and real microgravity on microbial behavior and metabolism in liquid cultures aboard spacecraft are most likely mediated by alterations of extracellular environment. The response of the cell to changes in the extracellular environment includes a cascade of cellular transport events that operate nutrient uptake, cellular waste disposal, solute transport and quorum-sensing signaling. The Suf along with other ABC membrane transporters were identified as differentially abundant in *S. typhimurium* in proteomic response to cultivation aboard spacecraft (Wilson et al., 2008). Spaceflight significantly affected the transport machinery of *E. coli*, up-regulating a number of transporters, as shown in multi-omics analysis (Li et al., 2015). The multi-omics based comparison of the strains after spaceflight and the control strains of *E. coli*, *K. pneumonia*, and *R. rubrum* showed that ontological categories "transmembrane transporter activity" were overrepresented among all differently expressed genes and differently abundant proteins during spaceflight (Mastroleo et al., 2009; Li et al., 2014, 2015). The genes encoding for multidrug efflux and arsenite membrane-bound transporters were 3 to 4 fold overexpressed in transcriptomic analysis of spores of *B. subtilus* exposed to simulated Mars conditions or/and real space (Nicholson et al., 2012). The genes encoding for probable metal-transporting P-type ATPase and dctA C4-dicarboxylate transport protein were overexpressed as suggested by post-flight transcriptomic analysis of *P. aeruginosa* (Crabbé et al., 2011). Microarray analysis identified that the group of membrane transport genes belongs to low-shear modeled microgravity (LSMMG) regulon of *Salmonella* and the gene *sbmA* encoding ABC superfamily transporter was up-regulated during spaceflight (Wilson et al., 2007). Post-flight proteotranscriptomic analysis of *R. rubrum* revealed up-regulated genes that are involved in solute transport and osmotic regulation, and are probably related to oxidative stress (Mastroleo et al., 2009). Antibiotic-producing *S. coelicolor* in conditions of simulated and real space microgravity displayed a significant up-regulation of several transporters which contribute to its enhanced bioactivity and BldK ABC transporter complex which is essential for aerial mycelium formation (microarray-based analysis in Huang et al., 2015).

Due to the lack of gravity-driven convective flows, extracellular mass transport becomes essentially limited to diffusion under the conditions of spaceflight and simulated microgravity. Cells cultured in liquid medium during spaceflight may experience a deficiency in oxygen and nutrients availability (Zea et al., 2016), which reflects altered transport functions. The elevated transport machinery of microgravity-affected microorganisms aims to facilitate not only nutrient uptake, but also cellular waste removal, distribution of solute and trafficking of quorum-sensing signaling molecules.

Chemotaxis, Cell Motility

Microgravity in conditions of spaceflight affects extracellular fluid properties, this way altering relationship between microbial cell and extracellular environment (Horneck et al., 2010). The involvement of flagellar apparatus and chemotaxis machinery after spaceflight and real space exposure has been detected applying –omics assisted analyses of several bacterial strains. 5.1-fold up-regulation of the *fliL* gene required for flagellar formation was indicated in the transcriptomic response of space-exposed spores of *B. subtilis* (Nicholson et al., 2012). The *flgG* gene encoding the flagellar basal-body rod protein was up-regulated in transcriptomic response of *S. marcescens* to spaceflight conditions, while down-regulation was shown in the same study for the *FliE* gene that encodes the flagellar hook-basal body complex protein (Wang et al., 2014). In addition, many *K. pneumoniae* genes affecting cell motility were differentially expressed in the strain exposed to simulated space condition (Li et al., 2014). The expression of flagellar assembly genes in LSMMG conditions was also increased in the transcriptome of the mutualistic bacterium *Vibrio fischeri* (Duscher et al., 2018). Flagellar assembly and bacterial chemotaxis were the most significantly enriched functional categories among all affected genes differently expressed by *E. coli* during spaceflight, e.g., genes encoding bacterial flagellin and methyl-accepting chemotaxis protein II (Li et al., 2015). Transcriptomic response of *R. rubrum* to spaceflight and simulated microgravity indicated

the induced expression (upregulated > 2.6-fold) of the gene encoding for Flagellar hook-associated protein 2 (FliD filament cap protein) (Mastroleo et al., 2009). Genes of *S. typhimurium* involved in motility and chemotaxis response were identified as differentially expressed in response to spaceflight cultivation (Wilson et al., 2007). Transcriptomic and proteomic analyses of *P. aeruginosa* exposed to spaceflight conditions revealed that several chemotaxis transducers were up-regulated in response to spaceflight (Crabbé et al., 2011).

The reported effects of simulated microgravity and spaceflight on the various physiological properties of microorganisms are associated with the potential disruption of the quiescent extracellular environment. The molecular components of bacterial motility and chemotaxis response are activated in microgravity-exposed microorganisms in order to gain a balanced connection between the cell and its environment. The induced flagellar action results in mixing of the local fluid surrounding of microbial cell and removal of the cell from its quiescent location. The induction of molecular machinery responsible for motility and chemotaxis can locally influence the correct redistribution and availability of nutrients, substrates, solutes and other biologically active molecules at the extracellular environment level.

Energy Production and Conversion

In line with the increased demand in energy needed to cope with stress in space environment, there are several post-flight –omics assisted observations of altered membrane bioenergetics and electron transport chains with elevated abundances of electron transfer proteins and ATP synthase. Comparative proteomic analysis of *B. pumilus* spores long-termly exposed to a variety of real space conditions at the ISS in the EXPOSE facility revealed the up-regulation of the alpha-ketoglutarate decarboxylase enzyme which is associated with menaquinone biosynthesis and involved in the membrane-associated electron transport system (Palaniappan et al., 1994; Vaishampayan et al., 2012). Further proteomic studies with space-exposed *B. pumilus* showed that the altered protein abundances in the category of energy metabolism might be a microbial strategy to better cope with stressful environments (Chiang et al., 2019). Post-flight proteotranscriptomic analysis of *R. rubrum* identified significant up-regulation of multiple clusters of genes relevant to energy production and conversion (succinate dehydrogenase, ubiquinone oxidoreductase) (Mastroleo et al., 2009). The *hydN* gene encoding Fe-S center-bearing protein responsible for electron transport from formate to hydrogen together with a set of *S. typhimurium* genes involved in the formation of the Hyc hydrogenase (respiratory enzyme of H_2-uptake) were differentially expressed in response to spaceflight cultivation (Wilson et al., 2007). The gene *hppA* encoding membrane-bound proton-translocating pyrophosphatase and five F_0F_1 ATP synthase subunits were up-regulated after spaceflight of *R. rubrum* (Mastroleo et al., 2009). The subunits of ATP synthase of microgravity-exposed *S. cerevisiae* have been differentially regulated during short-term spaceflight (Van Mulders et al., 2011). The down-regulation of CcoP2, a cytochrome with high affinity for oxygen, has been observed in proteomic analysis of the *P. aeruginosa* cells grown in spaceflight (Crabbé et al., 2011). This cytochrome is not active in the anaerobic lifestyle of *P. aeruginosa*, but is induced under microaerophilic conditions (Crabbé et al., 2011). The authors reported that *P. aeruginosa* adopted an anaerobic mode of growth during spaceflight, and switched to anaerobic metabolism, which was accompanied by the down-regulation of CcoP2 under oxygen-limiting conditions. Spaceflight induced mainly genes involved in anaerobic metabolism of this pathogen and anaerobic respiration occurred through denitrification, i.e., in the presence of the alternative electron acceptor nitrate or nitrite (Crabbé et al., 2011).

Microbial adaptation to spaceflight conditions may lead to alterations associated with energy sources utilization. Hereby, a corresponding molecular pull of energy-converting enzymes responsible for a switch from one energy source to another is affected in conditions of spaceflight and simulated microgravity. Energy management also facilitates the survival of outer space exposed microorganisms by modulating electron transfer proteins.

Iron Utilization and Uptake

Iron as the most abundant transition metal in biological systems is incorporated into protein cofactors and plays important regulatory, redox and catalytic roles in microbial world. Prokaryotes have evolved powerful iron assimilation and storage systems, which supply sufficient iron for growth and metabolism. Microorganisms show an enormous diversity and abundance of iron-dependent redox proteins, which majorly harbor iron within hemes and in the form of iron–sulfur (Fe–S) clusters. Bacteria and Archaea enormously depend on these two classes of cofactors for their energy metabolism. Iron availability influences the expression of bacterial genes encoding high-affinity iron uptake pathways and, in pathogenic microorganisms, virulence determinants (Butt and Thomas, 2017). The metal-specific repressor Fur (ferric uptake regulator) (Lee and Helmann, 2007) appears to be a very global and well-conserved regulator, which participates in regulation of iron uptake and homeostasis in bacteria. Fur coordinates the expression of various genes and acts as an iron-responsive, DNA-binding repressor protein (Hantke, 1987; Lee and Helmann, 2007). The Fur protein employs Fe(II) as a cofactor and binds to a "Fur box" with the palindromic consensus sequence GATAATGATAATCATTATC in the promoters of iron-regulated genes, resulting in repression of these genes, while under low-iron conditions, the Fur protein is released from this operator site and transcription takes place. The Fur repressor is involved in the transcriptional control of the operons encoding the pathways for the production of the siderophores (responsible for delivering the iron into the cells), virulence-associated genes, the manganese- and iron-containing superoxide dismutase genes and in the *fur* gene autoregulation (Hall and Foster, 1996; Lee and Helmann, 2007).

The Fur protein and iron utilization/storage system were shown to play a role in the *Salmonella* ground-based LSMMG (Wilson et al., 2002) and the spaceflight-induced multi-omics molecular responses (Wilson et al., 2002, 2008). LSMMG induces

acid resistance in *Salmonella* and Fur was shown to be essential in this process. The *fur* mutant strain of *Salmonella* did not demonstrate any detectable acid resistance to be induced by LSMMG (Wilson et al., 2002). Furthermore, several genes involved in iron metabolism were induced (*fepD* encoding for ferric enterobactin transporter, *STM1537* encoding for Ni/Fe-hydrogenase1 b-type cytochrome subunit, *hscB* responsible for assembly of Fe-S clusters) and down regulated (*feoB* encoding for ferrous iron transport protein, *yliG* putative Fe-S oxidoreductase, *sufC*, *sufS*) by LSMMG, as indicated by whole genome microarray analysis (Wilson et al., 2002). Additionally, the authors mention a number of potential Fur-binding sites that were located upstream of several different LSMMG regulated genes. The Fur-binding site-associated genes regulated by LSMMG included those identified to be regulated by Fur (*fepD*, *sufC*, *sufS*, and *feoB*) and those not earlier described as Fur regulated (Wilson et al., 2002). Wilson et al. (2007, 2008) reported that several molecular components of iron utilization/storage system were altered during spaceflight. Proteomic analysis showed that the abundances of Fur, iron-dependent alcohol dehydrogenase, bactoferrin, and electron transport protein with Fe-S center were increased after spaceflight, while a number of other proteins involved in iron utilization and uptake (e.g., cytoplasmic ferritin, siderophore receptor TonB, Fe-S cluster formation protein, and ferric enterobactin receptor) were underrepresented during growth of *S. typhimurium* in spaceflight (Wilson et al., 2007, 2008). These findings indicate the involvement of Fur in transmitting the LSMMG and spaceflight induced signals.

Proteotranscriptomic analysis of *P. aeruginosa* showed that the gene *bfrB* encoding bacterioferritin was down-regulated in cells grown on-board (Crabbé et al., 2011). Apart from the primarily function of iron storage, bacterioferritins participate in defense against oxidative stress and radical damage (Velayudhan et al., 2007). The down-regulation of *bfrB* in this case may be linked to the anerobiosis switch of *P. aeruginosa* during spaceflight (Crabbé et al., 2011). 4 to 6-fold down-regulation of several genes encoding putative iron (III) dicitrate transporting proteins was shown in transcriptomic analysis of spores of *B. subtilus* exposed to 1.5 year to real space conditions (Nicholson et al., 2012). The analysis of differential gene expression of *R. rubrum* in MESSAGE 2 spaceflight experiment (Mastroleo et al., 2009) revealed the up-regulation of the Fur repressor, which connects cellular iron status to oxidative stress by scavenging iron (Lee and Helmann, 2007), and the down-regulation of hfq, which negatively controls *fur* expression in *E. coli* (Vecerek et al., 2003). During MESSAGE 2 experiment the genes involved in the iron acquisition and redox balance, e.g., ferredoxin (Rru_A0077), Fe-S cluster-related gene (Rru_A1069), *dps*-related gene (Rru_A1499), superoxide dismutase (Rru_A1760) and bacterioferritin *bfr* (Rru_A2195) were induced (Mastroleo et al., 2009).

The analyzed –omics based investigations indicate that modeled microgravity and spaceflight conditions operate molecular iron-binding elements for their regulatory and oxidative stress pathways, encompassing a novel environmental signal.

GENETIC MACHINERY

The potential effects of space radiation target genetic stability of space-traveling microorganisms. Both by direct damage to DNA and indirect consequences due to ROS generation, radiation component of space environment affects genetic machinery of exposed microorganisms (**Figure 2**), causing a wide variety of changes starting from gene expression patterns (**Table 1**) and frequently leading to space-induced DNA mutagenesis (Horneck and Rabbow, 2007; Moeller et al., 2012). Global alterations in gene expression at the translational and transcriptional levels induced by adaptation of exposed microorganisms to radiation- and microgravity-filled space environment have been confirmed by proteomic and transcriptomic analyses (**Figure 2**), while genomics techniques revealed a number of mutant microbial strains after spaceflight (Vaishampayan et al., 2010; Chang et al., 2013a,b; Li et al., 2014; Zhang et al., 2015).

Translation, Ribosomal Structure, and Biogenesis

The multi-omics post-flight observations of *K. pneumonia*, *E. faecium* and *R. rubrum* cultivated on-board spacecraft revealed that the functional category "translation, ribosomal and biogenesis" was one of most highly represented category among all the up-regulated genes (Mastroleo et al., 2009; Chang et al., 2013a; Guo et al., 2015). More than 20 ribosomal protein-encoding genes of *R. rubrum*, 1 translation initiation-related gene, and 2 translation elongation-related genes have been found up-regulated in transcriptomic response to spaceflight (Mastroleo et al., 2009). Ribosomal apparatus of *R. rubrum, P. aeruginosa*, *S. typhimurium*, *B. pumilus*, *B. subtilis*, *B. cereus*, *S. cerevisiae* and *C. metallidurans* has been also massively affected in conditions of modeled microgravity (Wilson et al., 2002; Leroy et al., 2010; Mastroleo et al., 2013), spaceflight (Leys et al., 2009; Su et al., 2014; Zhang et al., 2015) and in real space conditions (Nicholson et al., 2012; Vaishampayan et al., 2012) with a number of down-regulated ribosomal genes and proteins as suggested by the multi-omics based analysis. Of 115 genes of *P. aeruginosa* that were down-regulated during spaceflight, 40 were involved in the synthesis of ribosomes (Crabbé et al., 2011). The *P. aeruginosa* genes encoding translational elongation factor (*fusA1*) and translation initiation factors IF-1 and IF-3 were down-regulated in transcriptomic response to spaceflight cultivation (Crabbé et al., 2011). Several enzymes involved in ribosomal protein translation (translation elongation factors TufA, Tsf) were more abundantly represented in proteomic analysis of cells of *C. metallidurans* after the exposure to spaceflight within the MESSAGE experiments (Leys et al., 2009).

The elevated level of translation-related genes and proteins (**Figure 2**) can support the higher abundances of proteins related to the metabolic and stress responses in microorganisms exposed to space conditions.

Transcription

One of the most noteworthy and challenging matters in the understanding of the effects of space environmental factors is

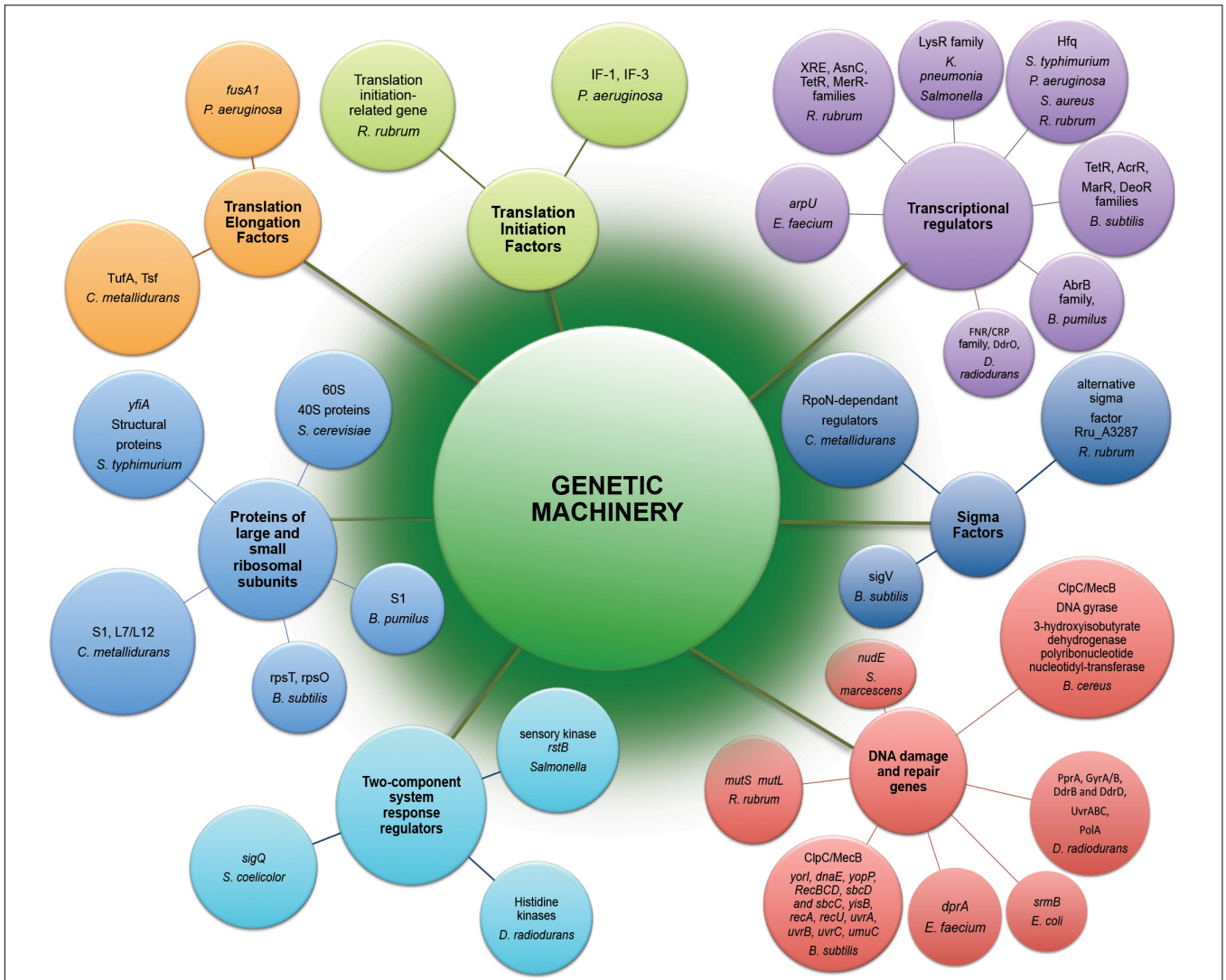

FIGURE 2 | Genetic machinery implicated in molecular response to exposure of microorganisms to the outer space environment. Represented are differently expressed genes and differently abundant proteins of microorganisms exposed to real and simulated space conditions (**Table 1**) revealed by means of –omics assisted methodological approaches.

the identification of global master regulators of space-induced response (**Figure 2**), that serve to globally reprogram microbial physiology in order to permit the adaptation of microorganisms to the space environment.

Transcriptomic analysis of *R. rubrum* (Mastroleo et al., 2009) cultivated aboard spacecraft, *B. subtilis* (Nicholson et al., 2012) and *B. pumilus* (Vaishampayan et al., 2012) spores exposed to outer space conditions and *Salmonella* in LSMMG conditions (Wilson et al., 2002) revealed a wide repertoire of transcriptional regulators involved in response to a long-term exposure to outer space. Interestingly, genomic analysis of *E. faecium* (Chang et al., 2013a) and *K. pneumonia* (Guo et al., 2015) mutant strains after spaceflight identified point mutations in genes encoding transcriptional regulators, including *arpU* gene that plays a role in cell wall growth and division by controlling the muramidase-2 export (Chang et al., 2013a). Remarkably high in *B. subtilis* spores exposed to simulated and real space conditions was 24- to 29-fold up-regulation of *fruR* transcriptional repressor of *fru* operon (DeoR family), which is implicated in metabolism of carbohydrates triggered in majority of space exposed microorganisms (Nicholson et al., 2012). Transcriptional regulator of AbrB family responsible for the repression of various starvation-induced differentiation processes was up-regulated in proteomic analysis of space-exposed spores of *B. pumilus* (Vaishampayan et al., 2012). The elevated transcript levels of several of *B. subtilis* master regulators were revealed in transcriptomic analysis; the stimulation of these master stress-responsive genes was higher in space-exposed spores of *B. subtilis*, than in spores exposed to simulated Mars environment (Nicholson et al., 2012).

Apart from the transcription factors, the *rstB* gene encoding a putative membrane sensory kinase was identified in microarray

analysis of *Salmonella* LSMMG response (Wilson et al., 2002), acting as part of a two-component system to accomplish signal transduction and reprogram the cell physiology in conditions of LSMMG. Multi-omics analyses of *B. subtilis*, *C. metallidurans*, *R. rubrum*, and *S. coelicolor* identified several sigma factors involved in response to the space conditions (Leys et al., 2009; Mastroleo et al., 2009; Nicholson et al., 2012; Huang et al., 2015). Proteometabolomic analysis of *D. radiodurans* exposed to simulated space conditions showed the involvement of the transcriptional regulator of FNR/CRP family and DdrO, the transcriptional regulator of HTH_3 family in response to UVC/vacuum combined stress (Ott et al., 2017). The RNA chaperone and global regulator Hfq (Sauter et al., 2003; Vogel and Luisi, 2011; Sauer, 2013) has been directly involved in mechanisms of spaceflight and LSMMG microbial responses (Wilson et al., 2007, 2008; Mastroleo et al., 2009; Castro et al., 2011; Crabbé et al., 2011) (**Figure 2**). Apart from the highly abundant transcriptional regulator of FNR/CRP family, specific histidine kinases might be also involved in the regulation of vacuum stress response in *D. radiodurans* as suggested by proteomic analysis (Ott et al., 2019b).

The adaptation of microorganisms to the spaceflight conditions and microbial survivability in the outer space environment is realized in the complex of responses, which are controlled under the regulation of specific genetic elements – master regulators of transcriptional response. The –omics based analyses revealed a number of upstream transcriptional regulators which affect downstream gene expression activity in response to space environmental parameters.

DNA Replication, Recombination, and Repair

Extremophilic microorganisms in the outer space environment tolerate radiation stress and cope with radiation-induced DNA damage by means of their DNA repair molecular machinery (**Figure 2**). A comparative multi-omic analysis of *B. cereus* and *E. faecium* strains after spaceflight (Chang et al., 2013a; Su et al., 2014) and transcriptomic analysis of *B. subtilis* long-termly exposed to simulated Martian and real outer space conditions (Nicholson et al., 2012) showed that the functional category of DNA replication, recombination, and repair was among the most abundantly represented categories of proteins and genes differently transcribed in comparison with a control ground strains. The DNA mismatch repair genes *mutS* and *mutL* were up-regulated in transcriptomic response to space flight of *R. rubrum* (Mastroleo et al., 2009). Putative replicative DNA helicase (*yorI*) and DNA polymerase III alpha-subunit 3 (*dnaE*) were 3- to 14-fold up-regulated in space-exposed and simulated Mars-exposed *B. subtilis* spores (Nicholson et al., 2012). The *srmB* gene encoding DNA helicase was up-regulated in *E. coli* under simulated microgravity conditions (Arunasri et al., 2013). A number of other up-regulated genes associated with DNA repair and recombination were identified in transcriptional response of *B. subtilis* to real and simulated space conditions (**Figure 2**) (Nicholson et al., 2012). Especially remarkable was 44-fold up-regulation of the gene *umuC* (*yqjW*) encoding Y-family DNA polymerase, responsible for translesion bypass DNA repair in space-exposed *B. subtilis* spores (Nicholson et al., 2012).

A recent proteomic analysis of *D. radiodurans* exposed to simulated space conditions indicated the up-regulation of DNA damage response proteins PprA, GyrA/B, DdrB and DdrD in UVC/vacuum-affected cells, along with high constitutive RecA levels (Ott et al., 2017). Moreover, UVC/vacuum stress conditions stimulated a number of proteins involved in detoxification process and aimed to remove damaged nucleotides from *D. radiodurans* cells (e.g., UvrB, a helixase subunit of the DNA excision repair endonuclease complex, MutT/nudix, and MutS2 families proteins involved in mismatch excision repair). The abundances of the proteins (recQ and ruvABC) responsible for recombinational DNA repair and the Mrr restriction system protein were also significantly increased (Ott et al., 2017). Furthermore, an increase in proteins of the UvrABC nucleotide excision repair machinery and polymerase PolA was observed during the 1st hours of recovery *D. radiodurans* after 90 days of exposure to simulated vacuum conditions of Low Earth Orbit (proteomic-based analyses in Ott et al., 2019b).

Obviously, "space travelers" utilize a striking up-regulation of DNA damage response genes and proteins as an important strategy to cope with space radiation induced DNA damage. Various DNA damage response systems react in order to handle with the stressful situation caused by spaceflight, outer space exposure and simulated space conditions.

GENERAL CELLULAR RESPONSES

Among other characteristics of the influence of the space environment on microbial cell behavior and physiology are numerous stress responses, altered tellurium resistance, biofilm formation, sporulation and virulence of several opportunistic and obligate pathogenic microorganisms.

General Stress Response

Proteins of general stress response function to protect cells, restore damage to cellular and molecular structures (e.g., DNA, the cell envelope, and proteins), and to provide microorganisms the ability to recover from the stress they experience. Overexpression of stress response genes was observed by real-time-PCR in *E. coli* under modeled reduced gravity conditions (Vukanti and Leff, 2012), in proteomic response of *C. metallidurans* grown aboard spacecraft (Leys et al., 2009) and in multi-omics analysis of *R. rubrum* exposed to spaceflight and simulated microgravity (Mastroleo et al., 2009, 2013) (**Figure 3**). Induction of stress-responsive proteins with the function of stress/protein folding and oxidative stress has been shown in proteomic analysis of *S. cerevisiae* aboard Soyuz TMA-9 (Van Mulders et al., 2011). Systems for monitoring protein quality within the cell devoted to control protein damage and misfolding implement in transcriptomic-assisted stress response of *B. subtilis* to real space and simulated Martian conditions (Nicholson et al., 2012) and proteomic response of *S. cerevisiae* to microgravity conditions during short-term spaceflight (Van Mulders et al., 2011) (**Figure 3**). The increased abundances

FIGURE 3 | Stress responses experienced by microorganisms in outer space real and simulated conditions. Proteins and genes of numerous stress responses with altered abundance and expression after exposure of microorganisms (**Table 1**) to the outer space real and simulated environment.

of a number of chaperons and proteases were observed in proteomic response of *D. radiodurans* to UVC/vacuum (Ott et al., 2017), implying the involvement of proteolytic regulation and quality monitoring in response to simulated space conditions. An increased abundance of *S. cerevisiae* ubiquitin in microgravity conditions was detected in proteomic analysis, indicating an increased degradosome activity and suggesting that cells of exposed microorganisms are prone to experience protein damage and/or misfolding as a consequence of exposure to space parameters (Van Mulders et al., 2011).

Various heat shock proteins and numerous chaperone proteins are frequently more abundantly represented in exposed microorganisms. Being involved in diverse metabolic processes and responsible for protein folding, these proteins can prevent or reverse protein misfolding. By binding to proteins, which are misfolded and damaged in response to the outer space environmental stresses, these molecular chaperones can direct the misfolded proteins to the associated proteases for degradation. The elevated level of different types of proteases under the influence of space-associated environmental factors indicates the involvement of quality monitoring and proteolytic regulation in response to outer space environmental stress.

Oxidative Stress Response

Comparative -omics assisted investigations revealed various universal ROS scavengers, e.g., superoxide dismutase (SOD), and redox active proteins (peroxiredoxin, thiol peroxidase, thioredoxin, catalase, sulfoxide reductase MsrA) induced in "real" space-exposed spores of *B. pumilus* and *B. subtilis*;

E. coli, *R. rubrum*, and *S. typhimurium* on-board of spacecraft, and *D. radiodurans* exposed to space simulating conditions, manifesting the up-regulation of antioxidant defense mechanisms during long-term spaceflight (**Figure 3**) (Wilson et al., 2008; Mastroleo et al., 2009; Nicholson et al., 2012; Vaishampayan et al., 2012; Ott et al., 2017). The PerR regulon consisting of a cluster of genes, which are stimulated in response to oxidative stress, was activated in transcriptomic analysis of *B. subtilis* spores long-termly exposed to ionizing radiation, vacuum, and extreme desiccation in outer space (Nicholson et al., 2012). Being essential for the resistance to oxidative stress, SOD (Fukai and Ushio-Fukai, 2011) by scavenging the superoxide (O^{2-}) radical, provides an efficient antioxidant defense in conditions of outer space. In opposite to its bacterial counterpart under the long-term influence of real space factors, SOD from spaceflight microgravity-exposed yeast *S. cerevisiae* along with the other oxidative stress protein peroxiredoxin was down-regulated in proteomic analysis after short-time space flight (Van Mulders et al., 2011). Together with the suppression of enzymes involved in oxidative metabolism, SOD down-regulation in microgravity conditions may indicate the shift of *S. cerevisiae* to anaerobiosis during spaceflight. *P. aeruginosa* has also shown an adaptation to anaerobic mode of growth during spaceflight with a number of up-regulated genes involved in anaerobic metabolism (Crabbé et al., 2011). The increased abundances of ROS scavenging proteins, e.g., peroxidases and catalases, were observed in proteomic analysis of *D. radiodurans* exposed to simulated Low Earth Orbit vacuum conditions (Ott et al., 2019b). The stress response genes contribute to the increased antibiotic tolerance of *E. coli* in microgravity during spaceflight aboard the ISS, as suggested by RNA-Seq assisted analysis (Aunins et al., 2018).

Mining data from –omics-assisted studies clearly shows that antioxidant defense mechanisms are important part of microbial responses to cope with space-induced oxidative damage.

Osmotic Stress Response

Results of post-flight proteotranscriptomic analysis of *E. coli* and *R. rubrum* indicated the altered expression of a number of genes involved in solute transport and osmotic regulation (**Figure 3**) (Mastroleo et al., 2009; Li et al., 2015; Zhang et al., 2015). The osmoprotectant glycine betaine transporter ProX of *R. rubrum* has been indicated as one of the very few proteins up-regulated in proteomic response under the conditions of simulation of ISS-ionizing radiation (Mastroleo et al., 2009). Osmotically inducible proteins were among up-regulated proteins in proteomic analyses of *S. typhimurium* and *E. coli* after spaceflight (Wilson et al., 2007; Zhang et al., 2015). *S. typhimurium* grown in conditions of modeled microgravity displayed increased resistance to multiple environmental stresses, including resistance to osmotic stress (Wilson et al., 2002). Notably, metabolomics analysis of cells of *D. radiodurans* exposed to simulated space conditions revealed the elevated level of a palmitoyl-derivative of carnitine, a quaternary amine compound with various physiological effects (Ott et al., 2017). Carnitine is a compatible solute and important osmoprotectant, which can augment thermotolerance, cryotolerance and barotolerance, thus influencing bacterial survival in extreme conditions (Meadows and Wargo, 2015). This compatible solute can help to cope with osmotic stress as a damaging desiccation effect of vacuum (Horneck et al., 2010; Frosler et al., 2017) by binding additional water molecules, stabilizing proteins and cell membranes, and thus blocking complete desiccation of the cell. The up-regulation of O-Palmitoyl-L-Carnitine chloride was suggested to play a role in the defense of *D. radiodurans* against combined stress conditions of UVC and vacuum (Ott et al., 2017).

Space environmental parameters inflict a cellular stress state that has the characteristics similar to an osmotic stress. Along with an activation of cell wall-associated machinery and integrity pathways, the production of osmoprotective compounds (e.g., compatible solutes) that increase the osmotolerance serve as a microbial strategy to cope with outer space environmental stressors.

Tellurium Resistance

Tellurium resistance does not necessarily constitute a distinct resistance determinant in microorganisms, but it may represent a resulting effect of a specific metabolic function, such as oxidative stress response (Taylor, 1999; Chasteen et al., 2009). Post-flight analysis of tellurium resistance of *R. rubrum* sent to the ISS in frames of MELiSSA project and in conditions of modeled microgravity indicated an enhanced expression of genes involved in tellurium resistance in transcriptomic analysis (**Figure 3**) (Mastroleo et al., 2009). The tellurium resistance proteins TerB and TerZ are associated with the resistance of *E. coli* against various damaging agents (e.g., heavy metal ions and UV radiation), and contribute to the preservation of the intracellular reducing environment, probably by directly reversing disulfide bonds (Slade and Radman, 2011). Oxidative stress-responsive proteins within tellurium resistance operon in *D. radiodurans* were found to be up-regulated immediately after gamma-irradiation (Slade and Radman, 2011). Moreover, TerB and TerD were up-regulated in proteomic response of *D. radiodurans* exposed to UVC/vacuum simulated space conditions (Ott et al., 2017). The enhanced tellurium resistance of exposed microorganisms can be either linked to another metabolic function or a part of metal sensing stress response system.

Sporulation

Frequently, space microbiology concentrates on spore-forming bacteria such as *Bacillus* due to the remarkable resistance of their spores to harsh conditions (Nicholson et al., 2000). Antibiotic-producing and spore-forming *Streptomyces* also represent additional interest due to the modulation of secondary metabolites production in space environment. The sporulation process of microgravity exposed *S. coelicolor* was intensified during spaceflight, and increased accumulation of the gray spore pigment and the fastened transition from aerial hyphae to mature spores were observed on-board the SHENZHOU-8 spacecraft (Huang et al., 2015). Global transcriptional analysis revealed the differential expression of genes involved in morphological differentiation and development of streptomycetes, which are mainly linked to aerial hyphae

erection, sporulation, spore germination, cell wall structure, spore structure, and development-associated secondary sigma factors (Huang et al., 2015).

Proteotranscriptomic analysis of *B. cereus* after short-term spaceflight showed the down-regulation protein MreB, which determines rod-shape of *B. cereus* (Su et al., 2014). A number of genes involved in sporulation were induced in transcriptional analysis during germination of *B. subtilis* spores after the exposure to simulated Martian and real space conditions (Nicholson et al., 2012). Significant up-regulation of the *cgeAB* operon involved in maturation of the outermost spore layer together with increased transcript levels of genes encoding minor and major acid-soluble spore proteins has been observed in this study. The genes *cotG*, *cotT*, and *cotVWXY* encoding protein components of the spore coat, the *safAcoxA* operon responsible for spore morphogenesis and spore cortex formation, and *rapAphrA* operon which controls initiation of sporulation were also significantly up-regulated in *B. subtilis* (Nicholson et al., 2012). Comparative proteomics analysis indicated that the outer spore coat protein A was modulated in spores of *B. pumilus* exposed to the UV- space–and UV-Mars–conditions (Vaishampayan et al., 2012).

Sporulation is a widely used strategy that helps to various spore-forming microorganisms to adapt and survive in harsh conditions of outer space. –Omics-assisted investigations helped to reveal the various molecular components involved in sporulation across different microbial species after exposure to the space environment.

Pathogenicity, Virulence, and Biofilm Formation

The molecular mechanisms underlying alterations of microbial virulence in space conditions have been successfully resolved with using state-of-the-art –omics technologies (**Figure 4**). A number of studies report that potentially pathogenic microorganisms display altered virulence and pathogenicity in real space or simulated microgravity conditions (Leys et al., 2004; Chopra et al., 2006; Taylor, 2015). Microbial morphogenic alterations have been described coherent with the enhanced pathogenicity of exposed microbes. Human opportunistic pathogen *Candida albicans* exhibited a morphogenic switch consistent with enhanced pathogenicity in simulated microgravity conditions (Altenburg et al., 2008). Microgravity induced the increased frequency of filamentous forms that contributes to the virulence and budding abnormalities (aberrant budding and cell clumping phenotype) of *C. albicans* and *S. cerevisiae* (Altenburg et al., 2008; Van Mulders et al., 2011). Spaceflight-cultured *C. albicans* exhibited random budding phenotype in accordance with the gene expression data (Crabbé et al., 2013). Genomic response analysis indicated that the expression of a set of genes involved in cell polarity and budding was significantly altered in these yeasts in simulated microgravity conditions. The conserved genes responsible for cell budding and separation were similarly down-regulated in microgravity exposed *C. albicans* and *S. cerevisiae*, thus suggesting that conservation of the genetic response takes place between the two distant yeast species (Altenburg et al., 2008; Van Mulders et al., 2011). Significant reduction in the expression of these genes appears to be consistent with the aberrant budding and cell-clumping phenotype of microgravity exposed cells. Increased virulence of *S. typhimurium* cultivated in spaceflight was accompanied by bacteria cellular aggregation, clumping and extracellular matrix formation, which is coherent with biofilm production (Wilson et al., 2007). Concomitantly, expression of *Salmonella* genes involved in biofilm formation was altered in microarray analysis during spaceflight (Wilson et al., 2007). A number of genes related to biofilm formation were up-regulated in transcriptomic profiling of *B. subtilis* during spaceflight aboard the ISS, which can be connected to the oxygen availability the in liquid cultures under the microgravity influence (Morrison et al., 2019).

The strain of human pathogen *K. pneumonia* returned from a spaceflight exhibited elevated biofilm forming properties as an important virulence characteristic (Li et al., 2014). The amount of biofilm-associated compound stearic acid (Saravanakumari and Mani, 2010; Vecino et al., 2015; Ge et al., 2016) was significantly elevated in cells of *D. radiodurans* exposed to vacuum and UVC-radiation (Ott et al., 2017). Although the cells of *D. radiodurans* do not naturally produce stearic acid in big quantities under non-stressed conditions (Melin et al., 1998), the observed accumulation of this biofilm-associated compound may lead to the high survival of *D. radiodurans* in dry multilayers under UVC/vacuum combined stress by preserving the structural integrity of cell membranes in conditions of vacuum-induced dehydration.

RNA-binding global regulatory protein Hfq has been shown to coordinate a regulatory response in bacterial reprogramming during spaceflight, altering bacterial gene expression and virulence under the influence of spaceflight conditions (multi-omics analyses in Wilson et al., 2007, 2008; Mastroleo et al., 2009; Crabbé et al., 2011). *P. aeruginosa* and human pathogen *B. cereus* cultured in the microgravity environment of spacecraft responded with the induction of several genes encoding virulence factors (Crabbé et al., 2011; Su et al., 2014). The obtained results of –omics studies of biofilm formation, microbial virulence and pathogenicity in space conditions and future follow-up investigations should continue to deliver novel molecular candidates for pharmacological intervention to prevent and control infectious diseases and to identify novel targets for vaccines and therapeutic development in order to keep crewmembers safe and healthy. This will ultimately facilitate long-term interplanetary transfer and productive space exploration.

SPACE SYSTEMS BIOLOGY – A FRAMEWORK FOR INTEGRATION OF OUTER SPACE PARAMETERS WITH OMICS TECHNOLOGY AND JOINED MATHEMATICAL MODELING

The –omics based approach has recently opened a window for a deep insight into molecular machinery implicated in

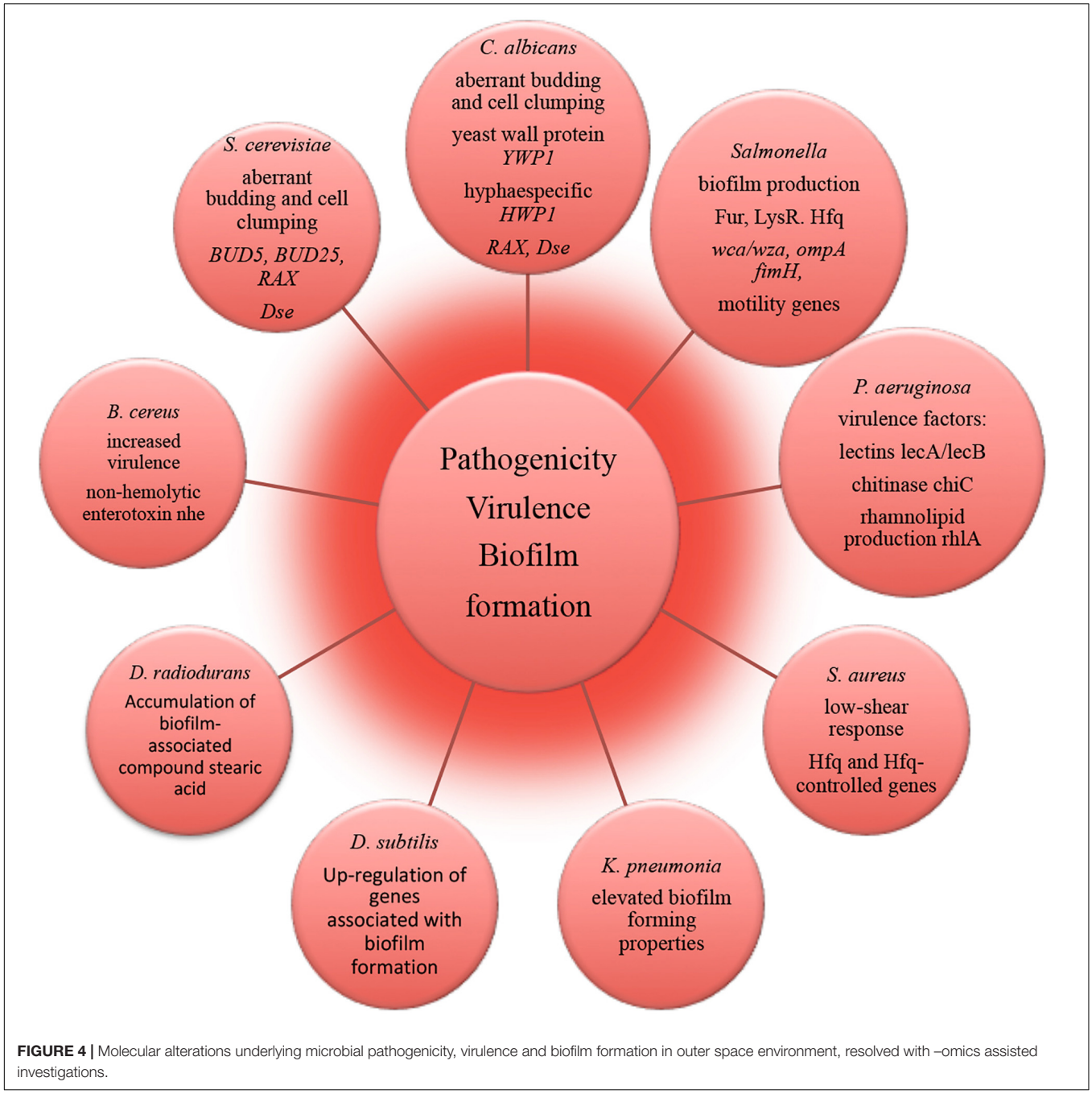

FIGURE 4 | Molecular alterations underlying microbial pathogenicity, virulence and biofilm formation in outer space environment, resolved with –omics assisted investigations.

survivability of space exposed microorganisms by revealing expression, metabolic functioning, and regulation of the genes and proteins encoded by the genomes of "space travelers." Metabolic alterations mediated by genetic regulations affect the diverse biological activities of space-exposed microorganisms (**Figure 1**). Space induced metabolic rearrangements trigger the restoration of energy status of exposed microbial cell (Mastroleo et al., 2009; Wang et al., 2014; Zhang et al., 2015). Frequently, the exposed microbial entity is posed in "energy saving mode" by the regulatory molecular network in order to reduce the need for synthesis of cellular material in non-growing cells and complement the increased energy demands for the maintenance of genetic stability and cellular integrity in the space environment. Several global regulatory molecules have been identified which orchestrate the molecular response of few space-exposed microorganisms (**Figure 2**). Of especial attention is a group of hypothetical proteins of "unknown function" which are often numerically abundantly represented in space responses (over 50% of space exposed *B. subtilis* genes) (Nicholson et al., 2012). One of the strategies to assign novel functions for these hypothetical proteins might be the exploration of new space-related environmental and stress conditions.

Experimental parameters during space exposure affect microbial survival rates and may lead to certain discrepancies in –omics assisted analysis of returned/exposed microorganisms. The composition of cultivation medium influences the microbial space response (Benoit and Klaus, 2007; Baker and Leff, 2006; Wilson et al., 2008), for instance, by providing specific antioxidants presented in rich medium, which may protect microbial cell against ionizing radiation. The majority of space experiments have been performed on-board of spaceflights, where microorganisms are cultivated in protected environment of spacecraft (**Table 1**). Only a few microbial species were exposed unprotected to real space conditions outside the ISS and then subsequently investigated with –omics techniques (Nicholson et al., 2012; Vaishampayan et al., 2012). There is an increasing demand in new space experiments to broad our knowledge of molecular mechanisms of microbial survivability under the conditions of real outer space or its selected parameters. Concomitantly, the design of space exposure experiments has to be critically assessed to accommodate sufficient number of independent biological repetitions enabling a comprehensive statistical analysis of obtained –omics data. This is an extremely necessary prerequisite to avoid artifacts during the evaluation of the multitude of effects of outer space environment on microorganisms. In many instances, a multi-omics post-flight analysis faces the problem of limited amount of the microbiological samples exposed to the space environment. In this connection, the development of valid technical approaches enabling simultaneous efficient extraction of DNA, RNA, proteins, and metabolites from a minimal amount of microbial cells is highly desirable to overcome this limiting step (Weckwerth et al., 2004; Valledor et al., 2014; Ott et al., 2017). Another important issue, which requires critical reassessment, is the frequent absence of detailed reports on the environmental conditions during space exposure of microorganisms and corresponding ground control experiments. Due to the high sensitivity of the –omics techniques used in post-flight analysis and the partial occurrence of uncontrolled conditions of the space experiments, the appearance of stress-related artifacts cannot be ruled out. Providing of a record of controlled parameters (e.g., temperature, humidity, pressure profiles) during flight, simulated, and control experiments is highly anticipated to achieve a comprehensive and artifacts-free analysis of the effects of the space environment on physiology and molecular machinery of microorganisms.

In addition to the proteotranscriptomic profiling, we propose that new space experiments should include a detailed

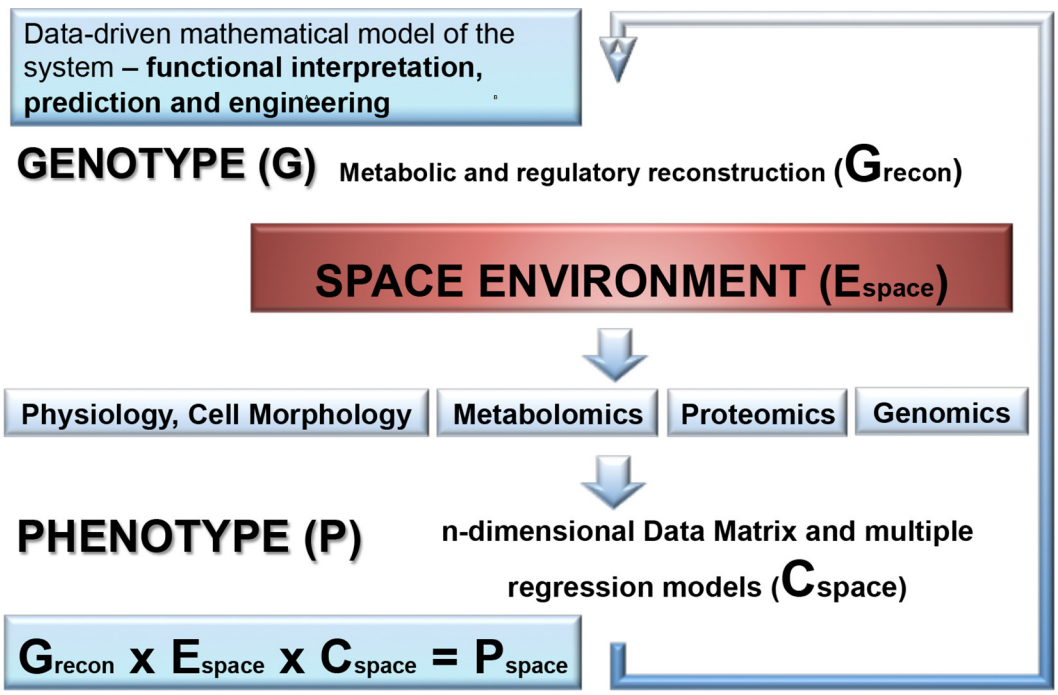

FIGURE 5 | A combination of molecular data with a genome-scale metabolic reconstruction of the microbial species exposed to the space environment. First, genome-scale metabolic and regulatory reconstruction of the respective microorganism is performed based on the available genome sequence and gene annotation information and results into a genotype matrix (G_{recon}). This provides the basic predictive metabolic model to eventually integrate statistical models of molecular data generated by OMICS technology, physiological and morphological data as well as environmental parameter which are accurately monitored in outer space conditions. The molecular and physio-morphometric data are correlated with environmental parameter by multiple regression methods and generate a comprehensive data covariance matrix times environmental data matrix ($C_{space} \times E_{space}$). The resulting data covariance model is eventually connected with the genotype matrix G_{recon} to generate a biomathematical data-driven regulatory and predictive model for the response trajectory of the microorganism in outer space conditions (P_{space}). Overall, this is an iterative process improving step by step the predictive models (for further information see Weckwerth et al., 2004; Weckwerth and Morgenthal, 2005; Weckwerth, 2011a, 2016, 2019; Sun and Weckwerth, 2012; Doerfler et al., 2013; Nägele et al., 2014, 2016; Sun et al., 2015).

metabolomic analysis of exposed microorganisms. This novel approach provides a rich source of new findings of fine molecular network regulating the space response (Ott et al., 2017, 2019a,b). Another aspect which is not yet addressed is the combination of molecular data with a genome-scale metabolic reconstruction of the respective species which is rather routine standard nowadays for the analysis of organisms (Weckwerth, 2011b). Summarizing the comprehensive review of metabolic alterations of microorganisms in space conditions reveals a multifactorial response trajectory which is not intuitively leading to a causal understanding. Thus, it is of utmost importance to integrate isolated biochemical parts into a global statistical and mathematical model. Here, we propose hybrid modeling approaches integrating statistical regression models and genome-scale metabolic reconstruction (Weckwerth, 2019). In **Figure 5** the proposed workflow for this hybrid modeling approach is shown: (i) for microorganisms with the available genome sequences genome-scale metabolic reconstruction is a straightforward approach (Thiele and Palsson, 2010; Weckwerth, 2011b); (ii) in a next step, –omics technology is applied as well as classical physiological and morphological parameter are measured to build a comprehensive statistical regression model of the response trajectory to environmental space conditions. Decisive for this regression model is the experimental design and the comprehensive monitoring of the environmental parameters. (iii) Finally, the statistical and the genome-scale models are joined by biomathematical approaches to represent a global model of metabolic regulation in outer space conditions (Weckwerth, 2019; Wilson et al., 2020). Based on a thorough hybrid modeling approach of the microbial systems in outer space as described above also metabolic engineering strategies can be developed upon revealing the elements of adaptation: from intrinsic protective mechanisms to elevated repair abilities, and a merging of these adaptation strategies.

AUTHOR CONTRIBUTIONS

Both authors conceived the review, conducted the literature search, created the figures, wrote and revised the final version of the manuscript.

FUNDING

The study was conducted within the MOMEDOS (Molecular Mechanisms of Deinococcus radiodurans survivability in Outer Space) project 854013, funded by the FFG (Österreichische Forschungsförderungsgesellschaft—https://www.ffg.at/, Austrian Space Applications Programme ASAP) to TM.

ACKNOWLEDGMENTS

The authors would like to acknowledge 18th EANA Conference European Astrobiology Network Association (Freie Universität Berlin, Germany, 24–28 September 2018) for giving a possibility to present partial data from this review article.

REFERENCES

Altenburg, S. D., Nielsen-Preiss, S. M., and Hyman, L. E. (2008). Increased filamentous growth of *Candida albicans* in simulated microgravity. *Genom. Proteom. Bioinf.* 6, 42–50. doi: 10.1016/S1672-0229(08)60019-4

Arunasri, K., Adil, M., Venu Charan, K., Suvro, C., Himabindu, R. S., and Shivaji, S. (2013). Effect of simulated microgravity on E. coli K12 MG1655 growth and gene expression. *PLoS One* 8:e57860. doi: 10.1371/journal.pone.s0057860

Aunins, T. R., Erickson, K. E., Prasad, N., Levy, S. E., Jones, A., Shrestha, S., et al. (2018). Spaceflight Modifies *Escherichia coli* gene expression in response to antibiotic exposure and reveals role of oxidative stress response. *Front. Microbiol.* 9:310. doi: 10.3389/fmicb.2018.00310

Baker, P. W., and Leff, L. (2006). Mir space station bacteria responses to modeled reduced gravity under starvation conditions. *Adv Space Res.* 38, 1152–1158. doi: 10.1111/j.1365-2672.2005.02593.x

Benoit, M. R., and Klaus, D. M. (2007). Microgravity, bacteria and the influence of motility. *Adv. Space Res.* 39, 1225–1232. doi: 10.1089/ast.2010.0536

Bertalanffy, L. V. (1940). Der organismus als physikalisches system betrachtet. *Naturwissenschaften* 33, 522–531.

Bertalanffy, L. V. (1969). General System Theory.

Blachowicz, A., Chiang, A. J., Elsaesser, A., Kalkum, M., Ehrenfreund, P., Stajich, J. E., et al. (2019). Proteomic and metabolomic characteristics of extremophilic fungi under simulated mars conditions. *Front. Microbiol.* 10:1013. doi: 10.3389/fmicb.2019.01013

Butt, A. T., and Thomas, M. S. (2017). Iron acquisition mechanisms and their role in the virulence of burkholderia species. *Front. Cell Infect. Microbiol.* 7:460. doi: 10.3389/fcimb.2018.00305

Castro, S. L., Nelman-Gonzalez, M., Nickerson, C. A., and Ott, C. M. (2011). Induction of attachment-independent biofilm formation and repression of Hfq expression by low-fluid-shear culture of Staphylococcus aureus. *Appl. Environ. Microbiol.* 77, 6368–6378. doi: 10.1128/AEM.00175-11

Chang, D., Zhu, Y., An, L., Liu, J., Su, L., Guo, Y., et al. (2013a). A multi-omic analysis of an Enterococcus faecium mutant reveals specific genetic mutations and dramatic changes in mRNA and protein expression. *BMC Microbiol.* 28:304. doi: 10.1186/1471-2180-13-304

Chang, D., Zhu, Y., Fang, X., Li, T., Wang, J., Guo, Y., et al. (2013b). Draft Genome Sequences of the Enterococcus faecium Strain LCT-EF258. *Genome Announc.* 1, e147–e112. doi: 10.1128/genomeA.00147-12

Chasteen, T. G., Fuentes, D. E., Tantaleán, J. C., and Vásquez, C. C. (2009). Tellurite: history, oxidative stress, and molecular mechanisms of resistance. *FEMS Microbiol. Rev.* 33, 820–832. doi: 10.1111/j.1574-6976.2009.00177.x

Chiang, A. J., Malli Mohan, G. B., Singh, N. K., Vaishampayan, P. A., Kalkum, M., and Venkateswaran, K. (2019). Alteration of proteomes in first- generation cultures of Bacillus pumilus spores exposed to outer space. *mSystems* 4:e00195-19. doi: 10.1128/mSystems.00195-19

Chopra, V., Fadl, A. A., Sha, J., Chopra, S., Galindo, C. L., and Chopra, A. K. (2006). Alterations in the virulence potential of enteric pathogens and bacterial-host cell interactions under simulated microgravity conditions. *J. Toxicol. Environ. Health* 69, 1345–1370. doi: 10.1080/15287390500361792

Cockell, C. S., Rettberg, P., Rabbow, E., and Olsson-Francis, K. (2011). Exposure of phototrophs to 548 days in low Earth orbit: microbial selection pressures in outer space and on early earth. *ISME J.* 5, 1671–1682. doi: 10.1038/ismej.2011.46

Crabbé, A., Nielsen-Preiss, S. M., Woolley, C. M., Barrila, J., Buchanan, K., McCracken, J., et al. (2013). Spaceflight enhances cell aggregation and random budding in *Candida albicans*. *PLoS One* 8:e80677. doi: 10.1371/journal.pone.0080677

Crabbé, A., Schurr, M. J., Monsieurs, P., Morici, L., Schurr, J., Wilson, J. W., et al. (2011). Transcriptional and proteomic responses of *Pseudomonas aeruginosa*

PAO1 to spaceflight conditions involve Hfq regulation and reveal a role for oxygen. *Appl. Environ. Microbiol.* 77, 1221–1230. doi: 10.1128/AEM.01582-10

Doerfler, H., Lyon, D., Nägele, T., Sun, X., Fragner, L., Hadacek, F., et al. (2013). Granger causality in integrated GC-MS and LC-MS metabolomics data reveals the interface of primary and secondary metabolism. *Metabolomics* 9, 564–574. doi: 10.1007/s11306-012-0470-0

Duscher, A. A., Conesa, A., Bishop, M., Vroom, M. M., Zubizarreta, S. D., and Foster, J. S. (2018). Transcriptional profiling of the mutualistic bacterium Vibrio fischeri and an hfq mutant under modeled microgravity. *NPJ Microgravity* 4:25. doi: 10.1038/s41526-018-0060-1

Frosler, J., Panitz, C., Wingender, J., Flemming, H. C., and Rettberg, P. (2017). Survival of deinococcus geothermalis in biofilms under desiccation and simulated space and martian conditions. *Astrobiology* 17, 431–447. doi: 10.1089/ast.2015.1431

Fukai, T., and Ushio-Fukai, M. (2011). Superoxide dismutases: role in redox signaling, vascular function, and diseases. *Antioxid. Redox Signal* 15, 1583–1606. doi: 10.1089/ars.2011.3999

Ge, X., Shi, X., Shi, L., Liu, J., Stone, V., Kong, F., et al. (2016). Involvement of NADH oxidase in biofilm formation in *Streptococcus sanguinis*. *PLoS One* 11:e0151142. doi: 10.1371/journal.pone.0151142

Goh, K., Chua, D., Beck, B., McKee, M. L., and Bhagwat, A. A. (2011). Arginine-dependentacid-resistance pathway in *Shigella* boydii. *Arch. Microbiol.* 193, 179–185. doi: 10.1007/s00203-010-0656-7

Guo, Y., Li, J., Liu, J., Wang, T., Li, Y., Yuan, Y., et al. (2015). Effects of Space Environment on Genome, Transcriptome, and Proteome of *Klebsiella pneumoniae*. *Arch. Med. Res.* 46, 609–618. doi: 10.1016/j.arcmed.2015.11.001

Guo, Y., Li, Y., Su, L., Chang, D., Liu, W., Wang, T., et al. (2014). Comparative genomic analysis of Klebsiella pneumonia (LCT-KP214) and a mutant strain (LCT-KP289) obtained after spaceflight. *BMC Genomics* 12:589. doi: 10.1186/1471-2164-15-589

Hall, H. K., and Foster, J. W. (1996). The role of fur in the acid tolerance response of *Salmonella* typhimurium is physiologically and genetically separable from its role in iron acquisition. *J. Bacteriol.* 178, 5683–5691. doi: 10.1128/jb.178.19.5683-5691.1996

Hantke, K. (1987). Selection procedure for deregulated iron transport mutants (fur) in *Escherichia coli* K 12: fur not only affects iron metabolism. *Mol. Gen. Genet.* 210, 135–139. doi: 10.1007/bf00337769

Hildebrandt, T., Knuesting, J., Berndt, C., Morgan, B., and Scheibe, R. (2015). Cytosolic thiol switches regulating basic cellular functions: GAPDH as an information hub? *Biol. Chem.* 396, 523–537. doi: 10.1515/hsz-2014-0295

Horneck, G., Klaus, D. M., and Mancinelli, R. L. (2010). Space microbiology. *Microbiol. Mol. Biol. Rev.* 74, 121–156. doi: 10.1128/MMBR.00016-09

Horneck, G., and Rabbow, E. (2007). Mutagenesis by outer space parameters other than cosmic rays. *Adv. Space Res.* 40, 445–454. doi: 10.1016/j.asr.2006.12.049

Horneck, G., Stöffler, D., Ott, S., Hornemann, U., Cockell, C. S., Moeller, R., et al. (2008). Microbial rock inhabitants survive hypervelocity impacts on Mars-like host planets: first phase of lithopanspermia experimentally tested. *Astrobiology* 1, 17–44. doi: 10.1089/ast.2007.0134

Huang, B., Liu, N., Rong, X., Ruan, J., and Huang, Y. (2015). Effects of simulated microgravity and spaceflight on morphological differentiation and secondary metabolism of Streptomyces coelicolor A3(2). *Appl. Microbiol. Biotechnol.* 99, 4409–4422. doi: 10.1007/s00253-015-6386-7

Ideker, T., Galitski, T., and Hood, L. (2001). A new approach to decoding life: systems biology. *Annu. Rev. Genom. Hum. G.* 2, 343–372. doi: 10.1146/annurev.genom.2.1.343

Kawaguchi, Y., Yang, Y., Kawashiri, N., Shiraishi, K., Takasu, M., Narumi, I., et al. (2013). The possible interplanetary transfer of microbes: assessing the viability of Deinococcus spp. under the ISS Environmental conditions for performing exposure experiments of microbes in the Tanpopo mission. *Orig. Life Evol. Biosph.* 43, 411–428. doi: 10.1007/s11084-013-9346-1

Kitano, H. (2000). Perspectives on systems biology. *New Gener. Comput.* 18, 199–216.

Lee, J. W., and Helmann, J. D. (2007). Functional specialization within the Fur family of metalloregulators. *Biometals* 20, 485–499. doi: 10.1007/s10534-006-9070-7

Leroy, B., Rosier, C., Erculisse, V., Leys, N., Mergeay, M., and Wattiez, R. (2010). Differential proteomic analysis using isotope-coded protein-labeling strategies: comparison, improvements and application to simulated microgravity effect on Cupriavidus metallidurans CH34. *Proteomics* 10, 2281–2291. doi: 10.1002/pmic.200900286

Levine, R. L., Moskovitz, J., and Stadtman, E. R. (2000). Oxidation of methionine in proteins: roles in antioxidant defense and cellular regulation. *IUBMB Life* 50, 301–307. doi: 10.1080/713803735

Leys, N., Baatout, S., Rosier, C., Dams, A., Heeren, C., Wattiez, R., et al. (2009). The response of Cupriavidus metallidurans CH34 to spaceflight in the international space station. *Antonie Van Leeuwenhoek* 96, 227–245. doi: 10.1007/s10482-009-9360-5

Leys, N. M., Hendrickx, L., De Boever, P., Baatout, S., and Mergeay, M. (2004). Space flight effects on bacterial physiology. *J. Biol. Regul. Homeost. Agents* 18, 193–199.

Li, J., Liu, F., Wang, Q., Ge, P., Woo, P. C., Yan, J., et al. (2014). Genomic and transcriptomic analysis of NDM-1 *Klebsiella pneumoniae* in spaceflight reveal mechanisms underlying environmental adaptability. *Sci. Rep.* 4:6216. doi: 10.1038/srep06216

Li, T., Chang, D., Xu, H., Chen, J., Su, L., Guo, Y., et al. (2015). Impact of a short-term exposure to spaceflight on the phenotype, genome, transcriptome and proteome of *Escherichia coli*. *Int. J. Astrobiology* 14, 435–444. doi: 10.1017/S1473550415000038

Liang, X., Zhang, L., Natarajan, S. K., and Becker, D. F. (2013). Proline mechanisms of stress survival. *Antioxid. Redox Signal* 20, 998–1011. doi: 10.1089/ars.2012.5074

Mastroleo, F., Van Houdt, R., Atkinson, S., Mergeay, M., Hendrickx, L., Wattiez, R., et al. (2013). Modelled microgravity cultivation modulates N-acylhomoserine lactone production in *Rhodospirillum rubrum* S1H independently of cell density. *Microbiology* 159, 2456–2466. doi: 10.1099/mic.0.066415-0

Mastroleo, F., Van Houdt, R., Leroy, B., Benotmane, M. A., Janssen, A., Mergeay, M., et al. (2009). Experimental design and environmental parameters affect *Rhodospirillum rubrum* S1H response to space flight. *ISME J.* 3, 1402–1419. doi: 10.1038/ismej.2009.74

Meadows, J. A., and Wargo, M. J. (2015). Carnitine in bacterial physiology and metabolism. *Microbiology* 161, 1161–1174. doi: 10.1099/mic.0.000080

Melin, A. M., Peuchant, E., Perromat, A., and Clerc, M. (1998). Sensitivity to oxidative damage of two Deinococcus radiodurans strains. *J. Appl. Microbiol.* 84, 531–537. doi: 10.1046/j.1365-2672.1998.00376.x

Minic, Z. (2015). Proteomic studies of the effects of different stress conditions on central carbon metabolism in microorganisms. *J. Proteomics Bioinform.* 8, 80–90. doi: 10.4172/jpb.1000355

Moeller, R., Reitz, G., The Protect Team Nicholson, W. L., and Horneck, G. (2012). Mutagenesis in bacterial spores exposed to space and simulated martian conditions: data from the EXPOSE-E spaceflight experiment PROTECT. *Astrobiology* 12, 457–468. doi: 10.1089/ast.2011.0739

Morgenthal, K., Wienkoop, S., Scholz, M., Selbig, J., and Weckwerth, W. (2005). Correlative GC-TOF-MS-based metabolite profiling and LC-MS-based protein profiling reveal time-related systemic regulation of metabolite-protein networks and improve pattern recognition for multiple biomarker selection. *Metabolomics* 1, 109–121.

Morrison, M. D., Fajardo-Cavazos, P., and Nicholson, W. L. (2019). Comparison of *Bacillus subtilis* transcriptome profiles from two separate missions to the international space station. *NPJ Microgravity* 5:1. doi: 10.1038/s41526-018-0061-0

Nägele, T., Furtauer, L., Nagler, M., Weiszmann, J., and Weckwerth, W. (2016). A strategy for functional interpretation of metabolomic time series data in context of metabolic network information. *Front. Mol. Biosci.* 3:6. doi: 10.3389/fmolb.2016.00006

Nägele, T., Mair, A., Sun, X., Fragner, L., Teige, M., and Weckwerth, W. (2014). Solving the differential biochemical Jacobian from metabolomics covariance data. *PLoS One* 9:e92299. doi: 10.1371/journal.pone.0092299

Nicholls, C., Li, H., and Liu, J. P. (2012). GAPDH: a common enzyme with uncommon functions. *Clin. Exp. Pharmacol. Physiol.* 39, 674–679. doi: 10.1111/j.1440-1681.2011.05599.x

Nicholson, W. L. (2009). Ancient micronauts: interplanetary transport of microbes by cosmic impacts. *Trends Microbiol.* 17, 243–250. doi: 10.1016/j.tim.2009.03.004

Nicholson, W. L., Moeller, R., Protect Team, and Horneck, G. (2012). Transcriptomic responses of germinating *Bacillus subtilis* spores exposed to 1.5

years of space and simulated martian conditions on the EXPOSE-E experiment PROTECT. *Astrobiology* 12, 469–486. doi: 10.1089/ast.2011.0748

Nicholson, W. L., Munakata, N., Horneck, G., Melosh, H. J., and Setlow, P. (2000). Resistance of Bacillus endospores to extreme terrestrial and extraterrestrial environments. *Microbiol. Mol. Biol. Rev.* 64, 548–572. doi: 10.1128/mmbr.64.3.548-572.2000

Orsini, S. S., Lewis, A. M., and Rice, K. C. (2017). Investigation of simulated microgravity effects on *Streptococcus mutans* physiology and global gene expression. *NPJ Microgravity* 3:4. doi: 10.1038/s41526-016-0006-4

Ott, E., Kawaguchi, Y., Kölbl, D., Chaturvedi, P., Yamagishi, N. K., et al. (2017). Proteometabolomic response of *Deinococcus radiodurans* exposed to UVC and vacuum conditions: initial studies prior to the *Tanpopo space* mission. *PLoS One* 12:e0189381. doi: 10.1371/journal.pone.0189381

Ott, E., Fuchs, F., Moeller, R., Hemmersbach, R., Kawaguchi, Y., Yamagishi, A., et al. (2019a). Molecular response of *Deinococcus radiodurans* to simulated microgravity explored by proteometabolomic approach. *Sci. Rep.* 9:18462. doi: 10.1038/s41598-019-54742-6

Ott, E., Kawaguchi, Y., Özgen, N., Yamagishi, A., Rabbow, E., Rettberg, P., et al. (2019b). Proteomic and metabolomic profiling of *Deinococcus radiodurans* recovering after exposure to simulated low earth orbit vacuum conditions. *Front. Microbiol.* 10:909. doi: 10.3389/fmicb.2019.00909

Palaniappan, C., Taber, H., and Meganathan, R. (1994). Biosynthesis of o-succinylbenzoic acid in *Bacillus subtilis*: identification of menD mutants and evidence against the involvement of the alpha-ketoglutarate dehydrogenase complex. *J. Bacteriol.* 176, 2648–2653. doi: 10.1128/jb.176.9.2648-2653.1994

Paulsen, C. E., and Carroll, K. S. (2013). Cysteine-mediated redox signaling: chemistry, biology and tools for discovery. *Chem. Rev.* 113, 4633–4679. doi: 10.1021/cr300163e

Rinaldo, S., Giardina, G., Mantoni, F., Paone, A., and Cutruzzolà, F. (2018). Beyond nitrogen metabolism: nitric oxide, cyclic-di-GMP and bacterial biofilms. *FEMS Microbiol. Lett.* 365:6. doi: 10.1093/femsle/fny029

Saffary, R., Nandakumar, R., Spencer, D., Robb, F. T., Davila, J. M., Swartz, M., et al. (2002). Microbial survival of space vacuum and extreme ultraviolet irradiation: strain isolation and analysis during a rocket flight. *FEMS Microbiol. Lett.* 215, 163–168. doi: 10.1111/j.1574-6968.2002.tb11386.x

Sancho, L. G., de la Torre, R., Horneck, G., Ascaso, C., de Los Rios, A., Pintado, A., et al. (2007). Lichens survive in space: results from the 2005 LICHENS experiment. *Astrobiology* 3, 443–454. doi: 10.1089/ast.2006.0046

Saravanakumari, P., and Mani, K. (2010). Structural characterization of a novel xylolipid biosurfactant from Lactococcus lactis and analysis of antibacterial activity against multi-drug resistant pathogens. *Biores. Technol.* 101, 8851–8854. doi: 10.1016/j.biortech.2010.06.104

Sauer, E. (2013). Structure and RNA-binding properties of the bacterial LSm protein Hfq. *RNA Biol.* 10, 610–618. doi: 10.4161/rna.24201

Sauter, C., Basquin, J., and Suck, D. (2003). Sm-like proteins in Eubacteria: the crystal structure of the Hfq protein from *Escherichia coli*. *Nucleic Acids Res.* 31, 4091–4098. doi: 10.1093/nar/gkg480

Selbmann, L., Zucconi, L., Isola, D., and Onofri, S. (2015). Rock black fungi: excellence in the extremes, from the Antarctic to space. *Curr. Genet.* 3, 335–345. doi: 10.1007/s00294-014-0457-7

Sirover, M. A. (2012). Subcellular dynamics of multifunctional protein regulation: mechanisms of GAPDH intracellular translocation. *J. Cell Biochem.* 113, 2193–2200. doi: 10.1002/jcb.24113

Sirover, M. A. (2014). Structural analysis of glyceraldehyde-3-phosphate dehydrogenase functional diversity. *Int. J. Biochem Cell Biol.* 57, 20–26. doi: 10.1016/j.biocel.2014.09.026

Slade, D., and Radman, M. (2011). Oxidative stress resistance in *Deinococcus radiodurans*. *Microbiol. Mol. Biol. Rev.* 75, 133–191. doi: 10.1128/MMBR.00015-10

Sturme, M. H., Kleerebezem, M., Nakayama, J., Akkermans, A. D., Vaugha, E. E., and de Vos, W. M. (2002). Cell to cell communication by autoinducing peptides in gram-positive bacteria. *Antonie Van Leeuwenhoek* 81, 233–243. doi: 10.1023/a:1020522919555

Su, L., Zhou, L., Liu, J., Cen, Z., Wu, C., Wang, T., et al. (2014). Phenotypic, genomic, transcriptomic and proteomic changes in Bacillus cereus after a short-term space flight. *Adv. Space Res.* 53, 18–29. doi: 10.1016/j.asr.2013.08.001

Sun, X., Langer, B., and Weckwerth, W. (2015). Challenges of inversely estimating jacobian from metabolomics data. *Front. Bioeng. Biotechnol.* 3:188. doi: 10.3389/fbioe.2015.00188

Sun, X., and Weckwerth, W. (2012). COVAIN: a toolbox for uni- and multivariate statistics, time-series and correlation network analysis and inverse estimation of the differential Jacobian from metabolomics covariance data. *Metabolomics* 8, 81–93. doi: 10.1007/s11306-012-0399-3

Taylor, D. E. (1999). Bacterial tellurite resistance. *Trends Microbiol.* 7, 111–115. doi: 10.1016/s0966-842x(99)01454-7

Taylor, P. W. (2015). Impact of space flight on bacterial virulence and antibiotic susceptibility. *Infect. Drug Resist.* 30, 249–262. doi: 10.2147/IDR.S67275

Thiele, I., and Palsson, B. O. (2010). A protocol for generating a high-quality genome-scale metabolic reconstruction. *Nat. Protoc.* 5, 93–121. doi: 10.1038/nprot.2009.203

Vaishampayan, P., Probst, A., Krishnamurthi, S., Ghosh, S., Osman, S., McDowall, A., et al. (2010). Bacillus horneckiae sp. nov., isolated from a spacecraft-assembly clean room. *Int. J. Syst. Evol. Microbiol.* 60, 1031–1037. doi: 10.1099/ijs.0.008979-0

Vaishampayan, P. A., Rabbow, E., Horneck, G., and Venkateswaran, K. J. (2012). Survival of Bacillus pumilus spores for a prolonged period of time in real space conditions. *Astrobiology* 12, 487–497. doi: 10.1089/ast.2011.0738

Valledor, L., Escandón, M., Meijón, M., Nukarinen, E., Cañal, M. J., and Weckwerth, W. (2014). A universal protocol for the combined isolation of metabolites, DNA, long RNAs, small RNAs, and proteins from plants and microorganisms. *Plant J.* 79, 173–180. doi: 10.1111/tpj.12546

Van Mulders, S. E., Stassen, C., Daenen, L., Devreese, B., and van Eijsden Siewers, V. (2011). The influence of microgravity on invasive growth in *Saccharomyces cerevisiae*. *Astrobiology* 11, 45–55. doi: 10.1089/ast.2010.0518

Vecerek, B., Moll, I., Afonyushkin, T., Kaberdin, V., and Bläsi, U. (2003). Interaction of the RNA chaperone Hfq with mRNAs: direct and indirect roles of Hfq in iron metabolism of *Escherichia coli*. *Mol. Microbiol.* 50, 897–909. doi: 10.1046/j.1365-2958.2003.03727.x

Vecino, X., Barbosa-Pereira, L., Devesa-Rey, R., Cruz, J. M., and Moldes, A. B. (2015). Optimization of extraction conditions and fatty acid characterization of Lactobacillus pentosus cell-bound biosurfactant/bioemulsifier. *J. Sci. Food Agric.* 95, 313–320. doi: 10.1002/jsfa.6720

Velayudhan, J., Castor, M., Richardson, A., Main-Hester, K. L., and Fang, F. C. (2007). The role of ferritins in the physiology of *Salmonella enterica* sv. Typhimurium: a unique role for ferritin B in iron-sulphur cluster repair and virulence. *Mol. Microbiol.* 63, 1495–1507. doi: 10.1111/j.1365-2958.2007.05600.x

Vogel, J., and Luisi, B. F. (2011). Hfq and its constellation of RNA. *Nat. Rev. Microbiol.* 15, 578–589. doi: 10.1038/nrmicro2615

Vukanti, R., and Leff, L. G. (2012). Expression of multiple stress response genes by *Escherichia coli* under modeled reduced gravity. *Microgravit. Sci. Tecnol.* 24, 267–279. doi: 10.1007/s12217-012-9310-0

Wang, Y., Yuan, Y., Liu, J., Su, L., Chang, D., Guo, Y., et al. (2014). Transcriptomic and proteomic responses of *Serratia marcescens* to spaceflight conditions involve large-scale changes in metabolic pathways. *Adv. Space Res.* 53, 1108–1117. doi: 10.1016/j.asr.2014.01.018

Wassmann, M., Moeller, R., Rabbow, E., Panitz, C., Horneck, G., Reitz, G., et al. (2012). Survival of spores of the UV-resistant Bacillus subtilis strain MW01 after exposure to low-earth orbit and simulated martian conditions: data from the space experiment ADAPT on EXPOSE-E. *Astrobiology* 5, 498–507. doi: 10.1089/ast.2011.0772

Weckwerth, W. (2003). Metabolomics in systems biology. *Annu. Rev. Plant. Biol.* 54, 669–689. doi: 10.1146/annurev.arplant.54.031902.135014

Weckwerth, W. (2011a). Green systems biology - From single genomes, proteomes and metabolomes to ecosystems research and biotechnology. *J. Proteomics.* 75, 284–305. doi: 10.1016/j.jprot.2011.07.010

Weckwerth, W. (2011b). Unpredictability of metabolism – the key role of metabolomics science in combination with next-generation genome sequencing. *Anal. Bioanal. Chem.* 400, 1967–1978. doi: 10.1007/s00216-011-4948-9

Weckwerth, W. (2016). *Systemtheoretische Konzepte der Genomweiten Molekularen Analyse und Datenintegration in der Biologie. Aus der Schriftenreihe der Hülsenberger Gespräche*. Hamburg: Heigener Europrint GmbH, 68–71.

Weckwerth, W. (2019). Toward a unification of system-theoretical principles in biology and ecology—the stochastic lyapunov matrix equation and its inverse application. *Front. Appl. Math. Stat.* 5:29. doi: 10.3389/fams.2019.00029

Weckwerth, W., and Morgenthal, K. (2005). Metabolomics: from pattern recognition to biological interpretation. *Drug Discov. Today* 10, 1551–1558. doi: 10.1016/S1359-6446(05)03609-3

Weckwerth, W., Wenzel, K., and Fiehn, O. (2004). Process for the integrated extraction, identification and quantification of metabolites, proteins and RNA to reveal their co-regulation in biochemical networks. *Proteomics* 4, 78–83. doi: 10.1002/pmic.200200500

Wilson, J. L., Nägele, T., Linke, M., Demel, F., Fritsch, S. D., Mayr, H. K., et al. (2020). Inverse data-driven modeling and multiomics analysis reveals phgdh as a metabolic checkpoint of macrophage polarization and proliferation. *Cell Rep.* 30, 1542–1552.e7. doi: 10.1016/j.celrep.2020.01.011

Wilson, J. W., Ott, C. M., Höner zu Bentrup, K., Ramamurthy, R., Quick, L., Porwollik, S., et al. (2007). Space flight alters bacterial gene expression and virulence and reveals a role for global regulator Hfq. *Proc. Natl. Acad. Sci. U.S.A* 104, 16299–163304. doi: 10.1073/pnas.0707155104

Wilson, J. W., Ott, C. M., Quick, L., Davis, R., Höner zu Bentrup, K., Crabbé, A., et al. (2008). Media ion composition controls regulatory and virulence response of *Salmonella* in spaceflight. *PLoS One* 3:e3923. doi: 10.1371/journal.pone.0003923

Wilson, J. W., Ramamurthy, R., Porwollik, S., McClelland, M., Hammond, T., Allen, P., et al. (2002). Microarray analysis identifies *Salmonella* genes belonging to the low-shear modeled microgravity regulon. *Proc. Natl. Acad. Sci. U.S.A.* 15, 13807–13812. doi: 10.1073/pnas.212387899

Zea, L., Larsen, M., Estante, F., Qvortrup, K., Moeller, R., Dias, et al. (2017). Phenotypic changes exhibited by *E. coli* cultured in space. *Front. Microbiol.* 8:1598. doi: 10.3389/fmicb.2017.01598

Zea, L., Prasad, N., Levy, S. E., Stodieck, L., Jones, A., Shrestha, S., et al. (2016). A molecular genetic basis explaining altered bacterial behavior in space. *PLoS One* 11:e0164359. doi: 10.1371/journal.pone.0164359

Zhang, X., Fang, X., and Liu, C. (2015). Genomic and proteomic analysis of *Escherichia coli* after spaceflight reveals changes involving metabolic pathways. *Arch. Med. Res.* 46, 181–185. doi: 10.1016/j.arcmed.2015.03.007

Zhao, B., and Houry, W. A. (2010). Acid stress response in enteropathogenic gammaproteobacteria: an aptitude for survival. *Biochem. Cell Biol.* 88, 301–314. doi: 10.1139/o09-182

Conflict of Interest: The authors declare that the research was conducted in the absence of any commercial or financial relationships that could be construed as a potential conflict of interest.

frontiers in Microbiology

ORIGINAL RESEARCH
published: 19 May 2020
doi: 10.3389/fmicb.2020.00948

Stromatolites as Biosignatures of Atmospheric Oxygenation: Carbonate Biomineralization and UV-C Resilience in a *Geitlerinema* sp. - Dominated Culture

*Rabja M. Popall[1], Henk Bolhuis[2], Gerard Muyzer[3] and Mónica Sánchez-Román[1]**

[1] Earth Sciences Department, Faculty of Science, Vrije Universiteit, Amsterdam, Netherlands, [2] Marine Microbiology & Biogeochemistry Department, Royal Netherlands Institute for Sea Research, Utrecht University, Den Hoorn, Netherlands, [3] Microbial Systems Ecology, Department of Freshwater and Marine Ecology, Institute for Biodiversity and Ecosystem Dynamics, University of Amsterdam, Amsterdam, Netherlands

Modern stromatolites are key to the record of past microbial activity preserved in fossil carbonate deposits. Mono-phototrophic cultures dominated by the cyanobacterium *Geitlerinema* sp. were obtained from a laboratory-maintained, low magnesium-calcite stromatolite originating from Lagoa Vermelha, Brazil. This lagoonal system has been described as a Precambrian analog, illustrating a period of photosynthetically induced atmospheric oxygenation, which created a global sanctuary from shortwave solar radiation and enabled the evolution of modern life on Earth. The enrichment cultures precipitate carbonates in minimal media, suggesting that cyanobacterial photosynthesis and extracellular polymeric substance production may be crucial in the mineralization of the studied stromatolite. We further show that *Geitlerinema* sp. can build and maintain filamentous mats under long-term UV-C exposure. Our results suggest that present day stromatolites dominated by cyanobacteria may be interpreted as biosignatures of atmospheric oxygenation and have implications for the search for putative biological traces on Mars.

Keywords: cyanobacteria, biomineralization, UV radiation, stromatolite, microbial carbonate, microbial mats, *Geitlerinema* sp., biosignatures

OPEN ACCESS

Edited by:
Akihiko Yamagishi, Tokyo University of Pharmacy and Life Sciences, Japan

Reviewed by:
Victoria Alexis Petryshyn, University of Southern California, United States
Crisogono Vasconcelos, ETH Zürich, Switzerland
Emmanuelle Gérard, UMR7154 Institut de Physique du Globe de Paris (IPGP), France
Fumito Shiraishi, Hiroshima University, Japan

****Correspondence:***
Mónica Sánchez-Román
m.sanchezroman@vu.nl;
sanchezromanmonica@gmail.com

Specialty section:
This article was submitted to Microbiological Chemistry and Geomicrobiology, a section of the journal Frontiers in Microbiology

Received: *21 October 2019*
Accepted: *21 April 2020*
Published: *19 May 2020*

Citation:
Popall RM, Bolhuis H, Muyzer G and Sánchez-Román M (2020) Stromatolites as Biosignatures of Atmospheric Oxygenation: Carbonate Biomineralization and UV-C Resilience in a Geitlerinema sp. - Dominated Culture. Front. Microbiol. 11:948. doi: 10.3389/fmicb.2020.00948

INTRODUCTION

Stromatolites are the oldest known fossil records of life on Earth. The organo-sedimentary structures are formed by complex interactions between microbial mat communities and their geochemical environment, thus providing insight into the ecosystem at the time of their genesis to approximately 3.5 Ga ago in the early Archean (Vasconcelos and McKenzie, 2009; Vasconcelos et al., 2014). Stromatolite abundance peaked in the Proterozoic and strongly decreased toward the Cambrian. This decline is attributed to the occurrence of metazoan grazers that started to put trophic pressure on microbial mats (Awramik, 1971). Next to predation, a decrease in sea

water carbonate saturation as well as increasingly complex ecosystems with niche diversification and eukaryotic competition are considered to have impacted stromatolite abundance after the Mesoproterozoic (Monty, 1973; Grotzinger, 1990; Riding, 2006). The rare modern stromatolites feature active microbial mat communities forming lithified discrete buildups, and can only be found in few natural environments (Foster et al., 2009; Suosaari et al., 2016). Those habitats are often characterized by an elevated salinity sheltering biofilms from animal grazing and continuous sediment disturbance (Douglas and Beveridge, 1998; Schieber, 2007). In accordance with their shallow aquatic environment, most of the extant stromatolites contain calcareous compounds. They are of great importance to the interpretation of ancient stromatolites and key to their record of past microbial activity forming lithified deposits (Decho and Kawaguchi, 2003; Vasconcelos et al., 2006; Vasconcelos and McKenzie, 2009; Kaźmierczak et al., 2015).

The functionally and structurally diversified modern stromatolites feature comprehensive communities in distinct layers (Vasconcelos and McKenzie, 2009). Comprising complete cycles of C, N, and S, microbial mats form a nearly closed minimal ecosystem and include the major functional groups of oxygenic photosynthetic primary producers (Cyanobacteria), aerobic heterotrophs, sulfur oxidizers, and anaerobic sulfate reducers along a vertical O_2 gradient (Visscher and Stolz, 2005). By definition, stromatolite growth is promoted "through accretion of laminae by the entrapment of sediment and by participation of carbonate, under active secretion or direct influence of microorganisms" (Altermann, 2008). The mechanism of trapping and binding sediment particles in the microbial mat is less significant in ancient carbonate stromatolites due to the lack of detritus from higher life forms in the Precambrian complementing carbonate sources of micrite and erosion, although some Archean microorganisms secreted envelopes of biopolymers which might be identical to extracellular polymeric substances (EPS) incorporating sedimentary material in present day biofilms (Kazmierczak, 2002). More relevant for such early stromatolites, however, is the biomineralization of calcite, aragonite, and dolomite by the microbial community (Kaźmierczak et al., 2015). Modern environments characterized by an increased salinity and absence of eukaryotic grazers and bioturbators (Vasconcelos et al., 2006), as well as alkaline lake (Kazmierczak and Kempe, 2006) and hot spring (Konhauser et al., 2001; Phoenix et al., 2006) stromatolites, likewise promote autochthonous input of material and are thus considered good textural analogs to Precambrian systems. In contrast, coarsely laminated structures such as Bahamian and Shark Bay stromatolites feature a relevant ratio of allochthonous grains in addition to *in situ* precipitation (Fairchild, 1991). The accumulation of autochthonous carbonates in a mat is the net result of precipitation and counterbalancing dissolution preceding diagenesis and amalgamation with the lithified stromatolite deposit (Visscher and Stolz, 2005). Carbonate precipitation is interpreted as a byproduct of photosynthetic and sulfate reducing metabolism promoting biomineral supersaturation in alkaline microenvironments (Visscher et al., 1998; Kaźmierczak et al., 2015), but only possible on suitable nucleation sites further reducing kinetic barriers (Kamennaya et al., 2012). An ideal matrix for crystal nucleation are the amphiphilic EPS, which feature a high uronic acid content and are suitable for binding both Mg/Ca cations and carbonate anions (Decho and Kawaguchi, 2003; Dittrich and Sibler, 2010). Top-layer cyanobacteria are not only photosynthetically active, but also the primary EPS producers of the system (Decho and Kawaguchi, 2003). This renders them key players contributing majorly to carbonate deposition in modern lithifying mats.

Molecular traces in the lithified stratum of previously studied stromatolites also confirm a significant contribution of sulfate reduction to lamina formation (Vasconcelos et al., 2014). A prominent sulfur cycle, however, was only established as a result of emerging oxygenic photosynthesis during the Great Oxygenation Event (GOE) (Canfield and Raiswell, 1999). While anaerobic photosynthesizers were most likely relevant for the formation of pre-GOE stromatolites (Bosak et al., 2007), the massive proliferation of oxygenic cyanobacteria facilitated a tremendous diversification of life and an increasingly oxygenated atmosphere (Shestakov and Karbysheva, 2017). During the simultaneous establishment of an atmospheric ozone shield, light-dependent cyanobacteria were exposed to the extremely damaging shortwave spectrum of ultraviolet (UV) solar radiation (Garcia-Pichel, 1998). Sedimentary habitats may have additionally aggravated the damaging effect of UV-C due to light-trapping effects, resulting in cyanobacterial mats developing highly effective adaptions such as chemical protectants, DNA repair mechanisms and phototaxis, a behavioral mechanism preserved in fossil stromatolites (Garcia-Pichel, 1998). The role of UV-C resilient cyanobacteria in the evolution of aerobic modern life-forms is not only of paleontological interest, but also significant to understand a possible existence of life on Mars. The finding of organic carbon on Mars recently sparked a new discussion on potential traces of past Martian biota (Eigenbrode et al., 2018). Present surface conditions on Mars are comparable to the ones of early Earth, neither providing an aerobic environment nor protection from UV-C wavelengths (Cockell, 2000). A stromatolitic record of oxygenic cyanobacterial photosynthesis may therefore be key to terraforming approaches as well.

Here, we studied a natural stromatolite maintained under controlled laboratory conditions originating from Lagoa Vermelha, Brazil. The formation of magnesium calcite and dolomite deposits in Lagoa Vermelha is the result of a unique biochemical environment considered to represent the shallow marine systems of early Earth (Vasconcelos et al., 2006). Bordering the South Atlantic, Lagoa Vermelha is part of a large lagoonal site. The proximity of an Atlantic upwelling zone accounts for semi-arid conditions, while periodical changes in surface area and water chemistry are enforced by a mean depth of 2 m (Vasconcelos et al., 2006; Spadafora et al., 2010). The microbial mats of Lagoa Vermelha and other modern stromatolites are essential to understand the biotic mechanisms of carbonate deposition in past systems. In consideration of this relationship, we analyze the microbial community composition by 16S rRNA gene amplicon sequencing and

carbonate deposition using stable C and O isotope analysis. Additional experiments were performed with *Geitlerinema* sp. enrichments to test their ability to mineralize carbonate and grow under long-term UV-C radiation.

MATERIALS AND METHODS

Origin and Sampling of the Studied Stromatolite

The studied stromatolite has been kept at room temperature in a hypersaline (>7% salt) aquarium at ETH Zurich, Switzerland, and currently at the Vrije Universiteit in Amsterdam, the Netherlands, for a total period of 15 years. An approximately 0.5 cm deep, 3 cm tall and 7 cm wide slice of the microbial mat was cut from the stromatolite (**Figure 1**). The biofilm covering the top layer was carefully removed to avoid potential contamination with non-associated algae. The slice was subdivided into smaller pieces according to the intended use and stored in saline solution if not immediately processed. An initial assessment of the nature of the phototrophic community was performed by fluorescence microscopy to distinguish between Chlorophyll *a* containing micro-eukaryotic alga and phycoerythrin containing cyanobacteria. Chlorophyll *a* was visualized using the Carl Zeiss Filter Set 09 (excitation 450–490 nm, emission 515 nm) and phycoerythrin was visualized using the Carl Zeiss Filter Set 20 (excitation 546 nm, emission 575–640 nm).

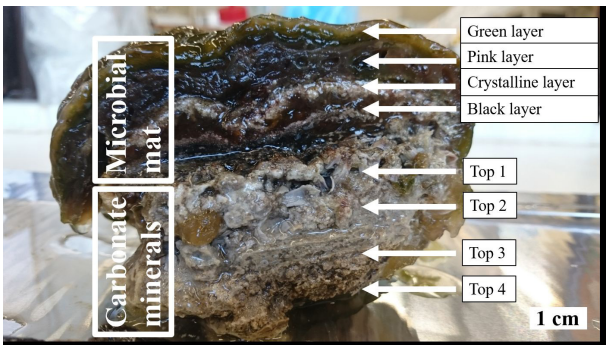

FIGURE 1 | Cross section of the studied stromatolite illustrating the layered microbial mat, which embeds the crystalline layer of unconsolidated precipitates, and relevant zones of the carbonate deposit below. The top green layer generally features photosynthetic cyanobacteria producing primary OM to be consumed by aerobic heterotrophic bacteria in the uppermost part of the layer below. The diverse community of this zone moreover comprises autotrophs, especially the purple sulfur bacteria which give the layer its characteristic pink color and are capable of microaerophilic or anoxygenic photosynthesis in the deeper parts of the zone. Below the distinct layer of unconsolidated precipitates composed of carbonate minerals such as magnesium calcite and/or dolomite, the community is dominated by strictly anoxic conditions and salvages (in-)organic metabolic products of the upper layers in association with less pronounced crystal deposits. The most prominent process in this black layer is sulfate reduction, next to obligate fermentation and other anoxygenic heterotrophy. The carbonate deposit in the lower half of the stromatolite comprises granulated as well as more compact strata toward the bottom.

Community Composition of Microbial Mat Layers

The microbial mat was dissected into four distinctive layers: The green top layer, the pink layer below, the crystalline layer, and the black bottom layer (**Figure 1**). All outer parts that were exposed to the external medium were thinly sliced off to avoid contamination. DNA was extracted from each layer using the MoBio PowerSoil DNA Isolation Kit with intensive bead beating for three cycles of 10 s beating at 3.5 m/s intensity and 40 s pause using the Omni Ruptor 24 Elite bead mill homogenizer (Omni Int., United States). 16S rRNA library preparation and Illumina sequencing were subsequently performed at BGI, China using bacterial (341F: ACTCCTACGGGAGGCAGCAG & 806R: GGACTACHVGGGTWTCTAAT) and archaeal (Arch349F: GYGCASCAGKCGMGAAW & Arch806R: GGACTACVSGGGTATCTAAT) specific 16S rRNA primers amplifying the V3-V4 region. Archaeal and bacterial sequences were clustered at a 95% sequence identify cutoff following the recommendations by Cardoso et al. (2017) and annotated following the QIIME version 1 pipeline (Caporaso et al., 2010) using the SILVA version 132 reference database (Quast et al., 2013). OTU abundances were normalized to relative abundance in percentage. The sequencing data is deposited in the NCBI small read archive and listed under BioProject ID PRJNA610984.

Unconsolidated and Lithified Carbonates

The morphology of unconsolidated precipitates was analyzed via scanning electron microscopy (SEM), while the chemical elemental composition was assessed with energy dispersive X-ray spectroscopy (EDS). Samples from the crystalline layer (**Figure 1**) were rinsed with ultrapure water and dried for 2 days at room temperature (RT). To remove halite residues, samples for later SEM runs were soaked in ultrapure water overnight. Additionally, the material was washed in ultrapure water and centrifuged at 10,000 × *g*, which was repeated five times. The final pellet was dried at RT. Microscopical analyses were conducted on a FEI Helios Nanolab G3 FIB-SEM. The samples were previewed under an optical microscope, fixed on mounts and coated with a platinum film of 5 nm thickness, before being observed in secondary electron mode at an accelerating voltage of HV = 10 kV and an emission current of 6.3 pA. Both unconsolidated precipitates and lithified deposit were further studied for C and O stable isotopes. The crystalline layer as well as four porous to compact laminae of the carbonate deposit ranked from top to bottom (**Figure 1**) were sampled, soaked in ultrapure water for 2 days and subsequently dried in an oven at 40°C. Isotope $\delta^{13}C$ and $\delta^{18}O$ values were established in relation to the Vienna Pee Dee Belemnite (VPDB) standard on a Finnigan MAT253 mass spectrometer using the Gasbench II. Sample size was corrected using the Vrije Universiteit Amsterdam in house carbonate standard (VICS), while the international IAEA-603 was measured as a control standard. The long-term standard deviation of the routinely analyzed in-house standard is <0.1‰ (1σ) for both carbon and oxygen isotope ratios. Isotopic values were established in four samples per layer.

Carbonate Biomineralization in a Cyanobacterium-Dominated Culture

Cultivation in Solid and Liquid Medium Under Promotion of Carbonate Biomineralization

A sample of the microbial mat was horizontally cut along the crystalline layer. The upper half consisting of green and pink layers was aerobically incubated in room-tempered sterile hypersaline solution under natural lighting. After 7 days, the culture was inoculated to ASN-III-CS growth medium plates ($n = 15$). The original ASN-III medium composition after Rippka et al. (1979) was modified to promote calcium/magnesium carbonate biomineralization and optimized over the course of the study. Additionally, the preparation procedure was adapted to avoid abiotic calcium carbonate precipitation (**Supplementary Table S1**). The cultures were incubated at 30°C and subjected to artificial illumination (40 W LED at 40 cm distance) in a 12 h light/12 h dark rhythm. After 10 weeks, each plate was individually wrapped in a translucent plastic bag to avoid agar desiccation. The plastic bags were punctured with a needle to allow gas exchange. Three weeks post-observation of cyanobacterial cultures, liquid ASN-III-CL medium (**Supplementary Table S1**) was inoculated with filamentous cell material from the agar cultures ($n = 3$). A sterile microscope slide was added to provide a retrievable surface for cellular growth and carbonate nucleation. The liquid cultures were incubated aerobically at 30°C and exposed to artificial illumination (40 W LED at 40 cm distance) in a 12 h light/12 h dark rhythm. Cell material was scraped from ASN-III-CS agar grown cultures for molecular analysis. DNA extraction, 16S amplicon sequencing and taxonomic assignment were performed as described above.

Identification of Carbonate Precipitates

Crystal nucleation and maturation were monitored with an optical microscope, while established carbonate crusts were analyzed via SEM-EDS. Cell material and carbonate crust were scraped off the agar in ASN-III-CS cultures and centrifuged for 90 s at 10,000 × *g*. The pellet was washed in ultrapure water and centrifuged at 10,000 × *g*, which was repeated three times. The pellet was then dried at RT. The material was put on mounts and coated with platinum as described above. Carbonate crusts from solid ASN-III-CS and organic material from liquid ASN-III-CL culture were furthermore assessed with transmission electron microscopy (TEM), EDS and electron diffraction (ED). One milliliter of cellular material settled on the microscope slide was sampled from liquid cultures and centrifuged for 10 min at 8,000 × *g* according to the preparation protocol in Benzerara et al. (2014). Subsequently, the pellet was washed with ultrapure water by centrifuging three times at 8,000 × *g* and resuspended in 200 µl of ultrapure water. All samples were treated ultrasonically in a bath sonicator for 60 s. 5 µl of dispersion were pipetted on a glow discharged TEM-grid for analysis on a FEI Talos F200X TEM. Material from solid cultures was examined in TEM bright field mode, while liquid cultures were additionally analyzed in STEM dark field mode and tilted between 30° and 60° if applicable. EDS was conducted to assess the elemental composition of sample compounds and ED to assign a crystalline or amorphous character. In addition, carbonate crusts from solid cultures were subjected to stable isotope analysis. Sample preparation and determination of $\delta^{13}C$ and $\delta^{18}O$ values was performed as described above.

Cyanobacterial Growth Under UV-C Radiation Stress

Free-floating cell material from liquid ASN-III-CL cultures was transferred to sterile saline solution which was used as inoculum for glass beakers containing solid ASN-III-US or liquid ASN-III-UL medium (**Supplementary Table S1**). The beakers were covered in a plastic wrap punctured with a fine needle to allow gas exchange. A sterile microscope slide was added to the liquid cultures as retrievable surface for cellular growth. Both solid ($n = 5$) and liquid ($n = 5$) cultures plus a negative control without bacterial cells each were placed in a laminar flow chamber beneath a UV-C tube (15 W, peak at 250 nm) mounted at 40 cm distance from the surface of the culture medium. The cultures were subjected to 12 h of both continuous UV-C and photosynthetically active radiation (PAR) combined (40 W LED, also at 40 cm distance), followed by 12 h of darkness, for a total period of 6 weeks. To avoid natural light exposure throughout the day, the chamber was completely covered in tinfoil. A control series, consisting of five solid and five liquid cultures with cells and one solid and one liquid culture without bacterial cells, was placed in an opaque box and exposed to PAR exclusively for 12 h light/12 h dark. Four weeks after the start of the experiment, one of the positive agar controls was added to the UV-C exposed experiment to monitor UVR effect on intact cyanobacterial mats. In response to the appearance of red precipitate in the liquid UVR-exposed experiments, negative controls of ASN-III-UL medium and sterile demineralized water covered in non-punctured plastic wrap were added to examine external contamination. Samples of red precipitate from a culture experiment were centrifuged at 10,000 × *g* for 90 s. The pellet was washed three times in ultrapure water and resuspended in 200 µl. The material was further prepared for TEM-EDS as described above before being examined in TEM bright field mode for imaging and with an EDS detector for elemental analysis. Cyanobacterial mat cover was monitored over a period of 6 weeks in all cultures. Organic material (OM) was prepared for and assessed via TEM-EDS and ED as described above.

RESULTS

Characterization of the Laboratory-Incubated Stromatolite

Microbial Community Composition of Mat Layers

Amplicon sequence analysis of the archaeal and bacteria 16S rRNA V3-V4 region revealed more bacterial than archaeal reads (**Figure 2** and **Supplementary Figure S1**). While the number of archaeal reads increased strongly from the green top layer to the black bottom layer, the bacterial reads showed a reverse tendency with most reads obtained in the top

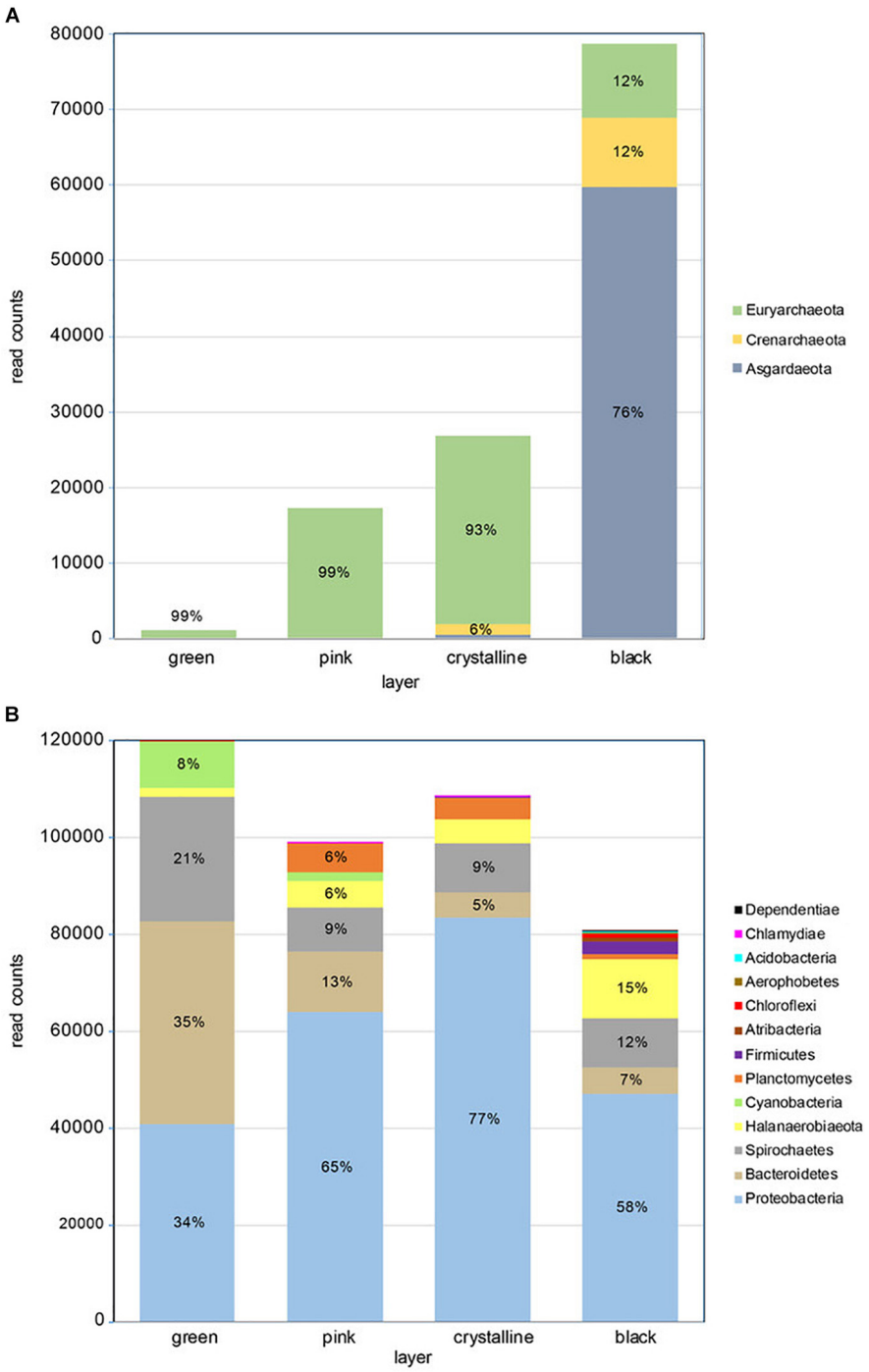

FIGURE 2 | Taxonomic composition of microbial mat layers showing **(A)** archaeal read counts and **(B)** bacterial read counts. The relative phyla frequency within a layer is indicated in percent if respective read counts constitute >5%.

layer and least in the bottom layer. Archaeal diversity was overall low with an estimated Chao-1 richness ranging from 6 in the top layer to 17.5 in the third, crystalline layer. Shannon diversity for the archaeal fraction was highest in the crystalline l (H = 1.03) and lowest black layer (H = 1.07) (**Supplementary Table S2**). Evenness was overall low with the two dominant archaeal OTUs, OTU_17 and OTU_29 making up 78% of the total community abundance. The Crystal layer is dominated by OTU_17 and OTU_13, assigned to the orders Methanosarcinales and Halobacteriales, respectively, and the black layer is dominated by OTU_29 and OTU_25, assigned to the classes Lokiarchaeia and Bathyarchaeia.

Diversity estimators for the bacterial community revealed a slight increase in Chao-1 richness from 96 to 135 from the top to the bottom layer (**Supplementary Table S2**). Shannon diversity index varied little between the three top layers and was highest in the bottom layer ($H = 3.22$). The evenness was overall low (0.13–0.20) indicative for a relative low number of dominant species. Indeed the 14 most abundant OTUs make up more than 75% of the total abundance.

Taxonomic annotation of the bacterial and archaeal OTUs was performed with QIIME using the SILVA version 132 reference database. This provides the taxonomic identifier of the best hits but does not give the percent identity to these hits. The OTUs were therefore also analyzed using standard online NCBI blastn algorithms. This revealed that the majority of the archaeal OTUs gave good hits (mean 98% identity) with nucleotide database (nt), but a very low identity (mean 86%) when comparing to the reference type-strain database (**Supplementary Table S3**).

The archaeal community in the top three layers mainly consists of Euryarchaeota (>90% of total abundance). These layers are dominated by methanogens of the genus *Methanohalophilus* and to a lesser extent of Halobacteria. The Halobacteria contribution is highest in the third layer (∼13%) but they form less than 0.3% of the archaeal population in the bottom layer. The black bottom layer is dominated by phylum *Asgardarchaeota*, class Lokiarchaeota (76% of total) that are neglectable in the other layers. The bottom layer furthermore contains uncultured members of the orders Bathyarchaeia (∼12%) and Thermoplasmata (∼11% - Marine Benthic Group D).

The bacterial community in the stromatolite is dominated by *Proteobacteria*, with a relative abundance increasing from 34% in the top layer to 77% in the third layer and decreasing to 58% in the lower layer (**Figure 2**), Bacteroidetes is the dominant phylum in the top layer (35%) and takes the second and third place in dominance in the subsequent layers. Other abundant phyla are *Spirochaetes* (13% of total bacterial community and present in all layers), *Halanaerobiaeota* (6% of total bacterial community and mainly present in the lower layers). *Cyanobacteria* are only significantly present in the top two layers (respectively, 8% and 2%) (**Supplementary Table S4**). Several genera and families were found that currently have no cultured representatives and no names could be provide but have the prefix _f or _g to indicate unknown family or genus, respectively. Two genera are dominantly found in all layers, *Marinospirillum* and *Marinobacter*, which make up 21% to 30% and 18% to 37%, respectively, in the lower three layers. In the top green layer, they are at a third and fourth place in relative abundance following an uncultured Balneolaceae genus (34%) and uncultured Spirochaeta 2 genus (21%). The top layer is furthermore characterized by the presence of the cyanobacterium *Geitlerinema* (6%). The lower layer is characterized by a relative higher abundance of potential sulfate reducing bacteria (*Desulfosalsimonas*, a novel Desulfobacteraceae genus and *Desulfovibrio*). Sequences derived from potential sulfur oxidizing bacteria were mainly found in the lowest black layer at 0.5% abundance and were annotated as Thiohalospira, a halophilic, obligately chemolithoautotrophic sulfur-oxidizing genus. Among these abundant genera we can recognize members that increase or decrease in abundance with depth of the layers and those that are more abundant in the two middle layers (**Supplementary Table S4**). A decrease in abundance from top to bottom is especially observed for members of the Balneolaceae_g, Spirochaeta 2, *Geitlerinema*, *Salinarimonas*. Genera that increase in abundance from top to bottom are more numerous and consist of amongst others *Marinospirillum*, *Halanaerobium*, *Sediminispirochaeta*, Oligoflexales_f_g and Marinilabiliaceae_g. The genus *Marinobacter* is especially abundant in the two middle layers. Finally, we identified genera which nearly exclusively reside in one of the four layers with an on average 50 times higher abundance than the sum of the other three layers or were absent in the other layers. Notably were Oligoflexales_f_g, Clostridiales_f_g and Desulfobacteraceae_g in the bottom layer, *Cryomorpha* in the top layer, *Defluviicoccus* in the second and *Pelagibius* in the third layer (**Supplementary Table S5**).

Unconsolidated and Lithified Carbonates

SEM-EDS analysis of the crystalline, third layer from the top identified the unconsolidated precipitates as magnesium calcite. The plate-shaped microcrystals (**Figure 3A**) measured 2–3 μm in length and occurred in aggregates of needle and cauliflower morphology. Aggregates were closely associated with each other, forming textures appearing poorly crystallized (**Figures 3C,D**). Spheroids below 1 μm in diameter were observed in association with layers of organic material (**Figures 3B,D**). The OM was layered, contained high rations of C and O and was, thus, related to EPS. All crystalline structures peaked in the C, Ca, and Mg spectra, while spheroids infrequently contained Si in addition (**Figures 3A,B**). The ratio of stable ^{12}C and ^{13}C isotopes varied between the crystalline layer and throughout the laminae of the carbonate deposit, averaging around a $\delta^{13}C$ value of −1.34 in relation to Vienna PeeDee Belemnite (VPDB). The $\delta^{13}C$ of the unconsolidated precipitates was most negative with a mean value of −2.33‰, with the value rising above zero in the first layer of the deposit, dropping slightly below zero in the porous layer below and sharply decreasing to mean isotopic ratios of −2.16‰ and −2.02‰, respectively, in the compact laminated and bottom layers of the deposit (**Table 1**). The delta values of stable ^{16}O and ^{18}O were relatively constant throughout the layers, fluctuating between 0.39‰ and 0.86‰ VPDB, respectively (**Table 1**).

Carbonate Biomineralization in Cyanobacteria-Dominated Culture

Growth and Taxonomic Composition of Cultures

Fifteen cyanobacterial enrichments were obtained through plating on ASN-III-CS agar and three enrichments through transferring cyanobacterial colonies from ASN-III-CS plates to liquid ASN-III-CL medium. The cyanobacteria formed dense, filamentous mats on agar (**Supplementary Figure S2**). In liquid medium, cellular growth was monitored on available surfaces (culture vessel, microscope slide) first, while more

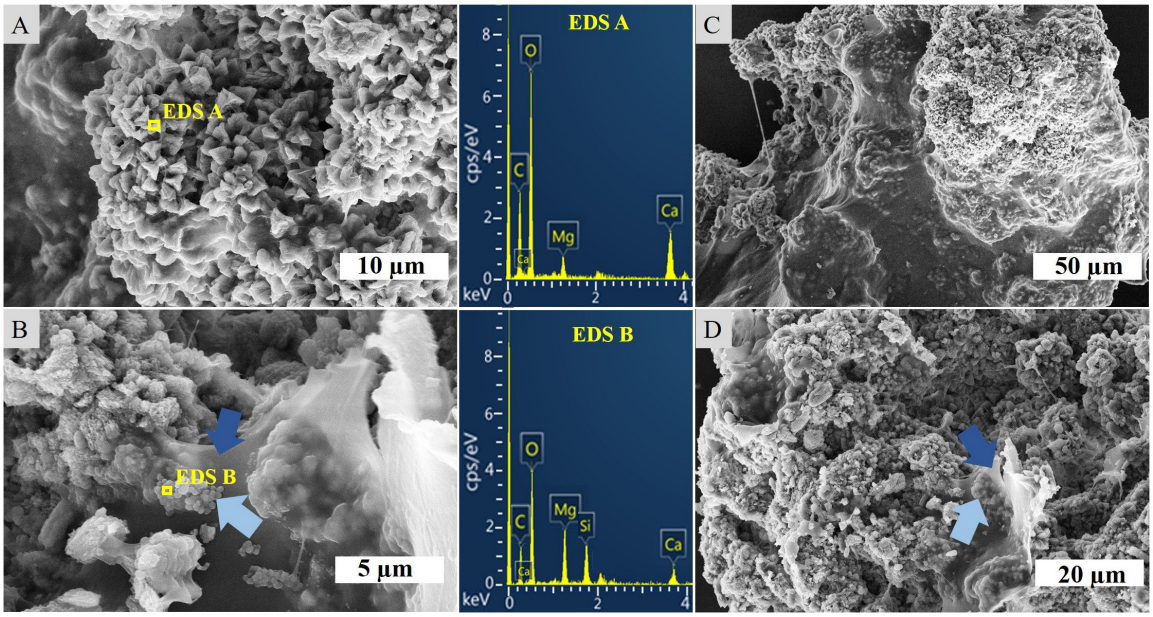

FIGURE 3 | SEM-EDS of the crystalline layer embedded in the stromatolitic microbial mat. **(A)** Imaging and EDS of larger, crystalline structures, **(B)** EDS of spheroids (light blue arrows) adhered to sheaths of EPS (dark blue arrows), **(C)** overview of a carbonate complex, and **(D)** granulated texture of crystalline microstructures and EPS.

mature filaments conglomerated in floating mats. The ASN-III-CL culture medium retained a clear color at all times, indicating the strong tendency of cells to associate with each other (**Supplementary Figure S3**). After 8 weeks of incubation, the bacterial cover started to die off on the increasingly desiccated agar base, while liquid cultures were maintained.

Both light- and dark-green mats showed similar morphological characteristics. While few coccoid cells of approximately 10 µm diameter could be observed, the vast majority of isolates appeared as flat-topped sheathed filaments of a variety of lengths. The single trichomes consisted of aligning rectangular cells about 2.7 µm in length and 1 µm in height (**Figure 4**). The majority of cultured cells showed strong red fluorescence when excited at 546 nm and not when excited at 450–490 nm, confirming the presence of phycoerythrin pigmentation characteristic for cyanobacteria (**Figure 4**). Molecular analysis identified the cyanobacterium as *Geitlerinema* sp. and the cultures as non-axenic containing also members of *Bacteroidetes* (averaging 15%) and *Proteobacteria* (averaging 12%). Since molecular analysis identified no other cyanobacteria in the enrichment cultures, the cultures are mono-phototrophic.

TABLE 1 | Mean isotope delta values throughout the layer of crystalline precipitates in the mat (Top 0) and the primary (Top 1), porous (Top 2), compact (Top 3), and bottom (Top 4) layer of the carbonate deposit.

	δ13C (‰ VPDB)	δ18O (‰ VPDB)
Top 0	−2.33	0.76
Top 1	0.17	0.39
Top 2	−0.35	0.55
Top 3	−2.16	0.64
Top 4	−2.02	0.86

All total of four samples was measured per layer. The long-term standard deviation of the routinely analyzed in-house standard is <0.1‰ (1σ).

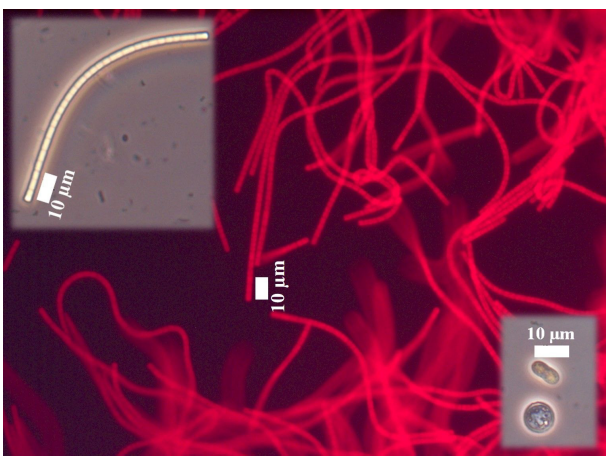

FIGURE 4 | Morphology of isolates from mixed agar culture under an optical microscope in standard adjustment (smaller pictures) and equipped with a green filter (big picture). The EPS appears as white to yellowish sheaths around the cyanobacterial cells.

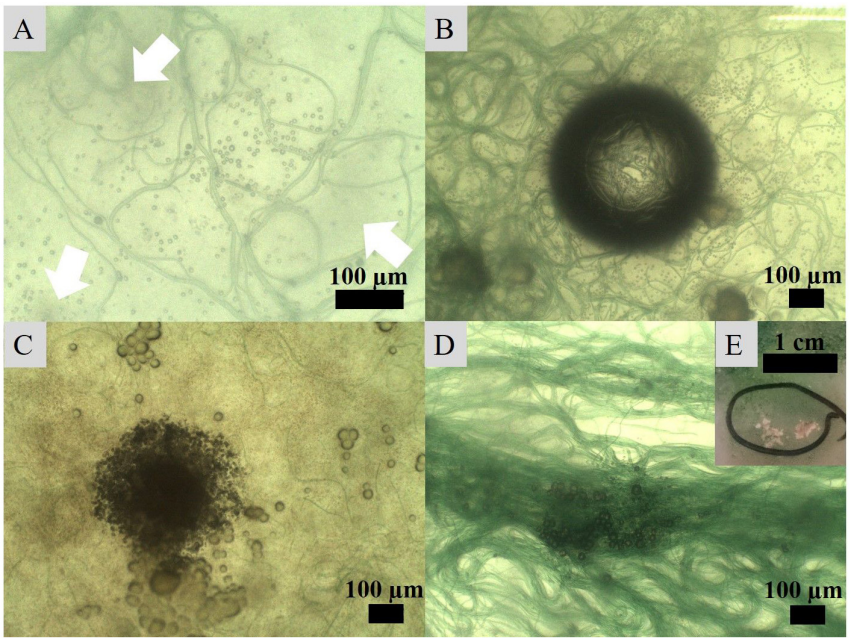

FIGURE 5 | Crystal nucleation and growth observed under an optical microscope. **(A)** Nucleation of globules in association with bacterial filaments and development of darker spots (indicated with arrows) in the medium, **(B)** increased number of nucleating crystals around filaments attracted to a CO_2 or O_2 bubble in the medium, **(C)** amalgamation of globules into granulated textures growing into **(D)** larger crystals on the surface of filament clusters and eventually **(E)** into carbonate crusts visible to the naked eye.

Characterization of Culture Carbonate Mineral Precipitates

Incubation of the *Geitlerinema* enrichment revealed nucleation of micro-globules after 17 days of incubation on seven agar plates. The dark spheres were approximately 1 µm in diameter and associated with filaments. In close proximity to many of the nucleation sites with denser filament coverage, the agar adopted cloudy spots of darker discoloration (**Figures 5A,B**). Over the course of the following weeks, the spheroids amalgamated in granulated textures and continued to grow in diameter (**Figures 5C,D**). Sixty days post-inoculation, white crusts visible to the naked eye and morphologically different from halite appeared on top of bacterial mats (**Figure 5E**). SEM-EDS analysis of this crust revealed magnesium calcite crystals. Imaging disclosed plate-shaped microstructures (**Figure 6A**) conglomerated in needle and cauliflower aggregates, which were in turn associated in granulated textures (**Figures 6B,C**). Additionally, spheroids below 1 µm in diameter could be monitored adhering to EPS layers (**Figures 6B,C**). EDS spectra of all morphology types revealed constantly high Ca and C peaks, while traces of Mg could be found sporadically (**Figures 6A,B**). A crystalline character was confirmed via electron diffraction pattern by TEM analysis (**Figure 6D**). ED patterns were composed of few distinct rings and scattered spots of varying intensities, which were indexed corresponding to the d-spacing values of calcite after Downs et al. (1993). Furthermore, completely calcified cells were disclosed via imaging and chemical elemental analysis (**Figure 6C**). The mean $\delta^{18}O$ of carbonate crusts resulted in 0.39‰ VPDB, while the average isotopic ratio of stable carbon isotopes had a value of −12.26‰ VPDB.

Neither extracellular crystals nor crusts could be observed in liquid cultures. TEM imaging revealed approximately round, intracellular inclusions of a range of diameters below 0.5 µm that were scattered irregularly within the cells and over the length of the filament (**Figure 7A**). The inclusions were often associated with each other, stayed in place upon tilting of the sample and featured similar atomic weights in HAADF-mode. EDS spectra revealed a high P ratio and lower Ca content, as well as elemental Mg, S and sometimes K peaks above the noise. A crystalline character could not be determined via TEM-ED (**Figure 7B**).

Cyanobacteria-Dominated Culture Growth Under UV-C Radiation Stress

Liquid cyanobacterial cultures exposed to UV-C radiation revealed the formation of red flakes within a week after the start of the experiment (**Figures 8B**, **9A**). The same phenomenon appeared in all ASN-III-UL negative control cultures (− cells) exposed to UV-C, both covered with punctured and non-punctured plastic wrap, but not in sterile demineralized water. EDS analysis of the flakes revealed high peaks in Fe and Mn (**Figure 9A**). While all ASN-III-US positive controls (+ cells, – UVC) were covered in a dense cyanobacterial mat within 1 month, no solid cultures could be monitored under UVR exposure (**Figure 8A**). After 6 weeks, cyanobacterial growth could be observed in two liquid UV-C exposed cultures, albeit exclusively beneath the added microscope slides. In liquid controls without UV-C, cyanobacterial growth was observed

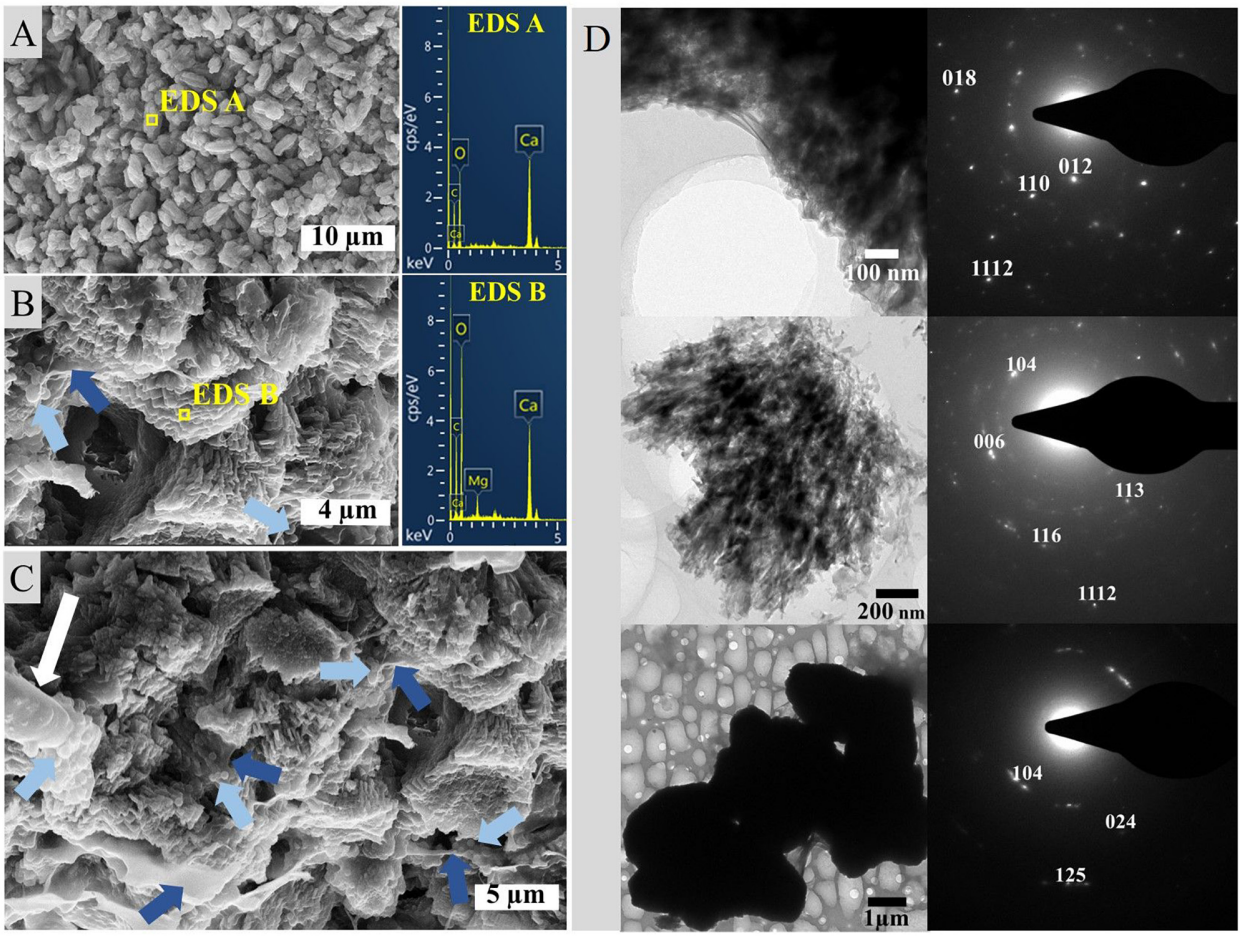

FIGURE 6 | SEM imaging and EDS analysis of carbonate crusts from agar cultures illustrating **(A)** needle morphology, **(B)** aggregate texture including nucleating spheroids (light blue arrows) in EPS sheaths (dark blue arrows) and **(C)** sheaths of EPS with nucleating spheroids as well as a calcified cell (white arrow) associated with spheroids on the far left, and **(D)** indexed ED patterns of calcite sample compounds.

in one culture only, and exclusively on the top side of the microscope slide (**Figures 8A,B**). When subjected to UV-C, the surface bacterial cover of a positive agar control significantly decreased within days and completely diminished after a week. Cyanobacterial filaments embedded in the subsurface agar (∼1 mm depth) were maintained (**Figure 8C**). Similar intracellular inclusions as in the culture experiments could be observed in both UV-C exposed and positive control filaments (**Figure 9E**). Correspondingly, the analysis of elemental composition and structure rendered approximately round structures peaking in the elemental P, Ca, Mg, S, and sporadically K spectra (**Figures 9A–D**).

DISCUSSION

Taxonomic Composition of Microbial Mat Layers

The Lagoa Vermelha microbial mat has been maintained for several years under controlled laboratory conditions to serve as a model ecosystem far from its place of origin (Vasconcelos et al., 2006, 2014; Vasconcelos and McKenzie, 2009). Since most natural communities change and adapt to laboratory conditions, it is difficult to extrapolate laboratory results to the field. However, here we show that several of the key functions (photosynthesis, presence of sulfur cycling taxa and calcification) remain intact with several of the natural key species performing these tasks (**Supplementary Tables S3, S4**).

The number of reads recovered by 16S rRNA amplicon sequencing using archaeal and bacterial primer sets revealed an inverse relationship in abundance between Archaea and Bacteria that, respectively, increase and decrease with depth (**Figure 2**). Although not quantitative, a potential higher archaeal abundance in the interior is consistent with studies on microbial mats in the natural stromatolite-forming Shark Bay area (Papineau et al., 2005; Wong et al., 2017). Also the overall microbial composition and the characteristic layering including a green photosynthetic layer, a white crystalline layer and a black sulfide rich layer are common for calcifying microbial mats such as from Shark Bay and Lagoa Vermelha

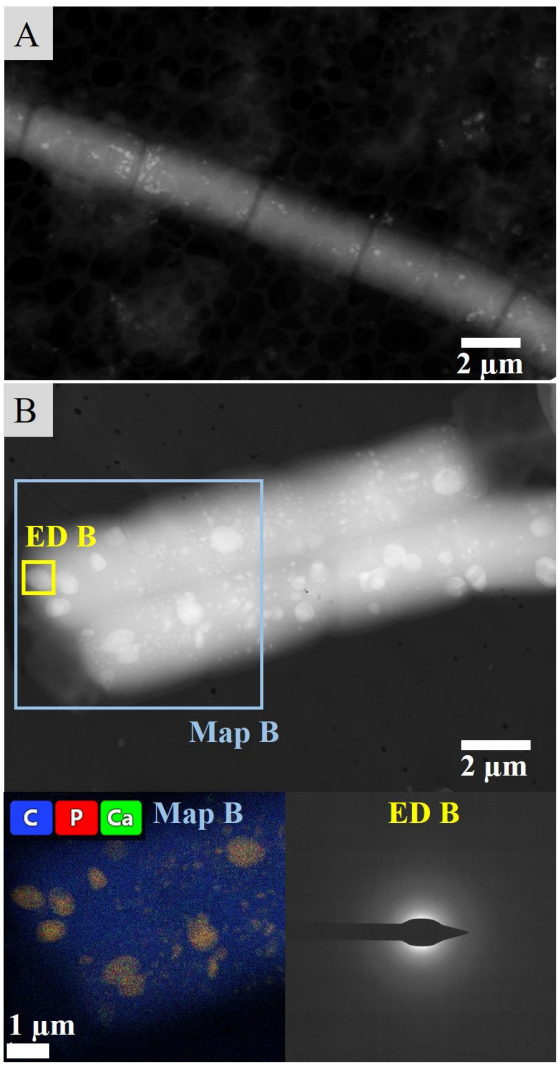

FIGURE 7 | Intracellular inclusions from liquid culture experiments. **(A)** Distribution of inclusions within the cells and throughout a filament visualized in HAADF mode. **(B)** Map and exemplary ED of intracellular granules.

(Vasconcelos et al., 2006). Hence, we consider the laboratory-incubated mats a suitable reference for natural stromatolite forming systems. The considerable incidence of Archaea in the bottom layer (**Figure 2**) is mostly attributed to the abundance of a novel group of Archaea that could only be assigned at the class level to Lokiarchaeia of the Asgard phylum using the SILVA version 132 as reference database. NCBI blast analysis returns a Methanothermobacter species (Euryarchaeota) as best blast hit albeit at only 78% sequence identity. We can rule out sequencing artifacts since many >99% sequence identity hits are found when compared to the nt database (**Supplementary Table S3**), with as best blast hits uncultivated species obtained from a molecular study of microbialites from hypersaline microbial mats. At this moment, we cannot give a conclusive identification, but members of the Asgard group, including Lokiarchaeia, have been observed before in stromatolites (Wong et al., 2018). Similarly, the archaeal OTUs annotated as Bathyarchaeia only have high sequence identity to cultivation independent obtained sequences from hypersaline environments and only a ∼80% identity with cultivated species. Little is known about this group of Archaea, but they may form a symbiotic association with Methanomicrobia with whom they often co-occur (Xiang et al., 2017). The genus *Methanohalophilus* within the order Methanosarcinales, is the most abundant archaeal genus in the top three layers and hints to an important contribution of potentially hydrogenotrophic methanogenesis in the mats. Hydrogenotrophic methanogenesis is considered an ancestral form of methane production (Bapteste et al., 2005; Wong et al., 2017; Lackner et al., 2018) and supports our interpretation that the Lagoa mat is a good analog of both modern and ancient stromatolites. The Thermoplasmata, represented by the Marine Benthic Group D and DHVEG-1 are found especially in the lower layers and may contribute to the sedimentary cycling of carbon, which might assign a key role of these organisms in lithifying mats (Zhou et al., 2019).

The overall composition is typical for microbial mats with a dominance of Proteobacteria, Bacteroidetes and Cyanobacteria, dependent on the sampling depth (Bolhuis and Stal, 2011). Primary production in the stromatolite type microbial mats is performed by oxygenic photosynthetic Cyanobacteria of the genus *Geitlerinema*, the dominant, filamentous cyanobacterium, *Dactylococcopsis*, a unicellular species and the filamentous genus of *Halomicronema* (**Supplementary Table S4**). Each of these salt tolerant cyanobacterial genera are frequently found in hypersaline environments (Oren, 2015) and stromatolites (Samylina and Zaytseva, 2019). Sulfur cycling is performed in the deepest layer by sulfur oxidizing bacteria (*Thiohalospira*) and sulfate reducing bacteria (order Desulfobacterales and Desulfovibrionales) (**Supplementary Table S4**). Sulfate reduction has been suggested to play a key role in the precipitation of carbonates in modern calcifying microbial mats, and recently a novel member of the *Desulfovibrionaceae* family has been linked to potential calcium carbonate deposition in a hypersaline environment (Spring et al., 2019).

The overall dominant genera are mainly anaerobic or microaerophilic heterotrophic bacteria, such as Balneolaceae_g, *Marinobacter* (facultative aerobe heterotrophs) and *Marinospirillum* (micro-aerophilic heterotroph) (**Supplementary Table S4**). Those genera may be involved in lamination formation requiring anoxic conditions and EPS nucleation sites (Vasconcelos et al., 2006).

Anaerobic, halophilic *Halanaerobium* taxa forming hydrogen and metabolizing C6 sugars, as well as *Spirochaeta* are potential fermenting bacteria. Fermentation can potentially counteract the calcification process, but may be prone to diel fluctuations (Dupraz et al., 2009). The presence of anaerobic phyla in the oxic top layers may be explained with sampling cross-overs or scattered anaerobic micro-zones (Wong et al., 2017). However, sulfate reducers, often considered as anaerobes, have also been found in (micro-)oxic regions

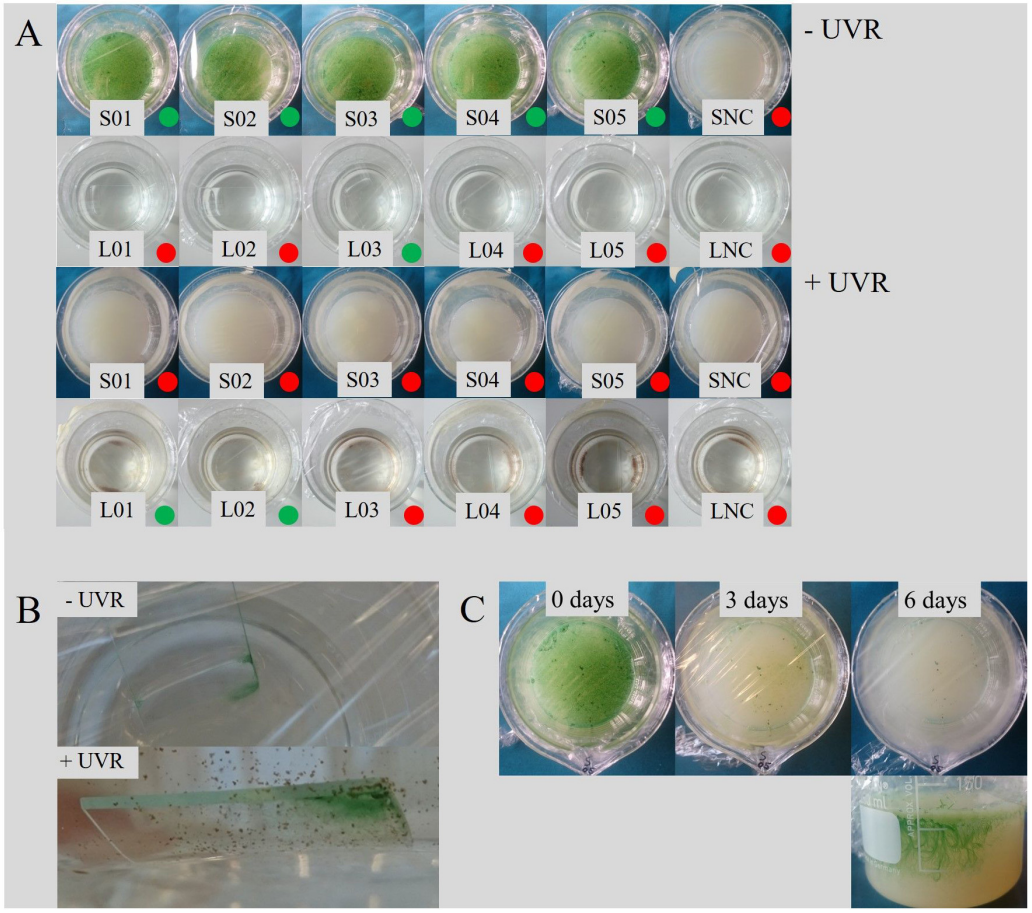

FIGURE 8 | Effects of UVR on cyanobacterial growth. **(A)** Growth in control series and UVR-exposed experiments after 6 weeks, distinguished in solid (S) and liquid (L) cultures including negative controls (NC). Cultures featuring bacterial growth are marked with a green dot, continuously sterile cultures with a red dot. In all liquid cultures subjected to UVR, including the NC, precipitation of red flakes could be observed (see also **B**). **(B)** Cyanobacterial growth occurred exclusively beneath the microscope slide in liquid culture subjected to UV-C, and on only top of the slide in the control. **(C)** Development of an intact cyanobacterial mat in agar culture after exposure to UVR.

of a mat suggesting active sulfur cycling within the upper layers (Minz et al., 1999a,b). The hypersaline nature of the microbial mat is reflected in the occurrence of halophilic species amongst the Archaea (*Halomarina* and *Halomicroarcula*) and halotolerant bacterial members (e.g., *Halanaerobium*, *Halomonas*) (**Supplementary Table S4**).

Precipitation and Lithification of a Laboratory-Incubated Stromatolite

The laboratory-controlled stromatolite continues to accrete carbonate mainly via *in situ* precipitation, which is similar to Precambrian systems and their modern analogs such as alkaline lake and Lagoa Vermelha stromatolites (Kazmierczak and Kempe, 2006; Vasconcelos et al., 2006). Spadafora et al. (2010) analyzed the mesostructure of the specimen we study here, and disclosed an overall autochthonous peloidal matrix, while allochthonous granules only constitute a marginal percentage of the total volume. In general, Lagoa Vermelha stromatolites are laminated on a sub-mm scale and have been described as good textural analogs to Precambrian forms (Vasconcelos et al., 2006, 2014; Spadafora et al., 2010). The mineralogical character of the studied precipitates (**Figure 3**) is consistent with the results of earlier analyses of lithifying microbial mats in Lagoa Vermelha (van Lith et al., 2002; Moreira et al., 2004; Vasconcelos et al., 2006, 2014), despite the stromatolite's transfer to a laboratory environment 15 years ago. A pronounced deviation from the natural system is the exclusive precipitation of magnesium calcite instead of additional dolomite. van Lith et al. (2002) disclose high salinity as a critical control on the formation of dolomite, which mainly occurs in early summer periods promoting evaporation in Lagoa Vermelha. The periodic fluctuation of water levels is not mimicked in the laboratory-incubated microbial mat. The hypersalinity may thus not be pronounced enough for dolomite precipitation on the stable laboratory-incubated stromatolite. The sediment presumably supplies a sufficient amount of Si to be sporadically trapped in the cyanobacterial EPS associated with magnesium calcite spheroids (**Figure 3B**).

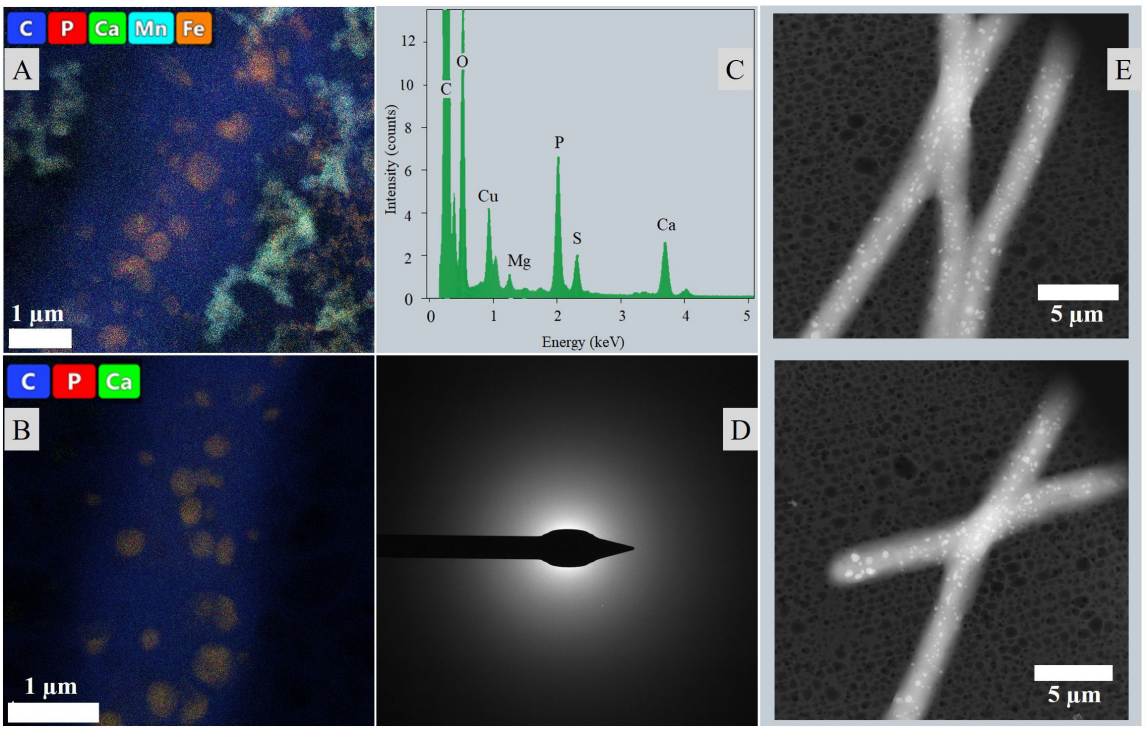

FIGURE 9 | Intracellular inclusions from the UVR experiment. **(A)** Map of a filament from liquid culture exposed to UVR surrounded by the Fe and Mn rich precipitated flakes. **(B)** Map of a filament from an agar control culture. **(C)** Representative EDS of the intracellular inclusions. **(D)** Representative ED of the intracellular inclusions. **(E)** Distribution of inclusions throughout the filaments and cells visualized in HAADF mode.

The varying $\delta^{13}C$ values (**Table 1**) throughout the carbonate stromatolite layers, which include primary precipitates (Top 0) and the amalgamated carbonate deposit (Top 1–Top 4) (**Figure 1**), indicate the contribution of different metabolic pathways to magnesium calcite deposition. Autotrophic carbon fixation features a strong preference for the lighter ^{12}C, which manifests in the OM itself after isotopic fractionation, e.g., in the ribulose biphosphate carboxylase (RuBisCO) reaction of the C3 photosynthetic Calvin cycle prevalent in cyanobacteria (Schidlowski, 2001). This depletes the dissolved inorganic carbon (DIC) pool of ^{12}C, thus increasing the ratio of heavy ^{13}C and accounting for relatively positive $\delta^{13}C$ values in locally formed inorganic material. Consequentially, values relatively negative compared to the equilibrium $\delta^{13}C_{DIC}$ point to heterotrophic incorporation of OM in diagenetic processes (Brady et al., 2013). While methanotrophy produces an extremely negative $\delta^{13}C$, sulfate reduction leads to a considerable decrease in the ^{13}C ratio of residual DIC as well. The layer of crystalline precipitates in the microbial mat features a relatively negative $\delta^{13}C$ (**Table 1**), conversely to the positive values of carbonate mediated via photosynthesis. It is likely that diagenetic processing by aerobic heterotrophic bacteria consuming cyanobacterial necromass and EPS, as well as sulfate reduction in the anoxic zone of the microbial mat produces an increased ^{12}C ratio in primary precipitates. Degradation of OM has been suggested to lead to formation of microbialites over time, while the upper mat layers presumably produce carbonates of globular morphology (Spring et al., 2019). Especially the significance of sulfate reducers in Lagoa Vermelha carbonate diagenesis has been shown before, since in addition to the consumption of organic compounds, this metabolic pathway produces alkalinity (Vasconcelos et al., 2006, 2014). Consequentially, the positive $\delta^{13}C$ value of the most recently amalgamated calcite in the Top 1 upper part of the deposit, as well as the merely negative $\delta^{13}C$ of the porous layer below indicate less prominent heterotrophic diagenesis, while the adjacent fine-grained layer and the very bottom of the stromatolite seem to incorporate a relatively higher ratio of metabolites enriched in ^{12}C. Next to the consumption of autotrophic necromass, photosynthesis itself may mediate ^{13}C enriched DIC in a CO_2 limited system. The laboratory growth conditions simulate the increased salinity of Lagoa Vermelha and thus decrease solubility of CO_2 (Weiss, 1974). It has been shown that the cyanobacterial response of concentrating inorganic HCO_3^- can elevate ^{13}C ratios in the OM, thus accounting for a DIC pool relatively more enriched in ^{12}C (Sharkey and Berry, 1985; Fielding et al., 1998). Therefore, a combination of both heterotrophy and operating carbon concentrating mechanisms (CCM) may lead to precipitation and diagenesis of carbonate with a more negative $\delta^{13}C$ than material mediated through regular C3 photosynthesis. The near zero $\delta^{18}O$ values throughout the layers indicate an approximate equilibrium of precipitated and lithified carbonates with the aquatic environment, as well as a relatively similar isotopic composition of the Lagoa Vermelha natural

seawater and the laboratory saline solution (including minor fluctuations) when comparing unconsolidated precipitates to the mature deposit.

Growth and Carbonate Precipitation in *Geitlerinema*-Dominated Culture

The cyanobacterial enrichment identified *Geitlerinema* sp. as the main constituent. This species is also the most abundant cyanobacterium present in the top layer of the laboratory stromatolite (**Supplementary Table S4**) and has been observed in natural stromatolites (Samylina and Zaytseva, 2019), while Vasconcelos et al. (2006) found the genus *Microcoleus* (Oscillatoriales) to be one of the dominant taxa in a Lagoa Vermelha microbial mat. *Geitlerinema* sp. showed a strong tendency to assemble in dense associations (**Supplementary Figure S3**) protecting the microbial mat against mechanical forces in a natural ecosystem. While bioturbation of the sediment is mostly non-prevalent and higher eukaryotic organisms such as Vertebrates and Crustacea have merely been found in Lagoa Vermelha (Vasconcelos et al., 2006), carbonate environments commonly feature pulses of sedimentation due to episodically heavy, abiotic disruptions such as storms and floods (Schieber, 2007). Culture growth on agar indicates a general adaption to the periodically semi-arid conditions with direct air exposure common in Lagoa Vermelha, with the gelatinous agar itself simulating a mat-like substrate.

The mono-phototrophic community featured precipitation of magnesium calcite on agar plates (**Figures 5**, **6**), but not in liquid medium. This suggests that a gel matrix favors mineral precipitation in the presence of *Geitlerinema* and that such media are good candidates to reproduce the substrate of natural microbial mats in general. Carvalho et al. (2018) studied a stromatolite from the same natural community as ours and disclosed a mean growth rate of 0.19 ± 0.03 mm/y. This indicates that the mat precipitates plus a section of the upper deposit layer of the stromatolite studied here have been formed in the laboratory and are especially valid to compare to the carbonates derived from cultures. Biominerals precipitated in those mono-phototrophic cultures are both chemically and morphologically similar to the ones precipitated in the natural microbial mat (**Figures 3**, **6**). While it is possible that other relevant cyanobacterial species were outcompeted in the experiment, this suggests a significant contribution of *Geitlerinema* to primary carbonate mineral precipitation on the studied stromatolite at least. A prominent difference in chemical composition, however, is the overall lower magnesium content in culture precipitates. This phenomenon is most likely accounted for by a shortage of magnesium in the growth medium (**Supplementary Table S1**). Mg^{2+} ions are generally present in significantly hydrated form and react slower than Ca^{2+} ions, making them less bioavailable and presumably requiring even higher initial concentrations than introduced in order to balance the disparity.

The solid, nutrient-rich agar surface promotes biomineralization in particular, since it is not subjected to fluid dynamics and allows a locally permanent change of the chemical milieu in an area beyond the bacterial EPS layers. Photosynthetically induced ion gradients are visible on the agar as spots of darker discoloration in the process and facilitate a local concentration of Ca^{2+} and Mg^{2+}, increasing both biomineral saturation state and pH (Kaźmierczak et al., 2015). An abiotic factor further assisting ion concentration and thus calcite formation is evaporation. The overall higher culture volume renders this parameter less significant in liquid medium, but cannot be neglected on agar plates subjected to high temperatures for prolonged periods of time. Evaporation entails the transition of the lighter stable oxygen isotope ^{16}O to the atmosphere, shifting the isotopic value of the remaining DIC pool to comparably positive $\delta^{18}O$ values. Since the $\delta^{18}O$ value of the laboratory distilled water is $-8.47‰$ SMOW, the average isotopic ratio of $0.39‰$ VPDB in culture-precipitated carbonates may indicate significant evaporation in the solid growth medium, which could also be observed in the gradual desiccation of agar plates over the course of the experiment, despite their transfer to plastic bags. However, carbonate precipitation was exclusively observed on top of cyanobacterial mats and in no more than half of agar cultures kept under identical conditions, rendering an abiotic precipitation unlikely and indicating cyanobacterial mediation. Interestingly, the $\delta^{18}O$ of morphologically similar carbonate precipitates embedded in the aquarium-kept stromatolite microbial mat is equally positive (**Table 1**).

In contrast, the $\delta^{13}C$ of -12.26 in carbonates derived from culture experiments, is extremely negative compared to the values derived from the carbonate layers of the stromatolite itself (**Table 1**) and simultaneously seems to contradict an abiotic and photosynthetic origin. The carbonate crusts were sampled in careful avoidance of OM, which could explain the distinctly negative value. However, the growth medium contains an extremely elevated carbonate concentration (**Supplementary Table S1**). While atmospheric CO_2 consists to approximately 99% of ^{12}C, inorganic (bi-) carbonate features a generally higher ^{13}C ratio (Sharkey and Berry, 1985). Similar to biomineralization and diagenetic processes on the stromatolite, a greater tendency to take up the heavier isotope from the abundant bicarbonate during C fixation may explain a lower isotopic discrimination than expected and thus exceedingly negative results in the DIC pool. The RuBisCO enzyme adds fixed CO_2 to ribulose-1,5-bisphosphate, eventually mediating the formation of carbohydrates during the photosynthetic dark reaction and resulting in a prominent isotopic fractionation (Schidlowski, 2001). Many cyanobacteria including *Geitlerinema* sp. (Batchu et al., 2019), however, are able to simultaneously take up inorganic HCO_3^-, which is assimilated in the cytoplasm and converted into CO_2 in the carboxysome. Such CCMs are not only activated in hypersaline or hot environments, but especially in alkaline conditions when CO_3^{2-} dominates and allow the cells to survive CO_2 limitation (Kamennaya et al., 2012).

The conversion of HCO_3^- into CO_2 for carboxylation consumes H^+ and contributes to the cell surface alkalization, where Ca^{2+} and Mg^{2+} ions are bound by the anionic EPS and precipitated with CO_3^{2-} generated from HCO_3^- as a result of the increased pH. Simultaneously, the alkaline milieu shifts the equilibrium of the bicarbonate buffer system to the

right, further increasing HCO_3^- and CO_3^{2-} concentrations (Kamennaya et al., 2012). In addition to the higher ionic bioavailability, the swift precipitation of calcium carbonate may also be explained by an additional accumulation of calcium cations via cellular Ca^{2+}/H^+ antiporters at this point, requiring even higher initial concentrations for comparable Mg^{2+} biomineralization. The nucleating carbonate crystals can be observed adhered to the EPS as globules typical for this phase (Smeets et al., 2015) (**Figures 6B,C**). Spheroids amalgamate in later stages and form calcite in different textures giving distinct electron diffraction signals but featuring an overall rather poorly crystallized character.

The irregular crystalline diffraction pattern (**Figure 6D**) distinguishes the comparably calcium-rich intracellular inclusions of cells cultured in liquid medium, which gave no measurable signal at all (**Figure 7B**). While it is possible that the ED detector was blocked by the considerable layer of OM or indicated intracellular calcium carbonate precipitates of a very low degree of crystallinity, the high phosphorous peak cannot be explained by the general P content in the cell since it is considerably concentrated in the inclusions (**Figure 7B**). The overall EDS spectrum (**Figure 9C**) is typical for polyphosphate (PolyP) granules, which are stored in the form of magnesium/calcium salts and formed by cyanobacterial taxa (Benzerara et al., 2014; Feng et al., 2018). Those P storage units have been described as "bioenergy fossils" and were probably already present in the prebiotic era (Achbergerová and Nahálka, 2011). Adopting several cellular functions such as energy supply and regulation of metabolic processes, PolyP granules can be interpreted as a stress response to starvation (Achbergerová and Nahálka, 2011; Racki et al., 2017), which indicates nutrient limitation in the aged liquid medium. The PolyP inclusions may represent another stable adaption of the cultured *Geitlerinema* to the dynamic conditions in Lagoa Vermelha, facilitating long-term mat survival and stromatolite growth. Concurrently, morphological, chemical and isotopic characteristics of the extracellular carbonate deposits document the mineralization of carbonates similar to the primary precipitates of the laboratory-incubated stromatolite and in the mono-phototrophic culture and represent an important precondition for the interpretation of *in situ* precipitated fossil stromatolites.

UV-C Resilience of *Geitlerinema*-Dominated Cultures

Another crucial factor for the evaluation of past terrestrial and a potential Martian atmospheric oxygenation is cyanobacterial resilience toward UV-C radiation. The high energy of UV photons is illustrated by the precipitation of iron- and manganese-rich flakes from liquid ASN-III medium in a presumably UV-C catalyzed abiotic reaction, since it is apparent in the absence of bacterial cells as well but not in cultures shielded from UVR (Anbar and Holland, 1992) (**Figures 8B**, **9A**). Interestingly, the growth medium contains a considerable amount of Fe, but only minuscule traces of Mn introduced by the trace metal mix (**Supplementary Table S1**), with no corresponding materials present in tools or vessels. A possible source of contamination may be the use of not entirely demineralized water containing residues of metal ions. Abiotic formation of putative manganese oxide via shortwave solar radiation could be relevant to early Earth conditions and potentially to conditions on Mars, since it is currently believed that a combination of both oxygen (or oxygen radicals) and microbial activity is required to overcome respective kinetic barriers (Spiro et al., 2010). The readily adsorbance of metal ions by bacteriogenic MnO_2 might render its presence especially meaningful for carbonate depositing systems, but further analysis of the composition of manganese-rich flakes precipitated by UV-C irradiation would be needed to gain insight into this process.

The highly energetic effect of the shortwave UV radiation did not allow bacterial growth on agar, as opposed to the liquid medium where cultivation of few mats could be observed (**Figure 8A**). In accordance with both cultivation experiment results and the significantly shortened time frame, this involved lack of extracellular precipitation but formation or maintenance of PolyP granules presumably facilitating stress acclimation (**Figure 9**).

A cyanobacterial key defense mechanism against UVR is the behavioral avoidance of damaging solar radiation concentrations. *Geitlerinema* species are capable of gliding motility and Oscillatoriales have been reported to migrate within microbial mats depending on the spectrum of incident wavelengths (Ramsing and Prufert-Bebout, 1994; Johansen et al., 2017). The natural mat system represents an ideal refuge, in which UVR tolerant species build a protective top layer for other, motile phototrophs and the deeper community (Quesada and Vincent, 1997). In the experimental set-up, the UV-C blocking microscope slide provides an abiotic type of shelter. In natural Early Earth and Mars analogs, porous rocks (Albanese et al., 2020), ice and dust (Rontó et al., 2003) might take a similar role. *Geitlerinema* filaments exclusively settled on the bottom side of the glass, as opposed to the positive control where mats formed on top of the slide (**Figure 8B**), closer to the PAR source. Cells apparently reached the refuge in two liquid cultures only (**Figure 8A**), potentially indicating an adverse distribution upon inoculation combined with an innate or UVR-induced, limited swimming ability. Indeed, it has been shown that long-term UVR exposure impairs gliding motility in filamentous cyanobacteria (Donkor and Haeder, 1991). At the same time, growth in liquid positive controls was even more limited, a phenomenon that may be explained by pronounced PAR absorption of the liquid medium. While solid medium cultures proliferated extensively in positive controls (**Figure 8A**), the agar surface did not provide any shelter from harmful irradiation. Similar to burial in sediments or mats, however, its subsurface evidently offers sufficient protection for the maintenance of pre-established filaments in a very shallow depth already (**Figure 8C**). This suggests that the cultures are not UV-C resistant enough to emerge primary mats from single cells in surface environments operating energy-intensive repair or blocking mechanisms, and that single cells may not be able to bury themselves in firm substrate and/or UVR environments. However, our experimental set-up does not account for an Archean "faint young sun," which featured a luminosity reduced up to 70% of present

solar radiation (Kasting, 2010). In Early Earth systems, the lower brightness of the sun might thus have facilitated the establishment of comparable photosynthesizing mats regardless. In any case, the cultivate features sufficient resilience to add to the community when sheltered by abiotic refuges or, accordingly, sessile cyanobacteria producing UV blocking agents. In a natural and non-PAR-permeable system, this is additionally dependent on unconstrained motility of phototactic mature filaments to simultaneously facilitate photosynthetic activity and avoidance of harmful solar radiation doses. These conclusions are not only relevant for astrobiological considerations, but also for modern terrestrial environments that promote cyanobacterial biomineralization and the formation of stromatolites subjected to elevated UVR intensities in high latitudes (Phoenix et al., 2006; Farías et al., 2013).

Our results suggest that modern *Geitlerinema* taxa are dependent on shelters enabling an escape from lethal doses of short-wave UVR. Even though this does not allow hard conclusions on the presence or absence of cyanobacteria in the Archean, it underlines the relevance of diversification in putative cyanobacterial mats during the Earth's oxygenation, which provided biotic refuges for motile phototactic cyanobacteria and eventually promoted a global UV-C sanctuary for the evolution of all present domains of life. Based on our observations, we propose that cyanobacteria-derived carbonate deposits are hotspots for traces of aerobic life and support further research on the performance of cyanobacteria under early Earth and Martian conditions. The consideration of biomineralizing anoxygenic photosynthetic taxa such as purple sulfur bacteria (Warthmann et al., 2011) may be an especially valuable addition to further attempts in shedding light on the evolution of aerobic life.

CONCLUSION

A metabolically diverse community accounts for precipitation and diagenesis of magnesium calcite on a laboratory-controlled stromatolite. Although not the overall dominant species, *Geitlerinema* sp. is the major cyanobacterial primary producer in this system and responsible for the oxygenation of the top layer. The *Geitlerinema* enrichment was shown to facilitate carbonate precipitation and was able to endure long-term exposure to highly energetic UV-C radiation. The unexpected large number of yet uncultivated Archaea related to the Asgard group may allow us to study this newly identified phylum and facilitate their cultivation and investigation, while the abiotic precipitation of putative manganese oxides via high-energy solar radiation might be of interest regarding the geochemical cycles of pre-GOE systems. Finally, this study will further contribute to our search for putative extraterrestrial live and especially fossilized biota as well as potential oxygenation of the presently UV-C permeable atmosphere on Mars.

DATA AVAILABILITY STATEMENT

The raw data supporting the conclusions of this article will be made available by the authors, without undue reservation, to any qualified researcher. The sequencing data has been submitted to the NCBI-SRA database under BioProject ID PRJNA610984.

AUTHOR CONTRIBUTIONS

MS-R performed conception and design of the study, assessed results and advised in practical execution, and manuscript writing. RP contributed to study design, conducted practical work, and assessed results as an internship part of the MSc track Freshwater and Marine Biology, University of Amsterdam, and also wrote the draft of the manuscript. HB performed both practical and analytical taxonomic assessment and contributed substantially to the writing and development of the manuscript. GM contributed as adviser, reviser and to the development of the manuscript. All authors contributed to manuscript revision, read and approved the submitted version.

FUNDING

This research was funded by the Origins Center, project 190438131 of the Dutch Research Council (NWO) and National Research Agenda (NWA).

ACKNOWLEDGMENTS

We greatly appreciate the support of Michele Grego (NIOZ, Texel) in morphological analysis of the cyanobacteria, as well as the work of Eric Hellebrand and Hans Meeldijk on the SEM/TEM at Utrecht University and the work of Suzan Verdegaal-Warmerdam on isotopic analysis at Vrije Universiteit, Amsterdam. Furthermore, we would like to thank the Systems Bioinformatics group, Vrije Universiteit for providing their lab facilities.

SUPPLEMENTARY MATERIAL

The Supplementary Material for this article can be found online at: https://www.frontiersin.org/articles/10.3389/fmicb.2020.00948/full#supplementary-material

REFERENCES

Achbergerová, L., and Nahálka, J. (2011). Polyphosphate - an ancient energy source and active metabolic regulator. *Microb. Cell Fact.* 10:63. doi: 10.1186/1475-2859-10-63

Albanese, D., Coleine, C., Rota-Stabelli, O., Onofri, S., Tringe, S. G., Stajich, J. E., et al. (2020). Antarctic cryptoendolithic bacterial lineages of pre-Cambrian origin as proxy for Mars colonization. *Microbiology* doi: 10.1101/2020.02.27.967604

Altermann, W. (2008). Accretion, trapping and binding of sediment in archean stromatolites—morphological expression of the antiquity of life. *Space Sci. Rev.* 135, 55–79.

Anbar, A. D., and Holland, H. D. (1992). The photochemistry of manganese and the origin of banded iron formations. *Geochim.*

Cosmochim. Acta 56, 2595–2603. doi: 10.1016/0016-7037(92)90346-K

Awramik, S. M. (1971). Precambrian columnar stromatolite diversity: reflection of metazoan appearance. *Science* 174, 825–827. doi: 10.1126/science.174.4011.825

Bapteste, E., Brochier, C., and Boucher, Y. (2005). Higher-level classification of the Archaea: evolution of methanogenesis and methanogens. *Archaea* 1, 353–363. doi: 10.1155/2005/859728

Batchu, N. K., Khater, S., Patil, S., Nagle, V., Das, G., Bhadra, B., et al. (2019). Whole genome sequence analysis of *Geitlerinema* sp. FC II unveils competitive edge of the strain in marine cultivation system for biofuel production. *Genomics* 111, 465–472. doi: 10.1016/j.ygeno.2018.03.004

Benzerara, K., Skouri-Panet, F., Li, J., Ferard, C., Gugger, M., Laurent, T., et al. (2014). Intracellular Ca-carbonate biomineralization is widespread in Cyanobacteria. *Proc. Natl. Acad. Sci. U.S.A.* 111, 10933–10938. doi: 10.1073/pnas.1403510111

Bolhuis, H., and Stal, L. J. (2011). Analysis of bacterial and archaeal diversity in coastal microbial mats using massive parallel 16S rRNA gene tag sequencing. *ISME J.* 5, 1701–1712. doi: 10.1038/ismej.2011.52

Bosak, T., Greene, S. E., and Newman, D. K. (2007). A likely role for anoxygenic photosynthetic microbes in the formation of ancient stromatolites. *Geobiology* 5, 119–126. doi: 10.1111/j.1472-4669.2007.00104.x

Brady, A. L., Druschel, G., Leoni, L., Lim, D. S. S., and Slater, G. F. (2013). Isotopic biosignatures in carbonate-rich, cyanobacteria-dominated microbial mats of the Cariboo Plateau, B.C. *Geobiology* 11, 437–456. doi: 10.1111/gbi.12050

Canfield, D. E., and Raiswell, R. (1999). The evolution of the sulfur cycle. *Am. J. Sci.* 299, 697–723.

Caporaso, J. G., Kuczynski, J., Stombaugh, J., Bittinger, K., Bushman, F. D., Costello, E. K., et al. (2010). QIIME allows analysis of high-throughput community sequencing data. *Nat. Methods* 7, 335–336. doi: 10.1038/nmeth.f.303

Cardoso, D. C., Sandionigi, A., Cretoiu, M. S., Casiraghi, M., Stal, L., and Bolhuis, H. (2017). Comparison of the active and resident community of a coastal microbial mat. *Sci. Rep.* 7:2969. doi: 10.1038/s41598-017-03095-z

Carvalho, C., Oliveira, M. I. N., Macario, K., Guimarães, R. B., Keim, C. N., Sabadini-Santos, E., et al. (2018). Stromatolite growth in Lagoa Vermelha, southeastern coast of Brazil: evidence of environmental changes. *Radiocarbon* 60, 383–393. doi: 10.1017/RDC.2017.126

Cockell, C. (2000). The ultraviolet environment of mars: biological implications past, present, and future. *Icarus* 146, 343–359. doi: 10.1006/icar.2000.6393

Decho, A. W., and Kawaguchi, T. (2003). "Extracellular polymers (EPS) and calcification within modern marine stromatolites," in *Fossil and Recent Biofilms*, eds W. E. Krumbein, D. M. Paterson, and G. A. Zavarzin (Dordrecht: Springer), 227–240. doi: 10.1007/978-94-017-0193-8_14

Dittrich, M., and Sibler, S. (2010). Calcium carbonate precipitation by cyanobacterial polysaccharides. *Geol. Soc. Lond. Spec. Publ.* 336, 51–63. doi: 10.1144/SP336.4

Donkor, V., and Haeder, D.-P. (1991). Effects of solar and ultraviolet radiation on motility, photomovement and pigmentation in filamentous, gliding cyanobacteria. *FEMS Microbiol. Lett.* 86, 159–168. doi: 10.1111/j.1574-6968.1991.tb04805.x

Douglas, S., and Beveridge, T. J. (1998). Mineral formation by bacteria in natural microbial communities. *FEMS Microbiol. Ecol.* 26, 79–88. doi: 10.1111/j.1574-6941.1998.tb00494.x

Downs, R. T., Bartelmehs, K. L., Gibbs, G. V., and Boisen, M. B. (1993). Interactive software for calculating and displaying X-ray or neutron powder diffractometer patterns of crystalline materials. *Am. Mineral.* 78, 1104–1107.

Dupraz, C., Reid, R. P., Braissant, O., Decho, A. W., Norman, R. S., and Visscher, P. T. (2009). Processes of carbonate precipitation in modern microbial mats. *Earth Sci. Rev.* 96, 141–162. doi: 10.1016/j.earscirev.2008.10.005

Eigenbrode, J. L., Summons, R. E., Steele, A., Freissinet, C., Millan, M., Navarro-González, R., et al. (2018). Organic matter preserved in 3-billion-year-old mudstones at Gale crater, Mars. *Science* 360, 1096–1101. doi: 10.1126/science.aas9185

Fairchild, I. J. (1991). Origins of carbonate in Neoproterozoic stromatolites and the identification of modern analogues. *Precambrian Res.* 53, 281–299. doi: 10.1016/0301-9268(91)90076-M

Farías, M. E., Rascovan, N., Toneatti, D. M., Albarracín, V. H., Flores, M. R., Poiré, D. G., et al. (2013). The discovery of stromatolites developing at 3570 m above sea level in a high-altitude volcanic lake Socompa, Argentinean Andes. *PLoS One* 8:e53497. doi: 10.1371/journal.pone.0053497

Feng, G., Dong, S., Huang, M., Zeng, M., Liu, Z., Zhao, Y., et al. (2018). Biogenic polyphosphate nanoparticles from a marine cyanobacterium *Synechococcus* sp. PCC 7002: production, characterization, and anti-inflammatory properties in vitro. *Mar. Drugs* 16:322. doi: 10.3390/md16090322

Fielding, A. S., Turpin, D. H., Guy, R. D., Calvert, S. E., Crawford, D. W., and Harrison, P. J. (1998). Influence of the carbon concentrating mechanism on carbon stable isotope discrimination by the marine diatom *Thalassiosira pseudonana*. *Can. J. Bot.* 76, 1098–1103. doi: 10.1139/b98-069

Foster, J. S., Green, S. J., Ahrendt, S. R., Golubic, S., Reid, R. P., Hetherington, K. L., et al. (2009). Molecular and morphological characterization of cyanobacterial diversity in the stromatolites of Highborne Cay, Bahamas. *ISME J.* 3, 573–587. doi: 10.1038/ismej.2008.129

Garcia-Pichel, F. (1998). Solar ultraviolet and the evolutionary history of cyanobacteria. *Orig. Life Evol. Biosph.* 28, 321–347. doi: 10.1023/a:1006545303412

Grotzinger, J. P. (1990). Geochemical model for Proterozoic stromatolite decline. *Am. J. Sci.* 290, 80–103.

Johansen, J. R., Strunecký, O., Bohunická, M., Čapková, K. Č, Raabová, L., Dvoøák, P., et al. (2017). A revision of the genus *Geitlerinema* and a description of the genus *Anagnostidinema* gen. nov. (Oscillatoriophycidae, Cyanobacteria). *Fac. Bibliogr.* 40, 114–126.

Kamennaya, N., Ajo-Franklin, C., Northen, T., and Jansson, C. (2012). Cyanobacteria as biocatalysts for carbonate mineralization. *Minerals* 2, 338–364. doi: 10.3390/min2040338

Kasting, J. F. (2010). Faint young Sun redux. *Nature* 464, 687–689. doi: 10.1038/464687a

Kazmierczak, J. (2002). Neoarchean biomineralization by benthic cyanobacteria. *Science* 298, 2351–2351. doi: 10.1126/science.1075933

Kaźmierczak, J., Fenchel, T., Kühl, M., Kempe, S., Kremer, B., Łącka, B., et al. (2015). CaCO3 precipitation in multilayered cyanobacterial mats: clues to explain the alternation of micrite and sparite layers in calcareous stromatolites. *Life* 5, 744–769. doi: 10.3390/life5010744

Kazmierczak, J., and Kempe, S. (2006). Genuine modern analogues of Precambrian stromatolites from caldera lakes of Niuafo'ou Island, Tonga. *Naturwissenschaften* 93, 119–126. doi: 10.1007/s00114-005-0066-x

Konhauser, K. O., Phoenix, V. R., Bottrell, S. H., Adams, D. G., and Head, I. M. (2001). Microbial-silica interactions in Icelandic hot spring sinter: possible analogues for some Precambrian siliceous stromatolites. *Sedimentology* 48, 415–433. doi: 10.1046/j.1365-3091.2001.00372.x

Lackner, N., Hintersonnleitner, A., Wagner, A. O., and Illmer, P. (2018). Hydrogenotrophic methanogenesis and autotrophic growth of *Methanosarcina thermophila*. *Archaea* 2018:4712608. doi: 10.1155/2018/4712608

Minz, D., Fishbain, S., Green, S. J., Muyzer, G., Cohen, Y., Rittmann, B. E., et al. (1999a). Unexpected population distribution in a microbial mat community: sulfate-reducing bacteria localized to the highly oxic chemocline in contrast to a eukaryotic preference for anoxia. *Appl. Environ. Microbiol.* 65, 4659–4665.

Minz, D., Flax, J. L., Green, S. J., Muyzer, G., Cohen, Y., Wagner, M., et al. (1999b). Diversity of sulfate-reducing bacteria in oxic and anoxic regions of a microbial mat characterized by comparative analysis of dissimilatory sulfite reductase genes. *Appl. Environ. Microbiol.* 65, 4666–4671.

Monty, C. (1973). Precambrian background and Phanerozoic history of stromatolitic communities, an overview. *Ann. Soc. Géol. Belg.* 96, 585–624.

Moreira, N. F., Walter, L. M., Vasconcelos, C., McKenzie, J. A., and McCall, P. J. (2004). Role of sulfide oxidation in dolomitization: sediment and pore-water geochemistry of a modern hypersaline lagoon system. *Geology* 32, 701–704. doi: 10.1130/G20353.1

Oren, A. (2015). Cyanobacteria in hypersaline environments: biodiversity and physiological properties. *Biodivers. Conserv.* 24, 781–798. doi: 10.1007/s10531-015-0882-z

Papineau, D., Walker, J. J., Mojzsis, S. J., and Pace, N. R. (2005). Composition and structure of microbial communities from stromatolites of Hamelin pool in shark bay, western Australia. *Appl. Environ. Microbiol.* 71, 4822–4832. doi: 10.1128/AEM.71.8.4822-4832.2005

Phoenix, V. R., Bennett, P. C., Engel, A. S., Tyler, S. W., and Ferris, F. G. (2006). Chilean high-altitude hot-spring sinters: a model system for UV screening

mechanisms by early Precambrian cyanobacteria. *Geobiology* 4, 15–28. doi: 10.1111/j.1472-4669.2006.00063.x

Quast, C., Pruesse, E., Yilmaz, P., Gerken, J., Schweer, T., Yarza, P., et al. (2013). The SILVA ribosomal RNA gene database project: improved data processing and web-based tools. *Nucleic Acids Res.* 41, D590–D596. doi: 10.1093/nar/gks1219

Quesada, A., and Vincent, W. F. (1997). Strategies of adaptation by Antarctic cyanobacteria to ultraviolet radiation. *Eur. J. Phycol.* 32, 335–342. doi: 10.1080/09670269710001737269

Racki, L. R., Tocheva, E. I., Dieterle, M. G., Sullivan, M. C., Jensen, G. J., and Newman, D. K. (2017). Polyphosphate granule biogenesis is temporally and functionally tied to cell cycle exit during starvation in *Pseudomonas aeruginosa*. *Proc. Natl. Acad. Sci. U.S.A.* 114, E2440–E2449. doi: 10.1073/pnas.1615575114

Ramsing, N. B., and Prufert-Bebout, L. (1994). "Motility of *Microcoleus chthonoplastes* subjected to different light intensities quantified by digital image analysis," in *Microbial Mats*, eds L. J. Stal and P. Caumette (Berlin: Springer), 183–191. doi: 10.1007/978-3-642-78991-5_19

Riding, R. (2006). Microbial carbonate abundance compared with fluctuations in metazoan diversity over geological time. *Sediment. Geol.* 185, 229–238. doi: 10.1016/j.sedgeo.2005.12.015

Rippka, R., Deruelles, J., Waterbury, J. B., Herdman, M., and Stanier, R. Y. (1979). Generic assignments, strain histories and properties of pure cultures of cyanobacteria. *J. Gen. Microbiol.* 111, 1–61.

Rontó, G., Bérces, A., Lammer, H., Cockell, C. S., Molina-Cuberos, G. J., Patel, M. R., et al. (2003). Solar UV irradiation conditions on the surface of mars. *Photochem. Photobiol.* 77, 34–40. doi: 10.1562/0031-8655200307700 34SUICOT2.0.CO2

Samylina, O. S., and Zaytseva, L. V. (2019). Characterization of modern dolomite stromatolites from hypersaline Petukhovskoe Soda Lake, Russia. *Lethaia* 52, 1–13. doi: 10.1111/let.12286

Schidlowski, M. (2001). Carbon isotopes as biogeochemical recorders of life over 3.8 Ga of Earth history: evolution of a concept. *Precambrian Res.* 106, 117–134.

Schieber, J. (2007). "Microbial mats on muddy substrates - examples of possible sedimentary features and underlying processes," in *Atlas of Microbial Mat Features Preserved within the Siliciclastic Rock Record*, eds J. Schieber, P. K. Bose, P. G. Eriksson, S. Banerjee, S. Sarkar, W. Altermann, et al. (Amsterdam: Elsevier), 117–134.

Sharkey, T., and Berry, J. (1985). "Carbon isotope fractionation of algae as influenced by an inducible carbon concentrating mechanism," in *Inorganic Carbon Uptake by Aquatic Photosynthetic Organisms*, ed. R. M. M. Crawford (Rockville, MD: American Society of Plant Physiologists), 389–401.

Shestakov, S. V., and Karbysheva, E. A. (2017). The origin and evolution of cyanobacteria. *Biol. Bull. Rev.* 7, 259–272. doi: 10.1134/S2079086417040090

Smeets, P. J. M., Cho, K. R., Kempen, R. G. E., Sommerdijk, N. A. J. M., and De Yoreo, J. J. (2015). Calcium carbonate nucleation driven by ion binding in a biomimetic matrix revealed by in situ electron microscopy. *Nat. Mater.* 14, 394–399. doi: 10.1038/nmat4193

Spadafora, A., Perri, E., Mckenzie, J. A., and Vasconcelos, C. (2010). Microbial biomineralization processes forming modern Ca:Mg carbonate stromatolites: biomineralization processes forming stromatolites. *Sedimentology* 57, 27–40. doi: 10.1111/j.1365-3091.2009.01083.x

Spiro, T. G., Bargar, J. R., Sposito, G., and Tebo, B. M. (2010). Bacteriogenic manganese oxides. *Acc. Chem. Res.* 43, 2–9. doi: 10.1021/ar800232a

Spring, S., Sorokin, D. Y., Verbarg, S., Rohde, M., Woyke, T., and Kyrpides, N. C. (2019). Sulfate-reducing bacteria that produce exopolymers thrive in the calcifying zone of a hypersaline cyanobacterial mat. *Front. Microbiol.* 10:862. doi: 10.3389/fmicb.2019.00862

Suosaari, E. P., Reid, R. P., Playford, P. E., Foster, J. S., Stolz, J. F., Casaburi, G., et al. (2016). New multi-scale perspectives on the stromatolites of Shark Bay, Western Australia. *Sci. Rep.* 6:20557. doi: 10.1038/srep20557

van Lith, Y., Vasconcelos, C., Warthmann, R., Martins, J. C. F., and McKenzie, J. A. (2002). Bacterial sulfate reduction and salinity: two controls on dolomite precipitation in Lagoa Vermelha and Brejo do Espinho (Brazil). *Hydrobiologia* 485, 35–49.

Vasconcelos, C., Dittrich, M., and McKenzie, J. A. (2014). Evidence of microbiocoenosis in the formation of laminae in modern stromatolites. *Facies* 60, 3–13.

Vasconcelos, C., and McKenzie, J. A. (2009). Geochemistry: the descent of minerals. *Science* 323, 218–219. doi: 10.1126/science.1168807

Vasconcelos, C., Warthmann, R., McKenzie, J. A., Visscher, P. T., Bittermann, A. G., and van Lith, Y. (2006). Lithifying microbial mats in Lagoa Vermelha, Brazil: modern Precambrian relics? *Sediment. Geol.* 185, 175–183. doi: 10.1016/j.sedgeo.2005.12.022

Visscher, P. T., Reid, R. P., Bebout, B. M., Hoeft, S. E., Macintyre, I. G., and Thompson, J. A. Jr. (1998). Formation of lithified micritic laminae in modern marine stromatolites (Bahamas): the role of sulfur cycling. *Am. Mineral.* 83, 1482–1493.

Visscher, P. T., and Stolz, J. F. (2005). Microbial mats as bioreactors: populations, processes, and products. *Palaeogeogr. Palaeoclimatol. Palaeoecol.* 219, 87–100. doi: 10.1016/j.palaeo.2004.10.016

Warthmann, R., Vasconcelos, C., Bittermann, A. G., and McKenzie, J. A. (2011). "The role of purple sulphur bacteria in carbonate precipitation of modern and possibly early Precambrian stromatolites," in *Advances in Stromatolite Geobiology*, eds J. Reitner, N.-V. Quéric, and G. Arp (Berlin: Springer), 141–149. doi: 10.1007/978-3-642-10415-2_9

Weiss, R. F. (1974). Carbon dioxide in water and seawater: the solubility of a non-ideal gas. *Mar. Chem.* 2, 203–215.

Wong, H. L., Visscher, P. T., White, R. A. III, Smith, D.-L., Patterson, M. M., and Burns, B. P. (2017). Dynamics of archaea at fine spatial scales in Shark Bay mat microbiomes. *Sci. Rep.* 7:46160. doi: 10.1038/srep46160

Wong, H. L., White, R. A., Visscher, P. T., Charlesworth, J. C., Vázquez-Campos, X., and Burns, B. P. (2018). Disentangling the drivers of functional complexity at the metagenomic level in Shark Bay microbial mat microbiomes. *ISME J.* 12, 2619–2639. doi: 10.1038/s41396-018-0208-8

Xiang, X., Wang, R., Wang, H., Gong, L., Man, B., and Xu, Y. (2017). Distribution of bathyarchaeota communities across different terrestrial settings and their potential ecological functions. *Sci. Rep.* 7:45028. doi: 10.1038/srep45028

Zhou, Z., Liu, Y., Lloyd, K. G., Pan, J., Yang, Y., Gu, J.-D., et al. (2019). Genomic and transcriptomic insights into the ecology and metabolism of benthic archaeal cosmopolitan, Thermoprofundales (MBG-D archaea). *ISME J.* 13, 885–901. doi: 10.1038/s41396-018-0321-8

Conflict of Interest: The authors declare that the research was conducted in the absence of any commercial or financial relationships that could be construed as a potential conflict of interest.

frontiers in Microbiology

ORIGINAL RESEARCH
published: 07 July 2020
doi: 10.3389/fmicb.2020.01284

Physicochemical Salt Solution Parameters Limit the Survival of *Planococcus halocryophilus* in Martian Cryobrines

Annemiek C. Waajen[1,2], Jacob Heinz[2], Alessandro Airo[2] and Dirk Schulze-Makuch[2,3,4,5]*

[1] UK Centre for Astrobiology, School of Physics and Astronomy, The University of Edinburgh, Edinburgh, United Kingdom, [2] Astrobiology Research Group, Center of Astronomy and Astrophysics, Technische Universität Berlin, Berlin, Germany, [3] School of the Environment, Washington State University, Pullman, WA, United States, [4] Section Geomicrobiology, GFZ German Research Centre for Geosciences, Potsdam, Germany, [5] Department of Experimental Limnology, Leibniz Institute of Freshwater Ecology and Inland Fisheries (IGB), Stechlin, Germany

OPEN ACCESS

Edited by:
Akihiko Yamagishi, Tokyo University of Pharmacy and Life Sciences, Japan

Reviewed by:
Jonathan Toner, University of Washington, United States
Adam Stevens, The University of Edinburgh, United Kingdom

***Correspondence:**
Annemiek C. Waajen
annemiek.waajen@ed.ac.uk

Specialty section:
This article was submitted to Extreme Microbiology, a section of the journal Frontiers in Microbiology

Received: *01 October 2019*
Accepted: *20 May 2020*
Published: *07 July 2020*

Citation:
Waajen AC, Heinz J, Airo A and Schulze-Makuch D (2020) Physicochemical Salt Solution Parameters Limit the Survival of Planococcus halocryophilus in Martian Cryobrines. Front. Microbiol. 11:1284. doi: 10.3389/fmicb.2020.01284

Microorganisms living in sub-zero environments can benefit from the presence of dissolved salts, as they significantly increase the temperature range of liquid water by lowering the freezing point. However, high concentrations of salts can reduce microbial growth and survival, and can evoke a physiological stress response. It remains poorly understood how the physicochemical parameters of brines (e.g. water activity, ionic strength, solubility and hydration shell strength between the ions and the surrounding water molecules) influence the survival of microorganisms. We used the cryo– and halotolerant bacterial strain *Planococcus halocryophilus* as a model organism to evaluate the degree of stress different salts assert. Cells were incubated in liquid media at −15°C containing single salts at eutectic concentrations ($CaCl_2$, LiCl, LiI, $MgBr_2$, $MgCl_2$, NaBr, NaCl, $NaClO_4$ and NaI). Four of these salts (LiCl, LiI, $MgBr_2$ and $NaClO_4$) were also investigated at concentrations with a low water activity (0.635) and, separately, with a high ionic strength (8 mol/L). Water activity of all solutions was measured at −15°C. This is the first time that water activity has been measured for such a large number of liquid salt solutions at constant sub-zero temperatures (−15°C). Colony-Forming Unit (CFU) counts show that the survival of *P. halocryophilus* has a negative correlation with the salt concentration, molecular weight of the anion and anion radius; and a positive correlation with the water activity and anions' hydration shell strength. The survival of *P. halocryophilus* did not show a significant correlation with the ionic strength, the molecular weight of the cation, the hydrated and unhydrated cation and hydrated anion radius, and the cations' hydration bond length. Thus, the water activity, salt concentration and anion parameters play the largest role in the survival of *P. halocryophilus* in concentrated brines. These findings improve our understanding of the limitations of microbial life in saline environments, which provides a basis for better evaluation of the habitability of extraterrestrial environments such as Martian cryobrines.

Keywords: *Planococcus halocryophilus*, salt stress, water activity, ionic strength, survival

INTRODUCTION

Liquid water is a requirement for life as we know it. Dissolved salts can depress the freezing point of water significantly. As this increases the temperature range of liquid water, this expands the habitable zone around stars (Kasting et al., 1993) and broadens the range of habitable environments on planets such as Mars.

Even though the long-term presence of liquid water on the surface of Mars is not possible due to the lack of a sufficiently dense atmosphere, liquid water could be temporarily stable under current Martian surface conditions as cryobrines, i.e., aqueous salty solutions with a eutectic temperature below 0°C (Möhlmann and Thomsen, 2011). The eutectic temperature is the lowest freezing temperature that can be obtained with a respective salt. This, in combination with the discovery of perchlorates on Mars (Hecht et al., 2009), suggests that perchlorate-rich brines could be present on Mars nowadays (Kereszturi et al., 2010; Chevrier and Rivera-Valentin, 2012; Martín-Torres et al., 2015; Ojha et al., 2015).

The existence of Martian cryobrine environments is supported by the recent putative discovery of a 1.5 km deep subsurface lake (Orosei et al., 2018). Although the lake water is assumed to have a temperature of −68°C, it remains presumably liquid because of its high concentration of dissolved salts (Fisher et al., 2010; Orosei et al., 2018). Furthermore, Martian Recurring Slope Lineae (RSL), i.e., seasonal dark streaks on steep slopes that slowly appear in spring and vanish in late summer (McEwen et al., 2011), have been suggested to be caused by the formation of surface cryobrines (Kereszturi et al., 2010; Chevrier and Rivera-Valentin, 2012; Ojha et al., 2015). This could indicate that potentially habitable cryobrine environments could exist temporarily near the Martian surface, supposedly containing sodium, calcium, or magnesium chlorides or perchlorates (Chevrier et al., 2009; McEwen et al., 2011).

The habitability of Martian cryobrines can be assessed through the study of extremotolerant organisms adapted to cold and saline environments on Earth, such as the halocryotolerant bacterium *Planococcus halocryophilus*. *P. halocryophilus* was isolated from Canadian permafrost soil and is capable of growth in 19 wt/vol% NaCl solution at −15°C (Mykytczuk et al., 2012, 2013). Furthermore, it has the highest bacterial perchlorate tolerance (13.6 wt/vol% $NaClO_4$ at +25°C) reported to date (Heinz et al., 2019). Only some fungi are known to tolerate higher perchlorate concentrations (Heinz et al., 2020). Hence, this halo- and cryotolerant organism is highly suitable as a model organism for studying the habitability of Martian cryobrines and was therefore used in this study.

Independent of such species-specific adaptations, all microorganisms are known to respond to salt stress through various molecular biological processes ranging from active transmembrane ion transport to dormancy. If a certain salt type or concentration generates a biochemical stress response, numerous defects can occur, such as protein denaturation or membrane damage, eventually leading to cell death. Deciphering the mechanisms by which each ion impedes microbial growth or survival is challenging, due to a potential overlap of different mechanisms that can additionally be highly species-dependent. At best, the toxicity of an ion correlates with a single physicochemical parameter either relating to the ion itself (e.g., ionic radius) or affected indirectly by the ion concentration (e.g., water activity). However, additional toxicities such as chemical reactivity (e.g., the reducing effect of ions like iodide) or biochemical toxicity [e.g., the interaction of calcium on extracellular polymeric substance (EPS)] can also influence microbial survival.

Research on the physicochemical parameters limiting the habitability of brines has largely focused on water activity, which is a measure of its thermodynamic availability (Tosca et al., 2008; Stevenson et al., 2015a,b). The maximum degree to which a salt can reduce the water activity also depends on its solubility, which is related to the hardness of the involved ions, which in turn derives from their charge/radius ratio. Ionic strength however, which is a measure for the strength of the electric field in a solution, has received less attention regarding the survival of microorganisms (Fox-Powell et al., 2016).

Several physicochemical parameters are influenced by the hardness of ions. The hardness of an ion is determined by the charge density of the respective ion, which is influenced by the charge/radius ratio of that ion. Hard ions have a high charge density, while soft ions have a low charge density. The Hard and Soft Acids and Bases (HSAB) theory states that salts consisting of hard cations and soft anions or vice versa are more soluble than salts consisting of either hard cations and hard anions or soft cations and soft anions (Pearson, 1968a,b). Furthermore, a higher solubility correlates with a lower minimal water activity in a saturated solution, as more water molecules are needed to dissolve the increased number of ions in the more concentrated solution. As water activity is one of the main parameters expected to influence microbial survival, the higher solubility, and thus the HSAB theory, might describe microbial survival. The link between these physicochemical parameters in light of the HSAB theory is investigated in this paper.

Heinz et al. (2018) investigated the survival of *P. halocryophilus* in various chloride and perchlorate solutions at different temperatures. The study showed that decreasing the temperature under high salt concentrations results in a higher survival of *P. halocryophilus*. The hypothesis for the higher survival at sub-zero temperatures is that besides the normal Arrhenius-like temperature dependence, the size and stability of hydration shells around the salt ions, which increases with decreasing temperatures, reduces the osmotic stress (Heinz et al., 2018). The size and stability of hydration shells depend on the hydration bond length (HBL) between the ion and the oxygen atom of the water molecules in the inner hydration shell (HBL-ion), which is determined by the charge and the radius of the ion (**Figure 1**). The radii of the ions taken into account in this study are the unhydrated or crystal ion radii and the hydrated or effective ion radii (Nightingale, 1959). As the size and stability of hydration shells differ between salts, this could influence microbial survival in brines containing these salts due to, for example, differences in ion transportation across the cell membrane.

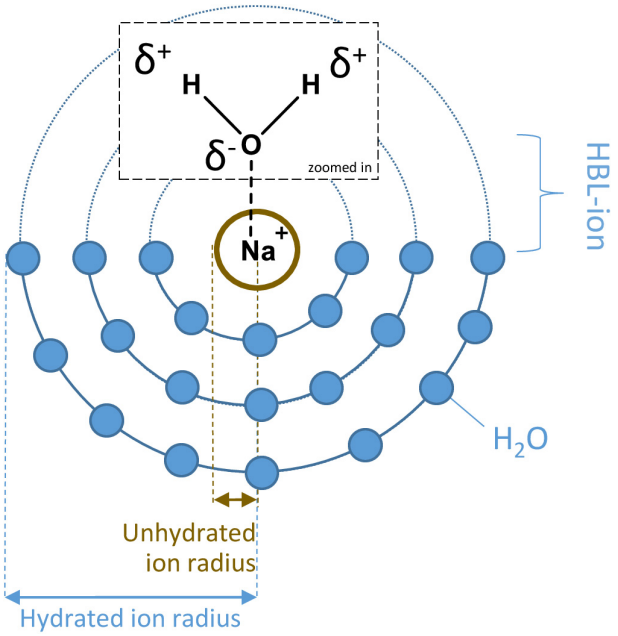

FIGURE 1 | An example of hydration spheres surrounding a sodium-ion in solution, including a depiction of the unhydrated and hydrated ion radius. The HBL-ion is the hydrogen bond length between the ion and the oxygen atom of the water molecules in the inner hydration shell surrounding the ion.

It remains unknown which physicochemical parameters of a salt solution have the greatest influence on the survival of *P. halocryophilus* and whether additional chemical reactivity or biochemical toxicity plays a role. A recent study by Heinz et al. (2019) suggests for chloride and perchlorate salt solutions that ion-specific factors of salts have a larger influence on the growth limitation of *P. halocryophilus* than general physicochemical parameters of the solution, such as water activity or ionic strength. In order to determine whether this applies to other salts, and to establish the relevance of other physicochemical salt parameters, we investigated the influence of a wide range of physicochemical parameters on the survival of *P. halocryophilus*. The investigated physicochemical parameters include water activity, ionic strength, HBL between the salt ions and water molecules, hydrated and unhydrated ion radii, salt concentration and ion molecular weight. Although an often-mentioned physicochemical salt parameter, chaotropicity of the ions could not be investigated due to the lack of quantitative data for most of the investigated salts.

MATERIALS AND METHODS

Planococcus halocryophilus Or1 (DSMZ 24743) was grown in liquid DSMZ #92 medium (30 g/L TSB; 3 g/L yeast) at +25°C in batch incubations without shaking. Cultures were transferred weekly to fresh medium. Death rate experiments were performed as described by Heinz et al. (2018). Briefly, 2 mL of *P. halocryophilus* Or1 cell suspension of growth medium +10 wt% NaCl at late exponential phase was stored at 4°C for 30–60 min and subsequently added to 8 mL of −15°C salt solution, resulting in a final salt concentrations as described in **Tables 1**, **2**. The death rate of *P. halocryophilus* was determined by plating sample aliquots and Colony-Forming Unit (CFU) determination. Death rate is defined as the decrease in CFU count per minute. CFU counts were plotted over time and the data was fitted with a logarithmic regression. For CFU determinations, culture samples were taken at multiple time points and diluted with −15°C phosphate-buffered saline (PBS) + 20 wt% NaCl (7 g/L $Na_2HPO_4.2H_2O$; 3 g/L KH_2PO_4; 250 g/L NaCl). Serial dilution was done in 1.5 mL reaction tubes with 900 µL PBS + 20% NaCl, followed by plating on 4°C DSMZ growth medium #92 agar plates containing no additional salt (30 g/L TSB; 3 g/L yeast; 15 g/L agar). Agar plates were incubated at +25°C. All experiments were either performed in technical and biological duplicates, or in technical triplicates.

The death rate of *P. halocryophilus*, calculated from the CFU counts, was investigated at the eutectic salt concentrations of the following salts: $CaCl_2$, LiCl, LiI, $MgBr_2$, $MgCl_2$, NaBr, NaCl, $NaClO_4$ and NaI. Death rate data in NaCl, $CaCl_2$ and $MgCl_2$ at eutectic concentrations were obtained by Heinz et al. (2018) using the same methodology as in this study. Additionally, death rates in LiCl, LiI, $MgBr_2$ and $NaClO_4$ were investigated at a water activity of 0.635 ± 0.02 at −15°C and separately at an ionic strength of 8 mol/L. The salt concentrations and physicochemical parameters at the tested conditions are shown in **Tables 1**, **2**. Water activity was measured in triplicate at −15°C using a humidity and temperature probe (HC2-AW, ROTRONIC Instruments (UK) Ltd, Crompton Fields). Three milliliter of salt solution was stored in the probe and the water activity was measured for several hours until stabilization. Additionally, the water activity of the solutions at +25°C were calculated using the Pitzer equation to compare these values with the measured water activity values at −15°C (Pitzer, 1973, 1975, 1991). Pitzer equation parameters were taken from Kim and Frederick (1988). The correlations between the death rate of *P. halocryophilus* and physicochemical parameters were determined with the help of univariate linear regression. The correlation coefficients of univariate linear regressions were all obtained from logarithmic regression lines.

RESULTS

Experiments at Eutectic Concentrations

Salt Concentration Dependent Parameters

Death rate and physicochemical salt parameter values at eutectic concentrations at −15°C are presented in **Table 1**. The quality of the correlations of parameters with the death rates are presented as R^2 values. The strength of the correlations is dependent on the slope of the correlation. The quality of the logarithmic regression of CFU counts determining the death rate at eutectic concentrations was high, as R^2 was higher than 0.8 for all salts except for $MgBr_2$, which had a lower quality (R^2 = 0.46) (data not shown). The investigated salt concentration dependent parameters were water activity and ionic strength. Salt

TABLE 1 | Chemical salt parameters at eutectic concentration for death rate experiments.

	Eutectic concentration		Salt concentration dependent parameters			Salt concentration independent parameters						Death rate results
Salt	**Concentration (wt%)**	**Molar concentration (mol/L)**	**Measured water activity at −15°C ± standard deviation**	**Calculated water activity at +25°C**	**Ionic strength (mol/L)**	**Hydrated cation radius[a] (Å)**	**Unhydrated cation radius[a] (Å)**	**Hydrated anion radius[a] (Å)**	**Unhydrated anion radius[a] (Å)**	**HBL-cation[a] (Å)**	**HBL-anion[a] (Å)**	**Death rate (min^{-1})**
$CaCl_2$	30.2[c]	3.90	0.5730 ± 0.0024	0.64	11.70	4.12	0.99	3.32	1.81	2.46[h]	3.21[h]	2.0×10^{-5}
LiCl	25.3[c]	7.99	0.4537 ± 0.0053	0.54	7.99	3.82	0.68	3.32	1.81	1.94[i]	3.21[h]	6.4×10^{-4}
LiI	51.5[e]	7.93	0.3941 ± 0.0033	0.39	7.93	3.82	0.68	3.31	2.16	1.94[i]	3.55[i]	6.6
$MgBr_2$	37.0[f]	3.19	0.5942 ± 0.0019	0.66	9.57	4.28	0.65	3.30	1.95	2.10[h]	3.47[j]	8.6×10^{-4}
$MgCl_2$	21.0[b]	2.79	0.6600 ± 0.0132	0.75	8.38	4.28	0.65	3.32	1.81	2.10[h]	3.21[h]	1.5×10^{-5}
NaBr	40.3[g]	6.56	0.6490 ± 0.0049	0.71	6.56	3.58	0.95	3.30	1.95	2.43[i]	3.47[j]	1.9×10^{-4}
NaCl	23.3[b]	5.20	0.7283 ± 0.0019	0.80	5.20	3.58	0.95	3.32	1.81	2.43[i]	3.21[h]	3.7×10^{-6}
$NaClO_4$	53.0[g]	9.06	0.6422 ± 0.0082	0.68	9.06	3.58	0.95	3.38	2.92	2.43[i]	3.68[k]	3.3×10^{-2}
NaI	47.1[g]	5.94	0.6758 ± 0.0070	0.72	5.94	3.58	0.95	3.31	2.16	2.43[i]	3.55[i]	6.0×10^{-1}

[φ] Hydration bond lengths between ions and oxygen atom of the water molecule in solution at +25°C. Water activity values were measured at −15°C and calculated for +25°C. Ionic strength values are calculated with the Pitzer equations (Pitzer, 1973, 1975, 1991). References: [a](Nightingale, 1959), [b](Heinz et al., 2018), [c](Conde, 2004), [d](Madan, 2012), [e](Hendricks, 1928), [f](Hennings, 2014), [g](Fegley and Osborne, 2013), [h](Bruni et al., 2012), [i](Mähler and Persson, 2012), [j](Kálmán et al., 1983), [k](Lindqvist-Reis et al., 1998).

TABLE 2 | Chemical salt parameters at non-eutectic concentrations for death rate experiments.

	Non-eutectic concentration		Salt concentration dependent parameters			Salt concentration independent parameters						Death rate results
Salt	**Concentration (wt%)**	**Molar concentration (mol/L)**	**Measured water activity at −15°C ± standard deviation**	**Calculated water activity at +25°C**	**Ionic strength (mol/L)**	**Hydrated cation radius[a] (Å)**	**Unhydrated cation radius[a] (Å)**	**Hydrated anion radius[a] (Å)**	**Unhydrated anion radius[a] (Å)**	**HBL-cation[a] (Å)**	**HBL-anion[a] (Å)**	**Death rate (min^{-1})**
LiCl	19.0	5.53	0.6157 ± 0.0033	0.70	5.53	3.82	0.68	3.32	1.81	1.94[b]	3.21[c]	2.8×10^{-4}
LiI	39.4	4.86	0.6333 ± 0.0027	0.70	4.86	3.82	0.68	3.31	2.16	1.94[b]	3.55[b]	2.3×10^{-1}
$MgBr_2$	35.0	2.92	0.6268 + 0.0100	0.70	8.77	4.28	0.65	3.30	1.95	2.10[c]	3.47[d]	2.7×10^{-3}
$NaClO_4$	51.3	8.60	0.6539 ± 0.0029	0.70	8.60	3.58	0.95	3.38	2.92	2.43[b]	3.68[e]	6.0×10^{-2}
LiCl	25.3	7.99	0.4537 ± 0.0053	0.54	7.99	3.82	0.68	3.32	1.81	1.94[b]	3.21[c]	7.6×10^{-4}
LiI	51.7	8.00	0.3941 + 0.0033	0.38	8.00	3.82	0.68	3.31	2.16	1.94[b]	3.55[b]	6.6
$MgBr_2$	32.9	2.66	0.6632 + 0.0032	0.74	7.99	4.28	0.65	3.30	1.95	2.10[c]	3.47[d]	3.1×10^{-3}
$NaClO_4$	49.5	8.01	0.6732 ± 0.0114	0.72	8.01	3.58	0.95	3.38	2.92	2.43[b]	3.68[e]	6.4×10^{-2}

[φ] Hydration bond lengths between ions and oxygen atom of water in solution at +25°C. Water activity values were measured at −15°C and calculated for +25°C. Ionic strength values are calculated with the Pitzer equations (Pitzer, 1973, 1975, 1991). References: [a](Nightingale, 1959), [b](Mähler and Persson, 2012), [c](Bruni et al., 2012), [d](Kálmán et al., 1983), [e](Lindqvist-Reis et al., 1998).

concentration itself was also investigated. A negative correlation between the death rate and the water activity at −15°C was observed (R^2 = 0.23; **Figure 2**). This negative correlation was confirmed when comparing salts with the same cation or anion (red and blue linear regression lines in **Figure 2**, respectively). No correlation was observed between the death rate and the ionic strength of the solution at the eutectic concentration (R^2 = 0.01; **Figure 3**). Moreover, there are no trends indicating a correlation for salts with the same cation or anion. A strong, positive correlation was found between salt concentrations and death rate (R^2 = 0.74; **Figure 4**), which was confirmed with positive trends in salts with the same cation, but not with the same anion.

Salt Concentration Independent Parameters

The investigated salt concentration independent parameters were the HBL-ion, ion molecular weight, hydrated ion radius and unhydrated ion radius. Strong, positive correlations were observed between the HBL-anion and death rate (R^2 = 0.62; **Figure 5**), and between the anion molecular weight and death rate (R^2 = 0.85; **Figure 6**). Although the correlations had a low quality; a weak, negative correlation was observed between the death rate and the cation molecular weight, the unhydrated cation radius and the HBL-cation, which were supported by negative trends in salts with the same anions (R^2 = 0.26, 0.04 and 0.06, respectively) (**Supplementary Figures S1–S3**). A strong, positive correlation was observed between the death rate and the unhydrated anion radius (R^2 = 0.34; **Supplementary Figure S4**). This is the opposite of the trends observed in the unhydrated cation radius. The negative correlation between the HBL-cation and death rate (**Supplementary Figure S3**) is contradictory to the HBL-anion results as described earlier (**Figure 5**). No correlation was observed between the death rate and the hydrated cation and anion radius (R^2 = 0.10 and 0.01, respectively; **Supplementary Figures S5, S6**).

Experiments at Non-eutectic Concentrations

Apart from the eutectic concentrations, the death rate of *P. halocryophilus* has also been investigated for several salts (LiCl, LiI, $MgBr_2$ and $NaClO_4$) at salt concentrations with either a constant water activity of 0.635 ± 0.02 at −15°C (**Figures 7A,C,E**), or a constant ionic strength of 8 mol/L (**Figures 7B,D,F**). Death rate and physicochemical salt parameter values at at non-eutectic concentration at −15°C are presented in **Table 2**. The quality of the logarithmic regression of CFU counts to determine the death rate at non-eutectic concentrations was high, as R^2 was higher than 0.8 for all salts (data not shown). At a water activity (at −15°C) of 0.635 ± 0.02, no correlation between the death rate and the ionic strength was found (R^2 = 0.003; **Figure 7A**), which is consistent with the results at eutectic concentrations. At an ionic strength of 8 mol/L, a strong, negative correlation with low quality (R^2 = 0.14) with the water activity at −15°C was observed (**Figure 7B**), which is consistent with the results at eutectic concentrations. Both conditions (constant water activity and constant ionic strength) showed similar results with each of the salt concentration independent salt parameters. The HBL-anion showed a strong, positive correlation at constant water activity (R^2 = 0.75; **Figure 7C**) and at constant ionic strength (R^2 = 0.42; **Figure 7D**), which is consistent with the results at eutectic concentrations. The unhydrated anion radius had a weak, positive correlation at a constant water activity at −15°C (R^2 = 0.41) and with a lower quality at constant ionic strength (R^2 = 0.15), respectively (**Figures 7E,F**), which is consistent with the results at eutectic concentrations. All other correlations with salt parameters at a water activity of 0.635 at −15°C (**Supplementary Figure S7**) and at an ionic strength of 8 mol/L (**Supplementary Figure S8**) had a low quality in both conditions ($R^2 \leq 0.15$).

DISCUSSION

Physicochemical Effects

We found correlations of higher quality ($R^2 > 0.4$) between several physicochemical parameters with the death rate of *P. halocryophilus*. These parameters are the salt concentration, HBL-anion and molecular weight of the anion. Correlations with a lower quality (R^2 between 0.2 and 0.4) were found between the death rate and the water activity at −15°C, unhydrated anion radius, and molecular weight of the cation, some of which only became apparent by examining salts with the same cation or anion. The correlations of the following parameters were considered unreliable as they had a low quality ($R^2 \leq 0.15$) and are therefore interpreted as no correlations; the ionic strength, hydrated and unhydrated cation radius, hydrated anion radius and HBL-cation. The correlations at eutectic concentrations were confirmed by the correlations at non-eutectic concentrations. The parameters systematically affecting the death rate are related to each other according to the HSAB theory.

Based on the HSAB theory (Pearson, 1968a), salts consisting of hard cations and hard anions or soft cations and soft anions are less soluble than salts consisting of hard cations and soft anions or vice versa. In this study all salts contain hard cations and single-charged anions ranging from hard to soft (Pearson, 1968b). Chlorine is considered hard, bromine borderline and iodine soft (Pearson, 1968b). The increase in anion softness correlates with an increase of the unhydrated anion radius and the anions' molecular mass. Increasing the anion softness in combination with the hard cations enhances the salts' solubility, resulting in higher eutectic concentrations. Although soft ions have a low charge density, and therefore less water molecules in the hydration sphere, the combination of a soft anion with a hard cation results in a higher solubility, which in turn decreases the water activity, as more water molecules are needed to dissolve the increased number of ions in the eutectic solution. This is the case for the tested salts at eutectic concentrations for the salt concentration and the measured water activity, except for NaBr and NaI, which have similar water activity values (**Table 1**). The relation between those parameters explains the observation of the positive correlation between the death rate and the unhydrated anion radius (**Supplementary Figure S6**), molecular anion weight (**Figure 6**) and salt concentration (**Figure 4**), while

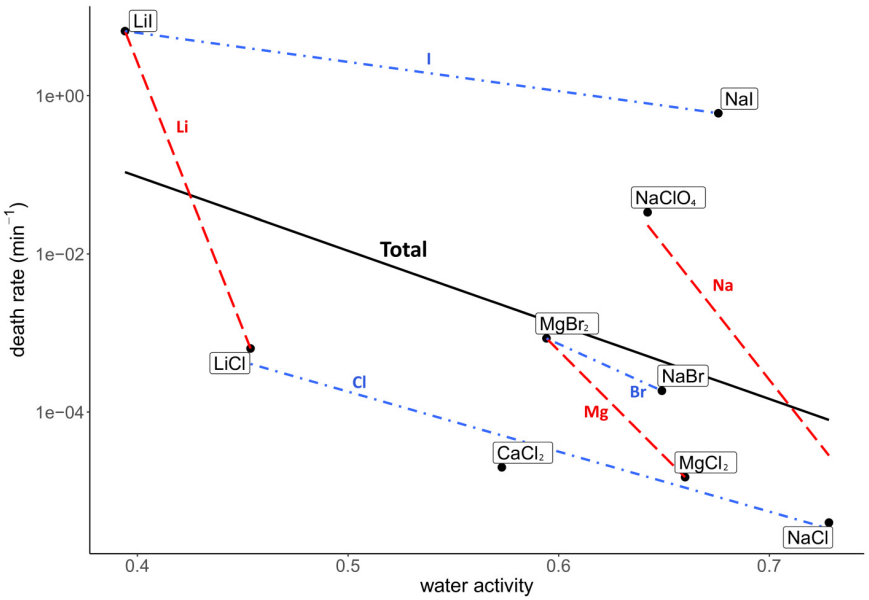

FIGURE 2 | Correlation between the death rate and water activity at −15°C at eutectic concentration. Regression of all salts is depicted in black (R^2 = 0.23). Regressions of salts with the same cations are depicted with red dashed lines, regressions of salts with the same anion are in blue dashdotted lines. The overall negative correlation is supported by the trends of salts with the same anion and cation, which all show a negative trend.

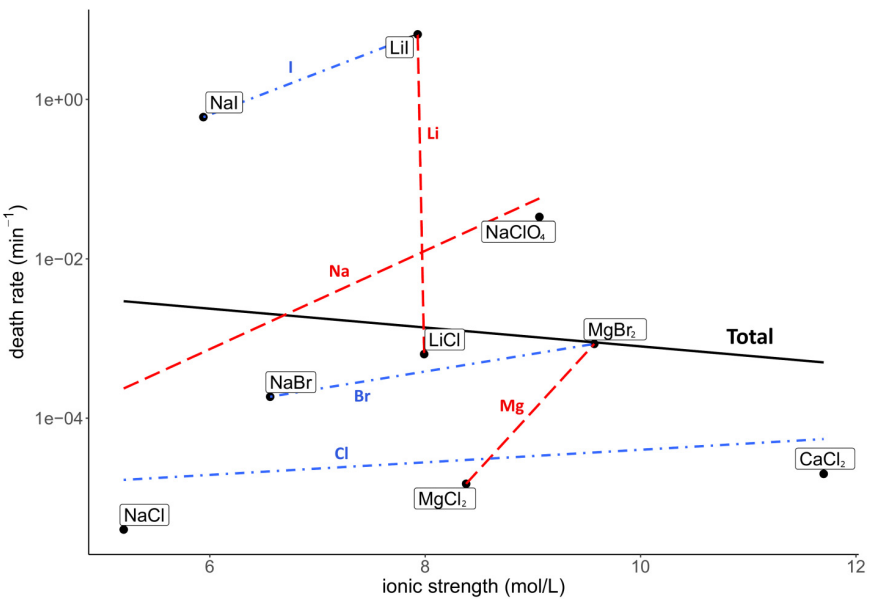

FIGURE 3 | Correlation between the death rate and ionic strength at eutectic concentration. Regression of all salts is depicted in black (R^2 = 0.01). Regressions of salts with the same cations are depicted with red dashed lines, regressions of salts with the same anion are in blue dashdotted lines. No overall correlation is seen, nor do the trend lines of salts with the same anion and cation show an indication of a correlation.

the water activity at −15°C shows a negative correlation with the death rate (**Figure 2**).

A correlation between the survival, i.e., the inverse of the death rate, and water activity is expected, as a low water activity correlates with a decreased percentage of free biologically available water molecules (Tosca et al., 2008; Stevenson et al., 2015a,b). All measured water activity values are lower than calculated water activity values of these solutions at +25°C (**Tables 1**, **2**). At lower temperatures, hydration shells are larger than at higher temperatures (Zavitsas, 2005; Heinz et al., 2018), resulting in a lower water activity of the surrounding solution. Although a lower water activity correlates to a

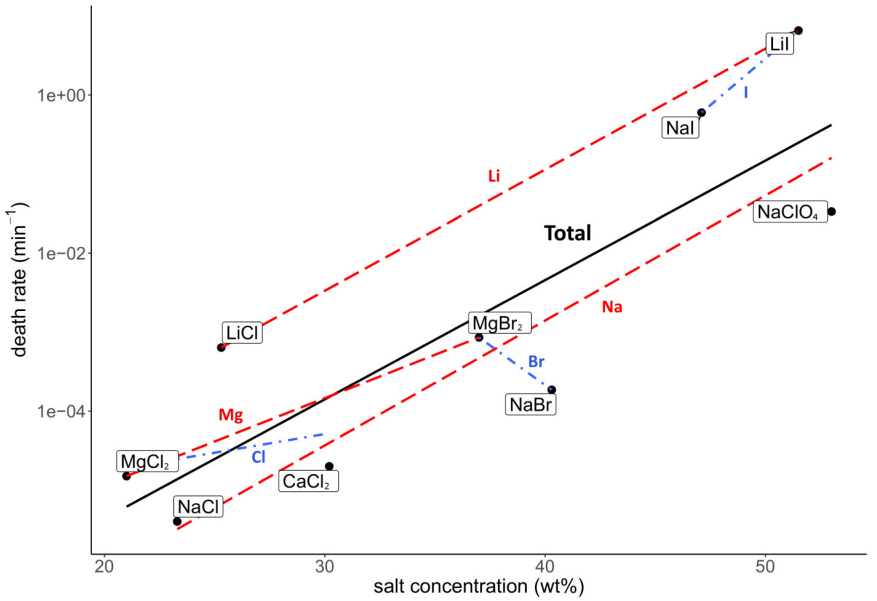

FIGURE 4 | Correlation between the death rate and salt concentration (wt%) at eutectic concentration. Regression of all salts is depicted in black (R^2 = 0.74). Regressions of salts with the same cations are depicted with red dashed lines, regressions of salts with the same anion are in blue dashdotted lines. The overall strong, positive correlation is supported by the trends of salts with the same cation, which all show a positive trend. However, salts with the same anion show no trends.

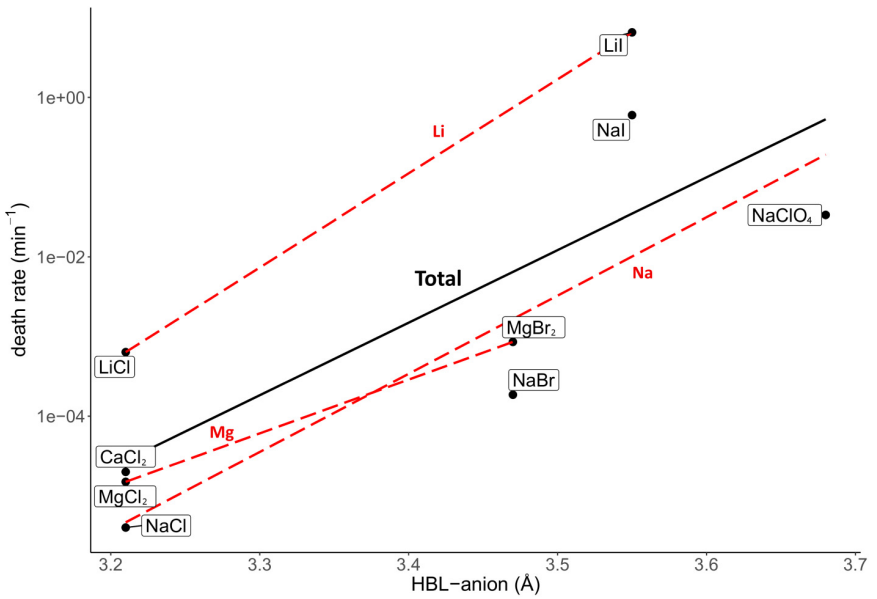

FIGURE 5 | Correlation between the death rate at eutectic concentration and hydration bond length between the anion and the oxygen atoms of the water molecules in the inner hydration shell (HBL-anion). Regression of all salts is depicted in black (R^2 = 0.62). Regressions of salts with the same cations are depicted with red dashed lines. The overall strong, positive correlation is supported by the trends of salts with the same anion, which all show a positive trend.

lower survivability, microbial survival increases by lowering the temperature of brines (Heinz et al., 2018). This insight indicates that the correlation between water activity, temperature and survival is more complex than previously thought and further research is recommended.

Our results indicate that the ionic strength does not influence survival (**Figure 3**). In contrast, Fox-Powell et al. (2016) showed ionic strength to limit bacterial growth. A potential explanation for the observed differences between these studies could be that our experiments investigated a smaller range of ionic strength

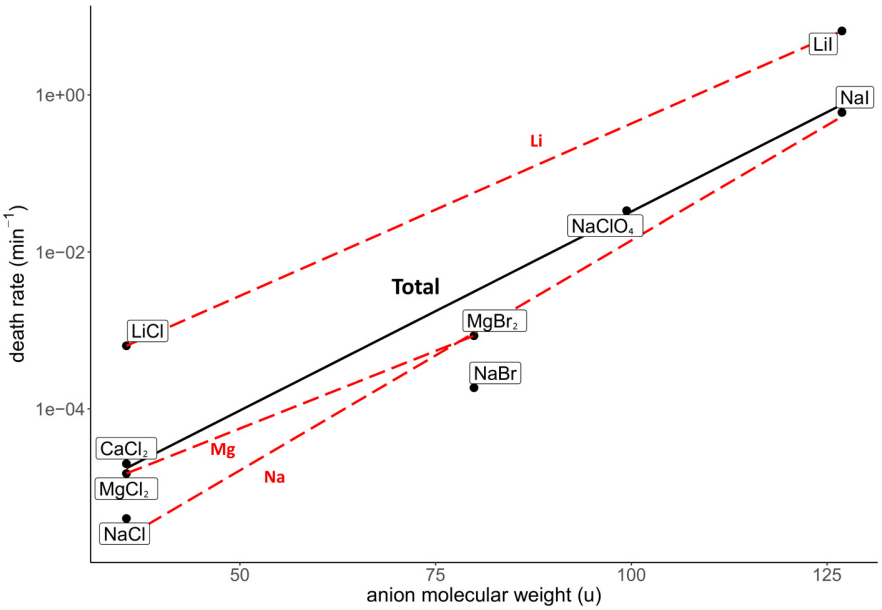

FIGURE 6 | Correlation between the death rate at eutectic concentration and molecular weight of the anion of the respective salts. Regression of all salts is depicted in black (R^2 = 0.85). Regressions of salts with the same cations are depicted with red dashed lines. The overall strong, positive correlation is supported by the trends of salts with the same anion, which all show a positive trend.

(4.9–11.7 mol/L) than Fox-Powell et al. (2016) (0–14 mol/L). Ionic strengths higher than 11.7 mol/L could have a negative effect on the survival of *P. halocryophilus* in the brines tested in the current paper. The lowest ionic strength that did not support growth in Fox-Powell et al. (2016) was 10.1 mol/L, while a different brine with an ionic strength of 12.1 mol/L did support microbial growth. Our research has only investigated one salt solution with an ionic strength larger than 10.1 mol/L, $CaCl_2$ at a eutectic concentration. Hence, further research on the effect of high ionic strengths on the survival of *P. halocryophilus* is needed.

Harder ions form shorter and stronger hydrogen bonds due to higher charge densities, resulting in more water molecules surrounding the ion. Hence, hydration shells around hard ions are stronger and larger, as more water molecules surround the ion and are more strongly bound to the ion. The effect of the hydration shell strength on the survival of *P. halocryophilus* had previously been proposed by Heinz et al. (2018). A potential cause for this putative correlation is that the ion's hydration shell is removed partially or completely by ion transport proteins prior to membrane transportation (Zhou et al., 2001; Gouaux and Mackinnon, 2005). Hence, stronger hydration shells (and thus shorter HBLs) require more energy for their removal from the ions and would therefore not be transported into the cell as much and as effectively as ions with longer HBLs. Stronger hydration shells would therefore correlate with a higher survival, i.e., lower death rate, which corroborates our observations of the hydration bond length of the anions (HBL-anion). However, our observations of the HBL-cation are not consistent with this hypothesis. There is a weak, negative correlation of low quality present between the HBL-cation and death rate, which was supported by negative trends when comparing salts with the same anion (a shorter HBL-cation correlates to a higher death rate). A possible explanation for the HBL-cation observation could be the fact that cations are significantly more hydrated at −15°C than at ambient temperatures (Zavitsas, 2005, 2016) while anions are usually less hydrated than their cationic counterparts (Ji, 1997, pp. 112–139). Thus, cations might have more difficulty to enter bacterial cells at −15°C because of a reduced ion mobility and permeability, which correlates with a decrease in the overall ion-specific toxicity (Seifriz, 1949). This effect could be sufficiently strong resulting in the absence of a strong correlation of survival with HBL-cation, while a strong correlation was present with the HBL-anion. Similar to our finding of more relevant anion-associated factors than those of the cation, a recent study shows that anions have the most important role in determining the maximum salt concentration suitable for growth of *P. halocryophilus*, thus influencing its survival (Heinz et al., 2019).

Non-physicochemical Effects

Additionally, non-physiochemical effects such as chemical reactivity or biochemical effects of the species-ion interactions could play a role in the survival of *P. halocryophilus*. It is generally observed that salt shock results in plasmolysis, which inhibits nutrient uptake and DNA replication, and triggers an ATP level increase in cells, leading to inhibition of macromolecular biosynthesis (Csonka, 1989). The presence of both monovalent and divalent ions are important for the stability of RNA structures, as monovalent ions encourage secondary structure formation of RNA, while divalent ions stabilize RNA structures by shielding electronegatively charged groups (Ramesh and Winkler, 2010). Moreover, a combination of mono- and divalent

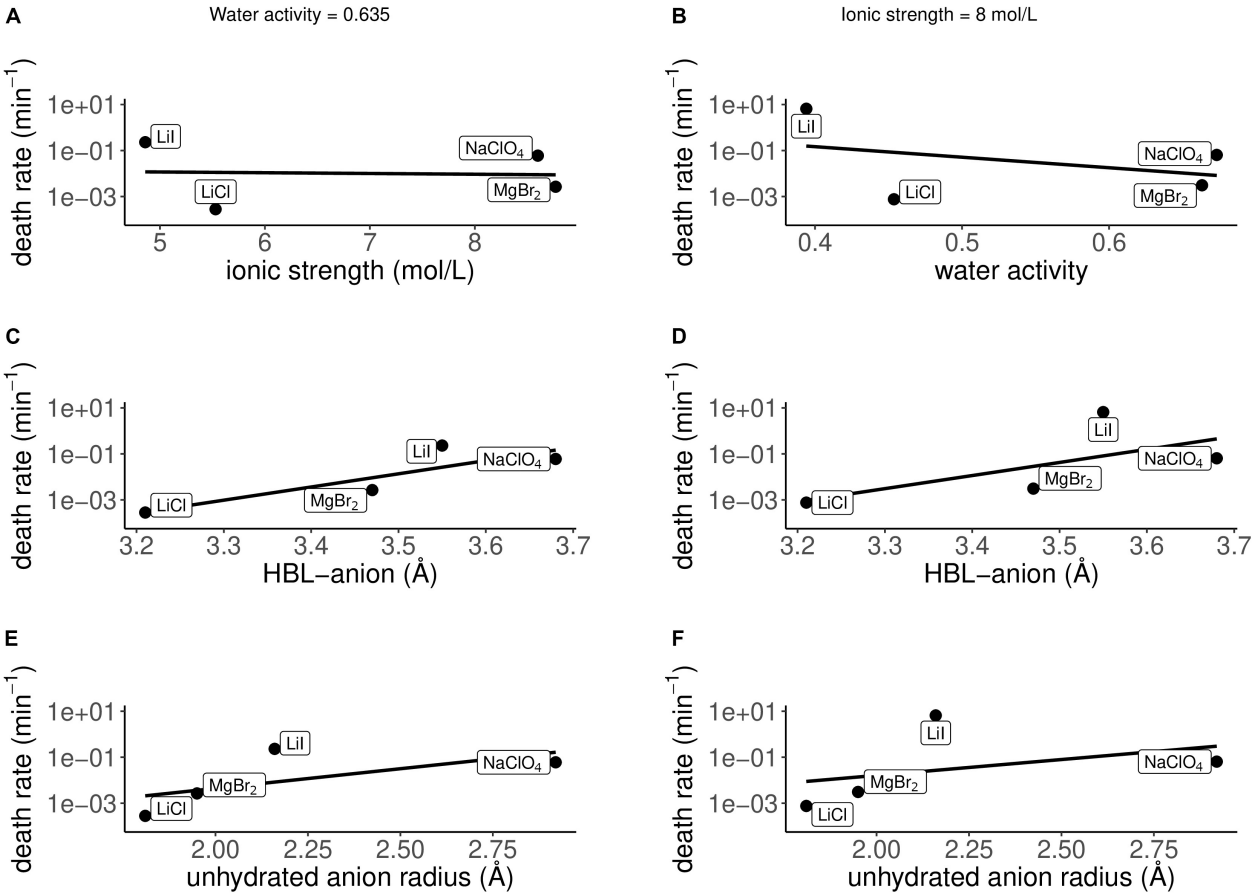

FIGURE 7 | Correlations between the death rate and several physicochemical parameters at non-eutectic conditions: constant water activity at −15°C = 0.635 ± 0.02 **(A,C,E)**, constant ionic strength = 8 mol/L **(B,D,F)**. **(A)** No correlation is observed between the death rate and the ionic strength at a water activity at −15°C of 0.635 (R^2 = 0.003). **(B)** A strong, negative correlation is observed between the death rate and the water activity at −15°C at an ionic strength of 8 mol/L (R^2 = 0.14). **(C)** A strong, positive correlation is observed between the death rate and the hydration bond length between the anion and the oxygen atoms of the water molecules in the inner hydration shell (HBL-anion) at a water activity at −15°C of 0.635 (R^2 = 0.75). **(D)** A strong, positive correlation is observed between the death rate and the hydration bond length between the anion and the oxygen atoms of the water molecules in the inner hydration shell (HBL-anion) at an ionic strength of 8 mol/L (R^2 = 0.42). **(E)** A weak, positive correlation is observed between the death rate and the unhydrated anion radius at a water activity at −15°C of 0.635 (R^2 = 0.41). **(F)** A weak, positive correlation is observed between the death rate and the unhydrated anion radius at an ionic strength of 8 mol/L (R^2 = 0.15).

ions ensure stable tertiary structures (Ramesh and Winkler, 2010). Magnesium, for example, effectively stabilizes tRNA tertiary structures (Draper et al., 2005). Therefore, changes in the ratio of mono- and divalent ions could influence the stability of biomolecules like RNA. Another biochemical effect could be influenced by different ion transportation mechanisms into and out of the cell. Ion transport of for example Na^+, Ca^{2+} and Cl^- over the cell membrane can occur actively and passively via membrane transporters (Maloney, 2002; Padan, 2009). Therefore, ion-specific transport regulation mechanisms could influence the effect different ions have on the survival of microorganisms.

Depending on the ion, the overall survival of an organism can be affected. Calcium ions have, for example, been shown to interact with EPS of sulfur-reducing bacteria (Braissant et al., 2007). Additionally, $CaCl_2$ is known to deflocculate sludge by the removal of EPS (Kavitha et al., 2015). In this study, the removal of EPS could have left the bacterial cells more exposed to the salt by reducing clumping, as observed previously (Heinz et al., 2019). Our study shows that the death rate in $CaCl_2$ is slightly higher than that in $MgCl_2$ or NaCl at their eutectic concentrations, but more calcium-containing salts would need to be tested to check if this effect occurs in more salts.

Chloride and bromide have little toxic effects on microorganisms (Flury and Papritz, 1993; Serrano, 1996). Bromide has previously shown to be comparably toxic as iodide to single-cell organisms (Flury and Papritz, 1993). However, iodide is a mildly reducing agent and can therefore induce reduction reactions with cell components causing cell damage. Additionally, iodide solutions contain minor amounts of iodine (I_2) capable of oxidizing cell components. Both types of redox reactions can be harmful to the cells and, hence, reduce their survival in iodide solutions. Furthermore, iodide has protein denaturing properties (Dzubiella, 2008). Indeed, our experiments showed an increased toxicity when comparing iodide-containing

salts to non-iodide-containing salts. In eutectic concentrations for example, the death-rate in LiI is 6.6 min^{-1}, while the death-rate in LiCl is only 6.4×10^{-4} min^{-1}, while the molar eutectic concentrations are similar (**Table 1**).

Not much is known about the microbial toxicity of dissolved perchlorate ions. In fact, dissimilatory perchlorate reduction is a common metabolic pathway in bacteria (Bardiya and Bae, 2011) and archaea (Liebensteiner et al., 2013), and perchlorate can be tolerated in high concentrations by eukaryotes, e.g., the halotolerant yeast *Debaryomyces hansenii* can tolerate 2.4 M $NaClO_4$ (Heinz et al., 2020). Furthermore, dissolved perchlorate ions are relatively inert and non-oxidizing due to kinetic barriers (Urbansky, 1998). Although sodium perchlorate was more damaging to the survival of *P. halocryophilus* than sodium chloride at eutectic concentrations, specific toxic parameters belonging to the perchlorate ion only might play a minor role and probably can be neglected.

Further research could decipher the effect of additional non-physicochemical parameters to bacterial survival and therefore elaborate the results of the currently investigated effects of physicochemical parameters.

Implications

Even though the addition of salt to aqueous environments would result in an increased temperature range of liquid water, and therefore would result in more potential habitable environments on Earth as well as on other planets, high salt concentrations have shown to have a detrimental effect on – even halotolerant – microorganisms. Our data shows that the survival of *P. halocryophilus* is affected by salinity and correlates simultaneously to multiple parameters which are chemically linked to each other. The water activity, salt concentration, hydration shell strength of the anion, anion molecular weight and unhydrated anion radius have shown to have the strongest correlation with the survival of *P. halocryophilus* in brines.

This study presents measured water activities for a large number of liquid salt solutions at constant sub-zero temperatures (−15°C) for the first time. As there are few datasets of water activity measurements in sub-zero liquid solutions (Toner and Catling, 2016), the dataset from this study gives a new, important insight of water activities in cryobrine environments relevant for planets such as Earth and Mars.

Together with water activity and salt concentration, the type of anion is the limiting factor for the survival of *P. halocryophilus* at low temperatures, and their toxicity is in turn correlated to their HBL, anion molecular weight and unhydrated radius. Thus, these parameters have the greatest influence on the habitability of saline environments, such as the abundant hygroscopic, saline environments and expected cryobrines on Mars, including the recently discovered putative subglacial lake (Orosei et al., 2018). These cryobrines haven been proposed to contain mainly chloride and perchlorate anions (Chevrier et al., 2009; McEwen et al., 2011). As *P. halocryophilus* has shown to have a high resistance to chloride and perchlorate containing brines (Heinz et al., 2019), this increases the probability of microbial life thriving in these environments. However, our results have shown that perchlorate containing salts are more damaging to the survival than chloride containing salts. This stresses the importance of anion brine composition, next to the importance of the salt concentration and water activity, when investigating the habitability of these brines. Hence, future Mars missions would need to take these environmental factors into account when investigating potential habitable environments.

DATA AVAILABILITY STATEMENT

The datasets generated for this study are available on request to the corresponding author.

AUTHOR CONTRIBUTIONS

AW and JH carried out the experimental work. AW performed the data analysis and wrote the first draft of the manuscript. All authors contributed to conception and design of the study, manuscript revision, and read and approved the submitted version.

FUNDING

This project was funded by European Research Council Advanced Grant "Habitability of Martian Environments" (HOME, no. 339231), by a NERC Doctoral Training Partnership grant (NE/L002558/1), and PCDS (Principal's Career Development Scholarship).

ACKNOWLEDGMENTS

We thank C. S. Cockell for providing AW with time for writing the manuscript and access to the laboratory in order to improve the manuscript. We also thank the two reviewers for their useful feedback on the manuscript.

SUPPLEMENTARY MATERIAL

The Supplementary Material for this article can be found online at: https://www.frontiersin.org/articles/10.3389/fmicb.2020.01284/full#supplementary-material

REFERENCES

Bardiya, N., and Bae, J. H. (2011). Dissimilatory perchlorate reduction: a review. *Microbiol. Res.* 166, 237–254. doi: 10.1016/j.micres.2010.11.005

Braissant, O., Decho, A. W., Dupraz, C., Glunk, C., Przekop, K. M., and Visscher, P. T. (2007). Exopolymeric substances of sulfate-reducing bacteria: interactions with calcium at alkaline pH and implication for formation of carbonate minerals. *Geobiology* 5, 401–411. doi: 10.1111/j.1472-4669.2007.00117.x

Bruni, F., Imberti, S., Mancinelli, R., and Ricci, M. A. (2012). Aqueous solutions of divalent chlorides: ions hydration shell and water structure. *J. Chem. Phys.* 136:064520. doi: 10.1063/1.3684633

Chevrier, V. F., Hanley, J., and Altheide, T. S. (2009). Stability of Perchlorate hydrates and their liquid solutions at the phoenix landing site, Mars. *Geophys. Res. Lett.* 36:L10202. doi: 10.1029/2009GL037497

Chevrier, V. F., and Rivera-Valentin, E. G. (2012). Formation of recurring slope lineae by liquid brines on present-day Mars. *Geophys. Res. Lett.* 39, 1–5. doi: 10.1029/2012GL054119

Conde, M. R. (2004). Properties of aqueous solutions of lithium and calcium chlorides: formulations for use in air conditioning equipment design. *Int. J. Ther. Sci.* 43, 367–382. doi: 10.1016/j.ijthermalsci.2003.09.003

Csonka, L. N. (1989). Physiological and genetic responses of bacteria to osmotic stress. *Microbiol. Rev.* 53, 121–147. doi: 10.1128/mmbr.53.1.121-147.1989

Draper, D. E., Grilley, D., and Soto, A. M. (2005). Ions and RNA Folding. *Annu. Rev. Biophys. Biomol. Struct.* 34, 221–243. doi: 10.1146/annurev.biophys.34.040204.144511

Dzubiella, J. (2008). Salt-Specific stability and denaturation of a short salt-bridge-forming α-helix. *J. Am. Chem. Soc.* 130, 14000–14007. doi: 10.1021/ja805562g

Fegley, B., and Osborne, R. (2013). *Practical Chemical Thermodynamics for Geoscientists*. Cambridge, MA: Academic Press.

Fisher, D. A., Hecht, M. H., Kounaves, S. P., and Catling, D. C. (2010). A perchlorate brine lubricated deformable bed facilitating flow of the North Polar Cap of Mars: possible mechanism for water table recharging. *J. Geophys. Res.* 115, 0–12. doi: 10.1029/2009JE003405

Flury, M., and Papritz, A. (1993). Bromide in the natural environment: occurrence and toxicity. *J. Environ. Qual.* 22, 747–758. doi: 10.2134/jeq1993.00472425002200040017x

Fox-Powell, M. G., Hallsworth, J. E., Cousins, C. R., and Cockell, C. S. (2016). Ionic strength is a barrier to the habitability of Mars. *Astrobiology* 16, 427–442. doi: 10.1089/ast.2015.1432

Gouaux, E., and Mackinnon, R. (2005). Principles of selective ion transport in channels and pumps. *Science* 310, 1461–1465. doi: 10.1126/science.1113666

Hecht, M. H., Kounaves, S. P., Quinn, R. C., West, S. J., Young, S. M. M., Ming, D. W., et al. (2009). Detection of perchlorate and the soluble chemistry of martian soil at the phoenix lander site. *Science* 325, 64–67. doi: 10.1126/science.1172466

Heinz, J., Krahn, T., and Schulze-Makuch, D. (2020). A new record for microbial perchlorate tolerance: fungal growth in $NaClO_4$ brines and its implications for putative life on Mars. *Life* 10:53. doi: 10.3390/life10050053

Heinz, J., Schirmack, J., Airo, A., Kounaves, S. P., and Schulze-Makuch, D. (2018). Enhanced Microbial Survivability in Subzero Brines. *Astrobiology* 18, 1171–1180. doi: 10.1089/ast.2017.1805

Heinz, J., Waajen, A. C., Airo, A., Alibrandi, A., Schirmack, J., and Schulze-Makuch, D. (2019). Bacterial growth in chloride and perchlorate brines: halotolerances and salt stress responses of *Planococcus halocryophilus*. *Astrobiology* 19, 1377–1387. doi: 10.1089/ast.2019.2069

Hendricks, S. B. (1928). The crystal structure of lithium iodide trihydrate. *Am. J. Sci.* 15, 403–409. doi: 10.2475/ajs.s5-15.89.403

Hennings, E. (2014). *Cryo Brines - Phasengleichgewichte von Salz-Wasser-Systemen Bei Tiefen Temperaturen*. PhD dissertation, Technischen Universität Bergakademie Freiberg, Freiberg.

Ji, G. L. (1997). "Electrostatic Adsorption of Anions," in *Chemistry of Variable Charge Soils*, 1st Edn, eds T. R. Yu and G. L. Ji (Oxford: Oxford University Press), 112–139.

Kálmán, E., Serke, I., and Pálinkás, G. (1983). Complex Formation in an aqueous $ZnBr_2$ Solution Based on Electron Diffraction. X-ray Scattering and Raman Spectra. *Zeitschrift Naturfoschung A* 38, 9–14. doi: 10.1515/zna-1983-0220

Kasting, J. F., Whitmire, D. P., and Reynolds, R. T. (1993). Habitable zones around main sequence stars. *Icarus* 101, 108–128. doi: 10.1006/icar.1993.1010

Kavitha, S., Saranya, T., Kaliappan, S., Kumar, A. S., Yeom, I. T., and Banu, J. R. (2015). Accelerating the Sludge Disintegration Potential of a Novel Bacterial Strain *Planococcus jake* 01 by $CaCl_2$ induced deflocculation. *Bioresour. Technol.* 175, 396–405. doi: 10.1016/j.biortech.2014.10.122

Kereszturi, A., Möhlmann, D., Berczi, S. Z., Ganti, T., Horvath, A., Kuti, A., et al. (2010). Indications of brine related local seepage phenomena on the northern hemisphere of Mars. *Icarus* 207, 149–164. doi: 10.1016/j.icarus.2009.10.012

Kim, H.-T., and Frederick, W. J. (1988). Evaluation of Pitzer ion interaction parameters of aqueous Electrolytes at 25 °C. 1. Single Salt Parameters. *J. Chem. Eng. Data* 33, 177–184. doi: 10.1021/je00052a035

Liebensteiner, M. G., Pinkse, M. W., Schaap, P. J., Stams, A. J., and Lomans, B. P. (2013). Archaeal (Per)chlorate reduction at high temperature: an interplay of biotic and abiotic reactions. *Science* 340, 85–87. doi: 10.1126/science.1233957

Lindqvist-Reis, P., Munoz-Paez, A., Diaz-Moreno, S., Pattanaik, S., Persson, I., and Sandström, M. (1998). The Structure of the hydrated gallium(III), indium(III), and chromium(III) ions in aqueous solution. A large angle X-ray scattering and EXAFS study. *Inorg. Chem.* 37, 6675–6683. doi: 10.1021/ic980750y

Madan, R. L. (2012). *Chemistry for Degree Students: (B.Sc. 2nd Year)*. New Delhi: S Chand & Company Ltd.

Mähler, J., and Persson, I. (2012). A study of the hydration of the alkali metal ions in aqueous solution. *Inorg. Chem.* 51, 425–438. doi: 10.1021/ic2018693

Maloney, P. C. (2002). "Bacterial membrane transport: superfamilies of transport proteins," in *Encyclopedia of Life Sciences* (Hoboken, NJ: John Wiley & Sons, Ltd). doi: 10.1002/9780470015902.a0001418.pub2

Martín-Torres, J. F., Zorzano, M. P., Valentín-Serrano, P., Harri, A. M., Genzer, M., Kemppinen, O., et al. (2015). Transient liquid water and water activity at Gale crater on Mars. *Nat. Geosci.* 8, 357–361. doi: 10.1038/ngeo2412

McEwen, A. S., Ojha, L., Dundas, C. M., Mattson, S. S., Byrne, S., Wray, J. J., et al. (2011). Seasonal flows on warm Martian slopes. *Science* 333, 740–743. doi: 10.1126/science.1204816

Möhlmann, D., and Thomsen, K. (2011). Properties of cryobrines on Mars. *Icarus* 212, 123–130. doi: 10.1016/j.icarus.2010.11.025

Mykytczuk, N. C. S., Foote, S. J., Omelon, C. R., Southam, G., Greer, C. W., and Whyte, L. G. (2013). Bacterial Growth at −15 °C; Molecular Insights from the Permafrost Bacterium *Planococcus halocryophilus* Or1. *ISME J.* 7, 1211–1226. doi: 10.1038/ismej.2013.8

Mykytczuk, N. C. S., Wilhelm, R. C., and Whyte, L. G. (2012). *Planococcus halocryophilus* sp. nov., an extreme sub-zero species from high Arctic permafrost. *Int. J. Syst. Evol. Microbiol.* 62(Pt 8), 1937–1944. doi: 10.1099/ijs.0.035782-0

Nightingale, E. R. (1959). Phenomenological theory of ion solvation. Effective radii of hydrated ions. *J. Phys. Chem.* 63, 1381–1387. doi: 10.1021/j150579a011

Ojha, L., Wilhelm, M. B., Murchie, S. L., Mcewen, A. S., Wray, J. J., Hanley, J., et al. (2015). Spectral evidence for hydrated salts in recurring slope lineae on Mars. *Nat. Geosci.* 8, 829–832. doi: 10.1038/ngeo2546

Orosei, R., Lauro, S. E., Pettinelli, E., Cicchetti, A., Coradini, M., Cosciotti, B., et al. (2018). Radar evidence of subglacial liquid water on Mars. *Science* 361, 490–493. doi: 10.1126/science.aar7268

Padan, E. (2009). "Bacterial membrane transport: organization of membrane activities," in *Encyclopedia of Life Sciences* (Hoboken, NJ: John Wiley & Sons, Ltd). doi: 10.1038/npg.els.000374

Pearson, R. G. (1968a). Hard and Soft Acids and Bases, HSAB, Part II: underlying theories. *J. Chem. Educ.* 45, 643–648. doi: 10.1021/ed045p581

Pearson, R. G. (1968b). Hard and Soft Acids and Bases, HSAB, Part I: fundamental Principles. *J. Chem. Educ.* 45, 581–587. doi: 10.1021/ed045p643

Pitzer, K. S. (1973). Thermodynamics of electrolytes. I. Theoretical basis and general equations. *J. Phys. Chem.* 77, 268–277. doi: 10.1021/j100621a026

Pitzer, K. S. (1975). Thermodynamics of electrolytes. V. Effects of Higher-Order Electrostatic Terms. *J. Solut. Chem.* 4, 249–265. doi: 10.1007/bf00646562

Pitzer, K. S. (1991). *Activity Coefficients in Electrolyte Solutions*. Boca Raton, FL: CRC PRESS.

Ramesh, A., and Winkler, W. C. (2010). Magnesium-Sensing Riboswitches in Bacteria. *RNA Biol.* 7, 77–83. doi: 10.4161/rna.7.1.10490

Seifriz, W. (1949). Toxicity and the chemical properties of ions. *Science* 110, 193–196. doi: 10.1126/science.110.2851.193

Serrano, R. (1996). Salt tolerance in plants and microorganisms: toxicity targets and defense responses. *Int. Rev. Cytol.* 165, 1–52. doi: 10.1016/s0074-7696(08)62219-6

Stevenson, A., Burkhardt, J., Cockell, C. S., Cray, J. A., Dijksterhuis, J., Fox-Powell, M., et al. (2015a). Multiplication of microbes below 0.690 water activity: implications for terrestrial and extraterrestrial life. *Environ. Microbiol.* 17, 257–277. doi: 10.1111/1462-2920.12598

Stevenson, A., Cray, J. A., Williams, J. P., Santos, R., Sahay, R., Neuenkirchen, N., et al. (2015b). Is there a common water-activity limit for the

three domains of life? *ISME J.* 9, 1333–1351. doi: 10.1038/ismej.2014.219

Toner, J. D., and Catling, D. C. (2016). Water activities of $NaClO_4$, $Ca(ClO_4)_2$, and $Mg(ClO_4)_2$ brines from experimental heat capacities: water activity >0.6 below 200 K. *Geochim. Cosmochim. Acta* 181, 164–174. doi: 10.1016/j.gca.2016.03.005

Tosca, N. J., Knoll, A. H., and McLennan, S. M. (2008). Water activity and the challenge for life on early Mars. *Science* 320, 1204–1207. doi: 10.1126/science.1155432

Urbansky, E. T. (1998). Perchlorate chemistry: implications for analysis and remediation. *Bioremed. J.* 2, 81–95. doi: 10.1080/10889869891214231

Zavitsas, A. A. (2005). Aqueous solutions of calcium ions: hydration numbers and the effect of temperature. *J. Phys. Chem. B* 109, 20636–20640. doi: 10.1021/jp053909i

Zavitsas, A. A. (2016). Comment on 'The size and structure of selected hydrated ions and implications for ion channel selectivity' by Z.-H. Yang, RSC. Adv., 2015, 5, 1213. *RSC Adv.* 6, 92771–92777. doi: 10.1039/c6ra13733d

Zhou, Y., Morais-Cabral, J. H., Kaufman, A., and MacKinnon, R. (2001). Chemistry of ion coordination and hydration revealed by a K+ channel-Fab complex at 2.0 Å Resolution. *Nature* 414, 43–48. doi: 10.1038/35102009

Conflict of Interest: The authors declare that the research was conducted in the absence of any commercial or financial relationships that could be construed as a potential conflict of interest.

The reviewer AS declared a shared affiliation with no collaboration, with one of the authors AW, to the handling editor at the time of review.

Advantages of publishing in Frontiers

OPEN ACCESS
Articles are free to read for greatest visibility and readership

FAST PUBLICATION
Around 90 days from submission to decision

HIGH QUALITY PEER-REVIEW
Rigorous, collaborative, and constructive peer-review

TRANSPARENT PEER-REVIEW
Editors and reviewers acknowledged by name on published articles

Frontiers
Avenue du Tribunal-Fédéral 34
1005 Lausanne | Switzerland

Visit us: www.frontiersin.org
Contact us: frontiersin.org/about/contact

REPRODUCIBILITY OF RESEARCH
Support open data and methods to enhance research reproducibility

DIGITAL PUBLISHING
Articles designed for optimal readership across devices

FOLLOW US
@frontiersin

IMPACT METRICS
Advanced article metrics track visibility across digital media

EXTENSIVE PROMOTION
Marketing and promotion of impactful research

LOOP RESEARCH NETWORK
Our network increases your article's readership